Charles University
Faculty of Science

Study programme: Immunology

Mgr. Matej Fabišik

Signalling pathways of leukocyte membrane receptors, their regulation and deficiencies

Signální dráhy membránových receptorů leukocytů, jejich regulace a poruchy

Doctoral thesis

Supervisor: Mgr. Tomáš Brdička, Ph.D.

Prague, 2020

Prohlášení

Prohlašuji, že jsem závěrečnou práci vypracoval samostatně a uvedl jsem veškeré použité informační zdroje a literature. Tato práce ani žádná její část nebyla předložena k získání jiného nebo stejného akademického titulu.

V Praze 29.6. 2021 Mgr. Matej Fabišik

Acknowledgements

I would like to thank my supervisor Dr. Tomáš Brdička for the opportunity to work in the field of immunology, support, help and calm approach. Many thanks belongs to all of the colleagues for friendly working environment, ideas and help. Finally, I want to thank to Julie Vacková and my family for their endless support.

Content

1. List of abbreviations

AMP – Adenosine monophosphate

BCP-ALL – B cell progenitor acute lymphoblastic leukaemia

BCR - B cell receptor

BM – Bone marrow

BMDC – Bone marrow derived dendritic cells

BMMF – Bone marrow derived macrophages

CD – Cluster of differentiation

CD – Crohn´s disease

CMO – Chronic multifocal osteomyelitis

CRMO – Chronic recurrent multifocal osteomyelitis

CR – Complement receptor

DAMP – Damage associated pattern

DSS – Dextran sodium sulphate

FACS – Fluorescence-activated cell sorting

fMLP – N-formyl-methionyl-leucyl-phenylalanine G-CSFR

– Granulocyte colony-stimulating factor receptor GM-CSF

– Granulocyte/monocyte colony stimulating factor GMP –

Guanosine monophosphate IBD – Inflammatory bowel

disease

IFNγ – Intereferon gamma

ITCH – Itchy E3 Ubiquitin Protein Ligase

ITAM – Immuno tyrosine activatory motif

ITIM – Immuno tyrosine inhibitory motif

KO – Knockout

LSK – Lineage^{-} Sca1^{+} c-Kit^{+} cells

LST1 – Leukocyte specific transcript 1

LPS – Lipopolysaccharide

MAP – Mitogen-activated protein

MHC – Major histocompatibility complex

NK – Naturla killer cells

NKT – Natural killer T cells

OPAL1 – Outcome predictor of acute leukaemia

1 PAMP – Pathogen associated pattern PKC –

Protein kinase C

PMA – Phorbol myristate acetate

PolyI:C – Polyinosinic:polycytidylic acid

PSTPIP2 – Proline-serine-threonine phosphatase-interacting protein 2

PTB – Phosphotyrosine binding

PTM – Post-translational modification

PTK – Protein-Tyrosine kinase

PTPN – Protein tyrosine phosphatases non-receptor type

qPCR – quantitative Polymerase chain reaction ROS –

Reactive oxygen species

SCIMP – SLP adapter and CSK-interacting membrane protein

SCID – Severe combine immuno-defficiency

SH – Src homology

SUMO – Small ubiquitin-like modifier

TCR – T cell receptor

TLR – Toll-like receptor

TNBS – Trinitrobenzene sulfonic acid

TnT – Tunneling nanotubes

TNF – Tumor necrosis factor

TRAP – Transmembrane adaptor protein

UC – Ulcerative colitis

WBP1L – WW domain binding protein 1-like

2. Abstract

Because of the profound effects of signal transduction on cell behaviour, the activity of signalling pathways must be carefully regulated. Otherwise, dysregulation of signalling might harm the organism by not responding to danger or by an excessively strong reaction. Therefore, various regulatory mechanisms became essential parts of signal transduction pathways. They affect these pathways at all levels, including ligands, receptors, signalling enzymes, adaptor proteins and other signalling mediators, as well as transcription factors further downstream. In this thesis, I present the results of the research on the role of transmembrane and membrane associated adaptor proteins LST1, SCIMP, PSTPIP2 and WBP1L in the regulation of leukocyte signalling and homeostasis.

Transmembrane adaptor protein LST1 is a short protein expressed in the cells of the myeloid lineage. Observation of *LST1*$^{-/-}$ mice revealed that these animals are overall healthy without visible phenotype, with the exception of mild reductions in myeloid, NK and NKT cell populations at the steady state. On the other hand, LST1 deficiency had significant protective effect during acute colitis induced by dextran sodium sulphate, suggesting the role of LST1 in the regulation of gut inflammation.

Studies on PSTPIP2 and SCIMP presented in this thesis are also focused on inflammation. They show the role of PSTPIP2 in the regulation of reactive oxygen species production and associated inflammatory bone damage and the function of SCIMP in the regulation of macrophage and dendritic cell responses to fungal cell wall components. Finally, this thesis describes novel transmembrane adaptor WBP1L and its role in the regulation of CXCR4 signalling and haematopoiesis.

3. Abstrakt

Buněčná signalizace má zásadní vliv na chování a funkci buněk, a proto musí být činnost signálních drah pečlivě regulována. Porucha regulace signalizace může poškodit organismus tím, že nezareaguje na nebezpečí nebo na něj zareaguje příliš silně. Proto se různé regulační mechanismy staly nezbytnou součástí signálních drah. Tyto mechanismy se uplatňují na všech úrovních, včetně ligandů, receptorů, signálních enzymů, adaptorových proteinů a dalších signálních mediátorů, jakož i transkripčních faktorů. V této práci předkládám výsledky výzkumu funkcí transmembránových a membránově asociovaných adaptorových proteinů LST1, SCIMP, PSTPIP2 a WBP1L při regulaci signalizace a homeostázy leukocytů.

Transmembránový adaptorový protein LST1 je krátký protein exprimovaný v buňkách myeloidní linie. Pozorování myší *LST1*$^{-/-}$ odhalilo, že tato zvířata jsou zdravá, bez viditelného fenotypu, s výjimkou mírného snížení populací myeloidních buněk, NK a NKT buněk v normálním stavu. Nedostatek LST1 měl naopak významný ochranný účinek při akutní kolitidě vyvolané dextran-sodium-sulfátem, což naznačuje úlohu LST1 v regulaci zánětu střev.

Studie PSTPIP2 a SCIMP prezentované v této práci se také zaměřují na zánět. Ukazují roli PSTPIP2 v regulaci produkce reaktivních forem kyslíku a souvisejícího zánětlivého poškození kostí a funkci SCIMP v regulaci odpovědi makrofágů a dendritických buněk na složky buněčných stěn hub. V neposlední řadě tato práce popisuje nový transmembránový adaptér WBP1L a jeho roli v regulaci signalizace CXCR4 a hematopoézy.

4. Introduction

Every cell gathers information from the environment through its senses - receptors. When a receptor recognizes its ligand, it triggers activation of signalling enzymes, followed by changes in gene expression, cellular metabolism and other processes regulated by this receptor. However, the cells can react only when the signal reaches its designated targets (proteins, enzymes or transcription factors). The process of sending the signal through the cell is called signal transduction. Signal transduction transmits signals from receptors to the designated places through the network of signalling pathways [1].

Receptors sharing similar structural features form receptor families. Signalling pathways of the same receptor family often use similar set of molecules for signal transduction. For example, Toll-like receptors (TLRs) recognize pathogens and danger associated molecular patterns (chaperons, DNA, RNA, LPS, peptidoglycans…) and their main signalling pathway depends on MYD88 adaptor protein. However, several TLRs, such as e.g. TLR4, also use adaptor protein TRIF. This variety of adaptor proteins activating different molecules, change the strength of signals and gives rise to specific patterns of pathway activity. It allows the cell to distinguish, which receptor was triggered and what response should occur, relying on a very tight regulation [2; 3].

Overall, signal transduction plays prominent role in the regulation of immune cells (leukocytes) and the immune system. Its perturbation can cause autoimmunity, insufficient or excessive immune reaction against pathogens and can be potentially harming for organism. To be able to prevent these unwanted outcomes, it is necessary to understand leukocyte signalling pathways and their regulation in sufficient detail.

4.1 Signalling pathway components

4.1.1 Ligands

Leukocytes react to ligands, which are associated with infection/danger or regulate behaviour of the cells. Infection/danger signals are known as DAMP (damage-associated molecular pattern) or PAMP (pathogen associated molecular pattern).

The DAMPs are ligands that are released upon damage inflicted on the organism. For example, when the cell within the organism undergoes destruction, its content, including organelles and intracellular molecules are released and sensed by leukocytes. These are usually molecules which are not available under the normal conditions in the extracellular space, such as DNA, RNA, ATP, chaperons and other intracellular proteins.

The PAMPs are molecules associated with foreign organisms. The most typical PAMPs include lipopolysaccharide (LPS) present in the cell walls of gram-negative bacteria, lipoteichoic acid of gram-positive bacteria, nucleic acids from viruses, mannans or β-glucans from fungi [4].

Hormones, growth factors, cytokines, and chemokines are ligands regulating response and behaviour of leukocytes. Hormones regulate many functions in the organism such as cell growth, differentiation or cell metabolism. In addition, they have a strong immunomodulatory effect on immune cells [5]. For example, glucocorticoids inhibit TLRs pro-inflammatory response by attenuation of AP-1, IRF3 and NF-κB signalling [6; 7; 8]. Glucocorticoids also directly stimulate expression of inhibitory proteins such as glucocorticoid-induced leucine zipper (GILZ), which inhibits MAP kinases, AP-1 and NF-κB [9]. Growth factors such as cytokines G-CSF, GM-CSF, M-CSF or SCF regulate proliferation and differentiation of the cell [10]. Chemokines are typically known for regulation of cell migration. However, their functions are also in the cell proliferation, survival, activation (degranulation, oxidative burst), phagocytosis enhancement and induction of cell adhesion [11; 12]. Cytokines regulate proliferation, activation, inhibition or polarisation of the cells for specific patterns of differentiation or behavior (M1-M2 macrophages, Th1, Th2 cells and others [13; 14]). These ligands are distributed in an

autocrine (influencing the producing cell itself) or paracrine (influencing other cells) manner.

4.1.2 Receptors and signal transduction molecules

Receptors are proteins, which recognize the ligands with high affinity and specificity and after their binding initiate a signalling cascade. In the cells there are two main categories of receptors: cell-surface and intracellular. After the activation, they use various intermediary proteins and other molecules to send the signal downstream. These intermediaries vary depending on the receptor and its mechanism of function. In this respect the most common types of receptors include G-protein coupled receptors, protein kinase associated receptors, receptors employing homotypic domain interactions, nuclear receptors and ligand-gated channels [1].

Cell-surface receptors consist of extracellular part, which usually contains ligand binding site, transmembrane domain anchoring receptor in the cell membrane, and intracellular part with signalling function.

Heterotrimeric G-protein coupled receptors (such as chemokine receptor CXCR4) undergo conformational changes upon ligand binding. This activates exchange of GDP for GTP in the Gα subunit of the heterotrimeric Gαβγ protein, which then dissociates from GPCR as subunits Gα and Gβγ. Both then directly or indirectly activate multiple signalling pathways, including, among others, ERK and P38 pathway and phospholipase Cβ, mediating production of diacylglycerol and inositol-1,4,5-trisphosphate, leading to subsequent activation of calcium signalling, AKT, JNK, MEK and ERK1/2 [15].

Ligand-gated ion channels open after ligand binding and cause influx or efflux of ions. This results in changes of membrane polarization and activation of signalling proteins. Typical ion in immune signalling is Ca^{2+}. For example, T cell stimulation via TCR results in efflux of Ca^{2+} from endoplasmatic reticulum (ER) into cytoplasm. This is triggered by binding of inositol-3-phosphate to calcium channels in the ER membrane. Subsequently, protein detector STIM responds to the decrease of Ca^{2+} concentration in ER and activates Calcium release activated channels (CRAC) in the plasma membrane. Activation of CRAC channels leads to further influx of Ca^{2+} ions

into the cytoplasm. Rise in Ca^{2+} concentration in the cytoplasm has various consequences. One of the best known is Ca^{2+} binding to protein calmodulin, which changes its conformation and activates phosphatase calcineurin, which then dephosphorylates and activates transcription factors of NF-AT family [16; 17].

Another type of receptors regulating immune cell behaviour are receptors associated with protein kinases. Protein kinases attach phosphate moiety to proteins. Some receptors, such as receptors for M-CSF or SCF, are themselves kinases, since they contain kinase domain in their intracellular part. Others interact with kinases non-covalently. Examples include, TCR, BCR and many others. When TCR encounters its ligand, it results in the activation of SRC family kinases, which then phosphorylate CD3 proteins of the TCR complex. Next, another kinase, ZAP70, is recruited to the phosphorylated CD3 proteins and sends signal further downstream [18]. Phosphorylation is rapid process, which can quickly change the protein cellular localisation (STAT transcription factors), interaction with partners (mediated by SH2 and PTB domains) or protein conformation and enzymatic activity (Src family kinases). Phospho-tyrosine containing sites are often present in the structure of adaptor proteins (LAT, LST1, SCIMP, SLP-65/76 etc.)[19; 20].

Signalling by a number of receptors recognizing molecular patterns associated with pathogens or receptors from TNF receptor family is dependent on another general mechanism, homotypic domain interactions, where two domains of the same type interact to transduce the signal. For example, TIR domains in the intracellular part of TLR4 or other TLRs bind TIR domains in the adaptor protein MYD88 to initiate signal transduction, which is further propagated via interactions of MYD88 death domain with the death domains of IRAK kinases [21; 22]. Another characteristic feature of this type of receptors is a common use of ubiquitination in the downstream signalling pathways. Ubiquitination is primarily a degradation signal. When poly-ubiquitin chain is formed on the protein via ubiquitin ligases, it undergoes proteasomal degradation. Degradation can regulate protein localisation (degradation in specific compartments), protein turnover or stability of activated signalling complexes. However, based on how the ubiquitin molecules are linked to polyubiquitin chains (via Lysine 6, 11, 27, 29, 33, 48, or 63), it can also serve as localisation signal or a binding site for other proteins [23]. A great example is signalling of TNF receptor, which is ubiquitinated, internalised and degraded upon

activation. However, ubiquitination also has multiple positive effects on its signalling. These include activation of transcription factor NF-κB mediated by ubiquitin induced degradation of its repressor - protein IκBα [24; 25; 26]. In addition, during activation of the TNF receptor, ubiquitin linked via K63 serves as a scaffold supporting recruitment of parts of the NF-kB signalling pathway (TAK1-TAB2-TAB3 komplex, NEMO-IKKa-IKKb complex, LUBAC complex) mediated by their ubiquitin binding domains [27; 28; 29].

Receptors for pathogens are located not only on the cell surface, but also in the endocytic vesicles and in the cytosol. Typical intracellular pathogens are viruses, which are recognised by DNA- and RNA-sensing intracellular receptors (e.g. TLR3,7,9 in the endosomes and NOD like receptors, RIG-I, or MDA5 in the cytosol) [3; 30]. Upon recognition of their ligands, they induce antiviral responses [1]. Other intracellular receptors such as nuclear receptors (e.g. androgen receptor, estrogen receptors) act like transcription factors [3].

4.1.3 Signalling regulation

Together, the receptors work as the senses of the cells for a wide variety of signals. However, the decision whether to respond and with what intensity depends on the regulation of signalling pathways. Moreover, multiple receptors can share parts of signalling pathways or their signalling can produce a similar outcome. Regulation of the signalling enables proper integration of these signals and ensures an adequate response.

Signalling pathway can be regulated from the outside or by its own components from within the pathway. Outside regulation is mediated by another pathway. For example, T cell signalling via TCR has positive effect of T cell activation and proliferation only when co-stimulation by CD28 receptor is present. Co-stimulation via CD28 enhances transcription of TCR induced genes and induces expression of proteins IL-2 and BCL-x_L, which serve as proliferation and survival factors. However, when the T cells are stimulated only by TCR without co-stimulation, activation induces T cells anergy [31; 32; 33; 34]. Regulation from within the signalling pathway occurs when proteins in the pathway actively regulate its other components. For example, ERK signalling pathway is negatively self-regulated via ERK1/2-mediated

phosphorylation of upstream pathway components (RAF, MEK1/2, etc.). This form of inhibition is fast and regulates the kinetics shortly after activation. Signalling pathways can also induce expression of genes with inhibitory function. However, this form of inhibition has longer kinetics due to longer time required for gene expression. [35].

Signalling is also regulated by utilisation and combination of different signalling modules. This way of regulation relies on changes in spatiotemporal localisation of these signalling modules in the cell or on differential activation of distinct pathways by receptors. Signalling module regulation is often mediated by adaptor proteins that bind multiple signalling complexes together and allow signalling cascades to proceed. A great illustrative example of regulation by signalling modules is TLR4 signal transduction. TLRs are localised at the plasma membrane (TLR1,2,4,5,6,10), or in the endosomes (TLR3, 7, 8, 9, 11, 12, 13) [3]. The canonical TLR signalling pathway (TLR1, 2, 4, 5, 6, 7, 8, 9, 10, 11, 12, 13) is initiated by MYD88 adaptor protein module, followed by phosphorylation, ubiqutination and degradation of IκBα. Degradation of this repressor protein allows the translocation of NF-kB transcription factor into the nucleus and expression of proinflammatory genes such as *IL-1* and *TNFa*. In addition, MYD88 adaptor also activates MAP kinase pathways (p38, ERK) [36; 37]. TLR3 utilises different module starting with TRIF adaptor protein, which signals through TBK1 and again activates NF-kB. In addition, it also activates IRF3, which induces production of type I interferons [38]. However, TLR4 is utilising both adaptor protein modules. Firstly, after ligand recognition, it begins to signal via MYD88. TLR4 is then internalized and interacts with TRIFF adaptor protein. Ultimately, activation of both signalling modules activates different pattern of signalling molecules, leading to corresponding gene expression and defence response [3].

Signalling pathways are fine and complex networks of proteins and other signalling molecules. Their precise regulation is essential to elicit an accurate response and maintain equilibrium between strength of defence and potential harm to organism [39; 40].

5. Adaptor proteins in immune signalling

5.1 Role of adaptor proteins in immune signalling

Adaptor proteins are characterized as proteins without enzymatic activity that facilitate co-localization of the components of cellular signalling cascades and create signalling hubs, locating other signalling proteins in close proximity to each other. We recognize transmembrane adaptor proteins, plasma membrane associated adaptor proteins and cytosolic adaptor proteins [19]. Adaptor proteins contain protein binding domains, which allow them to bind additional proteins and act as scaffolds or docking platforms. By promoting co-localization of signalling cascade components, they enhance the selectivity, specificity and potency of signalling. Typical binding domains of adaptor proteins include the modular binding domains, such as phospho-tyrosine binding domain, SH2 or SH3 domain, pleckstrin homology or WW domain. In addition adaptor proteins often contain short sequence motifs that bind modular binding domains in other proteins. Examples include proline-rich sequences recognized by SH3 domains, PxY motifs interacting with WW domains, or phosphotyrosine-based motifs binding to SH2 or PTB domains. Highly specialized examples of phosphotyrosine-based motifs include Immunoreceptor tyrosine-based activating motif (ITAM - YxxL/I$x_{(6-8)}$YxxL/I), or Immunoreceptor tyrosine-based inhibitory motif (ITIM - S/I/V/LxYxxI/V/L). After phosphorylation of their tyrosines, ITAM and ITIM serve as binding sites for SH2 domains of SYK-family kinases or SHP/SHIP phosphatases, respectively [41]. Localisation of adaptor proteins themselves is regulated by their interaction domains and motifs. Membrane adaptor proteins are also associated with cellular membranes by transmembrane domains or membrane binding domains, such as F-BAR or PH domain or via posttranslational modification with fatty acyl or other hydrophobic moiety [19; 20; 42; 43].

Transmembrane adaptor proteins (TRAPs) contain plasma membrane spanning domain, which localises the adaptor to the plasma membrane in the proximity of receptors. TRAPs usually have very short extracellular part, which is often without ligand or any known function, while their intracellular part contains various interaction motifs. Typical examples include proteins LAT, PAG, NTAL, SCIMP, LST1. Their membrane association is often supported by palmitoyl residue covalently bound to the adaptor at palmitoylation site close to the membrane spanning region [44]. Interestingly, TRAPs do not contain modular binding domains. On the other hand they

typically contain multiple phosphotyrosine-based motifs. Depending on the molecules these motifs recruit they either propagate/potentiate positive signals generated by receptors, or attenuate signalling, e.g. by recruiting protein tyrosine phosphatases (PTPs) [19; 41; 42].

Function of cytoplasmic adaptor proteins, like MYD88, TRIF, SLP65, SLP76 or GRB2 is similar, except that they are recruited to the receptor proximity by binding to the receptor itself or to membrane adaptor proteins and there they contribute to orchestrating signalling cascade in the cytoplasm. In addition to protein-binding motifs they also often contain one or more modular binding domains. Multiple motifs in the adaptor protein structure help organise their interaction partners and regulate downstream signalling [20; 42; 43].

The following chapters will describe signalling, regulation and function of the adaptor proteins important for this thesis.

5.2 Proline-serine-threonine phosphatase-interacting protein 2 (PSTPIP2)

PSTPIP2 belongs to the membrane associated adaptor protein family. It is associated with the plasma membrane via the phosphoinositide binding F-BAR domain at its N terminus [45]. The F-BAR domain is followed the C-terminal tail containing PEST phosphatases binding sequence [46] and tyrosine based phosphorylation motifs interacting with phosphoinositide phosphatase SHIP1 [47]. PSTPIP2 also binds negative regulator of SRC-family kinases CSK via an unknown binding site. PEST family of phosphatases contains three members: PEP/LYP, PTP-HSCF and PTP-PEST. They have rather pleiotropic functions, including negative regulation of lymphocyte activation, as well as regulation of cytoskeletal rearrangement and vesicle trafficking in processes such as adhesion, migration, phagocytosis, antigen capture and antigen presentation [48; 49]. SHIP1 is recruited to PSTPIP2 phosphorylation sites after their phosphorylation increases upon cell activation and contributes to inhibition of inflammasome-mediated processing of pre-IL-1β into its active form [50].

PSTPIP2 expression was reported mainly in myeloid cells. Mutation L98P in the mouse strain *Pstpip2*^{cmo} results in the loss of PSTPIP2 protein. As a consequence, these mice spontaneously develop autoinflammatory disease - Chronic multifocal

osteomyelitis (CMO), which is very similar to human Chronic recurrent multifocal osteomyelitis (CRMO) [45]. However, no *PSTPIP2* mutation has been identified in human CRMO patients up to date [51; 52; 53]. CMO disease symptoms manifest as inflammation of soft tissues in the paws, tail, and ears and as inflammatory destruction of the bones. Activated osteoclasts are the major cause of bone damage in *Pstpip2*^{cmo} mice [45; 54; 55]. However, neutrophil granulocytes and deregulated IL-1β expression are the main trigger of CMO. Mice lacking expression of IL-1β had attenuated disease or were completely healthy [56; 57; 58]. Because IL-1β is cleaved by Caspase-1, studies have been focusing on inflammasome function. They showed that deletion of Caspase-1 does not protect against the disease. The role of Caspase-1 was further found redundant with Caspase-8, which can also cleave IL-1β. Simultaneous inactivation of genes coding for Caspase-1 and 8 significantly, but again incompletely, protected mice against autoinflammation, suggesting that IL-1β activation and lack of inflammasome inhibition are important part of CMO disease initiation [56; 59; 60; 61]. Altogether, available data on the PSTPIP2 adaptor protein indicate that it functions as negative regulator of pro-inflammatory signalling.

5.3 SLP adapter and CSK-interacting membrane protein (SCIMP)

SCIMP is transmembrane adaptor protein discovered in the previous decade. It is expressed exclusively in antigen presenting cells – B cells, dendritic cells, monocytes and macrophages. It is located in tetraspanin enriched microdomains. Upon activation, SCIMP translocates to the immunological synapse between antigen presenting cell and T cell. It was suggested that there it regulates reverse signalling in the antigen presenting cell during the encounter with T cell. Stimulation of antigen recognition receptor BCR in B cells does not trigger phosphorylation of SCIMP. However, when antigen presenting molecules MHCIIgp were cross-linked by anti-MHCII antibodies, SCIMP was phosphorylated [62]. SCIMP was also phosphorylated after activation by LPS, Poly I:C, Pam3CSK4 and CpG and subsequently it bound proteins GRB2, SLP65, LYN and CSK kinase. [63; 64; 65; 66; 67].

5.4 WW Domain Binding Protein 1 Like (WBP1L)

WBP1L – WW domain binding protein 1-like, also known as OPAL1 – Outcome predictor of Acute Leukaemia was discovered as a potential marker of favourable prognosis of acute lymphoblastic leukaemia [160]. Later it was shown that its expression is increased in acute lymphoblastic leukaemia with *ETV6-RUNX1* gene fusion which was known to have good prognosis. We have speculated that WBP1L expression may be linked to this positive outcome. However, nothing was known about its physiological function or function in leukaemia on which we could base any suggestions or speculations about its role [68; 69; 70]. *WBP1L* has also been predicted in several genetic studies as a marker for schizophrenia, high blood pressure and it was associated with placental DNA methylation and birth weight affected by prenatal smoking [71; 72; 73; 74].

Structural analysis of WBP1L *in silico* discovered that it belongs to the transmembrane adaptor protein family. WBP1L contains C*C*CC*CC motif common to the Shisa-like proteins in its small extracellular part. In the intracellular domain WBP1L contains WW domain binding motifs (L-P-X-Y or P-P-X-Y), similar to those interacting with NEDD4 family ubiquitin ligases [75]. However, none of its interactions, effects on signalling pathways or physiological role had been addressed experimentally.

5.5 Leukocyte specific transcript 1 (LST1)

LST1 was found and cloned from an immunologically important genomic region, MHCIII locus [76; 77; 78]. Adjacent regions - MHCI and MHCII loci contain genes of antigen presenting molecules. The MHCIII locus contains genes participating in the regulation and activation of the immune system such as genes coding TNFα, complement proteins or lymphotoxins [78; 79]. Human *LST1* gene has 9 exons of which 5 are non coding. It undergoes immense splicing. A total of 16 splice variants of human *LST1* gene have been described [80; 81; 82]. In contrast, murine *Lst1* has only two splice variants [83].

LST1 is 97 amino acids long transmembrane adaptor protein with very short extracellular part containing dimerization cysteine and a glycosylation motif. In the

intracellular part, LST1 contains ITIM (defined as (L/V/I)*x*Y*xx*(L/V)) and ITIM-like (defined as (D/E)Y*x*E(V/I)(R/K)) motif. Studies showed an interaction between LST1 and RalGPS2-TalA-Sec5, which affects formation of long (up to 100 μm) membrane protrusions called Tunnelling nanotubes (TnT). TnTs mediate cell to cell contact and transfer of molecules between the cells (e.g. of MHCIgp) [84; 85; 86]. Additionally, previous work in our laboratory showed binding of phosphatases SHP1 and SHP2 to LST1 after phosphorylation of its ITIM motifs. Consistent with these data, LST1 inhibited Fc receptor-triggered total phosphorylation and calcium signalling after LST1 and Fc receptor co-crosslinking [87].

Expression of LST1 is still a widely discussed topic. Using our own antibody against human LST1, our group found expression of LST1 exclusively in myeloid immune cells, which was also confirmed by qPCR [87]. However, antibody 7E2 developed by Schiller et al [88] detected LST1 also in lymphoid (Jurkat, B cells) and non-hematopoietic cells (HeLa, Capan-1, HepG2) [88]. LST1 expression was found to be increased under inflammatory conditions. *LST1* mRNA was upregulated in cell lines stimulated with LPS and TNF, in samples from patients suffering from inflammatory bowel diseases (IBD) [89] and synovial fluid of rheumatoid arthritis (RA) patients [90; 91]. Moreover, LST1-deficient mice had more serious disease course and lower survival rate when challenged with influenza virus [92].

Overall, these results suggested its role not only in the Tunnelling nanotubes formation, but also in the regulation of immune response and inflammation. However, the exact processes and immune system activities regulated by LST1 have not been defined.

6. Inflammatory bowel diseases

6.1 Classification of inflammatory bowel diseases

Inflammatory bowel disease (IBD) is a group of disorders of small intestine and colon caused by a dysregulated immune system. The two major types of IBD are Crohn´s disease (CD) and Ulcerative colitis (UC) [93]. The Crohn´s disease displays transmural pleomorphic inflammation, which does not have to be continuous and can occur as multiple lesions. As a complication of the colon inflammation CD patients may develop fistulas, abscesses and often also granulomas and fissures in any part of the intestine. Symptoms unrelated to the colon are weight loss, fever, arthritis, pyoderma gangrenosum and sweet syndrome. In ulcerative colitis, inflammation is localised in colon and is mostly characterized by neutrophilic inflammation with crypt abscesses and pseudopolyps. The inflammation is continual and occurs in the submucosa/mucosa layer. Common complications are haemorrhage and toxic megacolon. Non-colon symptoms of UC are similar – weight loss, arthritis, sweet syndrome, pyoderma gangrenosum with addition of hepatitis and sclerosing cholangitis [94].

During last century incidence and prevalence of IBD have been increasing mainly in the western countries [95]. The IBD prevalence in the North America and European countries exceeds 0.3% [96]. Such prevalence represents a considerable burden for the healthcare system (capacity, financing) and patients, whose condition leads to a decrease in quality of life (anemia, disability, psychic disorders) [97; 98; 99; 100]. IBDs are complex diseases and for their development three factors are responsible: genetics, microbiota and nutrition. Relatives of patients with IBD have an increased risk of developing the disease, suggesting genetic factors influence onset of IBD [101; 102; 103]. IBD are also often associated with monogenetic immunodeficiencies and those patients have early onset of the disease [94]. Immunodefficiencies connected with IBD are caused by defects in the genes of innate (*NOD2/CARD11* [104], *CYBB* - chronic granulomatous disease) or adaptive immunity (BTK – agammaglobulinemia) or both (*IKBKG* - *NEMO* deficiency syndrome) [105], indicating multiple connections between immunity and IBD onset. Study in Sweden showed increased incidence of IBD in the second generation of former immigrants [106], connecting environmental factors (nutrition and microbiota) to the development of IBD as well. Even though, no single microbe or microbial milieu has been proven causal, IBD is strongly associated

with intestinal dysbiosis. Its changes have an important role in the onset of IBD in genetically predisposed individuals [107]. Dietary habits affect changes in microbiome as well. Several studies demonstrated association between reduced risk of IBD and diet rich in fruits and vegetables and, conversely, an increased risk of IBD connected to western diet rich in animal fats and refined sugar [108; 109; 110; 111].

Many animal models of spontaneous (*IL-10*$^{-/-}$ [112], *Muc2*$^{-/-}$ [113], *NEMO*$^{-/-}$ [114]) or chemically induced colitis (Trinitrobenzene sulfonic acid (TNBS) [115], Oxazolone [116], Dextran sodium sulphate (DSS) [117]) were developed. Studies of these models have helped identify genes and signalling pathways involved in the onset of IBD. They also have helped to identify resident microbiota, loss of oral tolerance, disruption of epithelial barrier or defects in immune system as factors that can initiate colon inflammation [118].

6.2 Dextran sodium sulphate induced colitis

The dextran sodium sulphate (DSS) is sulphated polysaccharide of various sizes (between 500 kDa to 5 kDa). After administration in drinking water for 5-7 days [119]), DSS begins to dissolve mucin layer in the guts, leaving epithelial layer unprotected. Epithelium is then colonised and damaged by intestinal microbiota. This event alarms the immune system, which triggers inflammatory reaction resulting in colitis. DSS induced colitis can be employed to induce and study both acute and chronic colitis. In the beginning of inflammatory reaction, myeloid immune cells (neutrophils, macrophages, dendritic cells and monocytes) migrate to the colon to defend it against colonizing microorganisms. This immune response further damages the epithelium. As a result, mice suffer from diarrhoea, rectal bleeding, shortening of the colon, dehydration and weight loss [120]. After repeated administration of DSS, inflammation shifts to chronic colitis [121; 122]. Because DSS colitis can develop in SCID mice without adaptive immunity, it was believed that acute DSS colitis is initiated by myeloid lineage cells [123]. However, later studies have shown that lymphoid lineage also plays a key role in the pathology of both, acute and chronic colitis [124; 125; 126; 127; 128].

Characteristic features of DSS colitis are activation, migration and proliferation of all immune cell subtypes [124; 129] and increased expression of pro-inflammatory

cytokines –TNFα, IFNγ, IL1β, IL6, IL12, IL17, IL18 [130]. Studies of DSS colitis showed exacerbated disease in the murine knockout models of the pattern recognition receptors (PRRs) like Dectin-1 [131] and TLR2/4 [132]. In agreement with these results, colitis severity improves after stimulation of these receptors [133; 134]. Surprisingly, stimulation of TLR3 and TLR9 receptors recognizing viral particles in the endosomes also diminished severity of colitis [135; 136]. Stimulation of these receptors leads to an increased inflammatory response, which protects colon by clearance of bacteria, cytokine production and strengthening of epithelium (mucus and tight-junction protein expression [130]). Cytokine-based studies showed heterogeneous group of phenotypes in genetically modified mice. Suspension of pro-inflammatory cytokine production, including IL-1β [137; 138], IL-17 [139], and IFNγ [140] is protective against DSS. However, deletion or inhibition of IL12 [141] or TNFα
[142] exacerbates colitis. Furthermore, mice lacking suppressive cytokines develop spontaneous colitis (IL-10) [112] or exacerbated symptoms (TGFβ) [143]. IL-18 is an intriguing cytokine in the regulation of the colitis. It has a dual role, which depends on the timing of stimulation. Addition of IL-18 before induction of the colitis protects the animals. However, addition of IL-18 during the colitis exacerbates the disease by inhibition of goblet cell maturation. Immature goblet cells then produce lower amount of mucus leaving epithelium unprotected [144; 145].

Although, IBD is extensively studied, pathology and regulation of the IBDs are still not fully understood and require deeper insight to discover other relevant factors and regulations.

7. Aims of the study

The main aim of my projects was to study unknown roles of recently discovered adaptor proteins in the signalling of the immune cells and describe outcomes of their deficiencies.

- The most important aim was to characterize the regulation of signalling by the adaptor protein LST1 in murine model and to describe the phenotype of LST1-deficient mice. The project focused on the study of LST1 expressed in the dendritic cells and macrophages and on the effect of LST1 deficiency on severity of chemically induced colitis (DSS colitis).

- Secondary aims included mainly characterization of adaptor proteins SCIMP, PSTPIP2 and WBP1L in murine models, especially with regard to their role in signal transduction and to the consequences of their deficiencies. The focus was on defining the role of SCIMP in Dectin-1 signalling in dendritic cells and macrophages, on studying the effect of ROS production in the development of Chronic Multifocal Osteomyelitis (CMO) in *Pstpip2*^{cmo} mice, and finally, on characterizing the role of WBP1L in CXCR4 signalling and in the regulation of haematopoiesis.

8. Results and discussion

8.1 Regulation of inflammatory response by transmembrane adaptor protein LST1

Human variant of LST1 protein was studied in our laboratory in the past. We described its structure and motif composition containing glycosylation site, palmitoylation site and ITIM motifs. We also performed a limited functional analysis in human cell lines and described its possible role as inhibitory regulator of myeloid cell signalling [87]. However, in order to expand our knowledge about LST1, we obtained an LST1 knockout murine model from Centre d'Immunophénomique (PHENOMIN-CIPHE, Aix Marseille) for detailed mechanistic study and its phenotype description.

8.1.1 LST1 detected on western blot shows glycosylation

For the detection on the western blot we used our newly generated antibody LST1/06 raised against intracellular part of LST1 of murine origin. LST1/06 antibody detects murine LST1 under non-reducing conditions. On SDS-PAGE it appears as unfocused double band with the mobility corresponding to 27-37 and 42-71 kDa, which is more than predicted based on its amino acid sequence, suggesting that LST1 forms multimers and/or that it undergoes post-translational modifications. We found that glycosylation of the protein is responsible for at least part of this anomaly. After addition of Tunikamycin, which blocks glycosylation process, LST1 was detectable as focused double band with lower molecular weight (29-48 kDa).

8.1.2 LST1 is expressed in myeloid cells and its expression is increased after inflammatory stimulation

Human LST1/A was found in human myeloid cell lines at mRNA and protein level [87]. Its mRNA expression was also found to be increased in IBD patient biopsy samples [89] and in the synovial fluid of arthritis patients [90]. We confirmed similar expression profile in the mouse primary cells where *Lst1* mRNA and protein were

exclusively expressed in the myeloid lineage cells (Dendritic cells, Macrophages, Granulocytes, Monocytes) and not in lymphoid cells (T, B NK cells). Interestingly, its expression in bone marrow derived macrophages and dendritic cells was increased when these cells were stimulated with pro-inflammatory stimuli (LPS, PolyI:C, TNFα, IFNγ) overnight, indicating possible role of LST1 in the regulation of inflammatory signalling.

8.1.3 LST1 influences the homeostasis of leukocyte populations

Confirmation of same LST1 expression profile in murine and human cells led us to examine LST1 expressing myeloid populations in more detail. Therefore, we analysed the abundance of myeloid cell subsets in murine lymphoid organs (spleen, bone marrow, lymph nodes) and in the colon, where LST1 was previously found overexpressed in IBD patient samples. Analysis showed decreased percentages of myeloid immune cells - mainly macrophages, dendritic cells and granulocytes and surprisingly also LST1 non-expressing NK and NKT cells in the spleen, bone marrow and colon. The decrease of *LST1*$^{-/-}$ NK and NKT cells suggest possible external regulation of these cells by LST1 expressing cells, which could be mediated by cytokines like IL-12, IL-15 or IL-18. Nevertheless, expression of these cytokines was not altered in the macrophages and dendritic cells. Cellularity of the analysed organs was not altered either. Therefore, changes in cell population numbers should be equal to the changes in the population percentages. The observed phenotype could be mediated by some generalized defect in cellular migration. However, the test of migratory capacity showed increased migration of *LST1*$^{-/-}$ macrophages towards CXCR4 receptor ligand - CXCL12. These results excluded general defect in cellular migration as a cause of the observed phenotype. In addition, they suggested the role of LST1 in the negative regulation of CXCR4-mediated signalling/migration.

8.1.4 *LST1*$^{-/-}$ mice are more resistant to DSS colitis

LST1 expression increased after cell activation with inflammatory stimuli. Therefore, we analysed mice treated with LPS, which we expected to enhance the differences between wild-type and *LST1*$^{-/-}$ animals. Induction of inflammatory

environment by intraperitoneal injection of LPS resulted in increased levels of B cells and granulocytes in the spleen of both, wild-type and *LST1*$^{-/-}$ mice. However, the differences between the two animal groups remained similar to the steady state after both 4 and 16 hours of treatment. In the plasma of treated mice we observed increase in total TNFα and IL-6 concentrations, but there was no significant difference between the strains. We obtained similar results for LPS-stimulated BMDC and BMDM. LPS treatment increased overall mRNA level of a number of cytokines, including *Tnfa, Il-1b, Il-6, Il-12, Il-15, Il-18, Il-10* and *Tgfb*. However, there were again no significant differences between the strains. NF-κB signalling (IκBα degradation) and expression levels of LST1 binding partners SHP1 and SHP2 also did not show any alterations after LPS stimulation. Thus, we concluded that LPS inflammatory model did not reveal any additional information about regulation of the immune system by LST1.

Because of the increased expression of the LST1 in the histological samples of IBD patients, we decided to test murine model of IBD – dextran sodium sulphate (DSS) colitis. 2.5% DSS was administered in the drinking water for 6 days and then replaced with pure water for another 2 days. DSS colitis is characterized by a breach of the epithelial barrier by microbiota and subsequent colon inflammation. Colon epithelium is firstly damaged by microbiota and then by immune cell inflammatory reaction [120]. Mice weight, stool consistency and occult bleeding were measured. These factors were then integrated into Disease activity index (DAI), describing severity of the colitis. At the end of the experiment, mice were sacrificed and we measured colon length and performed flow cytometry analysis of immune organs (spleen, lymph nodes) and colon.

LST1$^{-/-}$ mice showed significant resistance (lower DAI) within the first 6 days during the onset and progression of the disease. After replacing DSS with water the WT mice began to improve, while *LST1*$^{-/-}$ mice continued in the trend of increasing inflammation. Colon histological analysis showed smaller area of inflamed colonic lesions of the *LST1*$^{-/-}$ mice, even after DSS replacement with water. Since colon epithelium does not express LST1 protein, this effect is likely mediated by immune cells. Surprisingly, all these differences did not affect the body weight loss, which remained comparable between the strains during the entire course of the experiment. It is somewhat unexpected, since it should be strongly affected by the size of colonic

lesions, severity of diarrhoea and dehydration during colitis. Another unexpected result showed that, except for non-significant decrease of granulocyte percentages in the colon, there were no alterations in the myeloid populations during colitis. Even differences observed at the steady state diminished. Among the *LST1*$^{-/-}$ lymphoid populations we observed increased T cell percentages at day 5 and reduced CD4 T cell and NKT cell percentages at day 8. Furthermore, we were able to measure significantly reduced concentrations of TNFα and similar trend also for IL-6 in the *LST1*$^{-/-}$ colon at day 5 of the colitis, but not before and after acute phase of the inflammation.

Myeloid cells and cytokines produced by these cells belong to the first wave of colon immune defence, especially in the DSS colitis. Although we did not find differences in the percentages of *LST1*$^{-/-}$ myeloid leukocytes, we revealed differences in the levels of pro-inflammatory cytokines TNFα and IL-6 during DSS colitis. This observation could be explained by reduced percentages and numbers of myeloid cells in the steady state. They might result in lesser scale of inflammation and cytokine production at the beginning of DSS treatment, causing observed delayed kinetics of colitis. However, pro-inflammatory cytokines expressed by dysregulated T cells could also be a possible explanation and we cannot exclude the impact of LST1 itself on the scale of inflammation.

Up to date, LST1 was described as a possible marker for multiple inflammatory diseases (rheumatoid arthritis, influenza, inflammatory bowel diseases). This is the first evidence showing its direct impact in IBD model DSS colitis and on myeloid cells homeostasis. These two phenomena may be connected and result in the observed phenotype of resistance to the DSS colitis onset.

8.2 The Transmembrane adaptor protein SCIMP facilitates sustained Dectin-1 signalling in dendritic cells

SCIMP is a palmytoilated transmembrane adaptor protein expressed in antigen presenting cells (APC – macrophages, dendritic cells and B cells). It is localized at the plasma membrane in the tetraspanin-enriched microdomains, where other immunologically important molecules reside, including Dectin-1 and MHCIIgp. SCIMP phosphorylation was shown to substantially increase after MHCIIgp crosslinking in B cells. Thus, it was expected to regulate signalling on the APC side of the immunological synapse during antigen presentation to T cells. Its binding partners revealed by biochemical analysis include adaptor proteins SLP-65, SLP-76, and GRB2 and protein tyrosine kinase CSK. The role of CSK, a major negative regulator of Src-family kinases, seems to be mainly in SCIMP auto-regulation, while overall SCIMP function appears to be as a positive regulator of signalling [62]. In our follow-up work presented here, we described the role of SCIMP in the murine dendritic cells and macrophages. We focused mainly on signalling via Dectin-1, a pattern recognition receptor binding β-glucan in fungal cell walls and described the role of SCIMP in signal transduction and cytokine production downstream of Dectin-1.

8.2.1 SCIMP expression and leukocyte development in the *SCIMP*$^{-/-}$ mice

SCIMP expression was detected in mouse APCs – macrophages, dendritic cells and B cells. When we examined effect of SCIMP deletion on these and other murine immune populations, we did not find any alterations in leukocyte development and homeostasis in lymph nodes, spleen and bone marrow of *SCIMP*$^{-/-}$ mice. However, in B cells, the effect of SCIMP on the signalling was previously only demonstrated after MHCIIgp crosslinking [62]. Moreover, in the murine populations of B cells, we found highest expression of SCIMP in B cells located in the germinal centers of lymph nodes, where they encounter antigens and mature into antibody secreting cells. Importantly, this process requires the interaction between MHCIIgp on B cells and TCR on helper T cells. Thus, we tested effect of impaired MHCIIgp signalling during antigen presentation on function of B cells in vivo after immunization with model

antigens and in vitro after MHCIIgp crosslinking. However, we did not find any defects in antibody production or altered signalling by murine *SCIMP*$^{-/-}$ B cells.

Next, we have analysed bone marrow derived dendritic cells (BMDC) produced by culturing bone marrow cells in the presence of GM-CSF. We detected high expression of SCIMP in these cells. In contrast, bone marrow derived macrophages (BMDM) had surprisingly low SCIMP expression, but it was substantially increased after GM-CSF addition. Therefore, we wanted to know whether expression of SCIMP in BMDC is affected by the process of their generation. BMDCs were generated via alternative method using FLT3 ligand instead of GM-CSF. We found strong expression of SCIMP even in FLT3 ligand produced BMDC, however it was still upregulated by GM-CSF addition.

8.2.2 Phosphorylation and signalling of SCIMP upon activation

SCIMP contains several tyrosines in its intracellular part. When these tyrosines are phosphorylated, proteins SLP-65/76, GRB2 and CSK interact with SCIMP and modify or transmit the signal further downstream. Surprisingly, phosphorylation of SCIMP tyrosines was very low in dendritic cells after crosslinking of MHCIIgp. However, treatment with zymosan (β-glucan-rich solid particles made from the cell walls of Saccharomyces cerevisiae) induced very strong SCIMP phosphorylation. Based on the localization of SCIMP to the tetraspanin enriched microdomains and upregulated phosphorylation after zymosan exposure, we suggest that SCIMP is a part of Dectin-1 receptor signalling pathway. However, zymosan is also recognized by TLR2 receptor. To assess the role of TLR2, we obtained *Myd88*$^{-/-}$ mice that cannot signal via TLR2. SCIMP phosphorylation was not inhibited in the *Myd88*$^{-/-}$ BMDC. Therefore, we concluded SCIMP is a part of the Dectin-1, and not TLR2 pathway.

Downstream signalling of Dectin-1 is executed, in part, by MAP kinases ERK and P38. After zymosan stimulation, their phosphorylation was not altered by SCIMP deficiency during short time points after stimulation (up to 30 minutes). However, SCIMP was still phosphorylated in BMDC even 24 hours after zymosan addition. Therefore, we tested MAP kinase signalling during later time points. After 24 hours of zymosan stimulation, phosphorylation of ERK and P38 decreased in *SCIMP*$^{-/-}$BMDCs but was sustained in wild-type BMDC. This reduced activation of MAP

kinases led to lowered concentration of pro-inflammatory cytokines IL-6 and TNFα produced by *SCIMP*$^{-/-}$ BMDCs at late time points after activation. These results are consistent with already published data, showing IL-6 and TNFα regulation by MAP kinases and their importance for anti-fungal immunity [146; 147; 148; 149]. However, events leading to their late production are still not fully understood. Similarly, Dectin-1 signalling pathway regulation by SCIMP is also still not fully revealed, as is the case with other receptors such as multiple TLRs that also use SCIMP as their regulatory adaptor [150; 151].

8.3 Dysregulated NADPH oxidase promotes bone damage in murine model of autoinflammatory osteomyelitis

In the mouse strain *Pstpip2*^{cmo}, missense mutation in the gene coding adaptor protein PSTPIP2 leads to the loss of its expression at the protein level. As a result, these animals develop spontaneous inflammation of the bones, mainly in hind paws and tail, and in the surrounding soft tissue. This phenotype was named as chronic multifocal osteomyelitis (CMO), based on the resemblance with autoinflammatory disease chronic recurrent multifocal osteomyelitis (CRMO) [45]. Up to date, *Pstpip2*^{cmo} murine model serves as one of the best described models for studying autoinflammatory bone diseases.

PSTPIP2 is an adaptor protein associated with cellular membranes via an F-BAR domain. The F-BAR domain is followed by a C-terminal tail containing tyrosine phosphorylation motifs binding negative regulator of signalling SHIP-1[47]. In addition PSTPIP2 binds phosphatases from the PEST family via a sequence encompassing Tryptophan 232 [46] and CSK via unknown binding site [47]. The major cause of CMO disease in *Pstpip2*^{cmo} mice is deregulated activation and release of IL-1β cytokine by neutrophil granulocytes. It is dependent on inflammasome and Caspase-1 and Caspase-8 activation and to some extent also on neutrophil proteases [56; 59; 60; 61]. Previously, our laboratory has shown that the loss of PSTPIP2 increases signalling of ERK, AKT and P38, which are known to activate NLRP3 inflammasome [50] and upregulate IL-1β production [47]. Moreover, increased production of reactive oxygen species (ROS) by mitochondria and NADPH oxidase also leads to activation of NLRP3 inflammasome. In the study presented here, we have discovered additional mechanism of the CMO disease progression, which includes dysregulated NADPH oxidase activation and increased ROS production.

8.3.1 IL-1β and ROS production is dysregulated in the *Pstpip2*^{cmo} granulocytes

Since increased ROS generation is one of the factors contributing to activation of inflammasome and IL-1β production, we tested cells from *Pstpip2*^{cmo} bone marrow, which contains a major neutrophil deposit in the organism, for the ROS production. *Pstpip2*^{cmo} bone marrow cell stimulation by an inflammasome activator silica led to

much higher ROS production when compared to wild-type mice. ROS generation was similarly increased, when measured in purified *Pstpip2*^{cmo} neutrophils. Interestingly, neutrophils were producing significantly more ROS after multiple different stimuli, including LPS, TNFα, fMLP, PMA, and E. coli bacteria. Strikingly, they were producing increased amount of ROS even in the basal steady state. Potentiation of ROS production is one of the hallmarks of neutrophil priming [152]. Therefore, we suspected that *Pstpip2*^{cmo} granulocytes could be spontaneously primed. However, we did not observe any changes in several markers of neutrophil priming, including CD11b expression, actin reorganization and transcription of IL-1β coding gene. We were also interested, whether abrogation of IL-1β signalling in vivo is going to inhibit ROS production. To analyse this, we crossed the *Pstpip2*^{cmo} mice with the *Myd88*$^{-/-}$strain, to abrogate IL-1β signalling, since MYD88 is key adaptor essential for signaling by IL-1 receptor [153; 154]. As expected, double-deficient mice did not develop CMO disease due to the block in IL-1 receptor signaling and we did not observe any inflammation and bone damage. However, we still observed elevated ROS production after activation of the granulocytes by silica, demonstrating that increased ROS production is an IL-1β independent effect.

Phosphorylation of NADPH oxidase, including its p47phox subunit, is a key event leading to its activation [155; 156]. Importantly, *Pstpip2*^{cmo} granulocytes showed increased phosphorylation of p47phox, suggesting that increased NADPH oxidase phosphorylation in *Pstpip2*^{cmo} mice is responsible for increased ROS production. Protein kinases C (PKC) and also MAP kinases were previously shown to phosphorylate NADPH oxidase. We have also described increased ERK phosphorylation in *Pstpip2*^{cmo} granulocytes [47]. However, inhibition of ERK pathway did not have any effect on the intensity of ROS production. On the other hand, inhibition of protein kinase C almost completely inhibited phosphorylation of p47phox in the *Pstpip2*^{cmo} mice. Thus, we concluded that dysregulated phosphorylation of NADPH oxidase by PKC is responsible for its increased activity. However, the exact mechanism of why is this phosphorylation elevated is still unclear.

In order to elucidate the effect of ROS on CMO disease phenotype, detection of ROS-elicited luminescence was followed *in vivo* to observe production of ROS in living animals. Strikingly, we detected deregulated ROS production already in the freshly weaned mice *Pstpip2*^{cmo} mice, before the development CMO symptoms,

which typically begin to manifest at 7-8 weeks of age. This observation shows the onset of spontaneous ROS production prior to the onset of CMO symptoms. *Gp91phox*$^{-/-}$ neutrophils with NADPH oxidase deficiency are unable to produce ROS after stimulation. Nevertheless, double knockout *Pstpip2*^{cmo} *x gp91phox*$^{-/-}$ strain was still able to initiate CMO disease with slightly delayed kinetics even without functional NADPH oxidase. However, these mice did not show almost any signs of bone damage, only soft tissue inflammation. Therefore, ROS is not responsible for or able to initiate CMO itself, but it is necessary for the bone destruction accompanying this disease.

Our data suggest that PSTPIP2 is a regulator of NADPH oxidase. Loss of PSTPIP2 leads to elevated ROS production, which exacerbate bone inflammation and inflammatory bone damage during CMO disease. CMO osteoclastogenesis has been shown to be upregulated together with osteoclasts activity [157] and osteoclasts activity is known to be enhanced by ROS [158]. Thus, the effect of increased ROS in *Pstpip2*^{cmo} mouse is likely to stimulate osteoclasts, which leads to the subsequent bone destruction.

8.4 Transmembrane adaptor protein WBP1L regulates CXCR4 signalling and murine haematopoiesis

WW domain binding protein 1-like (WBP1L) was a poorly studied adaptor protein without known functions and binding partners. The bioinformatics analysis predicted WW domain binding motifs (L-P-X-Y or P-P-X-Y) that could potentially interact with WW domain containing proteins, such as NEDD4-family ubiquitin ligases [75]. In the study, we have confirmed this prediction and co-immunoprecipitated ubiquitin ligases WWP1, WWP2, ITCH and NEDD4 together with WBP1L. We have also confirmed that WW binding motifs in the intracellular part of the protein are interaction sites for these ubiquitin ligases. Further examination of the ligases auto-ubiquitination, which is the sign of their activation and regulation, revealed increased ubiquitination in the presence of WBP1L. Overall, the data suggested possible inhibitory role of WBP1L mediated by its interaction with NEDD4-family ubiquitin ligases.

WBP1L expression in the murine cells was evaluated by Geneinvestigator tool and by immunoblotting, which both revealed its broad expression in hematopoietic cells – T cells, B cells, neutrophils, monocytes, BMDC, BMDM and in hematopoietic progenitors. In addition, WBP1L is overexpressed in B cell progenitor acute lymphoblastic leukaemia (BCP-ALL) carrying *ETV6-RUNX1* fusion gene [69]. In agreement with these data, increased WBP1L expression was found in REH cells derived from *ETV6-RUNX1*$^{+}$ BCP-ALL. One of the best studied targets of NEDD4 ubiquitin ligases in the hematopoietic system is chemokine receptor CXCR4. It is a key receptor critical for proper hematopoiesis, retention of the progenitors in their niches in the bone marrow and the maintenance of hematopoietic stem cells. CXCR4 receptor co-transfection with WBP1L into HEK293 cells led to increased ubiquitination of the CXCR4. The ubiquitination was accompanied with expected reduction of the receptor levels. In agreement, shRNA downregulation of WBP1L in cells with its high expression (immortalised progenitors and REH cells) results into positive effect – increased ERK and AKT phosphorylation after stimulation with CXCR4 ligand CXCL12.

8.4.1 WBP1L affects development and homeostasis of the progenitor cells

In *WBP1L*$^{-/-}$ mice, we observed reduced numbers of Lin^{-}SCA1^{+}KIT^{+} (LSK) cells representing hematopoietic stem and early progenitor cells and increased B cell numbers in the bone marrow, as well as and increased percentages of marginal zone B cells and dendritic cells in the spleen. To elucidate function of LSK cells, we performed competitive transplantation of bone marrow cells. For that purpose we used congenic markers Ly5.1 and Ly5.2, which are alleles of *Cd45* protein recognizable via different antibodies. This approach allows to detect origin and genetic background after transplantation of donor cells to recipient animal with different congenic marker [159]. Therefore, we transplanted mixture of Ly5.2 *WBP1L*$^{-/-}$ and Ly5.1 WT cells into lethally irradiated Ly5.1 recipient animals and observed threefold increase of Ly5.2 *WBP1L*$^{-/-}$ cells engraftment. The more efficient engraftment could be potentially explained by hyperactivity of CXCR4 signalling in the primary bone marrow cells. However, we did not observe any difference of CXCR4 signalling in bone marrow cells. Adaptor proteins often have redundant functions and cells are able to compensate for their loss. Thus, we produced *WBP1L*$^{fl/fl}$*-CreERT* murine model of inducible knockout. Indeed, after acute deletion of WBP1L we observed increased CXCR4 signalling in several major bone marrow cell subsets (T cells, monocytes and neutrophils). In addition this deletion in KIT^{+} progenitor cells resulted in increased levels of CXCR4 and consequently, also increased CXCR4-induced ERK phosphorylation. These results correlated with increased levels of BM homing of the*WBP1L*$^{fl/fl}$*-CreERT* KIT+ progenitor cells with acutely deleted WBP1L.

Altogether the results show that WBP1L is a negative regulator of hematopoietic stem and progenitor cells. We also suggest that CXCR4 is a major actor of the observed phenotype. However, the regulation of CXCR4 by WBP1L should be further studied to discover exact effects and additional interacting molecules involved in the regulation of CXCR4 signalling. Also, we cannot exclude the broad influence of dysregulated NEDD4 family ubitquitin ligases and their other targets on the observed phenotype, which should be further addressed in the future.

9. Conclusions

The projects described in this thesis were focused on the adaptor protein functions in leukocytes. In order to study their function and the role in diseases at the organismal level, all studies were performed on the murine knockout models.

My first author publication studied transmembrane adaptor protein LST1. We confirmed expression pattern of the murine LST1 in the myeloid lineage cells. Moreover, we found that its expression was upregulated after pro-inflammatory stimuli. We discovered alterations in the *LST1*$^{-/-}$ leukocyte subset abundance, specifically a decrease in several myeloid cell subsets, as well as reduction of NK and NKT cell percentages in the bone marrow, spleen and colon. These changes were not accompanied by changes in cytokine production in LST1$^{-/-}$ cells. Since LST1 was found overexpressed in the patient samples suffering from inflammatory bowel diseases, we tested its effects on the severity of dextran sodium sulphate-induced colitis. This model revealed that *LST1*$^{-/-}$ mice are more protected during the onset of the DSS colitis. However, severity of the disease matched the WT animals at later time points. Thus, we concluded LST1 adaptor protein is not only an expression marker of IBD, but also plays an active part in the development and kinetics of the disease.

Second project was focused on SCIMP transmembrane adaptor of antigen presenting cells. In this study, we found SCIMP is contributing to signalling downstream of pattern recognition receptor (PRR) Dectin-1, which is important in anti-fungal immunity. Subsequently, we described SCIMP effects on ERK phosphorylation and pro-inflammatory cytokine production in the prolonged signalling after Dectin-1 stimulation by Zymosan.

In the project focused on membrane associated adaptor protein PSTPIP2, we expanded our knowledge about its signalling pathways responsible for disease Chronic Multifocal Osteomyelitis (CMO). We found NADPH oxidase dysregulation and subsequent increased ROS production is mainly responsible for bone destruction in the *Pstpip2*^{cmo} mouse model.

Last project studied transmembrane adaptor WBP1L. We discovered its interactions with NEDD4 family ubiquitin ligases ITCH, NEDD4, WWP1 and WWP2. We found that WBP1L promotes activation of these ubiquitin ligases and, as

a result, inhibition of their targets. One such target is the chemokine receptor CXCR4, which regulates hematopoietic progenitor cells homing and maintenance. The loss of WBP1L led to increased signalling downstream of CXCR4. In addition, *WBP1L*$^{-/-}$ bone marrow showed around 3-fold more efficient engraftment in the competitively transplanted mice.

10. Contributions

1. Regulation of inflammatory response by transmembrane adaptor protein LST1

This is my first author publications where I conducted majority of the experiments. I also substantially contributed to writing of the publication.

2. The Transmembrane adaptor protein SCIMP facilitates sustained dectin-1 signalling in dendritic cells

In this article I contributed to the animal work. In addition I was maintaining primary cells cultures. I also performed ERK signalling assays and immunoprecipitation assays.

3. Dysregulated NADPH oxidase promotes bone damage in murine model of autoinflammatory osteomyelitis

For the study of PSTPIP2 adaptor protein I contributed to the preparation and isolation of primary granulocytes. I also performed qPCR experiments and measurements of ROS production in the cells maintained in suspensions.

4. Transmembrane adaptor protein WBP1L regulates CXCR4 signalling and murine haematopoiesis

In this project studying protein WBP1L (OPAL1) I contributed to the animal work, primary cell preparation and flow cytometry experiments.

Prohlášení o podílu studenta na výsledcích

Prohlašuji, že se Matej Fabišik podílel na publikacích uvedených v této dizertační práci v rozsahu uvedeném v kapitole Contribution.

V Praze dne 29.6. 2021 Mgr. Tomáš Brdička, Ph.D.

11. References

[1] A. Nair, P. Chauhan, B. Saha, and K.F. Kubatzky, Conceptual Evolution of Cell Signaling. Int J Mol Sci 20 (2019).

[2] J.D. Jordan, and R. Iyengar, Modes of interactions between signaling pathways. Biochem Pharmacol 55 (1998) 1347-52.

[3] T. Kawasaki, and T. Kawai, Toll-like receptor signaling pathways. Front Immunol 5 (2014) 461.

[4] P. Matzinger, The danger model: a renewed sense of self. Science 296 (2002) 301-5.

[5] O. Bereshchenko, S. Bruscoli, and C. Riccardi, Glucocorticoids, Sex Hormones, and Immunity. Front Immunol 9 (2018) 1332.

[6] S.R. Cechin, and P. Buchwald, Effects of representative glucocorticoids on TNFalpha- and CD40L-induced NF-kappaB activation in sensor cells. Steroids 85 (2014) 36-43.

[7] T. Van Bogaert, K. De Bosscher, and C. Libert, Crosstalk between TNF and glucocorticoid receptor signaling pathways. Cytokine Growth Factor Rev 21 (2010) 275-86.

[8] D.W. Cain, and J.A. Cidlowski, Immune regulation by glucocorticoids. Nat Rev Immunol 17 (2017) 233-247.

[9] E. Beaulieu, and E.F. Morand, Role of GILZ in immune regulation, glucocorticoid actions and rheumatoid arthritis. Nat Rev Rheumatol 7 (2011) 340-8.

[10] R.L. Robker, and J.S. Richards, Hormone-induced proliferation and differentiation of granulosa cells: a coordinated balance of the cell cycle regulators cyclin D2 and p27Kip1. Mol Endocrinol 12 (1998) 924-40.

[11] C.E. Hughes, and R.J.B. Nibbs, A guide to chemokines and their receptors. FEBS J 285 (2018) 2944-2971.

[12] P. Lopez-Cotarelo, C. Gomez-Moreira, O. Criado-Garcia, L. Sanchez, and J.L. Rodriguez-Fernandez, Beyond Chemoattraction: Multifunctionality of Chemokine Receptors in Leukocytes. Trends Immunol 38 (2017) 927-941.

[13] F.O. Martinez, and S. Gordon, The M1 and M2 paradigm of macrophage activation: time for reassessment. F1000Prime Rep 6 (2014) 13.

[14] M.E. Martinez-Sanchez, L. Huerta, E.R. Alvarez-Buylla, and C. Villarreal Lujan, Role of Cytokine Combinations on CD4+ T Cell Differentiation, Partial Polarization, and Plasticity: Continuous Network Modeling Approach. Front Physiol 9 (2018) 877.

[15] S. Santagata, C. Ierano, A.M. Trotta, A. Capiluongo, F. Auletta, G. Guardascione, and S. Scala, CXCR4 and CXCR7 Signaling Pathways: A Focus on the Cross-Talk Between Cancer Cells and Tumor Microenvironment. Front Oncol 11 (2021) 591386.

[16] S. Feske, H. Wulff, and E.Y. Skolnik, Ion channels in innate and adaptive immunity. Annu Rev Immunol 33 (2015) 291-353.

[17] Y.J. Park, S.A. Yoo, M. Kim, and W.U. Kim, The Role of Calcium-Calcineurin-NFAT Signaling Pathway in Health and Autoimmune Diseases. Front Immunol 11 (2020) 195.

[18] L. Chen, and D.B. Flies, Molecular mechanisms of T cell co-stimulation and co-inhibition. Nat Rev Immunol 13 (2013) 227-42.

[19] O. Stepanek, P. Draber, and V. Horejsi, Palmitoylated transmembrane adaptor proteins in leukocyte signaling. Cell Signal 26 (2014) 895-902.

[20] A. Leo, J. Wienands, G. Baier, V. Horejsi, and B. Schraven, Adapters in lymphocyte signaling. J Clin Invest 109 (2002) 301-9.

[21] J.D. Nanson, B. Kobe, and T. Ve, Death, TIR, and RHIM: Self-assembling domains involved in innate immunity and cell-death signaling. J Leukoc Biol 105 (2019) 363-375.
[22] M. Yamamoto, K. Takeda, and S. Akira, TIR domain-containing adaptors define the specificity of TLR signaling. Mol Immunol 40 (2004) 861-8.
[23] M. Akutsu, I. Dikic, and A. Bremm, Ubiquitin chain diversity at a glance. J Cell Sci 129 (2016) 875-80.
[24] J. Fritsch, M. Stephan, V. Tchikov, S. Winoto-Morbach, S. Gubkina, D. Kabelitz, and S. Schutze, Cell fate decisions regulated by K63 ubiquitination of tumor necrosis factor receptor 1. Mol Cell Biol 34 (2014) 3214-28.
[25] N. Tarantino, J.Y. Tinevez, E.F. Crowell, B. Boisson, R. Henriques, M. Mhlanga, F. Agou, A. Israel, and E. Laplantine, TNF and IL-1 exhibit distinct ubiquitin requirements for inducing NEMO-IKK supramolecular structures. J Cell Biol 204 (2014) 231-45.
[26] K. Kliza, and K. Husnjak, Resolving the Complexity of Ubiquitin Networks. Front Mol Biosci 7 (2020) 21.
[27] C.K. Ea, L. Deng, Z.P. Xia, G. Pineda, and Z.J. Chen, Activation of IKK by TNFalpha requires site-specific ubiquitination of RIP1 and polyubiquitin binding by NEMO. Mol Cell 22 (2006) 245-57.
[28] E. Varfolomeev, and D. Vucic, Intracellular regulation of TNF activity in health and disease. Cytokine 101 (2018) 26-32.
[29] D. Oikawa, Y. Sato, H. Ito, and F. Tokunaga, Linear Ubiquitin Code: Its Writer, Erasers, Decoders, Inhibitors, and Implications in Disorders. Int J Mol Sci 21 (2020).
[30] Y.K. Kim, J.S. Shin, and M.H. Nahm, NOD-Like Receptors in Infection, Immunity, and Diseases. Yonsei Med J 57 (2016) 5-14.
[31] J.H. Esensten, Y.A. Helou, G. Chopra, A. Weiss, and J.A. Bluestone, CD28 Costimulation: From Mechanism to Therapy. Immunity 44 (2016) 973-88.
[32] L.H. Boise, A.J. Minn, P.J. Noel, C.H. June, M.A. Accavitti, T. Lindsten, and C.B. Thompson, CD28 costimulation can promote T cell survival by enhancing the expression of Bcl-xL. Immunity. 1995. 3: 87-98. J Immunol 185 (2010) 3788-99.
[33] T.H. Watts, Staying alive: T cell costimulation, CD28, and Bcl-xL. J Immunol 185 (2010) 3785-7.
[34] L.H. Boise, A.J. Minn, P.J. Noel, C.H. June, M.A. Accavitti, T. Lindsten, and C.B. Thompson, CD28 costimulation can promote T cell survival by enhancing the expression of Bcl-XL. Immunity 3 (1995) 87-98.
[35] D. Lake, S.A. Correa, and J. Muller, Negative feedback regulation of the ERK1/2 MAPK pathway. Cell Mol Life Sci 73 (2016) 4397-4413.
[36] A.A. Ajibade, H.Y. Wang, and R.F. Wang, Cell type-specific function of TAK1 in innate immune signaling. Trends Immunol 34 (2013) 307-16.
[37] A.A. Ajibade, Q. Wang, J. Cui, J. Zou, X. Xia, M. Wang, Y. Tong, W. Hui, D. Liu, B. Su, H.Y. Wang, and R.F. Wang, TAK1 negatively regulates NF-kappaB and p38 MAP kinase activation in Gr-1+CD11b+ neutrophils. Immunity 36 (2012) 43-54.
[38] M. Chang, W. Jin, and S.C. Sun, Peli1 facilitates TRIF-dependent Toll-like receptor signaling and proinflammatory cytokine production. Nat Immunol 10 (2009) 1089-95.

[39] T. Yamamoto, N. Tsutsumi, H. Tochio, H. Ohnishi, K. Kubota, Z. Kato, M. Shirakawa, and N. Kondo, Functional assessment of the mutational effects of human IRAK4 and MyD88 genes. Mol Immunol 58 (2014) 66-76.
[40] C. Picard, A. Puel, M. Bonnet, C.L. Ku, J. Bustamante, K. Yang, C. Soudais, S. Dupuis, J. Feinberg, C. Fieschi, C. Elbim, R. Hitchcock, D. Lammas, G. Davies, A. Al-Ghonaium, H. Al-Rayes, S. Al-Jumaah, S. Al-Hajjar, I.Z. Al-Mohsen, H.H. Frayha, R. Rucker, T.R. Hawn, A. Aderem, H. Tufenkeji, S. Haraguchi, N.K. Day, R.A. Good, M.A. Gougerot-Pocidalo, A. Ozinsky, and J.L. Casanova, Pyogenic bacterial infections in humans with IRAK-4 deficiency. Science 299 (2003) 2076-9.
[41] D.D. Billadeau, and P.J. Leibson, ITAMs versus ITIMs: striking a balance during cell regulation. J Clin Invest 109 (2002) 161-8.
[42] A. Csiszar, Structural and functional diversity of adaptor proteins involved in tyrosine kinase signalling. Bioessays 28 (2006) 465-79.
[43] M. Togni, J. Lindquist, A. Gerber, U. Kolsch, A. Hamm-Baarke, S. Kliche, and B. Schraven, The role of adaptor proteins in lymphocyte activation. Mol Immunol 41 (2004) 615-30.
[44] T. Chum, D. Glatzova, Z. Kvicalova, J. Malinsky, T. Brdicka, and M. Cebecauer, The role of palmitoylation and transmembrane domain in sorting of transmembrane adaptor proteins. J Cell Sci 129 (2016) 95-107.
[45] V. Chitu, P.J. Ferguson, R. de Bruijn, A.J. Schlueter, L.A. Ochoa, T.J. Waldschmidt, Y.G. Yeung, and E.R. Stanley, Primed innate immunity leads to autoinflammatory disease in PSTPIP2-deficient cmo mice. Blood 114 (2009) 2497-2505.
[46] Y. Wu, D. Dowbenko, and L.K. Lasky, PSTPIP 2, a second tyrosine phosphorylated, cytoskeletal-associated protein that binds a PEST-type protein-tyrosine phosphatase. J Biol Chem 273 (1998) 30487-30496.
[47] A. Drobek, J. Kralova, T. Skopcova, M. Kucova, P. Novak, P. Angelisova, P. Otahal, M. Alberich-Jorda, and T. Brdicka, PSTPIP2, a Protein Associated with Autoinflammatory Disease, Interacts with Inhibitory Enzymes SHIP1 and Csk. J Immunol 195 (2015) 3416-3426.
[48] A. Veillette, I. Rhee, C.M. Souza, and D. Davidson, PEST family phosphatases in immunity, autoimmunity, and autoinflammatory disorders. Immunol Rev 228 (2009) 312-324.
[49] M. Sztacho, S. Segeletz, M.A. Sanchez-Fernandez, C. Czupalla, C. Niehage, and B. Hoflack, BAR Proteins PSTPIP1/2 Regulate Podosome Dynamics and the Resorption Activity of Osteoclasts. Plos One 11 (2016).
[50] M.G. Ghonime, O.R. Shamaa, S. Das, R.A. Eldomany, T. Fernandes-Alnemri, E.S. Alnemri, M.A. Gavrilin, and M.D. Wewers, Inflammasome priming by lipopolysaccharide is dependent upon ERK signaling and proteasome function. J Immunol 192 (2014) 3881-8.
[51] P.J. Ferguson, M.A. Lokuta, H.I. El-Shanti, L. Muhle, X. Bing, and A. Huttenlocher, Neutrophil dysfunction in a family with a SAPHO syndrome-like phenotype. Arthritis Rheum 58 (2008) 3264-9.
[52] M. Hurtado-Nedelec, S. Chollet-Martin, D. Chapeton, J.P. Hugot, G. Hayem, and B. Gerard, Genetic susceptibility factors in a cohort of 38 patients with SAPHO syndrome: a study of PSTPIP2, NOD2, and LPIN2 genes. J Rheumatol 37 (2010) 401-9.
[53] A. Jansson, E.D. Renner, J. Ramser, A. Mayer, M. Haban, A. Meindl, V. Grote, J. Diebold, V. Jansson, K. Schneider, and B.H. Belohradsky, Classification of non-

bacterial osteitis: retrospective study of clinical, immunological and genetic aspects in 89 patients. Rheumatology (Oxford) 46 (2007) 154-60.
[54] P.J. Ferguson, X.Y. Bing, M.A. Vasef, L.A. Ochoa, A. Mahgoub, T.J. Waldschmidt, L.T. Tygrett, A.J. Schlueter, and H. El-Shanti, A missense mutation in pstpip2 is associated with the murine autoinflammatory disorder chronic multifocal osteomyelitis. Bone 38 (2006) 41-47.
[55] J. Grosse, V. Chitu, A. Marquardt, P. Hanke, C. Schmittwolf, L. Zeitlmann, P. Schropp, B. Barth, P. Yu, R. Paffenholz, G. Stumm, M. Nehls, and E.R. Stanley, Mutation of mouse Mayp/Pstpip2 causes a macrophage autoinflammatory disease. Blood 107 (2006) 3350-3358.
[56] S.L. Cassel, J.R. Janczy, X.Y. Bing, S.P. Wilson, A.K. Olivier, J.E. Otero, Y. Iwakura, D.M. Shayakhmetov, A.G. Bassuk, Y. Abu-Amer, K.A. Brogden, T.L. Burns, F.S. Sutterwala, and P.J. Ferguson, Inflammasome-independent IL-1 beta mediates autoinflammatory disease in Pstpip2-deficient mice. P Natl Acad Sci USA 111 (2014) 1072-1077.
[57] J.R. Lukens, P. Gurung, P. Vogel, G.R. Johnson, R.A. Carter, D.J. McGoldrick, S.R. Bandi, C.R. Calabrese, L. Vande Walle, M. Lamkanfi, and T.D. Kanneganti, Dietary modulation of the microbiome affects autoinflammatory disease. Nature 516 (2014) 246-+.
[58] J.R. Lukens, J.M. Gross, C. Calabrese, Y. Iwakura, M. Lamkanfi, P. Vogel, and T.D. Kanneganti, Critical role for inflammasome-independent IL-1 beta production in osteomyelitis. P Natl Acad Sci USA 111 (2014) 1066-1071.
[59] P. Gurung, and T.D. Kanneganti, Novel roles for caspase-8 in IL-1beta and inflammasome regulation. Am J Pathol 185 (2015) 17-25.
[60] P. Gurung, A. Burton, and T.D. Kanneganti, NLRP3 inflammasome plays a redundant role with caspase 8 to promote IL-1beta-mediated osteomyelitis. Proc Natl Acad Sci U S A 113 (2016) 4452-7.
[61] P.J. Ferguson, and R.M. Laxer, New discoveries in CRMO: IL-1beta, the neutrophil, and the microbiome implicated in disease pathogenesis in Pstpip2-deficient mice. Semin Immunopathol 37 (2015) 407-12.
[62] P. Draber, I. Vonkova, O. Stepanek, M. Hrdinka, M. Kucova, T. Skopcova, P. Otahal, P. Angelisova, V. Horejsi, M. Yeung, A. Weiss, and T. Brdicka, SCIMP, a transmembrane adaptor protein involved in major histocompatibility complex class II signaling. Mol Cell Biol 31 (2011) 4550-62.
[63] S. Saijo, N. Fujikado, T. Furuta, S.H. Chung, H. Kotaki, K. Seki, K. Sudo, S. Akira, Y. Adachi, N. Ohno, T. Kinjo, K. Nakamura, K. Kawakami, and Y. Iwakura, Dectin-1 is required for host defense against Pneumocystis carinii but not against Candida albicans. Nat Immunol 8 (2007) 39-46.
[64] M.J. Marakalala, S. Vautier, J. Potrykus, L.A. Walker, K.M. Shepardson, A. Hopke, H.M. Mora-Montes, A. Kerrigan, M.G. Netea, G.I. Murray, D.M. MacCallum, R. Wheeler, C.A. Munro, N.A.R. Gow, R.A. Cramer, A.J.P. Brown, and G.D. Brown, Differential Adaptation of Candida albicans In Vivo Modulates Immune Recognition by Dectin-1. Plos Pathog 9 (2013).
[65] G.D. Brown, J. Herre, D.L. Williams, J.A. Willment, A.S.J. Marshall, and S. Gordon, Dectin-1 mediates the biological effects of beta-glucans. J Exp Med 197 (2003) 1119-1124.
[66] M. Rahabi, G. Jacquemin, M. Prat, E. Meunier, M. AlaEddine, B. Bertrand, L. Lefevre, K. Benmoussa, P. Batigne, A. Aubouy, J. Auwerx, S. Kirzin, D. Bonnet, M. Danjoux, B. Pipy, L. Alric, H. Authier, and A. Coste, Divergent Roles for Macrophage C-type Lectin Receptors, Dectin-1 and Mannose

Receptors, in the Intestinal Inflammatory Response. Cell Rep 30 (2020) 4386-4398 e5.
[67] M.N. Erkelens, G. Goverse, T. Konijn, R. Molenaar, M.R. Beijer, J. Van den Bossche, K.E. de Goede, S.G.S. Verberk, W.J. de Jonge, J.M.M. den Haan, and R.E. Mebius, Intestinal Macrophages Balance Inflammatory Expression Profiles via Vitamin A and Dectin-1-Mediated Signaling. Front Immunol 11 (2020) 551.
[68] B. Neveu, J.F. Spinella, C. Richer, K. Lagace, P. Cassart, M. Lajoie, S. Jananji, S. Drouin, J. Healy, G.R. Hickson, and D. Sinnett, CLIC5: a novel ETV6 target gene in childhood acute lymphoblastic leukemia. Haematologica 101 (2016) 1534-1543.
[69] V. Kanderova, D. Kuzilkova, J. Stuchly, M. Vaskova, T. Brdicka, K. Fiser, O. Hrusak, F. Lund-Johansen, and T. Kalina, High-resolution Antibody Array Analysis of Childhood Acute Leukemia Cells. Mol Cell Proteomics 15 (2016) 1246-61.
[70] A. Holleman, M.L. den Boer, M.H. Cheok, K.M. Kazemier, D. Pei, J.R. Downing, G.E. Janka-Schaub, U. Gobel, U.B. Graubner, C.H. Pui, W.E. Evans, and R. Pieters, Expression of the outcome predictor in acute leukemia 1 (OPAL1) gene is not an independent prognostic factor in patients treated according to COALL or St Jude protocols. Blood 108 (2006) 1984-90.
[71] C. Li, Y.K. Kim, R. Dorajoo, H. Li, I.T. Lee, C.Y. Cheng, M. He, W.H. Sheu, X. Guo, S.K. Ganesh, J. He, J. Lee, J. Liu, Y. Hu, D.C. Rao, F.J. Tsai, J.Y. Koh, H. Hu, K.W. Liang, W. Palmas, J.E. Hixson, S. Han, Y.Y. Teo, Y. Wang, J. Chen, C.H. Lu, Y. Zheng, L. Gui, W.J. Lee, J. Yao, D. Gu, B.G. Han, X. Sim, L. Sun, J. Zhao, C.H. Chen, N. Kumari, Y. He, K.D. Taylor, L.J. Raffel, S. Moon, J.I. Rotter, Y.D. Ida Chen, T. Wu, T.Y. Wong, J.Y. Wu, X. Lin, E.S. Tai, B.J. Kim, and T.N. Kelly, Genome-Wide Association Study Meta-Analysis of Long-Term Average Blood Pressure in East Asians. Circ Cardiovasc Genet 10 (2017) e001527.
[72] A.R. Docherty, T.B. Bigdeli, A.C. Edwards, S. Bacanu, D. Lee, M.C. Neale, B.K. Wormley, D. Walsh, F.A. O'Neill, B.P. Riley, K.S. Kendler, and A.H. Fanous, Genome-wide gene pathway analysis of psychotic illness symptom dimensions based on a new schizophrenia-specific model of the OPCRIT. Schizophr Res 164 (2015) 181-6.
[73] H. Zhang, X. Mo, Z. Zhou, Z. Zhu, X. HuangFu, Z. Guo, and Y. Zhang, Detection of Putative Functional Single Nucleotide Polymorphisms in Blood Pressure Loci and Validation of Association Between Single Nucleotide Polymorphism in WBP1L and Hypertension in the Chinese Han Population. J Cardiovasc Pharmacol 73 (2019) 48-55.
[74] E. Morales, N. Vilahur, L.A. Salas, V. Motta, M.F. Fernandez, M. Murcia, S. Llop, A. Tardon, G. Fernandez-Tardon, L. Santa-Marina, M. Gallastegui, V. Bollati, X. Estivill, N. Olea, J. Sunyer, and M. Bustamante, Genome-wide DNA methylation study in human placenta identifies novel loci associated with maternal smoking during pregnancy. Int J Epidemiol 45 (2016) 1644-1655.
[75] J. Pei, and N.V. Grishin, Unexpected diversity in Shisa-like proteins suggests the importance of their roles as transmembrane adaptors. Cell Signal 24 (2012) 758-69.
[76] I. Holzinger, A. de Baey, G. Messer, G. Kick, H. Zwierzina, and E.H. Weiss, Cloning and genomic characterization of LST1: a new gene in the human TNF region. Immunogenetics 42 (1995) 315-22.

[77] A. de Baey, I. Holzinger, S. Scholz, E. Keller, E.H. Weiss, and E. Albert, Pvu II polymorphism in the primate homologue of the mouse B144 (LST-1). A novel marker gene within the tumor necrosis factor region. Hum Immunol 42 (1995) 9-14.
[78] S.R. Nalabolu, H. Shukla, G. Nallur, S. Parimoo, and S.M. Weissman, Genes in a 220-kb region spanning the TNF cluster in human MHC. Genomics 31 (1996) 215-22.
[79] Complete sequence and gene map of a human major histocompatibility complex. The MHC sequencing consortium. Nature 401 (1999) 921-3.
[80] U.H. Weidle, I. Rohwedder, F. Birzele, E.H. Weiss, and C. Schiller, LST1: A multifunctional gene encoded in the MHC class III region. Immunobiology 223 (2018) 699-708.
[81] M.J. Neville, and R.D. Campbell, Alternative splicing of the LST-1 gene located in the Major Histocompatibility Complex on human chromosome 6. DNA Seq 8 (1997) 155-60.
[82] I. Rollinger-Holzinger, B. Eibl, M. Pauly, U. Griesser, F. Hentges, B. Auer, G. Pall, P. Schratzberger, D. Niederwieser, E.H. Weiss, and H. Zwierzina, LST1: a gene with extensive alternative splicing and immunomodulatory function. J Immunol 164 (2000) 3169-76.
[83] A. de Baey, B. Fellerhoff, S. Maier, S. Martinozzi, U. Weidle, and E.H. Weiss, Complex expression pattern of the TNF region gene LST1 through differential regulation, initiation, and alternative splicing. Genomics 45 (1997) 591-600.
[84] A. D'Aloia, G. Berruti, B. Costa, C. Schiller, R. Ambrosini, V. Pastori, E. Martegani, and M. Ceriani, RalGPS2 is involved in tunneling nanotubes formation in 5637 bladder cancer cells. Exp Cell Res 362 (2018) 349-361.
[85] C. Schiller, K.N. Diakopoulos, I. Rohwedder, E. Kremmer, C. von Toerne, M. Ueffing, U.H. Weidle, H. Ohno, and E.H. Weiss, LST1 promotes the assembly of a molecular machinery responsible for tunneling nanotube formation. J Cell Sci 126 (2013) 767-77.
[86] C. Schiller, J.E. Huber, K.N. Diakopoulos, and E.H. Weiss, Tunneling nanotubes enable intercellular transfer of MHC class I molecules. Hum Immunol 74 (2013) 412-6.
[87] P. Draber, O. Stepanek, M. Hrdinka, A. Drobek, L. Chmatal, L. Mala, T. Ormsby, P. Angelisova, V. Horejsi, and T. Brdicka, LST1/A is a myeloid leukocyte-specific transmembrane adaptor protein recruiting protein tyrosine phosphatases SHP-1 and SHP-2 to the plasma membrane. J Biol Chem 287 (2012) 22812-21.
[88] C. Schiller, M.J. Nitschke, A. Seidl, E. Kremmer, and E.H. Weiss, Rat monoclonal antibodies specific for LST1 proteins. Hybridoma (Larchmt) 28 (2009) 281-6.
[89] J. Heidemann, M. Kebschull, P.R. Tepasse, and D. Bettenworth, Regulated expression of leukocyte-specific transcript (LST) 1 in human intestinal inflammation. Inflamm Res 63 (2014) 513-7.
[90] R.D. Fritsch-Stork, S.C. Silva-Cardoso, M.J. Groot Koerkamp, J.C. Broen, F.F. Lafeber, and J.W. Bijlsma, Expression of ERAP2 and LST1 is increased before start of therapy in rheumatoid arthritis patients with good clinical response to glucocorticoids. Clin Exp Rheumatol 34 (2016) 685-9.
[91] H. Mulcahy, K.P. O'Rourke, C. Adams, M.G. Molloy, and F. O'Gara, LST1 and NCR3 expression in autoimmune inflammation and in response to IFN-gamma, LPS and microbial infection. Immunogenetics 57 (2006) 893-903.

[92] S.R. Leist, H. Kollmus, B. Hatesuer, R.L. Lambertz, and K. Schughart, Lst1 deficiency has a minor impact on course and outcome of the host response to influenza A H1N1 infections in mice. Virol J 13 (2016) 17.
[93] R.J. Xavier, and D.K. Podolsky, Unravelling the pathogenesis of inflammatory bowel disease. Nature 448 (2007) 427-34.
[94] J.R. Kelsen, P. Russo, and K.E. Sullivan, Early-Onset Inflammatory Bowel Disease. Immunol Allergy Clin North Am 39 (2019) 63-79.
[95] N.A. Molodecky, I.S. Soon, D.M. Rabi, W.A. Ghali, M. Ferris, G. Chernoff, E.I. Benchimol, R. Panaccione, S. Ghosh, H.W. Barkema, and G.G. Kaplan, Increasing incidence and prevalence of the inflammatory bowel diseases with time, based on systematic review. Gastroenterology 142 (2012) 46-54 e42; quiz e30.
[96] S.C. Ng, H.Y. Shi, N. Hamidi, F.E. Underwood, W. Tang, E.I. Benchimol, R. Panaccione, S. Ghosh, J.C.Y. Wu, F.K.L. Chan, J.J.Y. Sung, and G.G. Kaplan, Worldwide incidence and prevalence of inflammatory bowel disease in the 21st century: a systematic review of population-based studies. Lancet 390 (2018) 2769-2778.
[97] R.P. Calixto, C. Flores, and C.F. Francesconi, Inflammatory Bowel Disease: Impact on Scores of Quality of Life, Depression and Anxiety in Patients Attending a Tertiary Care Center in Brazil. Arq Gastroenterol 55 (2018) 202-207.
[98] H.R. Clearfield, How does IBD affect quality of life? Inflamm Bowel Dis 14 Suppl 2 (2008) S45-6.
[99] C. Marinelli, E. Savarino, M. Inferrera, G. Lorenzon, A. Rigo, M. Ghisa, S. Facchin, R. D'Inca, and F. Zingone, Factors Influencing Disability and Quality of Life during Treatment: A Cross-Sectional Study on IBD Patients. Gastroenterol Res Pract 2019 (2019) 5354320.
[100] R. Neuendorf, A. Harding, N. Stello, D. Hanes, and H. Wahbeh, Depression and anxiety in patients with Inflammatory Bowel Disease: A systematic review. J Psychosom Res 87 (2016) 70-80.
[101] M. Orholm, V. Binder, T.I. Sorensen, L.P. Rasmussen, and K.O. Kyvik, Concordance of inflammatory bowel disease among Danish twins. Results of a nationwide study. Scand J Gastroenterol 35 (2000) 1075-81.
[102] N.P. Thompson, R. Driscoll, R.E. Pounder, and A.J. Wakefield, Genetics versus environment in inflammatory bowel disease: results of a British twin study. BMJ 312 (1996) 95-6.
[103] D. Laharie, S. Debeugny, M. Peeters, A. Van Gossum, C. Gower-Rousseau, J. Belaiche, R. Fiasse, J.L. Dupas, E. Lerebours, S. Piotte, A. Cortot, S. Vermeire, B. Grandbastien, and J.F. Colombel, Inflammatory bowel disease in spouses and their offspring. Gastroenterology 120 (2001) 816-9.
[104] S. Lesage, H. Zouali, J.P. Cezard, J.F. Colombel, J. Belaiche, S. Almer, C. Tysk, C. O'Morain, M. Gassull, V. Binder, Y. Finkel, R. Modigliani, C. Gower-Rousseau, J. Macry, F. Merlin, M. Chamaillard, A.S. Jannot, G. Thomas, J.P. Hugot, E.-I. Group, E. Group, and G. Group, CARD15/NOD2 mutational analysis and genotype-phenotype correlation in 612 patients with inflammatory bowel disease. Am J Hum Genet 70 (2002) 845-57.
[105] A. Fischer, J. Provot, J.P. Jais, A. Alcais, N. Mahlaoui, and C.F.P.I.D.s.g. members of the, Autoimmune and inflammatory manifestations occur frequently in patients with primary immunodeficiencies. J Allergy Clin Immunol 140 (2017) 1388-1393 e8.

[106] X. Li, J. Sundquist, K. Hemminki, and K. Sundquist, Risk of inflammatory bowel disease in first- and second-generation immigrants in Sweden: a nationwide follow-up study. Inflamm Bowel Dis 17 (2011) 1784-91.
[107] E.R. Lane, T.L. Zisman, and D.L. Suskind, The microbiota in inflammatory bowel disease: current and therapeutic insights. J Inflamm Res 10 (2017) 63-73.
[108] A.N. Ananthakrishnan, H. Khalili, G.G. Konijeti, L.M. Higuchi, P. de Silva, J.R. Korzenik, C.S. Fuchs, W.C. Willett, J.M. Richter, and A.T. Chan, A prospective study of long-term intake of dietary fiber and risk of Crohn's disease and ulcerative colitis. Gastroenterology 145 (2013) 970-7.
[109] I.B.D.i.E.S. Investigators, A. Tjonneland, K. Overvad, M.M. Bergmann, G. Nagel, J. Linseisen, G. Hallmans, R. Palmqvist, H. Sjodin, G. Hagglund, G. Berglund, S. Lindgren, O. Grip, D. Palli, N.E. Day, K.T. Khaw, S. Bingham, E. Riboli, H. Kennedy, and A. Hart, Linoleic acid, a dietary n-6 polyunsaturated fatty acid, and the aetiology of ulcerative colitis: a nested case-control study within a European prospective cohort study. Gut 58 (2009) 1606-11.
[110] M.C. Mentella, F. Scaldaferri, M. Pizzoferrato, A. Gasbarrini, and G.A.D. Miggiano, Nutrition, IBD and Gut Microbiota: A Review. Nutrients 12 (2020).
[111] A.N. Ananthakrishnan, H. Khalili, G.G. Konijeti, L.M. Higuchi, P. de Silva, C.S. Fuchs, W.C. Willett, J.M. Richter, and A.T. Chan, Long-term intake of dietary fat and risk of ulcerative colitis and Crohn's disease. Gut 63 (2014) 776-84.
[112] R. Kuhn, J. Lohler, D. Rennick, K. Rajewsky, and W. Muller, Interleukin-10-deficient mice develop chronic enterocolitis. Cell 75 (1993) 263-74.
[113] M. Van der Sluis, B.A. De Koning, A.C. De Bruijn, A. Velcich, J.P. Meijerink, J.B. Van Goudoever, H.A. Buller, J. Dekker, I. Van Seuningen, I.B. Renes, and A.W. Einerhand, Muc2-deficient mice spontaneously develop colitis, indicating that MUC2 is critical for colonic protection. Gastroenterology 131 (2006) 117-29.
[114] A. Nenci, C. Becker, A. Wullaert, R. Gareus, G. van Loo, S. Danese, M. Huth, A. Nikolaev, C. Neufert, B. Madison, D. Gumucio, M.F. Neurath, and M. Pasparakis, Epithelial NEMO links innate immunity to chronic intestinal inflammation. Nature 446 (2007) 557-61.
[115] M. Neurath, I. Fuss, and W. Strober, TNBS-colitis. Int Rev Immunol 19 (2000) 51-62.
[116] F. Heller, I.J. Fuss, E.E. Nieuwenhuis, R.S. Blumberg, and W. Strober, Oxazolone colitis, a Th2 colitis model resembling ulcerative colitis, is mediated by IL-13-producing NK-T cells. Immunity 17 (2002) 629-38.
[117] I. Okayasu, S. Hatakeyama, M. Yamada, T. Ohkusa, Y. Inagaki, and R. Nakaya, A novel method in the induction of reliable experimental acute and chronic ulcerative colitis in mice. Gastroenterology 98 (1990) 694-702.
[118] P. Kiesler, I.J. Fuss, and W. Strober, Experimental Models of Inflammatory Bowel Diseases. Cell Mol Gastroenterol Hepatol 1 (2015) 154-170.
[119] B. Chassaing, J.D. Aitken, M. Malleshappa, and M. Vijay-Kumar, Dextran sulfate sodium (DSS)-induced colitis in mice. Curr Protoc Immunol 104 (2014) 15 25 1-15 25 14.
[120] D.D. Eichele, and K.K. Kharbanda, Dextran sodium sulfate colitis murine model: An indispensable tool for advancing our understanding of inflammatory bowel diseases pathogenesis. World J Gastroenterol 23 (2017) 6016-6029.
[121] L.A. Dieleman, M.J. Palmen, H. Akol, E. Bloemena, A.S. Pena, S.G. Meuwissen, and E.P. Van Rees, Chronic experimental colitis induced by dextran sulphate

sodium (DSS) is characterized by Th1 and Th2 cytokines. Clin Exp Immunol 114 (1998) 385-91.
[122] J.F. Zhu, Y. Xu, J. Zhao, X. Li, X. Meng, T.Q. Wang, B.Y. Zou, P.Y. Zhao, Q. Liu, C.L. Lu, F.L. Zheng, and H.S. Liu, IL-33 Protects Mice against DSS-Induced Chronic Colitis by Increasing Both Regulatory B Cell and Regulatory T Cell Responses as Well as Decreasing Th17 Cell Response. J Immunol Res 2018 (2018) 1827901.
[123] L.A. Dieleman, B.U. Ridwan, G.S. Tennyson, K.W. Beagley, R.P. Bucy, and C.O. Elson, Dextran sulfate sodium-induced colitis occurs in severe combined immunodeficient mice. Gastroenterology 107 (1994) 1643-52.
[124] L.J. Hall, E. Faivre, A. Quinlan, F. Shanahan, K. Nally, and S. Melgar, Induction and activation of adaptive immune populations during acute and chronic phases of a murine model of experimental colitis. Dig Dis Sci 56 (2011) 79-89.
[125] X. Xu, Y. Wang, B. Zhang, X. Lan, S. Lu, P. Sun, X. Li, G. Shi, Y. Zhao, H. Han, C. Du, and H. Wang, Treatment of experimental colitis by endometrial regenerative cells through regulation of B lymphocytes in mice. Stem Cell Res Ther 9 (2018) 146.
[126] A.E. Troy, C. Zaph, Y. Du, B.C. Taylor, K.J. Guild, C.A. Hunter, C.J. Saris, and D. Artis, IL-27 regulates homeostasis of the intestinal CD4+ effector T cell pool and limits intestinal inflammation in a murine model of colitis. J Immunol 183 (2009) 2037-44.
[127] F. Wang, P.L. Peng, X. Lin, Y. Chang, J. Liu, R. Zhou, J.Y. Nie, W.G. Dong, Q. Zhao, and J. Li, Regulatory role of NKG2D+ NK cells in intestinal lamina propria by secreting double-edged Th1 cytokines in ulcerative colitis. Oncotarget 8 (2017) 98945-98952.
[128] K. Yanaba, A. Yoshizaki, Y. Asano, T. Kadono, T.F. Tedder, and S. Sato, IL-10-producing regulatory B10 cells inhibit intestinal injury in a mouse model. Am J Pathol 178 (2011) 735-43.
[129] A. Poggi, R. Benelli, R. Vene, D. Costa, N. Ferrari, F. Tosetti, and M.R. Zocchi, Human Gut-Associated Natural Killer Cells in Health and Disease. Front Immunol 10 (2019) 961.
[130] M. Perse, and A. Cerar, Dextran sodium sulphate colitis mouse model: traps and tricks. J Biomed Biotechnol 2012 (2012) 718617.
[131] I.D. Iliev, V.A. Funari, K.D. Taylor, Q. Nguyen, C.N. Reyes, S.P. Strom, J. Brown, C.A. Becker, P.R. Fleshner, M. Dubinsky, J.I. Rotter, H.L. Wang, D.P. McGovern, G.D. Brown, and D.M. Underhill, Interactions between commensal fungi and the C-type lectin receptor Dectin-1 influence colitis. Science 336 (2012) 1314-7.
[132] M.M. Heimesaat, A. Fischer, B. Siegmund, A. Kupz, J. Niebergall, D. Fuchs, H.K. Jahn, M. Freudenberg, C. Loddenkemper, A. Batra, H.A. Lehr, O. Liesenfeld, M. Blaut, U.B. Gobel, R.R. Schumann, and S. Bereswill, Shift towards pro-inflammatory intestinal bacteria aggravates acute murine colitis via Toll-like receptors 2 and 4. Plos One 2 (2007) e662.
[133] D.L. Gibson, M. Montero, M.J. Ropeleski, K.S. Bergstrom, C. Ma, S. Ghosh, H. Merkens, J. Huang, L.E. Mansson, H.P. Sham, K.M. McNagny, and B.A. Vallance, Interleukin-11 reduces TLR4-induced colitis in TLR2-deficient mice and restores intestinal STAT3 signaling. Gastroenterology 139 (2010) 1277-88.
[134] S. Rakoff-Nahoum, J. Paglino, F. Eslami-Varzaneh, S. Edberg, and R. Medzhitov, Recognition of commensal microflora by toll-like receptors is required for intestinal homeostasis. Cell 118 (2004) 229-41.

[135] M. Vijay-Kumar, H. Wu, J. Aitken, V.L. Kolachala, A.S. Neish, S.V. Sitaraman, and A.T. Gewirtz, Activation of toll-like receptor 3 protects against DSS-induced acute colitis. Inflamm Bowel Dis 13 (2007) 856-64.
[136] W.A. Rose, 2nd, K. Sakamoto, and C.A. Leifer, TLR9 is important for protection against intestinal damage and for intestinal repair. Sci Rep 2 (2012) 574.
[137] C. Bauer, P. Duewell, C. Mayer, H.A. Lehr, K.A. Fitzgerald, M. Dauer, J. Tschopp, S. Endres, E. Latz, and M. Schnurr, Colitis induced in mice with dextran sulfate sodium (DSS) is mediated by the NLRP3 inflammasome. Gut 59 (2010) 1192-9.
[138] Y. Arai, H. Takanashi, H. Kitagawa, and I. Okayasu, Involvement of interleukin-1 in the development of ulcerative colitis induced by dextran sulfate sodium in mice. Cytokine 10 (1998) 890-6.
[139] L.P. McLean, R.K. Cross, and T. Shea-Donohue, Combined blockade of IL-17A and IL-17F may prevent the development of experimental colitis. Immunotherapy 5 (2013) 923-5.
[140] V. Langer, E. Vivi, D. Regensburger, T.H. Winkler, M.J. Waldner, T. Rath, B. Schmid, L. Skottke, S. Lee, N.L. Jeon, T. Wohlfahrt, V. Kramer, P. Tripal, M. Schumann, S. Kersting, C. Handtrack, C.I. Geppert, K. Suchowski, R.H. Adams, C. Becker, A. Ramming, E. Naschberger, N. Britzen-Laurent, and M. Sturzl, IFN-gamma drives inflammatory bowel disease pathogenesis through VE-cadherin-directed vascular barrier disruption. J Clin Invest 129 (2019) 4691-4707.
[141] H. Takagi, T. Kanai, A. Okazawa, Y. Kishi, T. Sato, H. Takaishi, N. Inoue, H. Ogata, Y. Iwao, K. Hoshino, K. Takeda, S. Akira, M. Watanabe, H. Ishii, and T. Hibi, Contrasting action of IL-12 and IL-18 in the development of dextran sodium sulphate colitis in mice. Scand J Gastroenterol 38 (2003) 837-44.
[142] Y. Naito, T. Takagi, O. Handa, T. Ishikawa, S. Nakagawa, T. Yamaguchi, N. Yoshida, M. Minami, M. Kita, J. Imanishi, and T. Yoshikawa, Enhanced intestinal inflammation induced by dextran sulfate sodium in tumor necrosis factor-alpha deficient mice. J Gastroenterol Hepatol 18 (2003) 560-9.
[143] R. Rani, A.G. Smulian, D.R. Greaves, S.P. Hogan, and D.R. Herbert, TGF-beta limits IL-33 production and promotes the resolution of colitis through regulation of macrophage function. Eur J Immunol 41 (2011) 2000-9.
[144] R. Nowarski, R. Jackson, N. Gagliani, M.R. de Zoete, N.W. Palm, W. Bailis, J.S. Low, C.C. Harman, M. Graham, E. Elinav, and R.A. Flavell, Epithelial IL-18 Equilibrium Controls Barrier Function in Colitis. Cell 163 (2015) 1444-56.
[145] Z. Pu, Y. Che, W. Zhang, H. Sun, T. Meng, H. Xie, L. Cao, and H. Hao, Dual roles of IL-18 in colitis through regulation of the function and quantity of goblet cells. Int J Mol Med 43 (2019) 2291-2302.
[146] G. Sabio, and R.J. Davis, TNF and MAP kinase signalling pathways. Semin Immunol 26 (2014) 237-45.
[147] E. Cenci, A. Mencacci, A. Casagrande, P. Mosci, F. Bistoni, and L. Romani, Impaired antifungal effector activity but not inflammatory cell recruitment in interleukin-6-deficient mice with invasive pulmonary aspergillosis. J Infect Dis 184 (2001) 610-7.
[148] S.G. Filler, M.R. Yeaman, and D.C. Sheppard, Tumor necrosis factor inhibition and invasive fungal infections. Clin Infect Dis 41 Suppl 3 (2005) S208-12.
[149] W.A. Neveu, E. Bernardo, J.L. Allard, V. Nagaleekar, M.J. Wargo, R.J. Davis, Y. Iwakura, L.A. Whittaker, and M. Rincon, Fungal allergen beta-glucans trigger

p38 mitogen-activated protein kinase-mediated IL-6 translation in lung epithelial cells. Am J Respir Cell Mol Biol 45 (2011) 1133-41.
[150] L. Luo, N.J. Bokil, A.A. Wall, R. Kapetanovic, N.M. Lansdaal, F. Marceline, B.J. Burgess, S.J. Tong, Z. Guo, K. Alexandrov, I.L. Ross, M.L. Hibbs, J.L. Stow, and M.J. Sweet, SCIMP is a transmembrane non-TIR TLR adaptor that promotes proinflammatory cytokine production from macrophages. Nat Commun 8 (2017) 14133.
[151] L. Luo, J.E.B. Curson, L. Liu, A.A. Wall, N. Tuladhar, R.M. Lucas, M.J. Sweet, and J.L. Stow, SCIMP is a universal Toll-like receptor adaptor in macrophages. J Leukoc Biol 107 (2020) 251-262.
[152] I. Miralda, S.M. Uriarte, and K.R. McLeish, Multiple Phenotypic Changes Define Neutrophil Priming. Front Cell Infect Microbiol 7 (2017) 217.
[153] O. Adachi, T. Kawai, K. Takeda, M. Matsumoto, H. Tsutsui, M. Sakagami, K. Nakanishi, and S. Akira, Targeted disruption of the MyD88 gene results in loss of IL-1- and IL-18-mediated function. Immunity 9 (1998) 143-50.
[154] N. Warner, and G. Nunez, MyD88: a critical adaptor protein in innate immunity signal transduction. J Immunol 190 (2013) 3-4.
[155] J.L. Johnson, J.W. Park, J.E. Benna, L.P. Faust, O. Inanami, and B.M. Babior, Activation of p47(PHOX), a cytosolic subunit of the leukocyte NADPH oxidase. Phosphorylation of ser-359 or ser-370 precedes phosphorylation at other sites and is required for activity. J Biol Chem 273 (1998) 35147-52.
[156] S.A. Belambri, M. Hurtado-Nedelec, A. Senator, K. Makni-Maalej, M. Fay, M.A. Gougerot-Pocidalo, J.C. Marie, P.M. Dang, and J. El-Benna, Phosphorylation of p47phox is required for receptor-mediated NADPH oxidase/NOX2 activation in Epstein-Barr virus-transformed human B lymphocytes. Am J Blood Res 2 (2012) 187-93.
[157] V. Chitu, V. Nacu, J.F. Charles, W.M. Henne, H.T. McMahon, S. Nandi, H. Ketchum, R. Harris, M.C. Nakamura, and E.R. Stanley, PSTPIP2 deficiency in mice causes osteopenia and increased differentiation of multipotent myeloid precursors into osteoclasts. Blood 120 (2012) 3126-35.
[158] I.R. Garrett, B.F. Boyce, R.O. Oreffo, L. Bonewald, J. Poser, and G.R. Mundy, Oxygen-derived free radicals stimulate osteoclastic bone resorption in rodent bone in vitro and in vivo. J Clin Invest 85 (1990) 632-9.
[159] E.O. Kwarteng, and K.M. Heinonen, Competitive Transplants to Evaluate Hematopoietic Stem Cell Fitness. J Vis Exp (2016).
[160] Mosquera-Caro M, Helman P, Veroff R, et al. Identification, validation and cloning of a novel gene (OPAL1) and associated genes highly predictive of outcome in pediatric acute lymphoblastic leukemia using gene expression profiling [abstract]. Blood. (2003)

12. Reprint of publications

frontiers in Immunology

ORIGINAL RESEARCH
published: 27 April 2021
doi: 10.3389/fimmu.2021.618332

Regulation of Inflammatory Response by Transmembrane Adaptor Protein LST1

Matej Fabisik [1,2], Jolana Tureckova [3,4], Nataliia Pavliuchenko [1,2], Jarmila Kralova [1], Jana Balounova [4], Kristina Vicikova [4], Tereza Skopcova [1], Frantisek Spoutil[4], Jana Pokorna[1], Pavla Angelisova[1], Bernard Malissen[5], Jan Prochazka[3,4], Radislav Sedlacek[3,4] and Tomas Brdicka[1]*

[1] Laboratory of Leukocyte Signalling, Institute of Molecular Genetics of the Czech Academy of Sciences, Prague, Czechia, [2] Faculty of Science, Charles University, Prague, Czechia, [3] Laboratory of Transgenic Models of Diseases, Institute of Molecular Genetics of the Czech Academy of Sciences, Vestec, Czechia, [4] Czech Centre for Phenogenomics, Institute of Molecular Genetics of the Czech Academy of Sciences, Vestec, Czechia, [5] Centre d'Immunophe´nomique, Aix Marseille Universite´, INSERM, CNRS, Marseille, France

OPEN ACCESS

Edited by:
Liwu Li,
Virginia Tech, United States

Reviewed by:
Silvia Melgar,
University College Cork, Ireland
Philippe Georgel,
Universite´ de Strasbourg, France

*Correspondence: Tomas Brdicka
tomas.brdicka@img.cas.cz

Specialty section: This article was submitted to Molecular Innate Immunity, a section of the journal Frontiers in Immunology

Received: 16 October 2020
Accepted: 08 April 2021
Published: 27 April 2021

Citation:
Fabisik M, Tureckova J, Pavliuchenko N, Kralova J, Balounova J, Vicikova K, Skopcova T, Spoutil F, Pokorna J, Angelisova P, Malissen B, Prochazka J, Sedlacek R and Brdicka T (2021) Regulation of Inflammatory Response by Transmembrane Adaptor Protein LST1. Front. Immunol. 12:618332. doi: 10.3389/fimmu.2021.618332

LST1 is a small adaptor protein expressed in leukocytes of myeloid lineage. Due to the binding to protein tyrosine phosphatases SHP1 and SHP2 it was thought to have negative regulatory function in leukocyte signaling. It was also shown to be involved in cytoskeleton regulation and generation of tunneling nanotubes. LST1 gene is located in MHCIII locus close to many immunologically relevant genes. In addition, its expression increases under inflammatory conditions such as viral infection, rheumatoid arthritis and inflammatory bowel disease and its deficiency was shown to result in slightly increased sensitivity to influenza infection in mice. However, little else is known about its role in the immune system homeostasis and immune response. Here we show that similar to humans, LST1 is expressed in mice in the cells of the myeloid lineage. In vivo, its deficiency results in alterations in multiple leukocyte subset abundance in steady state and under inflammatory conditions. Moreover, LST1-deficient mice show significant level of resistance to dextran sodium sulphate (DSS) induced acute colitis, a model of inflammatory bowel disease. These data demonstrate that LST1 regulates leukocyte abundance in lymphoid organs and inflammatory response in the gut.

Keywords: LST1, inflammation, colitis, inflammatory bowel disease, myeloid cells

INTRODUCTION

Leukocyte-specific transcript 1 protein (LST1) is a small, 97 amino acid long, transmembrane adaptor protein. It is composed of a very short extracellular segment with a dimerization cysteine, a single transmembrane domain, immediately followed by a palmitoylation site, and a larger cytoplasmic tail with two immunoreceptor tyrosine-based inhibitory motifs (ITIM). Despite of its small size, at least 16 LST1 splice variants of various length (transmembrane and soluble isoforms) were described in human mRNA. However, only one of these variants LST1/A has been detected at the protein level (1–4). The role of this extensive splicing is not known. It has been

speculated that it might function as a transcription and translation regulation tool (5). Interestingly, only two RNA splice forms have been detected in mouse (2). In this report, we will refer to the protein expressed from human and murine LST1 genes only as LST1.

Our previous analysis of LST1 expression pattern by in-house generated monoclonal antibody LST1/02 recognizing human but not murine LST1 revealed its expression exclusively in leukocytes of the myeloid lineage (macrophages, dendritic cells, monocytes, granulocytes) and in related cell lines (U-937, THP-1) (1). However, there is a discrepancy between these results and results obtained with another monoclonal antibody 7E2, which showed expression of LST1 also in lymphoid (Jurkat, B cells) and non-hematopoietic cells (HeLa, Capan-1, HepG2) (3). LST1 expression appears to be regulated during inflammation. Increased expression of LST1 mRNA isoforms was detected in cell lines after treatment with pro-inflammatory compounds (LPS, TNFa). Its expression was also elevated in histological colon samples from patients with inflammatory bowel disease (IBD) (6) and in the synovial fluid of patients with rheumatoid arthritis (7).

LST1 is coded by LST1 gene (also known as B144) localized in MHCIII locus. This genomic site harbors many immunologically important genes, such as genes coding for Lymphotoxin-b, Tumor Necrosis Factor a, several complement proteins and others. High LST1 expression in leukocytes together with localization of its gene in one of the immunologically most important loci, raises a question about the function of LST1 in the immune system (8, 9). Previous work from our laboratory demonstrated that ITIM motifs in LST1 bind phosphatases SHP1 and SHP2 and suggested that it is a negative regulator of signaling in myeloid cells, although the processes that LST1 regulates in vivo were not defined (1).

In HeLa cells, overexpression of LST1 induced formation of tunneling nanotubes via interaction with RalA–M-Sec–exocyst complex, and transfer of MHC class I molecules through these nanotubes between the cells (10–12). In a genomic study, Lst1 was identified as a gene connected to host response to influenza virus (13). This was further corroborated by a subsequent study showing that LST1-deficient mice display higher susceptibility to influenza infection when compared to the wild type mice (14). Increased expression of LST1 in tissues affected by IBD or rheumatoid arthritis suggests that it may also be involved in other inflammatory conditions. In this work we describe basic features of LST1 deficient mice and analyze the role of LST1 in the dextran sodium sulphate (DSS)-induced colitis, a mouse model of IBD. We show that the LST1 deficiency results in alterations in innate leukocyte subset composition and in milder progress of DSS-induced colitis, demonstrating LST1 involvement in the regulation of leukocyte homeostasis and inflammation.

MATERIALS AND METHODS

Mice

LST1-deficient mouse strain LST1$^{tm1(KOMP)Vlcg}$ on C57Bl/6J genetic background (abbreviated as Lst1$^{-/-}$) was obtained from International Knockout Mouse Consortium. These animals were crossed to C57Bl/6J mice from Animal facility of the Institute of Molecular Genetics to obtain heterozygotes Lst1$^{-/-}$ x C57Bl/6J. Their homozygote offspring were used as littermates for comparative experiments at the age of 6 - 10 weeks. Animal experiments were approved by the Animal Care and Use Committee of the Institute of Molecular Genetics and were in agreement with local legal requirements and ethical guidelines.

Primary Cell Isolation and Activation

Animals were sacrificed by cervical dislocation and single cell suspensions were prepared. Lymph node and splenic cell suspensions were prepared by pressing the lymph node or spleen tissue through 42 mm cell strainer. Bone marrow cells were isolated by flushing femurs cut at the extremities with cold PBS/2% FCS using syringe and 30 Gauge needle. Erythrocytes were removed by lysis in ACK buffer (150 mM NH_4Cl, 0.1 mM EDTA (disodium salt), 1 mM $KHCO_3$). Colon lamina propria cells were isolated from entire colon. The colon was opened longitudinally, washed with cold PBS and then rocked for 1 hour in 10 ml solution of 5mM EDTA/2% FCS/HBSS without Ca^{2+} and Mg^{2+} at 4°C followed by washing with 10 ml HBSS/2% FCS. Colon was then cut to 3 mm pieces and digested with the solution containing collagenase II (2 mg/ml, Gibco #17101-015, CAS No. 9001-12-1) and DNase I (0.5mg/ml, Sigma powder DN25-100MG; CAS No. 9003-98-9) in DMEM/2% FCS with shaking (37°C, 2 × 30 min). After each digestion round, tissues were poured onto petri dish and triturated gently with plastic Pasteur pipette in order to obtain the lamina propria cells. Cell suspension was filtered through 100 µm Sysmex filters, centrifuged, resuspended in 5 ml of PBS/2% FCS and kept on ice. After the second round of digestion, cells were pooled together, centrifuged, resuspended in PBS/2% FCS and filtered again through 50 µm Sysmex filters to obtain single cell suspension of colon lamina propria cells. For murine colonic epithelial cell isolation, colon was opened longitudinally and washed vigorously in PBS on ice. Then it was cut to shorter fragments and incubated in 20 ml pre-heated HBSS, 3% FBS, 2 mM EDTA twice at 37°C. The suspension with released cells was then collected and filtered through 100 µm filter. Filtered cells were resuspended in 1 ml (1 min, 37°C) TrypLE™ Express Enzyme (Thermo Fischer Scientific, 12605010), resuspended by pipetting and filtered again through 40 µm filter into 15 ml tubes. TrypLE™ enzymes were neutralized by washing filter with 3 ml of HBSS (without Ca^{2+} and Mg^{2+}), 3% FBS, 2 mM EDTA (pH 8.0, ice cold). Cells were centrifuged for 10 min (4°C, 300 × g), stained with CD45 and EpCAM fluorescent antibodies and sorted on BD FACSAria™ cell sorter as CD45^{-} EpCAM^{++}. Bone marrow derived dendritic cells (BMDC) and bone marrow derived macrophages (BMDM) were generated from isolated mouse bone marrow cells by culturing in IMDM culture media supplemented with 10% FCS and 3% supernatant from J558 cells containing GM-CSF for 10 days (BMDC) or 5% supernatant from CMG 14-12 cells containing M-CSF for 7 days (BMDM) as described in detail here (15).

Glycosylation Assay

BMDM were plated in a 6-well plate at 2 × 10^6 cells per well and treated with Tunicamycin (Sigma) - 0.5 µg/ml and 1 µg/ml for

24 hours followed by lysis (300 µl 2× concentrated SDS-PAGE sample buffer). Lysed samples were sonicated, heated to 95°C for 10 minutes and analyzed by immunoblotting under non-reducing conditions.

Cell Activation

BMDM and BMDC were cultured overnight in DMEM without M-CSF/GM-CSF in a 12-well tissue culture plate (10^6 cells per well) and then incubated for indicated time-points with IFNg (Peprotech) – 50 ng/ml, TNFa (Peprotech) – 20 ng/ml, LPS (Sigma) – 100 ng/ml and PolyI:C (Invivogen, low molecular weight) – 20 µg/ml, GM-CSF – 3% supernatant from J558 cells. Subsequently, cells were lysed in 2 × concentrated SDS-PAGE sample buffer (128 mM Tris pH 6.8, 10% glycerol, 4% SDS, 1% DTT) and subjected to immunoblotting with indicated antibodies.

Antibodies

Flow cytometry antibodies are listed in Supplementary Table S1. LST1/06 mouse mAb recognizing murine LST1 on Western blots and in immunoprecipitation was generated by immunization of $Lst1^{-/-}$ mice with recombinant intracellular domain of murine LST1 (starting at Cys40) produced in Escherichia coli. After immunization, splenocytes were fused with Sp2/0 myeloma cells and antibody producing hybridomas were cloned by limiting dilution. Antibodies used for Western blot detection: SHP-1 (SH-PTP1 Antibody, C-19, Santa Cruz Biotechnology), SHP-2 (SH-PTP2 N-16, Santa Cruz Biotechnology), GAPDH (Anti-GAPDH antibody produced in rabbit, Sigma-Aldrich), IkBa (Cell Signaling Technology, #9242). Western blot ECL signals were detected with Azure c300 imaging system (Azure Biosystems) and quantified using AIDA image analyzer software (Elysia-raytest, Straubenhardt, Germany).

Flow Cytometry

Cells of bone marrow, spleen and lymph nodes were incubated with fluorescently labeled antibodies and Fc-receptor blocking antibody (2.4G2) and analyzed on BD™ LSRII flow cytometer (Becton Dickinson). Staining was divided into two sets – A (CD3, CD4, CD8, CD19, NK1.1), B (CD11b, CD11c, F4/80, Ly6C, Ly6G). Cell populations were gated as: CD4 T cells – $CD3^+$ $CD4^+$; CD8 T cells – $CD3^+$ $CD8^+$; B cells – $CD19^+$ $CD3^-$; NK cells – $NK1.1^+$ $CD3^-$; $NK1.1^+CD3^+$; Macrophages – $CD11b^{low}$ $F4/80^+$; Monocytes – $CD11b^+$ $Ly6C^{hi}$ $Ly6G^-$; Neutrophils – $CD11b^+$ $Ly6C^{med}$ $Ly6G^+$; Dendritic cells – $CD11b^+$ $CD11c^+$. Colon leukocytes were measured on BD™ FACSymphony flow cytometer (Becton Dickinson) according to International Mouse Phenotyping Consortium standards[1] and gated as CD45+ cells. Staining was divided into two sets – A (CD49d, CD4, Klrg1, CD44, CD8a, gdTCR, NK1.1, GITR, CD25, CD62L), B (Ly6G, CD19, Ly6C, CD11b, CD21/CD35, F4/80, Bst2, NK1.1, CD23, CD11c, MHCII). Populations were gated as: CD4 T cells – $CD5^+$ $CD4^+$; CD8 T cells – $CD5^+$ $CD8^+$; B cells – $CD19^+$ $MHCII^+$; NK cells – $CD5^-$ $CD161^+$; NKT cells – $CD5^+$ $CD161^+$; Monocytes – $CD11b^+$ $Ly6C^+$ $Ly6G^-$; Neutrophils – $CD11b^+$ $Ly6C^{med}$ $Ly6G^+$; Macrophages – $CD11b^+$ $F4/80^+$; Dendritic cells – $CD11b^{+/-}$ $MHCII^+$ $CD11c^+$. Data were analyzed in FlowJo™ software.

Cytokine Detection by ELISA

Blood from tail vein was collected into EDTA tubes (EDTA 1000A, ref. 078035, KABE LABORTECHNIK, GmbH) and centrifuged (16 000 × g, 10 min, 4°C). Supernatant (plasma) was then transfered to fresh tubes and frozen in -80°C. Colons were homogenized in 400 µl RIPA lysis buffer (20 mM TRIS pH 7.5, 150 mM NaCl, 1% Nonidet P-40, 1% sodium deoxycholate, 0.1% SDS) containing 5 mM iodoacetamide (Sigma-Aldrich) and diluted Protease Inhibitor Cocktail Set III (Calbiochem, Merck) using AvansAHM1 Homogenizer on ice (10 s, maximum speed). The homogenates were cleared by centrifugation and frozen in -80°C. Concentrations of cytokines in blood plasma or colonic lysates were determined using IL-6 and TNF alpha Mouse Uncoated ELISA Kit with Plates (88-7324-22, 88-7064-22, Thermo Fischer Scientific) according to the manufacturer´s protocols.

Bone MicroCT Analysis

Femurs of 28 mice were scanned in-vivo under 20% zoletile anesthesia in SkyScan 1176 (Bruker, Belgium) at the resolution of 8.67 µm with 0.5 mm aluminum filter (voltage = 50 kV, current = 250 µA, step rotation = 0.3°) with 180° rotation, and reconstructed in NRecon 1.6.10.4 (Bruker, Belgium) with parameters of smoothing = 4, ring artifact correction = 7, beam hardening correction = 23%, and spread of intensities from 0.007 to 0.11 AU. Only reconstructions without artifacts underwent analysis resulting in 42 femurs analyzed. The femurs were segmented in CT Analyzer 1.16.4.1 (Bruker, Belgium) and reoriented in DataViewer 1.5.2 (Bruker, Belgium). CT Analyzer was also used for semiautomatic selection of regions of interest (central diaphysis for cortical bone, and distal metaphysis for trabecular bone) and subsequent 2D and 3D analysis. Parameters describing bone volume, porosity, and structural complexity were recorded. Bone mineral density (BMD) and tissue mineral density (TMD) were recorded for trabeculae and corticals, respectively, based on the correlation with calibrated hydroxyapatite phantoms.

Induction of Inflammatory Response In Vivo

For LPS challenge, mice were intraperitoneally injected with LPS (50 µg per animal). After 4 and 16 hours blood samples were collected and then mice were sacrificed by cervical dislocation and splenocyte subsets analyzed. To induce colitis with dextran sodium sulphate (DSS), littermates of $Lst1^{-/-}$ and WT mice (males, 8 weeks old) were fed with 2,5% DSS dissolved in drinking water for 6 days to induce acute colitis. Starting on day 7, DSS solution was changed for plain water. Parameters defining disease activity index, i.e. stool consistency, occult bleeding (Hemoccult Fecal Occult Blood Test, Beckman Coulter) and body weight on days 0, 2, 4, 5, 6, 8 were measured during the experiment. Mice in control group were administered only plain water. On day 8, mice were anesthetized with isoflurane (0.3L/min) for collection of blood sample from the

1 https://www.mousephenotype.org/impress/ProcedureInfo?action=list&procID=1225&pipeID=7

eye vein and sacrificed. Colon length was recorded, organs were collected (spleen, mesenteric lymph nodes, blood sample and colon), processed into single cell suspensions and measured with BD™ FACSymphony flow cytometer. Disease Activity Index was evaluated as average of the three measured parameters (weight loss, stool consistency and occult bleeding index) on a particular day. Scoring values were normalized to day 0, which has an arbitrary value 0. Scoring system for body weight: 1, loss of 1% – 5% weight; 2, loss of 5% –10% weight; 3, loss of 10% –20% weight; 4, 20% and higher body weight loss. Stool consistency: 0, well-formed stool pellets; 1, loose stool pellets; 2, pasty and semi-formed stools that did not adhere to the anus (mild diarrhea); 3, slimy stool (moderate diarrhea); 4, severe watery diarrhea that adhered to the anus and contained with blood. Occult bleeding: 0, no blood; 2, positive Hemoccult test, and 4, gross rectal bleeding.

Histology

The entire colon was opened longitudinally, flushed with PBS and fixed in 4% neutral buffered formaldehyde for 48 hours as swiss roll. Samples were dehydrated, embedded in paraffin and sectioned at 5 mm and stained with hematoxylin-eosin. For histological evaluation, areas of inflammatory lesions were microscopically evaluated and quantified as described (16). Area of damaged colon epithelium was assessed in FIJI editor after recalculating pixel area to the real area in mm^2 (4-5 animals per group).

Migration Assay

Corning 6.5 mm diameter Transwell Permeable Supports with 8.0 µm pores were used. Inserts (upper well) with pores were coated with 100 µl fibronectin (50 µg/ml) for 2 hours at room temperature and washed two times with migration media (IMDM without antibiotics, 0.5% BSA). 10^5 macrophages were added into the insert with migration media and 600 µl of migration media with CXCL12 (100 ng/ml) into the bottom well. After 2 hours at 37°C, 5% CO_2 migrated cells were collected (attached cells were released with 0.2% EDTA in PBS). The collected cells were mixed with 10 µl of Flow Cytometry Absolute Count Standard™ (Bangs Laboratories) and counted in BD™ FACSymphony flow cytometer (Becton Dickinson).

Quantitative Real-Time PCR

The total cellular RNA was isolated using Quick-RNA Miniprep Plus kit and transcribed into cDNA by RevertAid RT Reverse Transcription Kit, both used according to manufacturer's instructions. The cDNA was then used as a template for real-time quantitative PCR performed on LightCycler 480 using SYBR Green I Master mix (Roche). Primers used in cytokine mRNA detection are listed in Supplementary Table S2.

Statistics

Student´s t-test (two-tailed, unpaired) and One-way ANOVA with Tukey posttest for P-values and two-sided Grubb´s test for outlier recognition was performed in Graphpad Prism Software. Bars in figures represent mean ± SD, if not stated otherwise. P values lower than 0.05 are marked with asterisks as follows: * $p \leq 0.05$, ** $p \leq 0.01$, *** $p \leq 0.005$, **** $p \leq 0.0001$.

RESULTS

Murine LST1 Is Glycosylated Transmembrane Adaptor Protein

LST1 is a small transmembrane adaptor protein, which makes homo-dimers via cysteine bridges (1). Our previously generated monoclonal antibody LST1/02 to human LST1 (1) did not recognize murine protein. For detection of murine LST1, we have generated a novel monoclonal antibody LST1/06, against recombinant intracellular segment of murine LST1 and verified its specificity (Figure 1A). It preferentially binds LST1 under non-reducing conditions, i.e. in its dimeric form, which can be detected on Western blot as a broad double-band of ca 27-37 and 42-71 kDa, depending on the cell type (Figures 1A, B, 2). Lower than expected electrophoretic mobility and presence of N-glycosylation motif (NxS) in the short extracellular sequence suggested that murine LST1 could be glycosylated. Indeed, after addition of glycosylation inhibitor tunicamycin to the BMDM, its apparent molecular mass decreased to ca 29-48 kDa (Figure 1B).

LST1 Protein Levels Are Increased by Pro-Inflammatory Stimuli

The LST1 protein expression analysis using LST1/06 antibody, revealed that LST1 expression in cells that were not activated by proinflammatory stimuli is relatively low. As a result, multiple background bands cross-reacting with LST1/06 antibody, including a band of a similar molecular weight as LST1, became apparent during prolonged Western blot exposures. However, the use of the $Lst1^{-/-}$ cells as controls allowed us to distinguish the specific signal. Under these conditions, LST1 could be detected in the cells of myeloid lineage, including macrophages (MF), neutrophils (Neu), monocytes (Mon), but not in lymphoid lineage cells (T, B cells and NK cells) (Figure 2A). Since it has been observed previously that LST1 expression is elevated by inflammatory stimuli in human cell lines and in inflamed colon tissue (6), we decided to test if LST1 expression is upregulated under inflammatory conditions in leukocytes of myeloid lineage. Indeed, we observed elevated expression of LST1 in vitro in murine BMDM and BMDC after overnight (16 hours) stimulation with IFNg, LPS, TNFa and PolyI:C (Figures 2B, C).

LST1 Deficiency Results in Sex-Dependent Alterations of Trabecular Bone Structure in Mice

$Lst1^{-/-}$ mice were born at standard Mendelian ratios without any manifestation of disease during their aging. The phenotypical analysis of this mouse strain presented on the website of International mouse phenotyping consortium[2] (17), showed slight increase in the bone mineral density in $Lst1^{-/-}$ animals, suggesting potential effect on the function of osteoclasts or overall bone homeostasis, which are known to be affected by immune system activity. Though the finding was not considered significant, low p-value associated with the data prompted us to re-evaluate these results. Our analysis by microcomputerized

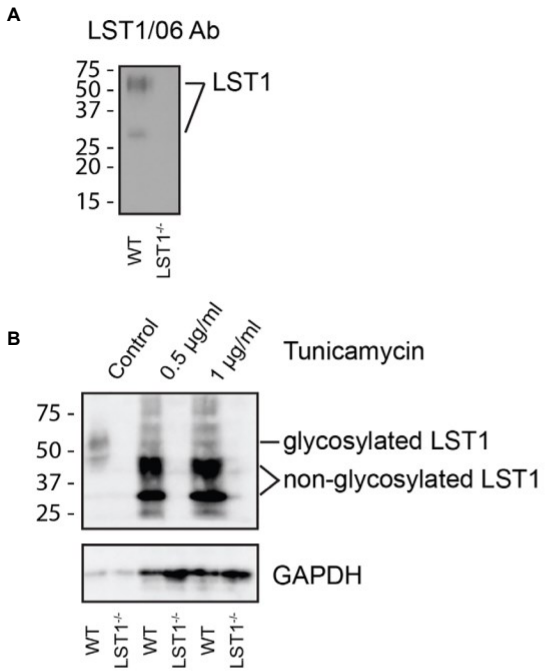

FIGURE 1 | Murine LST1 is a glycoprotein recognized by a newly developed antibody LST1/06. (A) Detection of murine LST1 by LST1/06 antibody in the LST1/06 immunoprecipitates from WT and Lst1$^{-/-}$ BMDM in non-reduced samples (n=3). (B) Murine BMDM were cultured in the presence of tunicamycin (0.5 and 1 µg/ml). Cells were lysed and LST1 immunoprecipitated and analyzed by immunoblotting with LST1/06 antibody under non-reducing conditions (n=3). Note the electrophoretic mobility shift after tunicamycin treatment, which is indicative of LST1 glycosylation.

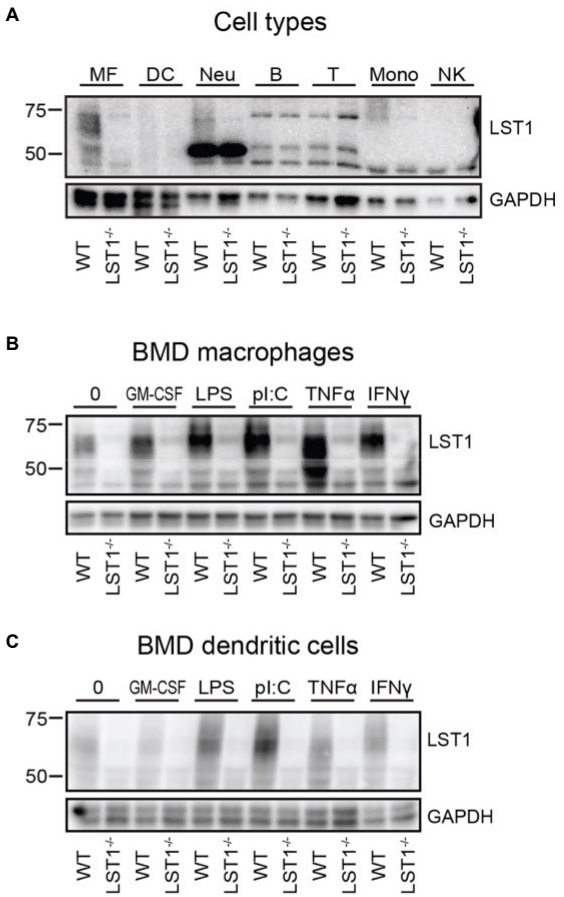

FIGURE 2 | Murine LST1 is expressed in the cells of myeloid lineage and its expression increases after pro-inflammatory stimuli. (A) Murine LST1 was detected in total cell lysates by immunoblotting (n=3). MF – bone marrow derived macrophages, DC – bone marrow derived dendritic cells, Neu – Neutrophils, B – B cells, T – T cells, Mono – monocytes, NK – NK cells. Its molecular weight varies between 42 to 71 kDa, likely due to the glycosylation. (B, C) Expression of LST1 in bone marrow derived macrophages (B) and dendritic cells (C) after treatment with various pro-inflammatory stimuli (n=3, see Materials and Methods for concentrations).

tomography (µCT) did not confirm any differences in the bone mineral density (not shown). On the other hand, it revealed reduced numbers of trabeculae in the trabecular bone tissue of Lst1$^{-/-}$ mice (Figures 3A, B). The trabeculae were also less segmented as demonstrated by the reduced ratio of trabecular bone surface and bone volume (Figure 3B). Interestingly, these differences were restricted only to male animals (Figures 3A,B; Supplementary Figure S1).

LST1 Deficient Mice Show Alterations in Leukocyte Subset Composition

Analysis of steady state lymphocyte populations in Lst1$^{-/-}$ mice revealed that while B cell and T cell subsets are without change and their percentages are comparable to the wild type mice (WT), other populations show reduced numbers. These include mainly bone marrow and splenic NK cells and splenic NKT cells (Figures 4A-C). Among the splenocytes of myeloid lineage, reduced percentages were observed for neutrophils, F4/80^{+} macrophages and to some extent also dendritic cells (Figure 4C). Reduced percentages were also observed for dendritic cells in the bone marrow (Figure 4A). Importantly, we also observed decrease in macrophage and dendritic cell percentages in the colon (Figure 4D). Total cell numbers were not significantly changed between the WT and Lst1$^{-/-}$ animals in any of the organs analyzed (Figure 4E). Reduced percentages of multiple leukocyte subsets could result from defect in cellular migration. To test the migratory capacity of LST1-deficient cells we analyzed chemokine-mediated migration of Lst1$^{-/-}$ bone marrow-derived macrophages in a transwell assay. Surprisingly, Lst1$^{-/-}$ cells migrated more efficiently towards CXCL12, ligand of chemokine receptor CXCR4, than WT cells (Figure 4F). At the same time CXCR4 expression was not affected by LST1 deficiency (Figure 4G). This finding suggests that LST1 negatively regulates CXCR4-mediated migration. It also shows that the migratory capacity of Lst1$^{-/-}$ cells is not compromised and that there is no general defect in cellular migration that could

2 https://www.mousephenotype.org/data/genes/MGI:1096324

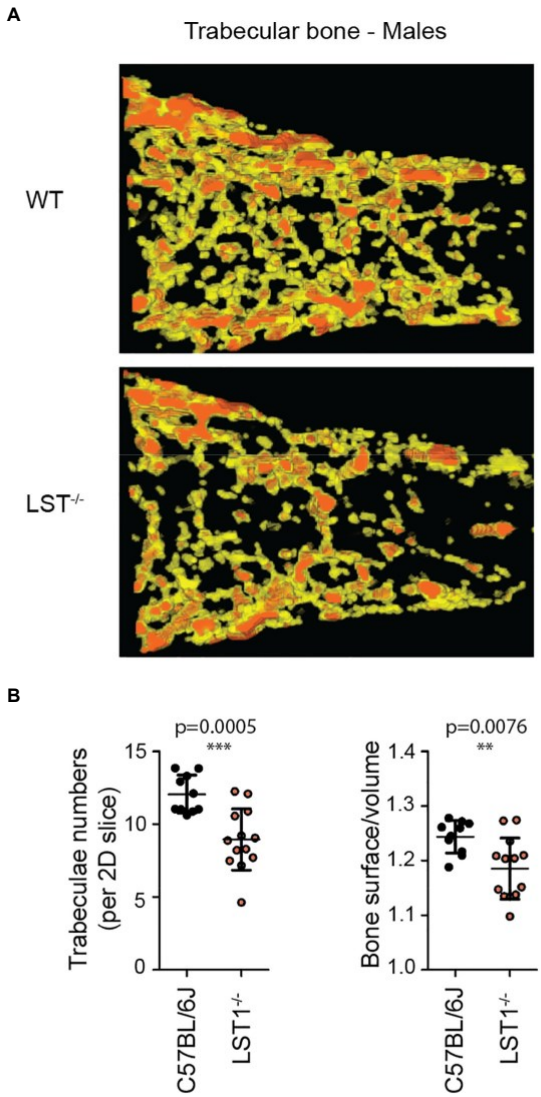

FIGURE 3 | Altered trabecular bone structure in Lst1$^{-/-}$ mice. (A) Representative picture of trabecular bone μCT scan of male bones with diminished numbers of trabeculae in Lst1$^{-/-}$ animals (B) Quantification of trabeculae numbers in 2D plane and ratio between trabecular bone surface and bone volume of WT (n=10) and Lst1$^{-/-}$ (n=13) mice. Lowered ratio is an evidence of reduced trabeculae segmentation. Dots in scatter plots represent biological replicates (hind limbs, i.e. two dots per mouse). Statistics evaluation was done by Student´s t-test (two-tailed, unpaired) and two-sided Grubb´s test. **p ≤ 0.01, ***p ≤ 0.005.

be responsible for reduced percentages of leukocyte subsets described above.

Normal Response of Lst1$^{-/-}$ Mice to LPS Challenge

Data showing increase in LST1 expression level after exposure to pro-inflammatory stimuli indicated that LST1 could be involved in the control of inflammation. In addition, we expected that the differences between WT and Lst1$^{-/-}$ mice will be more apparent under the conditions where LST1 expression is high in WT animals. Therefore, we decided to induce systemic inflammation in WT and Lst1$^{-/-}$ mice by intraperitoneal injection of LPS. In the spleens of both strains, this resulted in increased percentages of B cells and neutrophils and decreased percentages of other cell populations. When comparing WT and Lst1$^{-/-}$ mice, majority of the differences and trends observed in the steady state remained preserved or even enhanced. These included mainly reduced percentages of NK and NKT cells, monocytes, dendritic cells and similar (but outside the borderline of statistical significance) reduction in neutrophils (Figure 5A). Total numbers of splenocytes remained comparable (Figure 5B). In the bone marrow and blood, no additional alterations in Lst1$^{-/-}$ mice were observed (not shown). TNFa and IL-6 levels in the blood at 4 hours after LPS challenge were also not affected by LST1 deficiency (Supplementary Figure S2A). In BMDCs LST1 deficiency did not result in any alteration in LPS-induced cytokine mRNA expression, including IL-1b, IL-6, IL-12, TNFa, IL-15, IL-18, IL-10, and TGFb (Supplementary Figure S2B). Similar results were also obtained in a more limited analysis of BMDM (not shown). In line with these observations, LPS-induced NF-kB activation pathway in BMDM was not affected by LST1 deficiency (Supplementary Figure S2C). Moreover, expression of LST1 binding partners SHP1 and SHP2 also was not influenced by LST1 deficiency in LPS-treated BMDM (Supplementary Figure S2D) Thus, we concluded that LPS challenge did not reveal any new major differences between leukocyte subset composition and behavior in WT and Lst1$^{-/-}$ mice.

Lst1$^{-/-}$ Mice Show Increased Resistance to Acute Colitis Induced by DSS

Previously published article (6) showed elevated expression of LST1 in inflamed colon tissue from a patient with inflammatory bowel disease (IBD). This disease is characterized by an exaggerated immune response to commensal microbiota and breach of intestinal barrier. However, its etiology is still not completely understood. DSS-induced acute colitis is a widely used mouse model of IBD, where myeloid cells play a major role (18, 19). Due to LST1 expression in the target tissues and our data showing effects of LST1 deficiency on several myeloid populations, we decided to induce DSS colitis in Lst1$^{-/-}$ male mice to test the effects of LST1 deficiency on the severity of this disease. We used only males for this experiment, since they are more sensitive to DSS treatment (20). This way we reduced variability and a number of animals needed for this experiment and increased probability of detecting differences between WT and Lst1$^{-/-}$ mice. DSS at concentration 2.5% dissolved in drinking water was administered to the mice for 6 days. Then, DSS solution was changed for plain water for the remaining two days of the experiment (day 7 and 8). Mice were monitored for Lst1 mRNA expression and for number and area of inflammatory lesions, length of the colon and overall disease activity defined by Disease Activity Index – DAI (an integrated value encompassing weight loss, rectal bleeding and stool consistency). Lst1 mRNA expression in the colon tissue did not significantly change during the course of the experiment

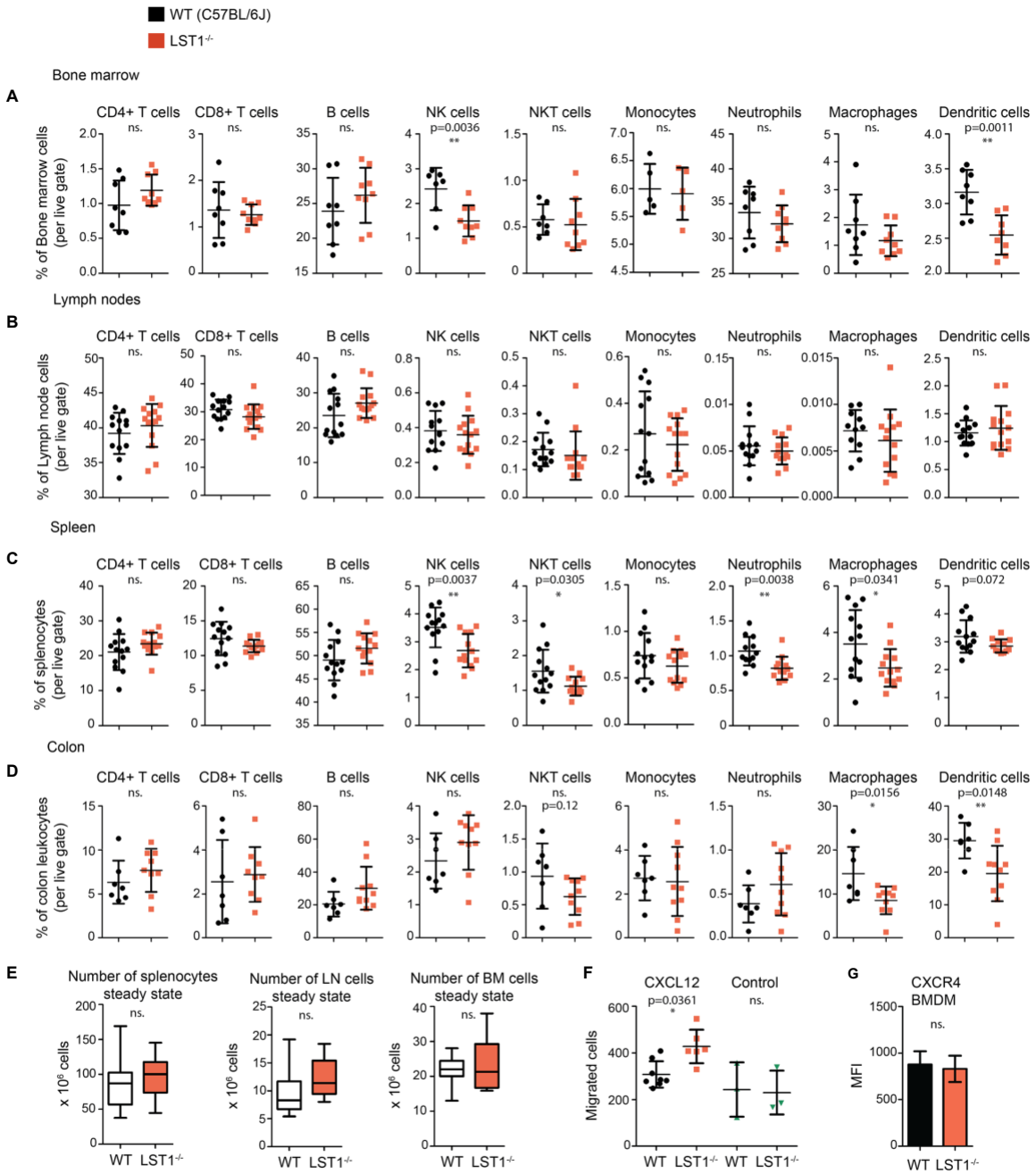

FIGURE 4 | Alterations of leukocyte subset percentages in Lst1$^{-/-}$ mice. (A–D) Steady state percentages of main leukocyte subsets (n=5-15) in the bone marrow (A), lymph nodes (B), spleen (C), and colon (D). Dots in scatter plots represent biological replicates. (E) Absolute numbers of cells in steady state spleen, bone marrow and lymph nodes (n=14-25). (F) Number of bone marrow derived macrophages (BMDM) that after 2 hours migrated towards CXCL12 (100 ng/ml) (n=6-8). Control samples were without CXCL12 chemo-attractant (n=3). (G) Quantification of CXCR4 expression on BMDM surface (n=6). Dots in scatter plots represent biological replicates. Statistics evaluation was done by Student´s t-test (two-tailed, unpaired) and two-sided Grubb´s test. *p ≤ 0.05, **p ≤ 0.01, ns, not significant.

and it was absent from isolated colonic epithelial cells. (Supplementary Figure S3A). Disease activity was similar in both WT and Lst1$^{-/-}$ mice until the day 4 of DSS treatment. However, from the sixth day on, the colitis DAI of Lst1$^{-/-}$ mice appeared significantly lower than that of WT animals (Figure 5C). Lst1$^{-/-}$ mice displayed less severe rectal bleeding, better stool consistency, and milder colon shortening than WT animals (Supplementary Figure S3B). Moreover, areas of damaged colonic epithelium were significantly smaller at days 6 and 8 in the Lst1$^{-/-}$ mice (Figures 5D, E). Expression of pro-inflammatory cytokines detected in colonic lysates was also reduced at day 5 of the experiment (Figure 5F). Surprisingly, these differences in

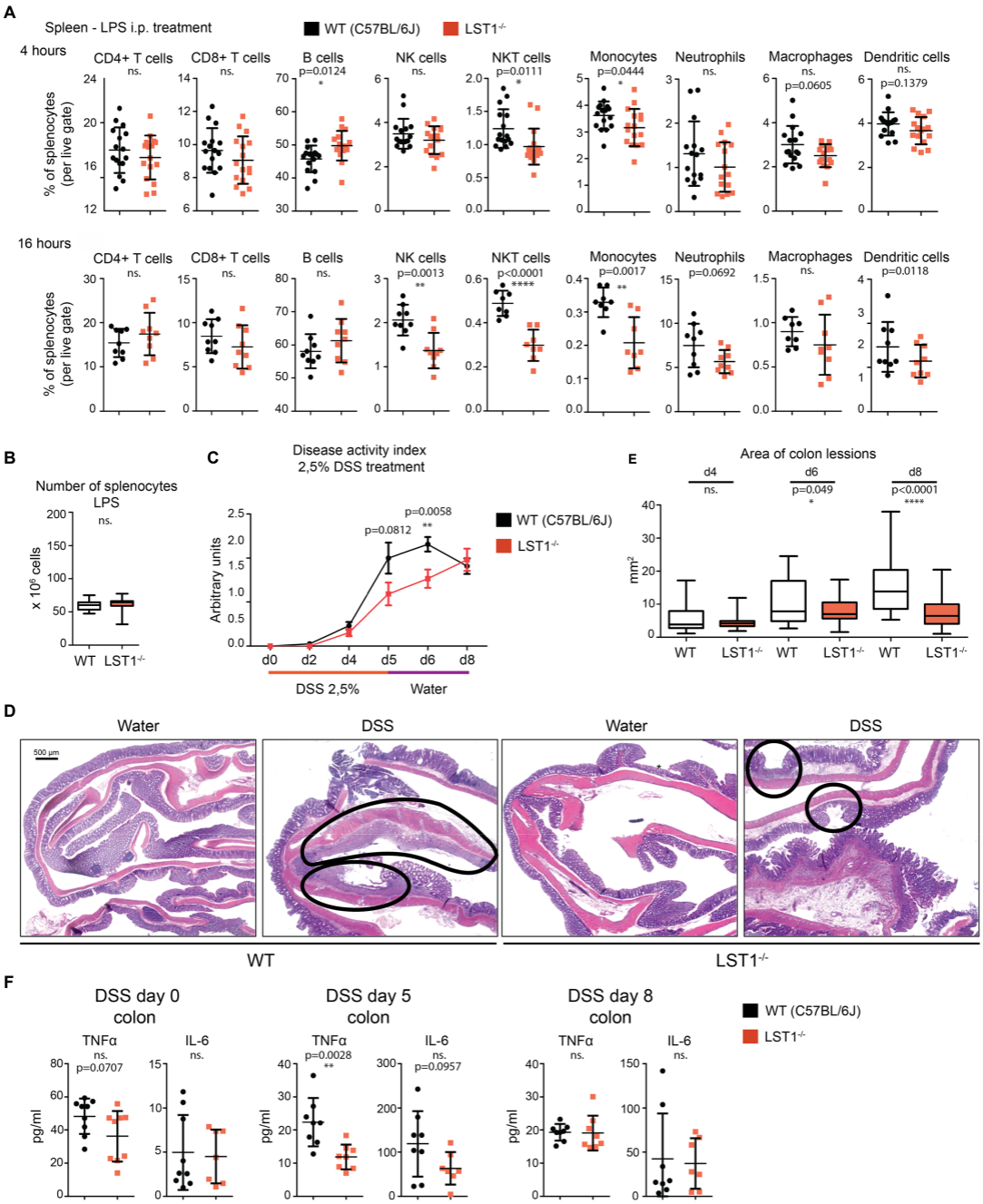

FIGURE 5 | Inflammatory response in Lst1$^{-/-}$ mice. (A) Percentages of major splenocytes subsets 4 and 16 hours after IP injection of LPS (n=8-9). Dots in scatter plots represent biological replicates. (B) Spleen cellularity 16 hours after LPS IP injection. (n=10) (C) DSS-induced colitis disease activity index (n=6-19 per time point) determined as described in Materials and Methods (higher numbers correspond to more severe symptoms) (D) Representative picture of colon sections stained with hematoxylin and eosin from control and DSS challenged WT and Lst1$^{-/-}$ mice. Lesions are highlighted with black line (100x magnification) (E) Quantitative evaluation of the size of colonic lesions induced by DSS treatment during multiple experiments (n=3-5 animals [26-56 lesions] per time point). (F) Concentrations of TNFa and IL-6 in colon homogenates from DSS-treated mice. Statistics evaluation was done by Student´s t-test (two-tailed, unpaired) and two-sided Grubb´s test. **p ≤ 0.01, ****p ≤ 0.0001, ns, not significant.

colon inflammation did not have an impact on body weight loss, which was similar for both genotypes (Supplementary Figure S3B). After changing DSS solution for plain water, WT mice began to recover more rapidly and the DAI reached the same values for both strains at the end of the experiment (Figure 5C). The differences in cytokine expression were also no longer detectable at day 8 (Figure 5F). On the other hand, colonic lesions in Lst1$^{-/-}$ animals were still significantly smaller at that

time point (Figure 5E). Surprisingly, flow cytometry analysis of leukocyte subsets in the colon did not show any striking differences between WT and Lst1$^{-/-}$ mice. DSS treatment resulted in multiple changes in myeloid immune cells percentages (Figure 4D, Supplementary Figure S3C). However, they were similar in both genotypes. In the lymphoid compartment, we observed slightly reduced Lst1$^{-/-}$ T cell percentages on day 5 which then recovered, and increased Lst1$^{-/-}$ CD4 T cell percentages could be observed on days 6 and 8 (Supplementary Figure S3C). Together, these data suggest that LST1 is not just an expression marker in colon samples of IBD patients but likely also an immune system regulator with moderate effects on leukocyte functions, homeostasis and development of colitis.

DISCUSSION

During the past two decades multiple observations have been made of elevated LST1 mRNA and protein levels under inflammatory conditions and during disease, including IBD, rheumatoid arthritis, and influenza (2, 6–8, 14, 21). Location of LST1 gene in MHCIII locus also suggests function in the regulation of immune response or inflammation. In spite of this, its role in these processes or in leukocyte homeostasis remained largely unknown. In this article, we provide data on LST1 protein expression in mice and show alterations in leukocyte subset composition caused by LST1 deficiency at steady state and under inflammatory conditions. In addition we bring evidence of LST1 effects on the severity of experimentally induced acute colitis.

Expression of LST1 protein has previously been analyzed in human cells and tissues with conflicting results. Monoclonal antibody LST1/02 recognizing human but not murine LST1, which was developed in our laboratory, revealed expression pattern largely restricted to the leukocytes of myeloid linage (1), while antibody developed by Schiller et al. showed broad expression pattern including expression outside hematopoietic system (3, 6). Here we describe another monoclonal antibody LST1/06, which recognizes murine LST1. It was generated separately from LST1/02 after immunization with recombinant protein comprising the entire cytoplasmic part of the murine LST1 and its specificity was validated on HEK293 transfectants expressing the murine LST1 (data not shown) and on LST1-deficient mice. The intensity of signals we obtain with LST1/06 antibody on Western blots is generally lower than the intensities we typically observe when using LST1/02 antibody on human samples. However, the reactivities of both antibodies are very similar, showing expression pattern restricted to myeloid cells and an absence in lymphocytes [Figure 2A and (1)]. Publically available data on human LST1 mRNA expression from Human Protein Atlas (22) and on mouse LST1 mRNA from ImmGen consortium (23) both support conclusions reached with our antibodies showing myeloid cell-restricted expression pattern, though low level of expression in other tissues cannot be completely excluded. Consistently with already published data (2, 6), pro-inflammatory stimuli enhanced expression of LST1 in myeloid cells.

LST1 deficiency in the mouse influences leukocyte homeostasis. We observed decreased percentages of myeloid cells in Lst1$^{-/-}$ mice. Significant reduction or at least a similar tendency were almost universally observed for majority of analyzed myeloid cell subsets in the bone marrow, spleen and colon, though the changes were usually relatively modest (Figures 4A–D). Some of the possible explanations of this phenotype include differences in chemokine receptor expression and differences in migration ability. We have analyzed expression of chemokine receptors CCR5, CCR6 and CXCR4 on leukocyte subsets in the spleen, bone marrow and colon at steady state and after DSS treatment, but we did not observe any significant differences between WT and Lst1$^{-/-}$ animals that could explain alterations in frequencies of these subsets (not shown). Intriguingly, Lst1$^{-/-}$ BMDM showed enhanced migration towards CXCL12. While this observation is interesting, it does not show any attenuation of migratory capacity and, as a result, cannot explain the reduced percentages of macrophages and other cell types in the lymphoid organs analyzed in this study. Reduced percentages were frequently observed also for LST1 non-expressing NK and NKT cells (Figures 4A, C). Since NK and NKT cells do not express LST1 the effect on these cells must be indirect, possibly mediated by myeloid cell-derived cytokines or other factors. We have tested mRNA expression of several cytokines that could affect NK cell numbers, including IL-15, IL-18, and IL-12 in Lst1$^{-/-}$ BMDCs and BMDMs. However, their levels were not altered in these cells (Supplementary Figure S2B and not shown). It is also possible that other cytokines were involved or that the NK cell supporting cytokine production in vivo was attenuated due to the diminished numbers of myeloid cells producing these cytokines rather than due to the reduction in cytokine expression levels.

Immune system of the gut and gut microbiota are known to have effects on bone homeostasis (24, 25). Germ-free mice were shown to have increased trabecular bone volume while gut dysbiosis after antibiotic treatment results in reduction in trabecular bone volume (26, 27). One could speculate that effects of LST1 on the activity of the immune system of the gut are linked to the alterations in trabecular bone structure observed in the present study. The experiments with the mouse model of DSS induced colitis suggested altered response to intestinal microbiota in Lst1$^{-/-}$ mice. On the other hand, we have not detected any changes in pro-inflammatory cytokine production in the steady state gut in Lst1$^{-/-}$ mice that could be a sign of altered activity of the gut immune system. In addition, during DSS-induced colitis, LST1 deficiency had mitigating effects on gut inflammation further arguing against the possibility that the lack of LST1 in the gut promoted inflammation-driven changes in trabecular bone structure. Chronic inflammation in other parts of the body could potentially also affect various parameters of the bone. However, so far we have not found any evidence of chronic inflammation in Lst1$^{-/-}$ mice. Finally, it is also possible that LST1 deficiency in the osteoclasts leads to alterations in their function and defects in trabecular bone formation. Currently available data do not provide sufficient support for any of these explanations and further research is needed to clarify this issue.

A number of polymorphisms have been detected in human LST1 gene (5). Some of these polymorphisms, thought to affect mainly LST1 gene expression and splicing, are associated with inflammatory conditions such as psoriasis, nephritis in systemic lupus erythromatosus and rheumatoid arthritis, or graft versus host disease severity (5). Moreover, expression of LST1 is increased in rheumatoid arthritis patients (7) and in colon samples from patients with inflammatory bowel disease (IBD) (6). These connections to IBD and various other inflammatory conditions, prompted us to test the effects of LST1 deficiency on inflammatory response and, in particular, on DSS-induced colitis in mice. DSS-induced collitis is one of the most widely used models of human IBD (28). Its overall symptoms and course are similar to this disease (19). DSS ingested by experimental animals with drinking water is cleaved into smaller fragments, penetrates colon barrier and dissolves the mucus layer. This leads to infiltration, colonization and damaging of colon epithelium by bacteria and viruses. Colonization of colon epithelia by bacteria is followed by infiltration of myeloid immune cells (neutrophils, dendritic cells, monocytes), causing acute colon inflammation and its symptoms (blood in the stool, colon shortage, diarrhea). Lymphoid cells (T, B, NK cells) and their interplay with myeloid immune cells also showed important impact on the severity of acute colitis (29–35).

Strikingly, Lst1$^{-/-}$ mice showed milder and delayed course of the disease. Disease Activity Index was significantly lower on the 6th day of DSS treatment. These results were also confirmed by histology, which showed less severe destruction of colon epithelium (Figures 5D, E). In the final part of the experiment, after changing DSS solution for plain water on day 6, DAI of WT animals improved while in the Lst1$^{-/-}$ mice DAI kept rising even after DSS solution was changed for plain water. On day 8, DAI reached the same severity as already improving WT mice. Data from mouse and patient samples show that resident and newly infiltrating myeloid immune cells are responsible for the first wave of immune response during DSS induced colitis (36). Reduced myeloid cell percentages in Lst1$^{-/-}$ colon and lymphatic tissue might explain the slower kinetics of disease development. On the other hand, LST1 may also be contributing to the resolution of inflammation. This could explain why the DAI in Lst1$^{-/-}$ mice was still raising after day 6, when the WT mice were already in the process of healing. However, there are currently no data addressing the role of LST1 in the resolution of inflammation. Additional possibilities include direct effects of LST1 expressed by epithelial cells on their barrier function or compensatory changes in SHP1 and SHP2 expression in myeloid cells. However, we could not detect any Lst1 mRNA in colonic epithelial cells nor any compensatory changes in SHP1/2 expression in LPS-treated BMDM. On the other hand, we observed significant reduction in TNFa expression in the gut on day 5 of DSS colitis and a similar trend for IL-6. TNFa is known to be involved in the pathogenesis of IBD and can be upstream of IL-6 expression (37). It is produced not only by myeloid cells, but also by Th1 cells. Myeloid cell numbers in the gut and their ability to produce TNFa *in vitro* were not affected by LST1 deficiency. On the other hand, overall T cell numbers were reduced in the gut on day 5 of DSS colitis. Since T cells do not express LST1, their reduced numbers could be the result of altered chemokine expression by myeloid cells or altered kinetics of dendritic cell-mediated antigen presentation, T cell activation or differentiation in Lst1$^{-/-}$ mice. Any of these changes could lead to transient reduction in Th1 cell numbers in the gut and reduced TNFa production. However, these hypotheses have to be further elucidated in future studies. Molecules and molecular mechanisms affecting the course and outcome of DSS-induced collitis often play a role in human IBD (19). Our results suggest that defects in LST1 expression and LST1 polymorphisms should be considered in future studies of this and related diseases in humans.

DATA AVAILABILITY STATEMENT

The raw data supporting the conclusions of this article will be made available by the authors, without undue reservation.

ETHICS STATEMENT

The animal study was reviewed and approved by Animal Care and Use Committee of the Institute of Molecular Genetics.

AUTHOR CONTRIBUTIONS

MF and JT with contribution from NP, JK, JB and TS performed majority of experiments and data analysis. JT, JB, KV and MF performed analysis of mouse colitis model. NP carried out analysis of LST1 and SHP1/2 expression analysis and ELISA assays. MF, JK, TS and NP performed flow cytometry analysis of healthy mice. FS and JPr carried out mCT analysis. JPo and PA generated LST1/06 hybridoma and corresponding monoclonal antibody. TB, JPr and RS contributed to experimental design and data analysis. BM assisted with Lst1$^{-/-}$ mice rederivation and preliminary phenotype analysis. TB, BM and RS secured funding and supervised the study. TB and MF wrote the paper. All authors contributed to the article and approved the submitted version.

FUNDING

This study was supported by Czech Science Foundation (GACR, project P302-12-G101) and by institutional funding from Institute of Molecular Genetics, CAS (RVO68378050). The results were obtained using the research infrastructure of the Czech Center for Phenogenomics supported by the projects of the Ministry of Education, Youth and Sports (MEYS) LM2018126 and OP RDI CZ.1.05/2.1.00/19.0395, and CZ.1.05/ 1.1.00/02.0109 provided by the MEYS and ERDF, and OP RDE CZ.02.1.01/0.0/0.0/16_013/0001789 by MEYS and ESIF. Centre d'Immunophénomique is supported by the Investissement

d'Avenir program PHENOMIN (French National Infrastructure for mouse Phenogenomics; ANR-10-INBS-07).

ACKNOWLEDGMENTS

We want to acknowledge staff of the Institute of Molecular Genetics flow cytometry core facility for excellent support and help. We also thank Tomas Brabec from the Laboratory of Immunobiology, Institute of Molecular Genetics CAS, Prague, for help with colonic epithelium isolation. Finally, we thank nonparticipant members of Laboratory of Leukocyte Signalling and Laboratory of Hematooncology for fruitful discussion, ideas and friendly working environment.

SUPPLEMENTARY MATERIAL

The Supplementary Material for this article can be found online at: https://www.frontiersin.org/articles/10.3389/fimmu.2021.618332/full#supplementary-material

REFERENCES

1. Draber P, Stepanek O, Hrdinka M, Drobek A, Chmatal L, Mala L, et al. LST1/A is a Myeloid Leukocyte-Specific Transmembrane Adaptor Protein Recruiting Protein Tyrosine Phosphatases SHP-1 and SHP-2 to the Plasma Membrane. J Biol Chem (2012) 287(27):22812–21. doi: 10.1074/jbc.M112.339143
2. de Baey A, Fellerhoff B, Maier S, Martinozzi S, Weidle U, Weiss EH. Complex Expression Pattern of the TNF Region Gene LST1 Through Differential Regulation, Initiation, and Alternative Splicing. Genomics (1997) 45(3):591– 600. doi: 10.1006/geno.1997.4963
3. Schiller C, Nitschke MJ, Seidl A, Kremmer E, Weiss EH. Rat Monoclonal Antibodies Specific for LST1 Proteins. Hybridoma (Larchmt) (2009) 28 (4):281–6. doi: 10.1089/hyb.2009.0021
4. Rollinger-Holzinger I, Eibl B, Pauly M, Griesser U, Hentges F, Auer B, et al. LST1: A Gene With Extensive Alternative Splicing and Immunomodulatory Function. J Immunol (2000) 164(6):3169–76. doi: 10.4049/jimmunol.164.6.3169
5. Weidle UH, Rohwedder I, Birzele F, Weiss EH, Schiller C. LST1: A Multifunctional Gene Encoded in the MHC Class III Region. Immunobiology (2018) 223(11):699–708. doi: 10.1016/j.imbio.2018.07.018
6. Heidemann J, Kebschull M, Tepasse PR, Bettenworth D. Regulated Expression of Leukocyte-Specific Transcript (LST) 1 in Human Intestinal Inflammation. Inflamm Res (2014) 63(7):513–7. doi: 10.1007/s00011-014-0732-6
7. Fritsch-Stork RD, Silva-Cardoso SC, Groot Koerkamp MJ, Broen JC, Lafeber FF, Bijlsma JW. Expression of ERAP2 and LST1 is Increased Before Start of Therapy in Rheumatoid Arthritis Patients With Good Clinical Response to Glucocorticoids. Clin Exp Rheumatol (2016) 34(4):685–9.
8. Yau AC, Tuncel J, Haag S, Norin U, Houtman M, Padyukov L, et al. Conserved 33-kb Haplotype in the MHC Class III Region Regulates Chronic Arthritis. Proc Natl Acad Sci USA (2016) 113(26):E3716–24. doi: 10.1073/pnas.1600567113
9. Nalabolu SR, Shukla H, Nallur G, Parimoo S, Weissman SM. Genes in a 220-kb Region Spanning the TNF Cluster in Human MHC. Genomics (1996) 31 (2):215–22. doi: 10.1006/geno.1996.0034
10. D'Aloia A, Berruti G, Costa B, Schiller C, Ambrosini R, Pastori V, et al. RalGPS2 is Involved in Tunneling Nanotubes Formation in 5637 Bladder Cancer Cells. Exp Cell Res (2018) 362(2):349–61. doi: 10.1016/ j.yexcr.2017.11.036
11. Schiller C, Huber JE, Diakopoulos KN, Weiss EH. Tunneling Nanotubes Enable Intercellular Transfer of MHC Class I Molecules. Hum Immunol (2013) 74(4):412–6. doi: 10.1016/j.humimm.2012.11.026
12. Schiller C, Diakopoulos KN, Rohwedder I, Kremmer E, von Toerne C, Ueffing M, et al. LST1 Promotes the Assembly of a Molecular Machinery Responsible for Tunneling Nanotube Formation. J Cell Sci (2013) 126(Pt 3):767–77. doi: 10.1242/jcs.114033
13. Nedelko T, Kollmus H, Klawonn F, Spijker S, Lu L, Hessman M, et al. Distinct Gene Loci Control the Host Response to Influenza H1N1 Virus Infection in a Time-Dependent Manner. BMC Genomics (2012) 13:411. doi: 10.1186/1471-2164-13-411
14. Leist SR, Kollmus H, Hatesuer B, Lambertz RL, Schughart K. Lst1 Deficiency has a Minor Impact on Course and Outcome of the Host Response to Influenza A H1N1 Infections in Mice. Virol J (2016) 13:17. doi: 10.1186/ s12985-016-0471-0
15. Kralova J, Glatzova D, Borna S, Brdicka T. Expression of Fluorescent Fusion Proteins in Murine Bone Marrow-Derived Dendritic Cells and Macrophages. J Vis Exp (2018) 140:e58081. doi: 10.3791/58081
16. Brauer R, Tureckova J, Kanchev I, Khoylou M, Skarda J, Prochazka J, et al. MMP-19 Deficiency Causes Aggravation of Colitis Due to Defects in Innate Immune Cell Function. Mucosal Immunol (2016) 9(4):974–85. doi: 10.1038/mi.2015.117
17. Dickinson ME, Flenniken AM, Ji X, Teboul L, Wong MD, White JK, et al. High-Throughput Discovery of Novel Developmental Phenotypes. Nature (2016) 537(7621):508–14. doi: 10.1038/nature19356
18. Dieleman LA, Ridwan BU, Tennyson GS, Beagley KW, Bucy RP, Elson CO. Dextran Sulfate Sodium-Induced Colitis Occurs in Severe Combined Immunodeficient Mice. Gastroenterology (1994) 107(6):1643–52. doi: 10.1016/0016-5085(94)90803-6
19. Eichele DD, Kharbanda KK. Dextran Sodium Sulfate Colitis Murine Model: An Indispensable Tool for Advancing Our Understanding of Inflammatory Bowel Diseases Pathogenesis. World J Gastroenterol (2017) 23(33):6016–29. doi: 10.3748/wjg.v23.i33.6016
20. Mahler M, Bristol IJ, Leiter EH, Workman AE, Birkenmeier EH, Elson CO, et al. Differential Susceptibility of Inbred Mouse Strains to Dextran Sulfate Sodium-Induced Colitis. Am J Physiol (1998) 274(3):G544–51. doi: 10.1152/ ajpgi.1998.274.3.G544
21. Pommerenke C, Wilk E, Srivastava B, Schulze A, Novoselova N, Geffers R, et al. Global Transcriptome Analysis in Influenza-Infected Mouse Lungs Reveals the Kinetics of Innate and Adaptive Host Immune Responses. PloS One (2012) 7(7):e41169. doi: 10.1371/journal.pone.0041169
22. Uhlén M, Fagerberg L, Hallström BM, Lindskog C, Oksvold P, Mardinoglu A, et al. Proteomics. Tissue-based Map of the Human Proteome. Science (2015) 347(6220):1260419. doi: 10.1126/science.1260419
23. Heng TS, Painter MW. The Immunological Genome Project: Networks of Gene Expression in Immune Cells. Nat Immunol (2008) 9(10):1091–4. doi: 10.1038/ni1008-1091
24. Cooney OD, Nagareddy PR, Murphy AJ, Lee MKS. Healthy Gut, Healthy Bones: Targeting the Gut Microbiome to Promote Bone Health. Front Endocrinol (Lausanne) (2021) 11:620466. doi: 10.3389/fendo.2020.620466
25. Castaneda M, Strong JM, Alabi DA, Hernandez CJ. The Gut Microbiome and Bone Strength. Curr Osteoporos Rep (2020) 18(6):677–83. doi: 10.1007/ s11914-020-00627-x
26. Sjögren K, Engdahl C, Henning P, Lerner UH, Tremaroli V, Lagerquist MK, et al. The Gut Microbiota Regulates Bone Mass in Mice. J Bone Miner Res (2012) 27(6):1357–67. doi: 10.1002/jbmr.1588
27. Schepper JD, Collins FL, Rios-Arce ND, Raehtz S, Schaefer L, Gardinier JD, et al. Probiotic Lactobacillus Reuteri Prevents Postantibiotic Bone Loss by Reducing Intestinal Dysbiosis and Preventing Barrier Disruption. J Bone Miner Res (2019) 34(4):681–98. doi: 10.1002/jbmr.3635
28. Kiesler P, Fuss IJ, Strober W. Experimental Models of Inflammatory Bowel Diseases. Cell Mol Gastroenterol Hepatol (2015) 1(2):154–70. doi: 10.1016/ j.jcmgh.2015.01.006
29. Kwon SH, Seo EB, Lee SH, Cho CH, Kim SJ, Kim SJ, et al. T Cell-Specific Knockout of STAT3 Ameliorates Dextran Sulfate Sodium-Induced Colitis by Reducing the Inflammatory Response. Immune Netw (2018) 18(4):e30. doi: 10.4110/in.2018.18.e30
30. Troy AE, Zaph C, Du Y, Taylor BC, Guild KJ, Hunter CA, et al. IL-27 Regulates Homeostasis of the Intestinal CD4+ Effector T Cell Pool and Limits

Intestinal Inflammation in a Murine Model of Colitis. J Immunol (2009) 183 (3):2037–44. doi: 10.4049/jimmunol.0802918

31. Yanaba K, Yoshizaki A, Asano Y, Kadono T, Tedder TF, Sato S. IL-10-Producing Regulatory B10 Cells Inhibit Intestinal Injury in a Mouse Model. Am J Pathol (2011) 178(2):735–43. doi: 10.1016/j.ajpath.2010.10.022
32. Xu X, Wang Y, Zhang B, Lan X, Lu S, Sun P, et al. Treatment of Experimental Colitis by Endometrial Regenerative Cells Through Regulation of B Lymphocytes in Mice. Stem Cell Res Ther (2018) 9(1):146. doi: 10.1186/s13287-018-0874-5
33. Yoshihara K, Yajima T, Kubo C, Yoshikai Y. Role of Interleukin 15 in Colitis Induced by Dextran Sulphate Sodium in Mice. Gut (2006) 55(3):334–41. doi: 10.1136/gut.2005.076000
34. Wang F, Peng PL, Lin X, Chang Y, Liu J, Zhou R, et al. Regulatory Role of NKG2D+ NK Cells in Intestinal Lamina Propria by Secreting Double-Edged Th1 Cytokines in Ulcerative Colitis. Oncotarget (2017) 8(58):98945–52. doi: 10.18632/oncotarget.22132
35. Hall LJ, Murphy CT, Quinlan A, Hurley G, Shanahan F, Nally K, et al. Natural Killer Cells Protect Mice From DSS-induced Colitis by Regulating Neutrophil Function Via the NKG2A Receptor. Mucosal Immunol (2013) 6(5):1016–26. doi: 10.1038/mi.2012.140
36. Liu H, Dasgupta S, Fu Y, Bailey B, Roy C, Lightcap E, et al. Subsets of Mononuclear Phagocytes are Enriched in the Inflamed Colons of Patients With IBD. BMC Immunol (2019) 20(1):42. doi: 10.1186/s12865-019-0322-z
37. Műzes G, MolnárB, Tulassay Z, Sipos F. Changes of the Cytokine Profile in Inflammatory Bowel Diseases. World J Gastroenterol (2012) 18(41):5848–61. doi: 10.3748/wjg.v18.i41.5848

Conflict of Interest: The authors declare that the research was conducted in the absence of any commercial or financial relationships that could be construed as a potential conflict of interest.

Supplementary Material

Supplementary Figures

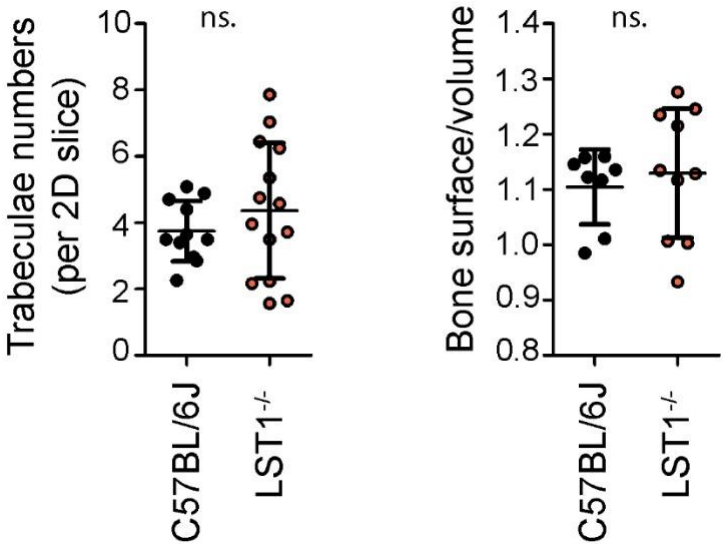

Supplementary figure S1. Trabecular bone structure in *Lst1*$^{-/-}$ female mice. Quantification of trabeculae numbers in 2D plane and ratio between trabecular bone surface and bone volume did not show any differences between female WT and *Lst1*$^{-/-}$ (n=8-14) mice. Statistics evaluation was performed by Student´s t-test (two-tailed, unpaired) and two-sided Grubb´s test.

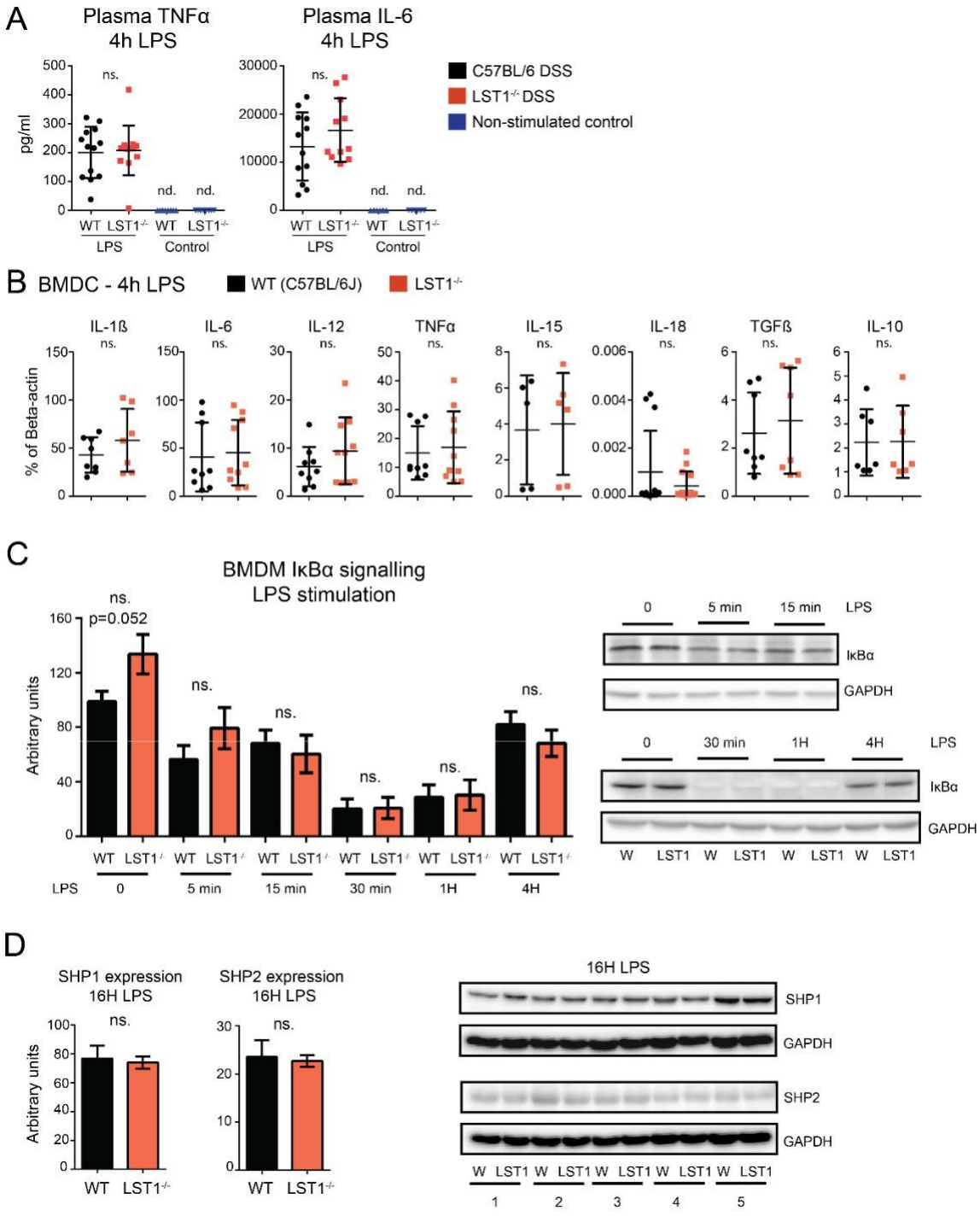

Supplementary figure S2. Inflammatory response in LST1$^{-/-}$ mice. (**A**) TNFα and IL-6 levels in plasma measured by ELISA 4 hours after intraperitoneal LPS injection (n=11- 13) (**B**) Cytokine mRNA expression measured by quantitative real-time PCR in BMDC after 4 hours of stimulation with LPS (100 ng/ml), expression was normalized to β-actin. (n=5-13) (**C**) IκBα degradation in BMDM stimulated with LPS (100 ng/ml). Quantification and representative immunoblot (n=4- 9) (**D**) Expression of SHP1 and SHP2 phosphatases in BMDM after 16 hour incubation with LPS (100 ng/ml) (n=5). Statistics evaluation was done by Student´s t-test (two-tailed, unpaired), One-way ANOVA with Tukey post test and two-sided Grubb´s test.

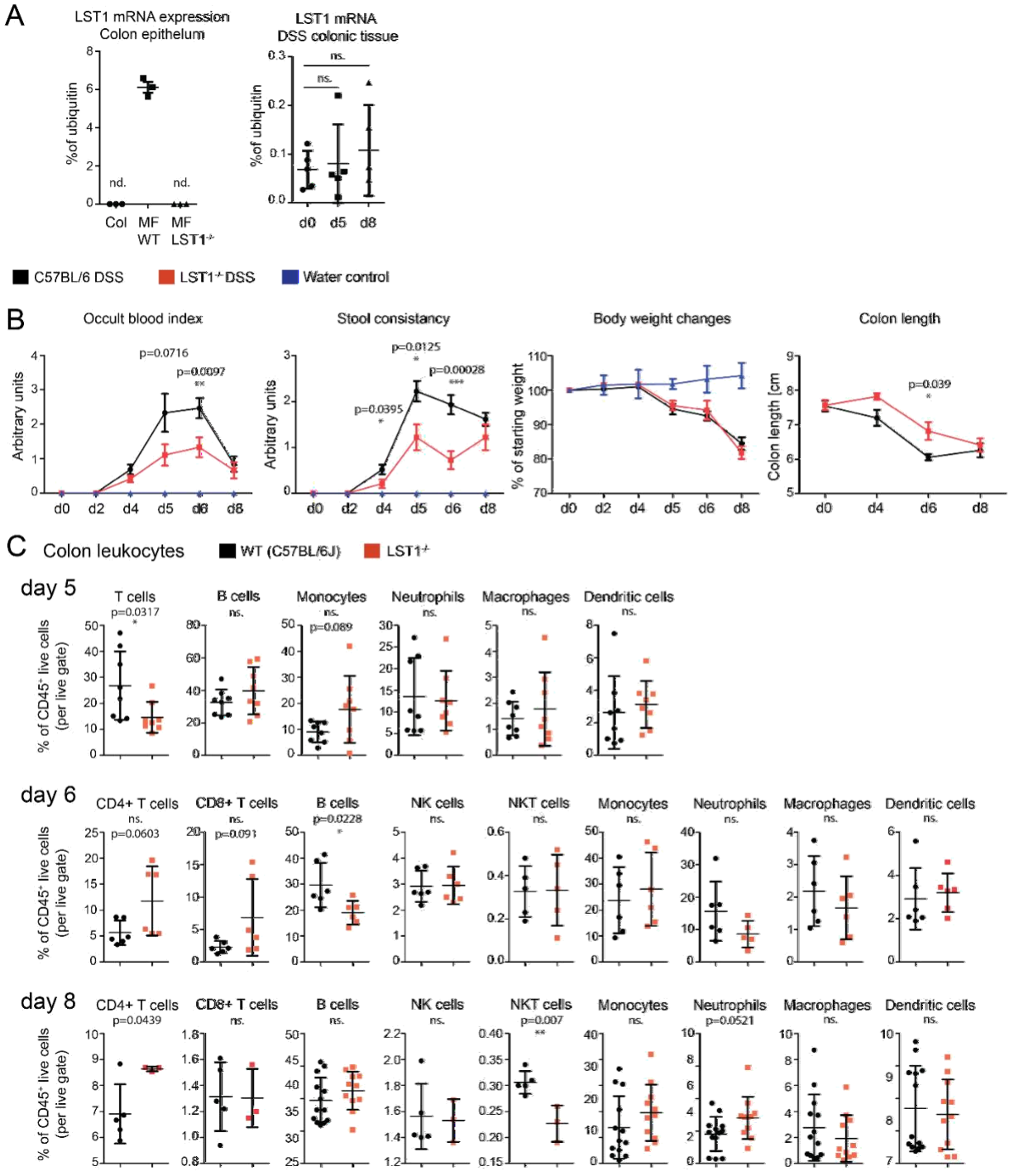

Supplementary figure S3. DSS-induced colitis in LST1$^{-/-}$ mice. (**A**) Expression of LST1 mRNA in colon epithelium cells compared to the WT macrophages and LST1$^{-/-}$ macrophages (n=2, technical triplicates from representative experiment are shown), and of LST1 mRNA in colonic tissue from DSS-treated mice (n=5), expression was normalized to ubiquitin. (**B**) Parameters used for calculation of disease activity index in Figure 5C and changes in colon length, an additional parameter characterizing the disease severity (n=5-20). (**C**) Leukocyte subsets present in the colon at day 5, 6 and day 8 after the initiation of DSS treatment (n=3-13). Statistics evaluation was done by Student´s t-test (two-tailed, unpaired), One-way ANOVA with Tukey post test and two-sided Grubb´s test.

Supplementary tables

Supplementary Table S1. List of flow cytometry antibodies

Marker	Fluorophore – Company - Clone	Fluorophore – Company - Clone
CD8a	PE-CF594 – BD Biosciences – 53-6.7	FITC – ExBio – 53-6.7
NK1.1	APC – BD Biosciences – PK136	PB – Biolegend – PK136
Ly6G	BV421 – BD Biosciences – 1A8	e450 – Biolegend – 1A8
	BV510 – Biolegend – 1A8	
CD19	BV510 – BD Biosciences – 1D3	APC – Biolegend – 605
Ly6C	FITC – BD Biosciences – AL-21	PE-Cy7 – Biolegend – HK1.4
CD11b	PerCP-Cy5.5 – Biolegend – M1/70	PE – Biolegend – M1/70
F4/80	PE-Dazzle594 – Biolegend – BM8	A488 – Biolegend – BM8
CD11c	PE-Cy7 – BD Biosciences – HL3	APC – Biolegend – N418
Fc block	2.4g2 supernatant (produced in lab.)	2G4 – BD Biosciences
CD45	A700 – Biolegend – 30-F11	APC – Biolegend – 104
CD44	PE – Biolegend – IM7	
CD49	BV510 – BD Biosciences – R1-2	
CD5	BV421– BD Biosciences – 53-7.3	
CD4	FITC – BD Biosciences – RM4-5	
Klrg1	PerCP-Cy5.5 – Biolegend – 2F1/KLRG1	
γδTCR	BV605 – BD Biosciences – GL3	
GITR	BV711 – BD Biosciences – DTA-1	
CD25	PE-CY7 – BD Biosciences – PC61	
CD62L	APC-CY7– BD Biosciences – MEL14	
CD21/CD35	PE – BD Biosciences – 7G6	
Bst2	BV605 – Biolegend – 927	
CXCR4	APC – Biolegend – L276F12	
CCR5	PE – Biolegend – HM-CCR5	
CCR6	BV785 – Biolegend – 29-2L17	
CCR7	APC-eFluor 780 – eBioscience – 4B12	
sCD23	BV711 – BD Biosciences – B3B4	
MHCII	APC-Cy7 – Biolegend – M5/114.15.2	
EpCAM	APC – Biolegend - G8.8	
Ghost Dye™	UV450 – Tonbo biosciences –13-0868	

Supplementary Table 2. List of qRT-PCR primers

	Forward	Reverse
IL-1β	TGT-AAT-GAA-AGA-CGG-CAC-ACC	TCT-TCT-TTG-GGT-ATT-GCT-TGG
IL-6	TGA-TGG-ATG-CTA-CCA-AAC-TGG	TTC-ATG-TAC-TCC-AGG-TAG-CTA-TGG
IL-10	CAG-AGC-CAC-ATG-CTC-CTA-GA	TGT-CCA-GCT-GGT-CCT-TTG-TT
IL-12	CCA-GGT-GTC-TTA-GCC-AGT-CC	GCA-GTG-CAG-GAA-TAA-TGT-TTC-A
IL-15	AAC-AGC-TCA-GAG-AGG-TCA-GGA	CCA-TGA-AGA-GGC-AGT-GCT-TT
IL-18	GAC-AAC-ACG-CTT-TAC-TTT-ATA-CGG	CAG-TGA-AGT-CGG-CCA-AAG-TT
TNFα	TCT-TCT-CAT-TCC-TGC-TTG-TGG	GGT-CTG-GGC-CAT-AGA-ACT-GA
TGFβ	TGG-AGC-AAC-ATG-TGG-AAC-TC	CAG-CAG-CCG-GTT-ACC-AAG
Beta-actin	GAT-CTG-GCA-CCA-CAC-CTT-CT	GGG-GTG-TTG-AAG-GTC-TCA-AA
Ubiquitin	ATG-TGA-AGG-CCA-AGA-TCC-AG	TAA-TAG-CCA-CCC-CTC-AGA-CG
LST1	CTG-ATG-ACA-ATG-GGA-TCT-GGT	CAG-GAT-GAT-GAC-AAG-CAG-GA

THE JOURNAL OF BIOLOGICAL CHEMISTRY VOL. 291, NO. 32, pp. 16530 –16540, August 5, 2016

The Transmembrane Adaptor Protein SCIMP Facilitates Sustained Dectin-1 Signaling in Dendritic Cells*□S

Received for publication, January 21, 2016, and in revised form, June 3, 2016 Published, JBC Papers in Press, June 10, 2016, DOI 10.1074/jbc.M116.717157

Jarmila Kralova‡1, Matej Fabisik‡1, Jana Pokorna§, Tereza Skopcova‡, Bernard Malissen¶2, and Tomas Brdicka‡3

From the Laboratories of ‡Leukocyte Signaling and §Molecular Immunology, Institute of Molecular Genetics, Academy of Sciences of the Czech Republic, 14220 Prague, Czech Republic and the ¶Centre d'Immunophénomique, PHENOMIN-CIPHE, Aix Marseille Université UM2, INSERM US012, CNRS UMS3367, 13288 Marseille, France

Transmembrane adaptor proteins are molecules specialized in recruiting cytoplasmic proteins to the proximity of the cell membrane as part of the signal transduction process. A member of this family, SLP65/SLP76, Csk-interacting membrane protein (SCIMP), recruits a complex of SLP65/SLP76 and Grb2 adaptor proteins, known to be involved in the activation of PLC 1/2, Ras, and other pathways. SCIMP expression is restricted to anti-gen-presenting cells. In a previous cell line-based study, it was shown that, in B cells, SCIMP contributes to the reverse signal-ing in the immunological synapse, downstream of MHCII glyco-proteins. There it mainly facilitates the activation of ERK MAP kinases. However, its importance for MHCII glycoprotein-de-pendent ERK signaling in primary B cells has not been analyzed. Moreover, its role in macrophages and dendritic cells has remained largely unknown. Here we present the results of our analysis of SCIMP-deficient mice. In these mice, we did not observe any defects in B cell signaling and B cell-dependent responses. On the other hand, we found that, in dendritic cells and macrophages, SCIMP expression is up-regulated after exposure to GM-CSF or the Dectin-1 agonist zymosan. Moreover, we found that SCIMP is strongly phosphorylated after Dectin-1 stimulation and that it participates in signal transduc-tion downstream of this important pattern recognition recep-tor. Our analysis of SCIMP-deficient dendritic cells revealed that SCIMP specifically contributes to sustaining long-term MAP kinase signaling and cytokine production downstream of Dectin-1 because of an increased expression and sustained phos-phorylation lasting at least 24 h after signal initiation.

Dectin-1 is a pattern recognition receptor from the C-type lectin receptor family (1). It is expressed in macrophages, den-dritic cells, neutrophils, and a subset of T and B cells (2– 4). Through its carbohydrate recognition domain, it specifically recognizes *b*-1,3-glucan (5), which is a typical component of fungal cell walls (6). Dectin-1 is considered a major receptor for *b*-glucans and plays an important role in the defense against various species of pathogenic fungi in mice, including *Candida albicans, Aspergillus fumigatus, and Pneumocystis carinii* (7–11). The importance of dectin-1 for antifungal defense has also been demonstrated by studies of human patients with dis-rupted dectin-1 function who display increased mucosal colo-nization with *Candida* species and suffer from recurrent muco-cutaneous fungal infections (12, 13).

Dectin-1 signaling is initiated by phosphorylation of the hemITAM motif in its intracellular tail, leading to the recruitment and activation of the protein tyrosine kinase Syk. This is followed by sequential activation of PLC*g*2 and PKC*d*. Stimulation of this pathway as well as of additional Syk-independent pathways results in the activation of the transcription factors NF-*k*B, nuclear factor of activated T cells (NFAT), and IRF1/5 and initiation of signaling by the MAP kinases ERK, p38, and JNK, which then contribute to downstream cellular responses (14 –16). Activation of Dectin-1 leads to phagocytosis of fungi or any other *b*-glucan-containing particles. In addition, it also triggers the production of reactive oxygen species and proin-flammatory cytokines (7, 17, 18). Cytokines produced in response to Dectin-1 stimulation also promote Th1 and Th17 polarization of helper T cells necessary for defeating fungal infection (14 –16). Interestingly, only *b*-glucan in the form of particles can elicit the full activity of Dectin-1, whereas soluble *b*-glucans, which also bind to the receptor, lack strong activat-ing properties and can inhibit the responses to particulate *b*-glucan (19). The difference is thought to be caused by the ability of particulate *b*-glucan to induce the formation of a phagocytic synapse that excludes CD45 and CD148 phospha-tases (19).

As any important receptor, Dectin-1 is tightly regulated. This regulation occurs not only at the level of signaling pathways but also at the level of expression. Dectin-1 is highly up-regulated after IL-4, IL-13, and GM-CSF treatment, whereas IL-10, LPS, and dexamethasone down-regulate its expression (20).

To elicit the full antifungal immune response, Dectin-1 cooperates with several TLRs[4] (most importantly TLR2) (17). Its function is also complemented by other C-type lectin recep-tors, such as Dectin-2, which recognizes mannan structures in

* This work was supported by Czech Science Foundation (GACR, Project P302/12/1712) and received institutional funding from IMG ASCR (RVO 68378050). The authors declare that they have no conflicts of interest with the contents of this article.

□S This article contains supplemental Movie 1.

[1] Supported in part by the Faculty of Science, Charles University, Prague.
[2] Supported by PHENOMIN CIPHE.

[3] To whom correspondence should be addressed: Laboratory of Leukocyte Signaling, Institute of Molecular Genetics of the Academy of Sciences of the Czech Republic, Videnska 1083, 14220 Prague, Czech Republic. Tel.: 420-241062467; Fax: 420-244472282; E-mail: tomas.brdicka@img.cas.cz.

[4] The abbreviations used are: TLR, Toll-like receptor; gp, glycoprotein; SCIMP, SLP76/SLP65-interacting membrane adaptor protein; APC, antigen-pre-senting cell; CFSE, 5-(and 6)-carboxyfluorescein diacetate succinimidyl ester; NP, 4-hydroxy-3-nitrophenylacetyl; BMDC, bone marrow-derived dendritic cell; BMMF, bone marrow-derived macrophage; IMDM, Iscove's modified Dulbecco's medium.

fungal cell walls (1). In addition, Dectin-1 interacts with tetras-panin molecules, which form the basis of tetraspanin-enriched microdomains and were suggested to be involved in Dectin-1 trafficking (21–23). However, the effects of tetraspanins on Dectin-1 signal transduction are at present unclear.

Tetraspanin-enriched microdomains in some Dectin-1-ex-pressing cells also interact with MHCII glycoproteins (MHCIIgp) and a small palmitoylated transmembrane adaptor protein, SCIMP (23–25). Expression of SCIMP is highly specific for the tissues of the immune system, where it is confined to the pro-fessional antigen-presenting cells (dendritic cells, B cells, and macrophages). In B cells, SCIMP is phosphorylated after MHCIIgp cross-linking, and it is thought to be involved in the reverse signaling at the APC side of the immunological synapse. In the K46 B cell line, it was shown to be mainly responsible for supporting ERK signaling upon MHCIIgp stimulation (24).

The SCIMP molecule has four potential tyrosine phosphor-ylation sites. When phosphorylated, it binds Grb2, SLP-65, or SLP-76 and Csk via their Src homology 2 (SH2) domains. Through a proline-rich sequence, SCIMP is constitutively asso-ciated with the Src family kinase Lyn. Despite the interaction with a negative regulator of the Src family kinases Csk, SCIMP plays an overall positive regulatory function mediated by the recruitment of the Grb2 SLP-65 complex, whereas Csk binding seems to be only responsible for negative feedback regulation of this process (24, 25).

Here we have investigated SCIMP function *in vivo* using a SCIMP-deficient mouse model. Although we did not observe any effects of SCIMP deficiency on MHCIIgp signaling, we found that it is involved in the signaling by Dectin-1 in dendritic cells and macrophages, where it is important for sustaining pro-longed MAP kinase activity and pro-inflammatory cytokine production.

Results

Normal Leukocyte Development and Distribution in SCIMP-deficient Mice—To determine the physiological function of SCIMP, we obtained the SCIMP-deficient mouse strain Scimp$^{tm1a(KOMP)Wtsi}$ (hereafter termed Scimp $^{/}$) from the International Knockout Mouse Consortium (for details, see "Experimental Procedures"). First we verified SCIMP defi-ciency at the protein level. As expected, there was no detectable SCIMP protein present in the lysates of Scimp $^{/}$ splenocytes and dendritic cells (Fig. 1*A*).

Next, we assessed leukocyte development and leukocyte sub-set representation in lymphoid organs obtained from SCIMP-deficient mice. Bone marrows, spleens, lymph nodes, and peripheral blood were isolated from 6- to 8-week-old wild-type and Scimp $^{/}$ animals. After preparation of single cell suspen-sions, a multiparametric flow cytometry analysis was carried out. This analysis determined the percentages of T cells, B cells, and their subpopulations as well as the representation of major myeloid cell subsets. However, Scimp $^{/}$ mice did not show any statistically significant differences from wild-type animals under steady-state conditions (Fig. 1, *B–E*).

Normal Function of SCIMP-deficient B Cells—In B cells, SCIMP was shown to be involved in signal transduction down-stream of MHCIIgp (24). Moreover, we found that GL7 ger-minal center B cells express higher levels of SCIMP than naïve B cells (Fig. 2*A*). This suggests that SCIMP may participate in signaling in B cells during the process of obtaining antigen-specific T cell help in the germinal centers of lymphoid follicles. This eventually results in B cell differentiation into plasma cells and secretion of specific antibodies. To test the effect of SCIMP deficiency on this process, we immunized wild -type and Scimp $^{/}$ mice intradermally with ovalbumin. After the immu-nization, we collected the serum from immunized animals and measured antigen-specific IgM and IgG by ELISA. Although there was a significant increase in immunoglobulin production after immunization, there were no significant differences between wild-type and Scimp $^{/}$ animals in the detected levels of antigen-specific IgM or IgG (Fig. 2*B*). Similar results were also obtained when we used different antigen (a small recom-binant fragment from ARHGEF4 protein, data not shown).

Another option was that SCIMP may support the function of B cells as antigen-presenting cells. To test this, we performed a B cell antigen presentation assay. Scimp $^{/}$ and wild-type mice were crossed with the transgenic mouse strain B1– 8i express-ing B cell antigen receptor (BCR) specific for 4-hydroxy-3-ni-trophenylacetyl (NP) hapten. Then we isolated B cells from these mice and fed them with NP-ovalbumin to allow its pro-cessing and presentation on MHCII molecules. Next we tested the ability of these B cells to stimulate OTII T cells expressing transgenic T cell antigen receptor (TCR) specific for ovalbumin peptide. The proliferation and activation of antigen-specific T cells were measured by flow cytometry (Fig. 2*C*). Similar to the previous experiment, we did not observe any differences between WT and Scimp $^{/}$ B cells in their ability to activate antigen-specific T cells.

Finally, we also tested signaling downstream of MHCIIgp in SCIMP-deficient B cells. Specifically, we analyzed ERK MAP kinase activation triggered by MHCIIgp cross-linking, which was shown previously to be reduced in the K46 B cell line after SCIMP down-regulation (24). However, in contrast to the K46 B cell line, murine purified B cells isolated from Scimp $^{/}$ spleen did not show any defects in ERK phosphorylation when compared with wild-type B cells (Fig. 2*D*). Moreover, calcium responses after MHCIIgp and IgM cross-linking were also not altered (Fig. 2*E*). This lack of differences at the single cell level *in vitro* may explain the lack of differences during the antigen presentation assay and antigen-specific antibody response *in vivo*.

SCIMP Expression in Myeloid Cells—SCIMP is expressed not only in the B cell lineage but also in myeloid cells, such as den-dritic cells and macrophages. Strong expression of SCIMP was observed in dendritic cells differentiated from human mono-cytes using GM-CSF- and IL-4-supplemented medium (24). Interestingly, in bone marrow-derived macrophages (BMMFs), SCIMP expression is relatively low. However, it can be strongly up-regulated after GM-CSF treatment (Fig. 3*A*). Therefore, we wanted to find out whether SCIMP expression in BMDCs pre-pared by culturing bone marrow cells in GM-CSF-containing medium is caused by the presence of GM-CSF or whether it is their intrinsic quality. To test this, we used another method of BMDC generation from bone marrow cells that employs Flt3L instead of GM-CSF. As Fig. 3*B* shows, SCIMP is expressed even

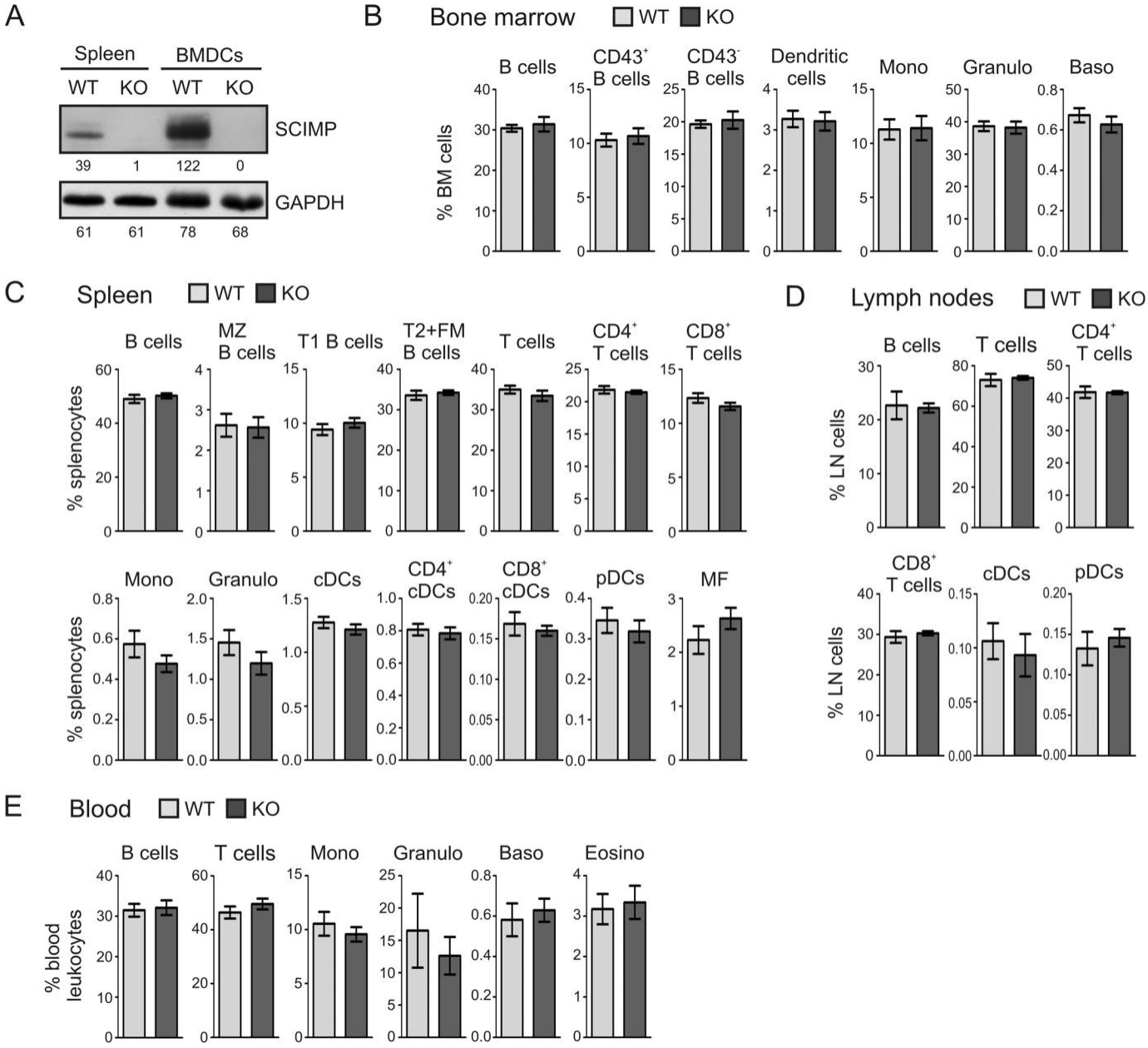

FIGURE 1. **Verification of SCIMP protein deficiency and leukocyte subset analysis in Scimp $^{/}$ mice.** *A*, lysates of splenocytes and BMDCs prepared from WT and Scimp $^{/}$ (*KO*) mice were probed for the presence of SCIMP and GAPDH (loading control) by Western blotting. *B–E*, percentages of major leukocyte subsets in the bone marrows (*B*), spleens (*C*), lymph nodes (*D*), and peripheral blood (*E*) of WT and Scimp $^{/}$ mice determined by flow cytometry. The individual subpopulations were gated as follows. Bone marrow: B cells (B220), CD43 B cells (B220 , CD43), CD43 B cells (B220 , CD43), dendritic cells (F4/80 , Ly6C , CD11b^{low}, CD11c^{hi}), monocytes (*Mono*, F4/80 , CD11b , Gr1^{low}, Ly6C^{hi}), granulocytes (*Granulo*, F4/80 , Ly6C , Gr1^{hi}), and basophils (*Baso*, ckit , CD49b , Fc*e*R). Spleen and lymph nodes: B cells (CD19), MZ B cells (B220 , IgM^{hi}, IgD , CD1d), T1 B cells (B220 , IgM , IgD), T2 FM B cells (B220 , IgD), T cells (CD3), CD4 T cells (CD3 , CD4), CD8 T cells (CD3 , CD8), monocytes (F4/80 , CD11b , Gr1^{low}, Ly6C^{hi}), granulocytes (CD3 , CD19 , CD11b , Gr1^{hi}), classical dendritic cells (CD11c , Ly6C), CD4 classical dendritic cells (CD11c , Ly6C ,CD4), CD8 classical dendritic cells (CD11c , Ly6C ,CD8), plasma-cytoid dendritic cells (CD11c^{low}, Ly6C , B220), and macrophages (CD11b^{low}, F4/80). Peripheral blood: B cells (CD19), T cells (CD3), monocytes (SSA^{low}, CD11b), granulocytes (CD11b , LyG^{hi}, Ly6C^{low}), basophils (ckit , CD49b , Fc*e*R*Ia*), and eosinophils (*Eosino*, CD11b , Ly6C^{low}, Ly6G , SSA^{hi}).

in BMDCs differentiated by Flt3L, although it is still further up-regulated after GM-CSF exposure (Fig. 3*B*).

Finally, to assess SCIMP expression in dendritic cells *in vivo*, we sorted classical dendritic cells from murine spleens and ana-lyzed SCIMP expression in these cells by Western blotting. These results clearly showed the presence of SCIMP in primary DCs (Fig. 3*C*). From these results we can conclude that SCIMP is expressed in dendritic cells *in vitro* and *in vivo* and that its expression is enhanced by the presence of GM-CSF.

SCIMP Is Phosphorylated After Stimulation of Dendritic Cells and Macrophages with Zymosan—Because of the strong SCIMP expression in BMDCs, we decided to search for its func-tion in this cell type. Surprisingly, we observed only a marginal increase in SCIMP phosphorylation after MHCIIgp cross-link-ing on the surface of these cells (Fig. 4*A*). Thus we hypothesized that, in BMDCs, SCIMP acts downstream of a different recep-tor. Dectin-1 was a very good candidate because, similar to SCIMP, it is present in tetraspanin-enriched microdomains

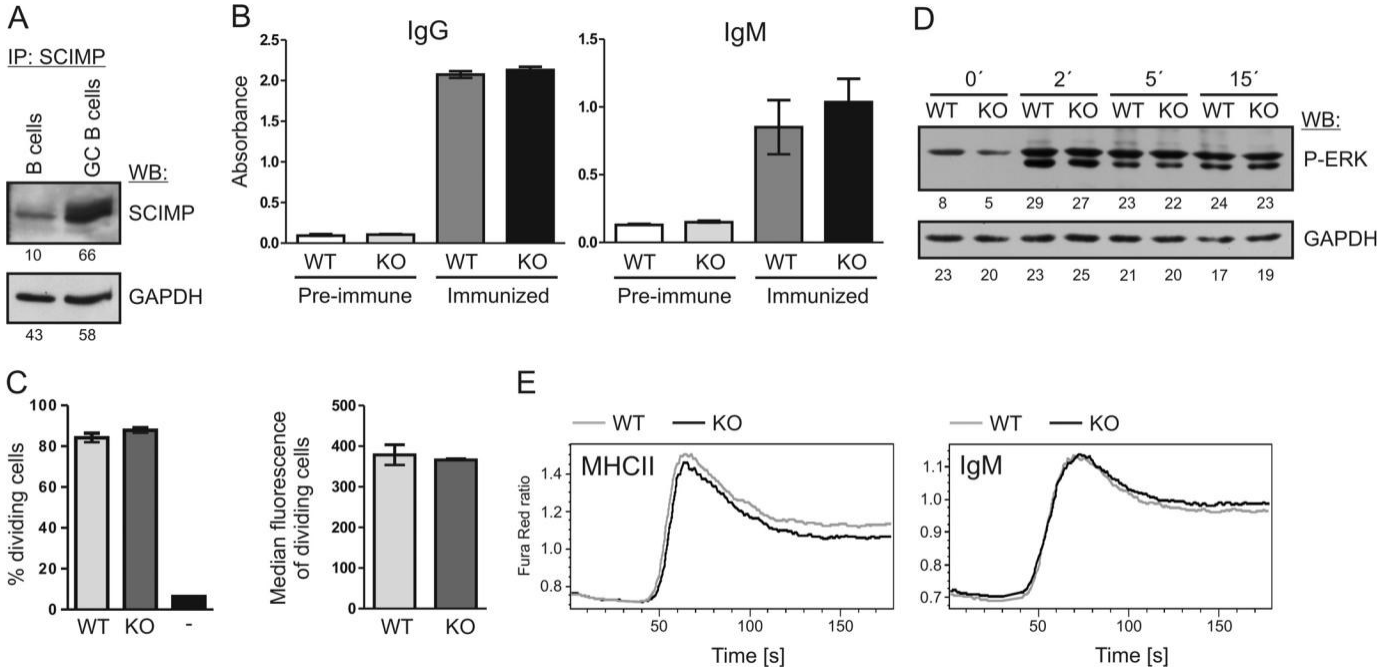

FIGURE 2. **Normal responses of Scimp $^{/}$ B cells.** *A*, sorted naïve mouse B cells from control mouse or GL7 germinal center (*GC*) B cells from sheep red blood cell-immunized mice were lysed in SDS-PAGE sample buffer and probed for SCIMP protein by immunoblotting. GAPDH staining served as a loading control. *IP*, immunoprecipitation; *WB*, Western blotting. *B*, sera from WT (*n* 5) or Scimp $^{/}$ (*KO*, *n* 6) mice immunized intradermally with ovalbumin in incomplete Freund adjuvant were collected, and immunoglobulins specific to ovalbumin were detected by ELISA. As a control, preimmune sera from the same mice were used. *C*, proliferation of OTII transgenic T cells labeled with CFSE was measured after 48 h co-culture with NP-ovalbumin-fed B1– 8i transgenic B cells (WT or Scimp $^{/}$) by flow cytometry. T cells cultured alone served as a negative control ( ). Percentages of dividing cells and median CFSE fluorescence of cells that underwent at least one division are shown. *D*, ERK1/2 phosphorylation after MHCIIgp cross-linking in WT and Scimp $^{/}$ primary splenic B cells was analyzed by immunoblotting. *E*, splenocytes isolated from WT and Scimp $^{/}$ mice were stained with APC-conjugated anti-CD3 and anti-CD11b antibodies. The increase in calcium flux after MHCIIgp or IgM cross-linking was evaluated in B cells (gated as CD3 CD11b) using a Fura Red calcium-sensitive probe.

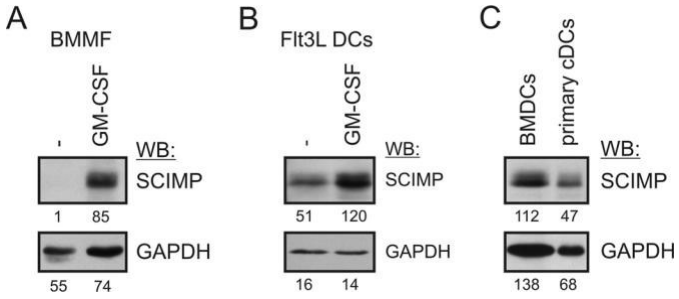

FIGURE 3. **Expression of SCIMP and its regulation in dendritic cells and macrophages.** *A*, BMMFs were differentiated from bone marrow cells for 7 days in M-CSF-containing medium. On day 7, the medium was replaced with GM-CSF-containing medium, and after an additional 24 h, cells were lysed in SDS-PAGE sample buffer. SCIMP was detected by immunoblotting. *WB*, West-ern blotting. *B*, dendritic cells were generated using Flt3L- and stem cell fac-tor-containing medium. On day 8, plasmacytoid dendritic cells were removed using anti-mPDCA-1 magnetic beads, and the rest of the dendritic cells were cultured for 24 h in GM-CSF-containing medium followed by analysis of SCIMP expression by immunoblotting. *C*, splenic cDCs (CD11c , B220 , Ly6C) were sorted from the spleens of wild-type mice, lysed, and subjected to immunoblotting with SCIMP and GAPDH antibodies. BMDCs served as a positive control.

(24), and it is up-regulated in the presence of GM-CSF. We used zymosan as a well established Dectin-1 activator. Zymosan is a preparation of small particles rich in the Dectin-1 ligand *b*-glu-can, prepared from the yeast *Saccharomyces cerevisiae* (26). Strikingly, treatment of BMDCs with zymosan resulted in a strong increase of SCIMP phosphorylation (Fig. 4*B*). Moreover, SCIMP localized into zymosan-containing phagosomes and remained there for at least 30 min (Fig. 4*C* and supplemental Movie 1). SCIMP phosphorylation was very stable, with only a minor reduction during the 30-min experiment (Fig. 4*D*). A similar observation was also made with BMMFs (Fig. 4*E*).

SCIMP Is Involved in Dectin-1 Signaling—Dectin-1 signal transduction is initiated by Src family kinases and Syk (15). To test which kinases are responsible for SCIMP phosphorylation after zymosan treatment, we stimulated BMDCs with zymosan in the presence of specific inhibitors of Src family kinases and Syk. The results suggested that both Src family and Syk kinases are required for SCIMP phosphorylation after zymosan treat-ment because SCIMP phosphorylation was most profoundly reduced when both Src family kinase (PP2) and Syk (Syk inhib-itor IV) inhibitors were combined (Fig. 5*A*).

The composition of zymosan is relatively complex. In addi-tion to *b*-glucan, it also contains mannans (ligands of Dectin-2) and TLR2 ligands (26, 27). To confirm Dectin-1 involvement in the induction of SCIMP phosphorylation, we exploited the much stronger responsiveness of Dectin-1 to particulate *b*-glu-can than to soluble *b*-glucan as a unique feature of this receptor. As a result, many aspects of Dectin-1 signaling after stimulation with particulate *b*-glucan can be inhibited by soluble forms of *b*-glucan (19). Thus, in the next experiment, we stimulated BMDCs with zymosan particles in the presence or absence of soluble *b*-glucan. Indeed, treatment with soluble *b*-glucan sub-stantially inhibited SCIMP phosphorylation, whereas soluble mannan had no effect (Fig. 5*B*), suggesting that SCIMP is indeed a part of the Dectin-1 signaling pathway. To further support this conclusion, we investigated SCIMP phosphoryla-tion in MyD88-deficient BMDCs, which have impaired func-tion of multiple TLRs, including TLR2, the main TLR activated

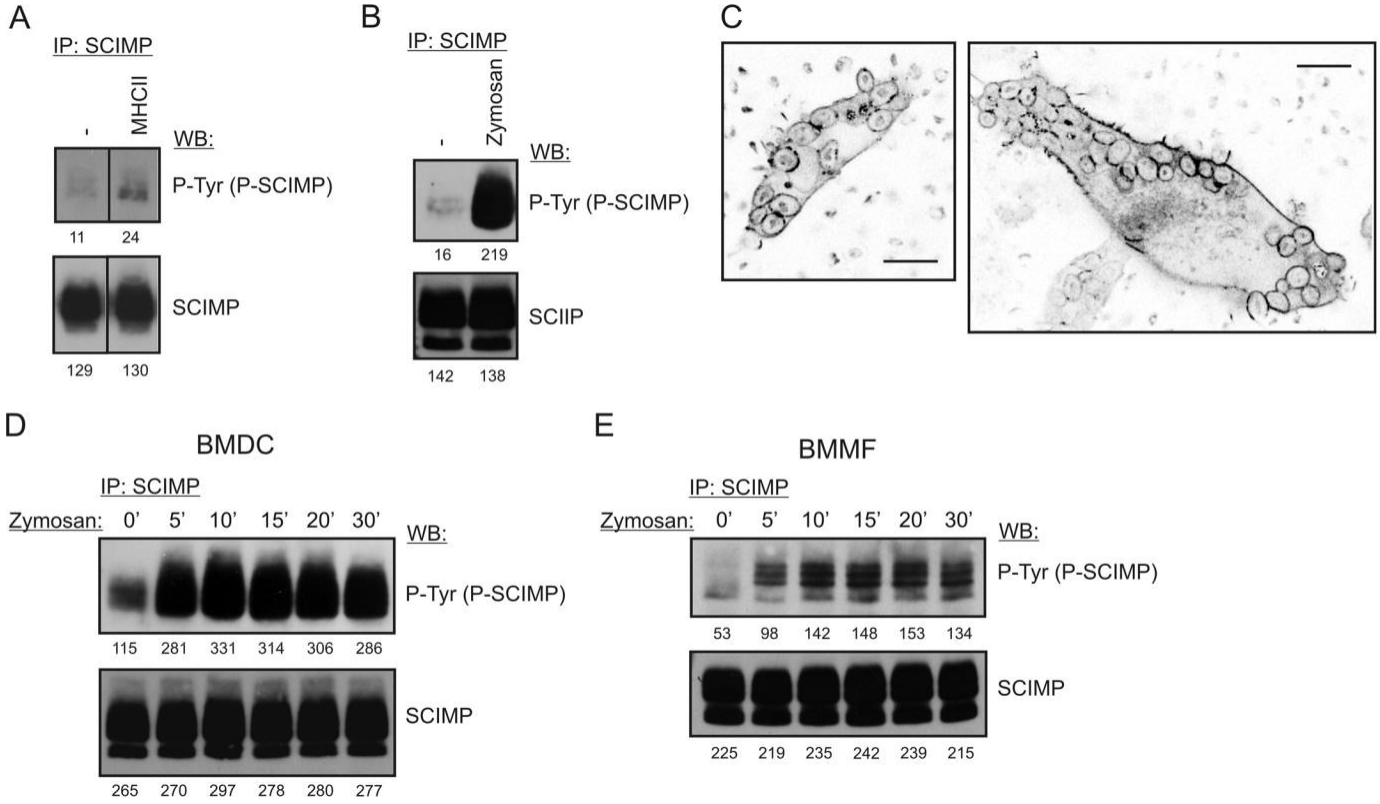

FIGURE 4. **SCIMP is phosphorylated in response to zymosan stimulation.** *A*, SCIMP phosphorylation in SCIMP immunoprecipitates (*IP*) prepared from BMDCs stimulated for 5 min by MHCIIgp cross-linking. *WB*, Western blotting. *B*, SCIMP phosphorylation in SCIMP immunoprecipitates prepared from BMDCs stimulated for 5 min with 300 *m*g/ml zymosan. *C*, localization of SCIMP-YFP into zymosan-containing phagosomes in BMDCs retrovirally transduced with a SCIMP-YFP coding construct. Zymosan is visible because of its strong autofluorescence. *Scale bars* 10 *m*m. *D*, sustained SCIMP phosphorylation in SCIMP immunoprecipitates prepared from BMDCs stimulated for the indicated times with 300 *m*g/ml zymosan. *E*, sustained SCIMP phosphorylation in SCIMP immunoprecipitates prepared from BMMFs stimulated for the indicated times with 300 *m*g/ml zymosan.

by zymosan (17, 28, 29). SCIMP phosphorylation was not affected by the disruption of TLR signaling (Fig. 5*C*). Based on these experiments, we concluded that Dectin-1 is responsible for inducing SCIMP phosphorylation after zymosan treatment.

SCIMP Is Important for Sustained MAP Kinase Signaling and Cytokine Production After Stimulation with Zymosan—To test the functional significance of SCIMP in Dectin-1 signaling, we first measured ERK activation in zymosan-stimulated BMDCs because the ERK pathway was affected in the previous study of the SCIMP-deficient K46 B cell line (24). We stimulated BMDCs with zymosan for 30 min and followed ERK phosphor-ylation in the lysates prepared from these cells at various time points. Surprisingly, we could not detect any reproducible dif-ferences in ERK phosphorylation between wild-type and Scimp $^{/}$ BMDCs (Fig. 6*A*). Similar results were also obtained for p38 and JNK MAP kinases (Fig. 6*A* and data not shown). We also crossed Scimp $^{/}$ mice with a MyD88-deficient strain to avoid interference from the TLR pathways. However, even in MyD88-deficient BMDCs, no differences in signaling caused by SCIMP deficiency could be detected (data not shown).

As shown in Fig. 4*D*, SCIMP phosphorylation after zymosan activation was stable for at least 30 min. When we analyzed this further, we found that increased SCIMP phosphorylation could be observed even as late as 24 h after addition of zymosan (Fig. 6*B*). However, it also seemed that the amount of SCIMP immu-noprecipitated from zymosan-treated cells was higher. Indeed, when we tested cell lysates from untreated and zymosan-acti-vated BMDCs, we observed that SCIMP expression was up-regulated after zymosan-mediated activation (Fig. 6*C*). Therefore, we decided to investigate the signaling downstream of Dectin-1 in Scimp $^{/}$ BMDCs at 24 h after initiation of signaling. To avoid interference from TLR pathways, we used mice with a MyD88-deficient genetic background for this experiment. Consistent with the long-lasting SCIMP phosphorylation, we observed a significant reduction of ERK and p38 phosphoryla-tion in SCIMP-deficient BMDCs at this late time point (Fig. 6, *D* and *E*). This effect seemed selective for MAP kinase signaling because we did not detect any differences in the phosphoryla-tion of PKC*d* in the same samples (Fig. 6*F*). We also tested the activation status of JNK and the members of the NF-*k*B path-way (p65 and IKK*a*/*b*), but we could not detect any phosphor-ylation of these proteins, which at this late stage of signaling could have already been down-regulated.

Finally, we tested whether the defects in MAP kinase signal-ing influence downstream functional responses in dendritic cells. In a recent study, activation of the ERK pathway was shown to be critical for inflammatory cytokine production in BMMFs (30). Because we were unable to detect any significant defects in cytokine production in Scimp $^{/}$ BMDCs during the typical experimental setup, where the readout was measured within the first 24 h of stimulation (data not shown), we focused our analysis on late phases of cytokine production beyond the 24-h time frame. At these late phases, the alterations to sus-tained MAP kinase activity observed in Scimp $^{/}$ BMDCs were

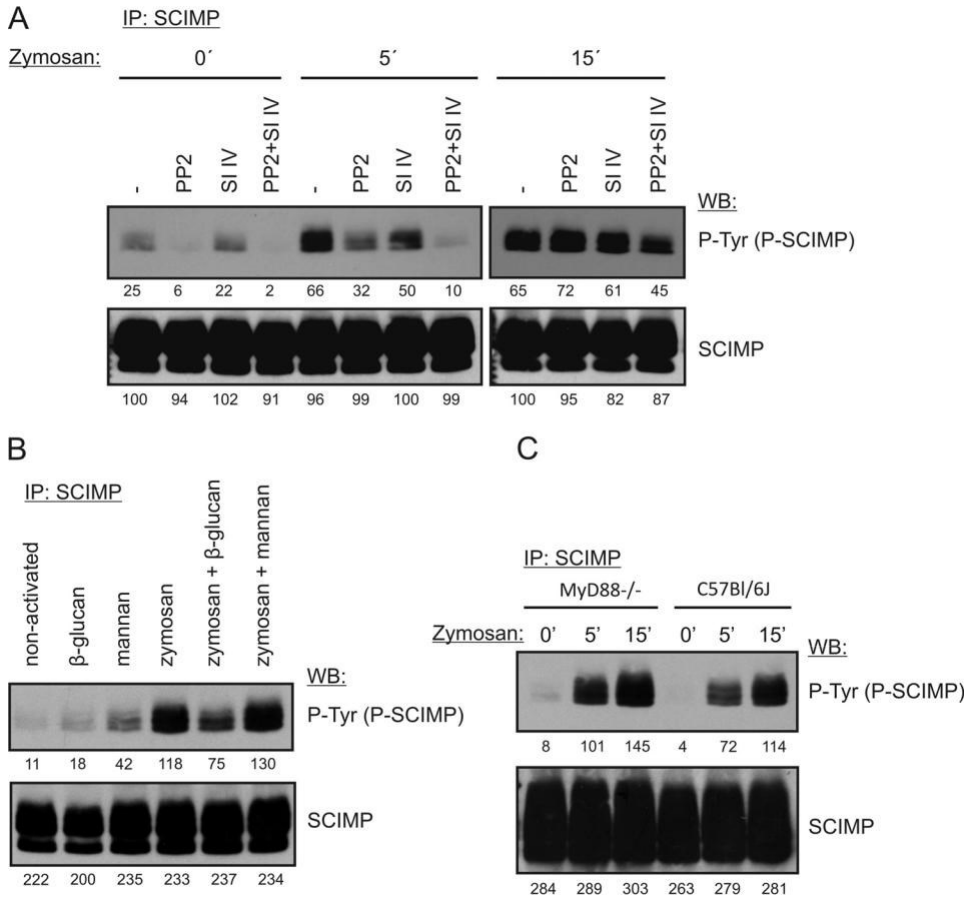

FIGURE 5. **SCIMP is part of the Dectin-1 signaling pathway.** *A*, BMDCs were incubated with 10 *m*M PP2 or 2 *m*M Syk inhibitor IV (*SI IV*) or a combination of them for 5 min. Next, 300 *m*g/ml zymosan was added, and cells were incubated in its presence for the indicated times, lysed, and subjected to SCIMP immunopre-cipitation (*IP*) followed by immunoblotting with phosphotyrosine (*P-Tyr*) and SCIMP antibodies. *WB*, Western blotting. *B*, BMDCs were incubated at 37 °C with 600 *m*g/ml mannan or 600 *m*g/ml soluble *b*-glucan alone or in combination with 300 *m*g/ml zymosan. The level of SCIMP phosphorylation was detected as in *A*. *C*, MyD88-deficient or wild-type BMDCs were activated with 300 *m*g/ml zymosan for 5 or 15 min, and SCIMP phosphorylation was detected as in *A*.

more likely to have an effect. To measure the prolonged cytokine production, we washed away cytokines produced during the initial 48 h of stimulation and then cultured the cells for an additional 24 h before collecting the supernatants. This way we obtained samples containing only the cytokines produced between 48 –72 h after zymosan stimulation. Under these conditions, we observed a significant reduction in the production of TNF*a* and IL-6 by Scimp/MyD88 $^{/}$ BMDCs compared with MyD88 $^{/}$ cells (Fig. 6*G*). These data are in agreement with our observations that SCIMP deficiency affects mainly the late phases of Dectin-1 signaling.

Discussion

In this article, we describe an initial analysis of SCIMP-defi-cient mice. Analysis of lymphocyte subsets in these mice at steady state showed that SCIMP is dispensable for leukocyte development and homeostasis. On the other hand, our results also showed that SCIMP is involved in Dectin-1 signaling, where it appears to be selectively involved in sustaining long-term ERK and p38 MAP kinase activation and pro-inflamma-tory cytokine production.

An earlier cell line-based study from our laboratory (24) suggested that, in B cells, SCIMP is involved in the reverse signaling at the B cell side of the immunological synapse downstream of MHCII glycoproteins. Specifically, it showed that SCIMP accumulates at the APC side of the immunological synapse and that shRNA-mediated SCIMP down-regulation results in a defect in ERK signaling downstream of MHCIIgp in the K46 murine B cell line. However, our analysis of primary murine B cells from SCIMP-deficient mice showed that, in contrast to the K46 B cell line, SCIMP deficiency has no significant impact on ERK signaling elicited by MHCIIgp cross-linking in primary mouse B cells. One possible explanation was that the K46 cell line may be more related to activated B cells, such as those present in the germinal center (31). Indeed, germinal center B cells express higher levels of SCIMP than naïve B cells and thus seem more likely to be affected by the loss of SCIMP. Nevertheless, we have not observed any effects of SCIMP deficiency on germinal center B cell numbers in Scimp $^{/}$ mice, and our experiments with isolated germinal center B cells did not reveal any differences in MHCIIgp signaling between WT and Scimp $^{/}$ GC B cells (data not shown). Moreover, intact antibody production by Scimp $^{/}$ mice (Fig. 2*B*) also suggested that germinal center reaction is not affected by SCIMP deficiency.

We also tested a possible involvement of SCIMP in MHCIIgp signaling in dendritic cells. However, despite the high levels of SCIMP in these cells, MHCIIgp cross-linking resulted only in a

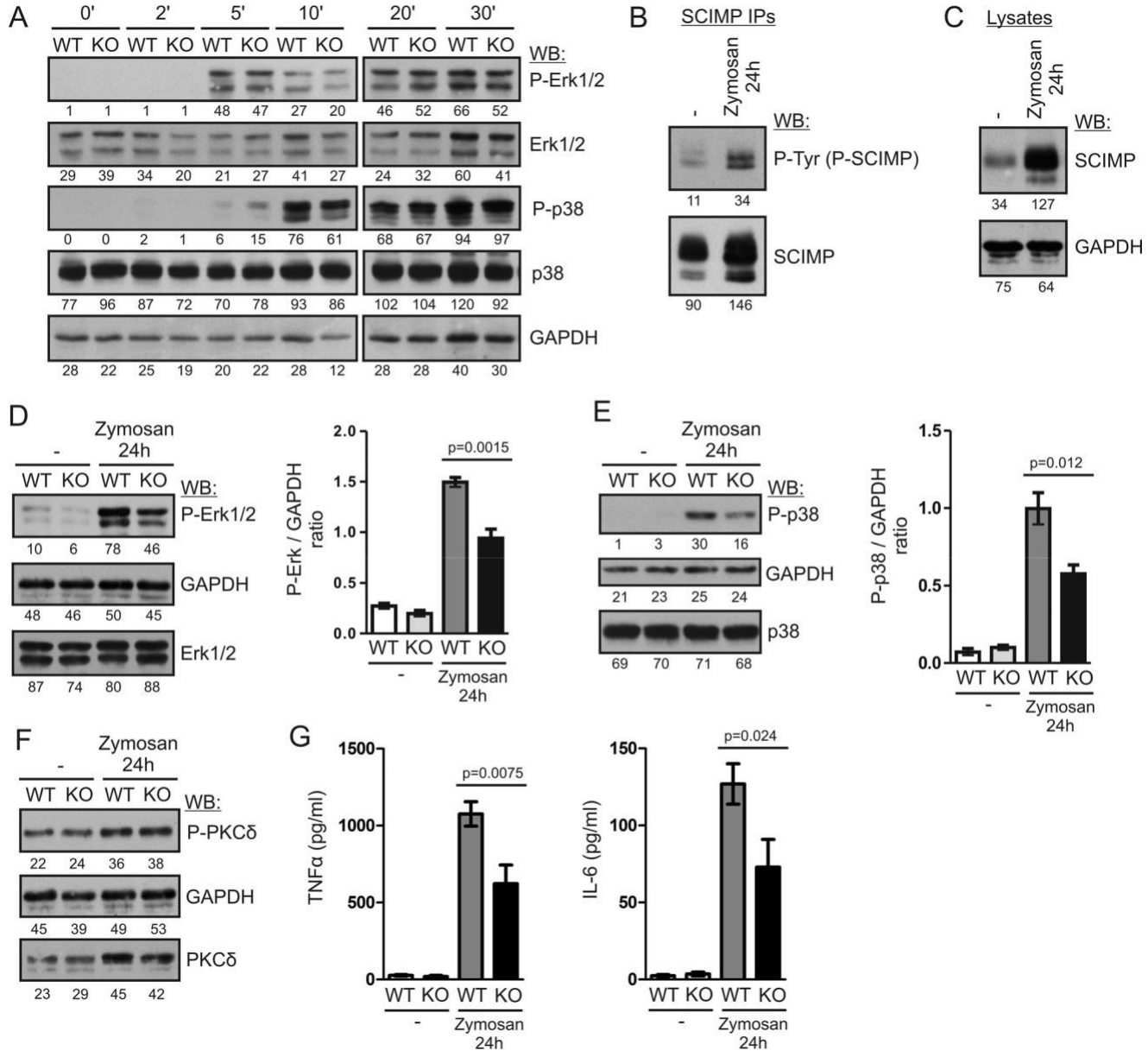

FIGURE 6. **SCIMP enhances long-term MAP kinase activation and pro-inflammatory cytokine production after stimulation with zymosan.** *A*, BMDCs from WT and Scimp $^{/}$ (*KO*) mice were stimulated with 300 mg/ml zymosan for the indicated times, and ERK1/2 and p38 phosphorylation was analyzed by immunoblotting. *WB*, Western blotting. *B*, BMDCs from C57Bl/6J mice were stimulated with 300 mg/ml zymosan for 24 h or left unstimulated, lysed, and subjected to SCIMP immunoprecipitation followed by immunoblotting with phosphotyrosine (*P-Tyr*) and SCIMP antibodies. *C*, levels of SCIMP protein in the lysates of BMDCs stimulated with 300 mg/ml zymosan for 24 h or left unstimulated were analyzed by immunoblotting with SCIMP antibodies. *D*, phosphory-lation of ERK1/2 in the lysates of WT and Scimp $^{/}$ BMDCs stimulated with zymosan for 24 h or left unstimulated (*left panel*). The *right panel* shows the results of densitometric quantification of ERK phosphorylation in samples prepared from 4 mice/genotype. *E*, a similar analysis of p38 phosphorylation in the samples from *D*. *F*, a similar analysis of PKCd phosphorylation. *G*, late production of TNFa and IL-6 by WT and Scimp $^{/}$ BMDCs. BMDCs were stimulated with 300 mg/ml zymosan for 48 h, washed, and cultured for an additional 24 h in the absence of stimulus. After this period, culture supernatants were collected and analyzed by ELISA for the presence of TNFa and IL-6. In the experiments shown in *B*–*G*, mice with a MyD88-deficient genetic background were used.

marginal increase in SCIMP phosphorylation, suggesting that, in dendritic cells, SCIMP may function differently from B cells and act downstream of a different receptor. Our candidate-based approach led to the identification of the *b*-glucan recep-tor Dectin-1 as a receptor employing SCIMP in its signal trans-duction. Because both SCIMP and Dectin-1 are associated with tetraspanins (21, 22), we hypothesized that, via tetraspanin-enriched microdomains, SCIMP and Dectin-1 may interact and, as a result, that SCIMP may be involved in coupling of Dectin-1 to downstream signaling pathways. Indeed, in both dendritic cells and GM-CSF-activated macrophages, SCIMP is strongly phosphorylated after Dectin-1 stimulation with zymosan. However, zymosan also contains ligands for additional pattern recognition receptors, and so we performed a series of experiments indicating that Dectin-1 is indeed the receptor triggering SCIMP phosphorylation. These experiments showed that SCIMP phosphorylation induced by zymosan treatment is not affected in Myd88 $^{/}$ dendritic cells with dysfunctional TLR signaling. In addition, zymosan-triggered SCIMP phosphorylation was inhibited by soluble *b*-glucan, which can spe-

cifically bind to the receptor but does not fully activate it (19). In contrast, a soluble form of mannan, another major zymosan component, did not inhibit SCIMP phosphorylation after zymosan treatment. Interestingly, soluble mannan alone elicited moderate SCIMP phosphorylation, suggesting that there may be a minor contribution from a mannan receptor, such as Dectin-2 (32), to zymosan-induced SCIMP phosphorylation.

SCIMP phosphorylation lasts for many hours after the encounter with zymosan. Moreover, zymosan stimulation also enhances SCIMP expression. Because SCIMP typically displays a certain level of constitutive phosphorylation even in quiescent cells, SCIMP protein up-regulation can contribute to the increased phosphorylation observed at the very late time points. However, the relative contribution of increased SCIMP expression and Dectin-1-induced phosphorylation to global levels of phosphorylated SCIMP remains unclear. Phosphoryl-ated SCIMP appears to be important for sustaining ERK and p38 activation for prolonged periods of time. The precise mech-anism of how SCIMP mediates ERK and p38 signaling is not entirely clear. Dectin-1 activates, by an unclear mechanism, PLC*g*2, which is indispensable for ERK activation (33). PLC*g*2 products also activate PKC*d*, which then phosphorylates the adaptor protein CARD9, resulting in activation of the NF-*k*B pathway (15). A recent study showed that CARD9 also plays a critical role in ERK activation by bringing together Ras and RasGRF1, resulting in the activation of Ras and ERK further downstream (30). However, the existence of CARD9-indepen-dent pathways cannot be ruled out. Previously published data showed that SCIMP binds the SLP65/SLP76 adaptor proteins, which are known to be involved in PLC*g*1/2 activation (24, 34). In addition, SCIMP also binds Grb2, which can then recruit Sos proteins, well characterized exchange factors for Ras and acti-vators of the Ras/ERK pathway. Products of PLC*g*2 also activate another family of Ras exchange factors, RasGRP proteins, which activate Ras downstream of TCR, BCR, and other immu-noreceptors (35). Clearly, there are multiple options of how SCIMP can contribute to Dectin-1-dependent ERK activation. It certainly is not the only player connecting Dectin-1 to the ERK pathway, and especially at the early stages of signaling, other pathways dominate the response. However, at the very late stages of Dectin-1 stimulation, SCIMP activity becomes more apparent.

In addition to ERK, SCIMP also contributes to the activation of p38 MAP kinase. The mechanism of p38 activation down-stream of Dectin-1 is less well understood. In contrast to ERK, it was shown to be independent of CARD9 (30). Our observations of similar defects in ERK and p38 activation in SCIMP-deficient animals together with unperturbed PKC*d* activity suggest that SCIMP affects a CARD9-independent pathway that may be involved in the activation of both of these MAP kinases.

Dectin-1 is an important innate immune receptor recogniz-ing a number of pathogenic fungi. It supports the immune response by mediating phagocytosis of these pathogens by trig-gering an oxidative burst and by inducing the production of cytokines (7, 17, 18). We have analyzed all of these downstream responses in BMDCs from SCIMP-deficient mice, but we did not observe any differences between WT and SCIMP-deficient cells when stimulated by zymosan (data not shown). The only exceptions were the late phases of TNF*a* and IL-6 production (Fig. 6*G*). Our data are consistent with previous observations that ERK signaling is required for the production of TNF*a* and IL-6 downstream of Dectin-1 (30, 36). p38 signaling in macrophages and dendritic cells has also been shown to contribute to pro-inflammatory cytokine production (37, 38). Although the precise function of the late sustained production of these cytokines still remains to be clarified, the role of these cytokines in antifungal defense has already been well established. Mice defi-cient in TNF*a* or IL-6 were shown to be highly susceptible to fungal infections (39 – 42). Moreover, the use of agents blocking the function of TNF*a* or IL-6 in human patients is also associ-ated with an increased incidence of infection with opportunis-tic fungi (43).

Taken together, our study describes a novel branch of Dec-tin-1 signaling that is driven by the small transmembrane adap-tor SCIMP. Our data suggest that the early and late phases of Dectin-1 signaling are differentially regulated. The late sus-tained phase of Dectin-1 signaling is partly dependent on SCIMP, which in dendritic cells promotes MAP kinase signal-ing and production of TNF*a* and IL-6, important mediators of the inflammatory response during fungal infections.

Experimental Procedures

Antibodies—Antibodies to the following antigens were used for Western blotting detection: GAPDH (Sigma-Aldrich); phospho-ERK (Thr-202/Tyr-204), phospho-PKC*d*/*u* (Ser-643/ 676), PKC*d*, phospho-p38 (Thr-180/182), and p38 MAPK, (Cell Signaling Technology); ERK1/2 (Promega); and phospho-tyro-sine (4G10, Upstate Biotechnology). Rabbit polyclonal antibod-ies against murine SCIMP were described earlier (24). For the flow cytometry analysis, antibodies against the following mouse antigens conjugated to the indicated fluorophores were used: CD3-PE-Cy7, CD5-PE, CD11b-FITC, CD11b-PE, CD11b-APC, CD19-eFluor 660, CD19-FITC, CD23-Dye 647, F4/80-FITC, Gr1-PB, Ly6G-FITC, CD49b (DX5)-APC, c-kit-PE, Gr1-PE, Ly6C-PE-Cy7, B220-FITC, IgM- FITC, MHCII-FITC, Fc*e*RI*a*-PB, and CD86-APC (Biolegend); CD1d-FITC, CD4-PE, CD8-e450, CD11c-APC, CD43-PE, GL7-FITC, B220-e450, IgD-APC, and CD80-APC (eBiosciences); and CD3-APC and CD8-FITC (EXBIO). The anti-IgM-Dy547 antibody was con-jugated in-house. For MACS purification, anti-CD43, anti-CD11b, anti-CD19, anti-FITC, and anti- mPDCA-1 MicroBeads (Miltenyi Biotec, Bergisch Gladbach, Germany) were used. Other antibodies used in this study were anti-mouse I-A/I-E-biotin (Biolegend), HRP-conjugated goat anti-mouse IgG (Sigma-Aldrich), HRP-conjugated goat anti-rabbit IgG Fc fragment-specific, goat anti-mouse IgM $F(ab)_2$ (Jackson Immu-noResearch Laboratories), Fc Bloc (2.4G2) (BD Biosciences), and HRP-conjugated goat anti-rabbit polyclonal antibody (Bio-Rad).

Other Reagents—We also used mannan from *S. cerevisiae* (Sigma-Aldrich), zymosan A from *S. cerevisiae* (Sigma-Aldrich), streptavidin (Jackson ImmunoResearch Laborato-ries), CFSE (5-(and 6)-carboxyfluorescein diacetate succinimi-dyl ester; eBioscience), and NP(14)-ovalbumin (Bioresearch Technologies, Inc.). Soluble *b*-glucan (Wellmune Soluble) was a kind gift from Bengt Hansson (Biogredia AB, Sandef-

jord, Norway). The Src family kinase inhibitor PP2 and Syk inhibitor IV (BAY 61-3606) were from Calbiochem/Merck (Darmstadt, Germany).

Mice—The SCIMP-deficient mouse strain Scimp$^{tm1a(KOMP)Wtsi}$ on the C57Bl/6J genetic background (throughout this article labeled as Scimp $^{/}$) was generated at the Wellcome Trust Sanger Institute (Cambridge, UK) within International Knock-out Mouse Consortium Project 24100 and was directly obtained from the Wellcome Trust Sanger Institute. B1– 8i B cell antigen receptor-transgenic mice (44), the OTII transgenic mouse strain (C57BL/6-Tg(TcraTcrb)425Cbn/Crl), and the Myd88-deficient mouse strain (B6.129P2(SJL)-Myd88tm1. 1Defr/J) derived from Myd88fl mice (45) were obtained from The Jackson Laboratory (Bar Harbor, ME). C57Bl/6J for com-parative experiments originated from crossing Scimp $^{/}$ heterozygotes. Other C57Bl/6J mice were from the animal facil-ity of the Institute of Molecular Genetics of the Academy of Sciences of the Czech Republic (IMG ASCR) (Prague, Czech Republic). All experiments in this work conducted on animals were approved by the Animal Care and Use Committee of the Institute of Molecular Genetics and were in agreement with local legal requirements and ethical guidelines.

Cell Lines and Primary Cells—Primary mouse B cells were isolated from spleens of Scimp $^{/}$ and C57Bl/6J mice by nega-tive selection using anti-CD43 and anti-CD11b MicroBeads (Miltenyi Biotec) on an AutoMACS magnetic cell sorter (Milte-nyi Biotec) and subsequently cultured in Iscove's modified Dul-becco's medium (IMDM). BMMFs were differentiated from mouse bone marrow cells in DMEM conditioned with 10% L929 culture supernatant containing M-CSF for 7–9 days. BMDCs were differentiated in DMEM conditioned with 3% LUTZ cell culture supernatant containing GM-CSF for 10 –12 days. Ftl3L-generated dendritic cells were cultured in 100 ng/ml rmFLT3L (Peprotech) and RPMI medium supple-mented with stem cell factor (supernatant from HEK293 cells transfected with a stem cell factor-coding construct) for 8 days, and then plasmacytoid dendritic cells were removed using anti- mPDCA- 1 microbeads on an AutoMACS, and the rest of the dendritic cells were used further.

To prepare primary classical dendritic cells, splenocytes from C57Bl/6J mice were incubated with Fc bloc, CD3-FITC, IgM-FITC, and Ter119-FITC and precleared on an AutoMACS using anti-FITC magnetic beads (Miltenyi Biotec). The nega-tive fraction was further stained with B220-e450, Ly6C-PE_Cy7, and CD11c-APC and sorted by BD Influx FACS (BD Biosciences) for classical DCs (CD11c , B220 , Ly6C) (46). For GL7 germinal center B cell purification, all splenic B cells were first purified from mice immunized intraperitoneally with sheep red blood cells by negative selection using CD11b and CD43 microbeads on an AutoMACS magnetic cell separator. The obtained B cells were then stained with GL-7-FITC anti-body, followed by positive selection with anti-FITC magnetic beads using the same AutoMACS separator. Phoenix Eco cells were obtained from Origene and cultured in DMEM. All media were supplemented with 10% fetal calf serum and antibiotics. The cells were cultured at 37 °C in 5% CO_2.

DNA Constructs, Transfection, and Transduction—The mouse SCIMP-YFP construct coding for full-length mouse SCIMP tagged at the C terminus with yellow fluorescent protein was cloned into the pMSCV-LNGFR retroviral vector. Lipofectamine 2000 (Invitrogen/Thermo Fisher Scientific) was used according to the protocol of the manufacturer for the transfection of SCIMP-YFP/pMSCV-LNGFR construct to Phoenix Eco cells to produce viral particles. Retrovirus-containing supernatants were then harvested, supplemented with Polybrene (10 mg/ml, Sigma-Aldrich), and added to the freshly isolated bone marrow cells. The cells were then centrifuged at 1250 *g* for 90 min at 30 °C and differentiated into BMDCs or BMMFs.

Cell Activation, Lysis, and Immunoprecipitation—To test the effect of zymosan and other activators on BMDCs, fully differentiated BMDCs were plated on 6-well plates (2 10^6 cells/ well) in culture medium and allowed to adhere to the plastic overnight. Then the medium was changed for DMEM without GM-CSF. After 2 h, zymosan in DMEM was added to a final concentration of 300 *m*g/ml. The activation of cells was stopped after the indicated time periods by lysis in SDS-PAGE sample buffer. For immunoprecipitation, the cells (BMDCs or BMMFs) were plated on 10-cm dishes and activated as above or by biotinylated anti mouse I-A/I-E antibody (Biolegend, 10 *m*g/ml), followed by cross-linking with 10 *m*g/ml streptavidin (Jackson ImmunoResearch Laboratories). They were then lysed in lysis buffer containing 1% laurylmaltoside (Calbiochem/ Merck), 20 mM Tris (pH 7.5), 150 mM NaCl, 5 mM iodoacet-amide, 5 mM NaF, 1 mM Na_3VO_4, 2 mM EDTA, and 100 diluted protease inhibitor mixture set III (Calbiochem) for 30 min on ice. Postnuclear supernatants were incubated for 1–2 h with anti-SCIMP rabbit antiserum followed by 1–2 h of incu-bation with protein A/G Plus-agarose beads (Santa Cruz Bio-technology) at 4 °C. After washing, the immunoprecipitates were eluted with 40 *m*l of SDS-PAGE sample buffer.

B cell stimulations were carried out in suspension. B cells were resuspended in a concentration of 5 10^7/ml in IMDM and activated by labeling with 10 *m*g/ml biotinylated anti-mouse I-A/I-E antibody, followed by cross-linking with 10 *m*g/ml streptavidin in IMDM at 37 °C for the indicated time intervals. The activation of cells was stopped by addition of an equal volume of 2 concentrated SDS-PAGE sample buffer. Western blotting quantification was performed by densitome-try of scanned films using AIDA image analyzer software (Ely-sia-raytest, Straubenhardt, Germany), and the obtained values were inserted into the figures below the individual blots.

Flow Cytometry—Single cell suspensions were prepared from spleens, lymph nodes, bone marrow, and peripheral blood from 6- to 8-week-old mice. Erythrocytes were lysed with ACK buffer (150 mM NH_4Cl, 0.1 mM EDTA (disodium salt), and 1 mM $KHCO_3$). The remaining cells were incubated with Fc-bloc and fluorophore-conjugated antibodies and analyzed on a BD LSRII Flow cytometer. For calcium response measurement, a single cell suspension of splenocytes (after erythrocyte lysis in ACK buffer) was loaded with 2 *m*M calcium indicator Fura Red (Invitrogen) and subsequently stained with anti-CD3-APC and anti-CD11b-APC. Samples were analyzed using a BD LSRII flow cytometer for 30 s at rest and then another 150 s after activation (either with 10 *m*g/ml anti-mouse IgM F(ab)2 anti-body (Jackson ImmunoResearch Laboratories) or with 10

*m*g/ml streptavidin, which cross-linked MHCIIgp molecules on B cells preincubated with biotinylated anti-I-A/I-E antibody (Biolegend). The relative calcium concentration was measured as a ratio of the Fura Red fluorescence intensity elicited by exci-tation wavelengths of 405 nm (emission measured at 635–720 nm) and 488 nm (emission measured at 655– 695 nm). Data were analyzed using FlowJo software (TreeStar).

Antigen Presentation Assay—For the antigen-presentation assay, we modified a method published previously (47). CD4 T cells isolated from lymph nodes of OTII mice using negative selection (CD11b, CD8, CD19-FITC) on AutoMACS were cul-tured for 2 days in RPMI medium supplemented with 100 ng/ml anti-CD3 antibody and 2 units/ml IL2 for 48 h. B cells negatively selected on AutoMACS were fed for 1 h with 10 mg/ml NP-ovalbumin at 37 °C, washed with PBS, and cultured in a ratio of 1:1 with CFSE-stained T cells. After 48 h, cell pro-liferation was measured using a BD LSRII flow cytometer.

Immunization—For antibody detection, Scimp $^{/}$ and C57Bl/6J mice, 6 – 8 weeks old, were intradermally injected with 100 *m*g of ovalbumin/mouse in incomplete Freund adjuvant. The second immunization followed 21 days after the first immunization. Serum from mice was collected on day 10 after the second immunization. Antibody concentration was measured by ELISA.

Cytokine Detection—Concentrations of TNF*a* and IL-6 in BMDC culture supernatants were determined by Ready-SET-Go! ELISA kits from eBioscience according to the instructions of the manufacturer.

Microscopy—For live cell microscopy, BMDCs and BMMFs expressing SCIMP-YFP were transferred into Lab-Tek cham-bered coverglass (Nunc, Thermo Fisher Scientific), and strongly autofluorescent zymosan particles were subsequently added. Cells were observed in a climate chamber (37 °C, 5% CO_2) under a Leica TCS SP5 confocal microscope using a 63 objective lens (Leica Microsystems). Data were analyzed using LAS AF software (Leica Microsystems).

Author Contributions—J. K. conducted the majority of the experiments, analyzed the results, and wrote most of the paper. M. F. was involved in the preparation of BMDCs and conducted the part of the experiments addressing the expression and function of SCIMP in BMDCs. J. P. performed the analysis of antibody production by Scimp $^{/}$ mice. T. S. performed part of the BMDC biochemical analysis. B. M. designed and conducted part of the flow cytometry analysis. T. B. conceptualized and supervised the project, conducted some of the biochemical experiments, and wrote the paper with J. K. All authors reviewed the results and approved the final version of the manuscript.

Acknowledgments—We thank the International Knockout Mouse Consortium and the Wellcome Trust Sanger Institute for providing us with Scimp $^{/}$ mice. We also thank Bengt Hansson from Biogredia AB (Sandefjord, Norway) for providing us with a generous amount of soluble b-glucan (Wellmune Soluble). We also acknowledge the Microscopy Centre, IMG ASCR (Prague, Czech Republic) for support with obtaining the scientific data presented in this paper.

References

1. Hardison, S. E., and Brown, G. D. (2012) C-type lectin receptors orchestrate antifungal immunity. *Nat. Immunol.* **13,** 817– 822
2. Seo, B. S., Lee, S. H., Lee, J. E., Yoo, Y. C., Lee, J., and Park, S. R. (2013) Dectin-1 stimulation selectively reinforces LPS-driven IgG1 production by mouse B cells. *Immune Netw.* **13,** 205–212
3. Taylor, P. R., Brown, G. D., Reid, D. M., Willment, J. A., Martinez-Pomares, L., Gordon, S., and Wong, S. Y. (2002) The *b*-glucan receptor, dectin-1, is predominantly expressed on the surface of cells of the monocyte/macrophage and neutrophil lineages. *J. Immunol.* **169,** 3876 –3882
4. Willment, J. A., Marshall, A. S., Reid, D. M., Williams, D. L., Wong, S. Y., Gordon, S., and Brown, G. D. (2005) The human *b*-glucan receptor is widely expressed and functionally equivalent to murine Dectin-1 on primary cells. *Eur. J. Immunol.* **35,** 1539 –1547
5. Brown, G. D., and Gordon, S. (2001) Immune recognition: a new receptor for *b*-glucans. *Nature* **413,** 36 –37
6. Barreto-Bergter, E., and Figueiredo, R. T. (2014) Fungal glycans and the innate immune recognition. *Front. Cell. Infect. Microbiol.* **4,** 145
7. Brown, G. D., Herre, J., Williams, D. L., Willment, J. A., Marshall, A. S., and Gordon, S. (2003) Dectin-1 mediates the biological effects of *b*-glucans. *J. Exp. Med.* **197,** 1119 –1124
8. Brown, G. D., Taylor, P. R., Reid, D. M., Willment, J. A., Williams, D. L., Martinez-Pomares, L., Wong, S. Y., and Gordon, S. (2002) Dectin-1 is a major *b*-glucan receptor on macrophages. *J. Exp. Med.* **196,** 407– 412
9. Saijo, S., Fujikado, N., Furuta, T., Chung, S. H., Kotaki, H., Seki, K., Sudo, K., Akira, S., Adachi, Y., Ohno, N., Kinjo, T., Nakamura, K., Kawakami, K., and Iwakura, Y. (2007) Dectin-1 is required for host defense against *Pneu-mocystis carinii* but not against *Candida albicans*. *Nat. Immunol.* **8,** 39–46
10. Marakalala, M. J., Vautier, S., Potrykus, J., Walker, L. A., Shepardson, K. M., Hopke, A., Mora-Montes, H. M., Kerrigan, A., Netea, M. G., Murray, G. I., Maccallum, D. M., Wheeler, R., Munro, C. A., Gow, N. A., Cramer, R. A., *et al.* (2013) Differential adaptation of *Candida albicans in vivo* modulates immune recognition by dectin-1. *PLoS Pathog.* **9,** e1003315
11. Steele, C., Rapaka, R. R., Metz, A., Pop, S. M., Williams, D. L., Gordon, S., Kolls, J. K., and Brown, G. D. (2005) The *b*-glucan receptor dectin-1 rec-ognizes specific morphologies of *Aspergillus fumigatus*. *PLoS Pathog.* **1,** e42
12. Ferwerda, B., Ferwerda, G., Plantinga, T. S., Willment, J. A., van Spriel, A. B., Venselaar, H., Elbers, C. C., Johnson, M. D., Cambi, A., Huysamen, C., Jacobs, L., Jansen, T., Verheijen, K., Masthoff, L., Morré, S. A., *et al.* (2009) Human dectin-1 deficiency and mucocutaneous fungal infections. *N. Engl. J. Med.* **361,** 1760 –1767
13. Plantinga, T. S., van der Velden, W. J., Ferwerda, B., van Spriel, A. B., Adema, G., Feuth, T., Donnelly, J. P., Brown, G. D., Kullberg, B. J., Blijlevens, N. M., and Netea, M. G. (2009) Early stop polymorphism in human DECTIN-1 is associated with increased *Candida* colonization in hematopoietic stem cell transplant recipients. *Clin. Infect. Dis.* **49,** 724 –732
14. Sancho, D., and Reis e Sousa, C. (2012) Signaling by myeloid C-type lectin receptors in immunity and homeostasis. *Annu. Rev. Immunol.* **30,** 491–529
15. Brubaker, S. W., Bonham, K. S., Zanoni, I., and Kagan, J. C. (2015) Innate immune pattern recognition: a cell biological perspective. *Annu. Rev. Im-munol.* **33,** 257–290
16. Dambuza, I. M., and Brown, G. D. (2015) C-type lectins in immunity: recent developments. *Curr. Opin. Immunol.* **32,** 21–27
17. Gantner, B. N., Simmons, R. M., Canavera, S. J., Akira, S., and Underhill, D. M. (2003) Collaborative induction of inflammatory responses by dectin-1 and Toll-like receptor 2. *J. Exp. Med.* **197,** 1107–1117
18. Rogers, N. C., Slack, E. C., Edwards, A. D., Nolte, M. A., Schulz, O., Schweighoffer, E., Williams, D. L., Gordon, S., Tybulewicz, V. L., Brown, G. D., and Reis e Sousa, C. (2005) Syk-dependent cytokine induction by Dectin-1 reveals a novel pattern recognition pathway for C type lectins. *Immunity* **22,** 507–517
19. Goodridge, H. S., Reyes, C. N., Becker, C. A., Katsumoto, T. R., Ma, J., Wolf, A. J., Bose, N., Chan, A. S., Magee, A. S., Danielson, M. E., Weiss, A.,

Vasilakos, J. P., and Underhill, D. M. (2011) Activation of the innate immune receptor Dectin-1 upon formation of a "phagocytic synapse." *Nature* **472,** 471– 475

20. Willment, J. A., Lin, H. H., Reid, D. M., Taylor, P. R., Williams, D. L., Wong, S. Y., Gordon, S., and Brown, G. D. (2003) Dectin-1 expression and func-tion are enhanced on alternatively activated and GM-CSF-treated macro-phages and are negatively regulated by IL-10, dexamethasone, and lipopo-lysaccharide. *J. Immunol.* **171,** 4569 – 4573
21. Mantegazza, A. R., Barrio, M. M., Moutel, S., Bover, L., Weck, M., Brossart, P., Teillaud, J.-L., and Mordoh, J. (2004) CD63 tetraspanin slows down cell migration and translocates to the endosomal-lysosomal-MIICs route after extracellular stimuli in human immature dendritic cells. *Blood* **104,** 1183–1190
22. Meyer-Wentrup, F., Figdor, C. G., Ansems, M., Brossart, P., Wright, M. D., Adema, G. J., and van Spriel, A. B. (2007) Dectin-1 interaction with tetras-panin CD37 inhibits IL-6 production. *J. Immunol.* **178,** 154 –162
23. Berditchevski, F., and Odintsova, E. (2007) Tetraspanins as regulators of protein trafficking. *Traffic* **8,** 89 –96
24. Draber, P., Vonkova, I., Stepanek, O., Hrdinka, M., Kucova, M., Skopcova, T., Otahal, P., Angelisova, P., Horejsi, V., Yeung, M., Weiss, A., and Brdicka, T. (2011) SCIMP, a transmembrane adaptor protein involved in major histocompatibility complex class II signaling. *Mol. Cell. Biol.* **31,** 4550 – 4562
25. Stepanek, O., Draber, P., and Horejsi, V. (2014) Palmitoylated transmembrane adaptor proteins in leukocyte signaling. *Cell. Signal.* **26,** 895–902
26. Di Carlo, F. J., and Fiore, J. V. (1958) On the composition of zymosan. *Science* **127,** 756 –757
27. Underhill, D. M., Ozinsky, A., Hajjar, A. M., Stevens, A., Wilson, C. B., Bassetti, M., and Aderem, A. (1999) The Toll-like receptor 2 is recruited to macrophage phagosomes and discriminates between pathogens. *Nature* **401,** 811– 815
28. Takeuchi, O., Kaufmann, A., Grote, K., Kawai, T., Hoshino, K., Morr, M., Mühlradt, P. F., and Akira, S. (2000) Cutting edge: preferentially the R-ste-reoisomer of the mycoplasmal lipopeptide macrophage-activating lipo-peptide-2 activates immune cells through a toll-like receptor 2- and MyD88-dependent signaling pathway. *J. Immunol.* **164,** 554 –557
29. Akira, S. (2000) Toll-like receptors: lessons from knockout mice. *Biochem. Soc. Trans.* **28,** 551–556
30. Jia, X. M., Tang, B., Zhu, L. L., Liu, Y. H., Zhao, X. Q., Gorjestani, S., Hsu, Y.M., Yang, L., Guan, J. H., Xu, G. T., and Lin, X. (2014) CARD9 mediates Dectin-1-induced ERK activation by linking Ras-GRF1 to H-Ras for anti-fungal immunity. *J. Exp. Med.* **211,** 2307–2321
31. André, P., Cambier, J. C., Wade, T. K., Raetz, T., and Wade, W. F. (1994) Distinct structural compartmentalization of the signal transducing func-tions of major histocompatibility complex class II (Ia) molecules. *J. Exp. Med.* **179,** 763–768
32. McGreal, E. P., Rosas, M., Brown, G. D., Zamze, S., Wong, S. Y., Gordon, S., Martinez-Pomares, L., and Taylor, P. R. (2006) The carbohydrate-rec-ognition domain of Dectin-2 is a C-type lectin with specificity for high mannose. *Glycobiology* **16,** 422– 430
33. Xu, S., Huo, J., Lee, K.-G., Kurosaki, T., and Lam, K.-P. (2009) Phospho-lipase C*g*2 is critical for Dectin-1-mediated Ca^2 flux and cytokine pro-duction in dendritic cells. *J. Biol. Chem.* **284,** 7038 –7046
34. Koretzky, G. A., Abtahian, F., and Silverman, M. A. (2006) SLP76 and SLP65: complex regulation of signalling in lymphocytes and beyond. *Nat. Rev. Immunol.* **6,** 67–78
35. Jun, J. E., Rubio, I., and Roose, J. P. (2013) Regulation of ras exchange factors and cellular localization of ras activation by lipid messengers in T cells. *Front. Immunol.* **4,** 239
36. Slack, E. C., Robinson, M. J., Hernanz-Falcón, P., Brown, G. D., Williams, D. L., Schweighoffer, E., Tybulewicz, V. L., and Reis e Sousa, C. (2007) Syk-dependent ERK activation regulates IL-2 and IL-10 production by DC stimulated with zymosan. *Eur. J. Immunol.* **37,** 1600 –1612
37. Zhu, W., Downey, J. S., Gu, J., Di Padova, F., Gram, H., and Han, J. (2000) Regulation of TNF expression by multiple mitogen-activated protein ki-nase pathways. *J. Immunol.* **164,** 6349 – 6358
38. Wu, Y.-J., Wu, Y.-H., Mo, S.-T., Hsiao, H.-W., He, Y.-W., and Lai, M.-Z. (2015) Cellular FLIP inhibits myeloid cell activation by suppressing selec-tive innate signaling. *J. Immunol.* **195,** 2612–2623
39. Cenci, E., Mencacci, A., Casagrande, A., Mosci, P., Bistoni, F., and Romani, L. (2001) Impaired antifungal effector activity but not inflammatory cell recruitment in interleukin-6-deficient mice with invasive pulmonary aspergillosis. *J. Infect. Dis.* **184,** 610 – 617
40. Romani, L., Mencacci, A., Cenci, E., Spaccapelo, R., Toniatti, C., Puccetti, P., Bistoni, F., and Poli, V. (1996) Impaired neutrophil response and CD4 T helper cell 1 development in interleukin 6-deficient mice infected with *Candida albicans*. *J. Exp. Med.* **183,** 1345–1355
41. van Enckevort, F. H., Netea, M. G., Hermus, A. R., Sweep, C. G., Meis, J. F., Van der Meer, J. W., and Kullberg, B. J. (1999) Increased susceptibility to systemic candidiasis in interleukin-6 deficient mice. *Med. Mycol.* **37,** 419 – 426
42. Filler, S. G., Yeaman, M. R., and Sheppard, D. C. (2005) Tumor necrosis factor inhibition and invasive fungal infections. *Clin. Infect. Dis.* **41,** S208-S212
43. Vallabhaneni, S., and Chiller, T. M. (2016) Fungal infections and new biologic therapies. *Curr. Rheumatol. Rep.* **18,** 29
44. Sonoda, E., Pewzner-Jung, Y., Schwers, S., Taki, S., Jung, S., Eilat, D., and Rajewsky, K. (1997) B cell development under the condition of allelic in-clusion. *Immunity* **6,** 225–233
45. Hou, B., Reizis, B., and DeFranco, A. L. (2008) Toll-like receptors activate innate and adaptive immunity by using dendritic cell-intrinsic and -ex-trinsic mechanisms. *Immunity* **29,** 272–282
46. Edwards, A. D., Diebold, S. S., Slack, E. M., Tomizawa, H., Hemmi, H., Kaisho, T., Akira, S., and Reis e Sousa, C. (2003) Toll-like receptor expres-sion in murine DC subsets: lack of TLR7 expression by CD8 *a* DC cor-relates with unresponsiveness to imidazoquinolines. *Eur. J. Immunol.* **33,** 827– 833
47. Chatterjee, P., Tiwari, R. K., Rath, S., Bal, V., and George, A. (2012) Mod-ulation of antigen presentation and B cell receptor signaling in B cells of beige mice. *J. Immunol.* **188,** 2695–2702

The Journal of Immunology

Dysregulated NADPH Oxidase Promotes Bone Damage in Murine Model of Autoinflammatory Osteomyelitis

Jarmila Kralova, Ales Drobek, Jan Prochazka, Frantisek Spoutil, Matej Fabisik, Daniela Glatzova, Simon Borna, Jana Pokorna, Tereza Skopcova, Pavla Angelisova, Martin Gregor, Pavel Kovarik, Radislav Sedlacek and Tomas Brdicka

J Immunol 2020; 204:1607-1620; Prepublished online 5 February 2020;
doi: 10.4049/jimmunol.1900953
http://www.jimmunol.org/content/204/6/1607

The Journal of Immunology is published twice each month by The American Association of Immunologists, Inc., 1451 Rockville Pike, Suite 650, Rockville, MD 20852

Print ISSN: 0022-1767 Online ISSN: 1550-6606.

Dysregulated NADPH Oxidase Promotes Bone Damage in Murine Model of Autoinflammatory Osteomyelitis

Jarmila Kralova,*,[1] Ales Drobek,*,†,[1] Jan Prochazka,‡,x,[1] Frantisek Spoutil,x Matej Fabisik,*,{ Daniela Glatzova,*,{ Simon Borna,*,{ Jana Pokorna,* Tereza Skopcova,* Pavla Angelisova,* Martin Gregor,‖ Pavel Kovarik,# Radislav Sedlacek,‡,x and Tomas Brdicka*

Autoinflammatory diseases are characterized by dysregulation of the innate immune system, leading to spontaneous inflammation. Pstpip2^{cmo} mouse strain is a well-characterized model of this class of disorders. Because of the mutation leading to the lack of adaptor protein PSTPIP2, these animals suffer from autoinflammatory chronic multifocal osteomyelitis similar to several human syndromes. Current evidence suggests that it is driven by hyperproduction of IL-1b by neutrophil granulocytes. In this study, we show that in addition to IL-1b, PSTPIP2 also negatively regulates pathways governing reactive oxygen species generation by neutrophil NOX2 NADPH oxidase. Pstpip2^{cmo} neutrophils display highly elevated superoxide production in response to a range of stimuli. Inactivation of NOX2 NADPH oxidase in Pstpip2^{cmo} mice did not affect IL-1b levels, and the autoinflammatory process was initiated with similar kinetics. However, the bone destruction was almost completely alleviated, suggesting that dysregulated NADPH oxidase activity is a key factor promoting autoinflammatory bone damage in Pstpip2^{cmo} mice. The Journal of Immunology, 2020, 204: 1607–1620.

Autoinflammatory diseases represent a distinct class of disorders of the innate immune system. They are char-acterized by a pathological inflammation that typically arises spontaneously without detectable extrinsic cause and in the absence of autoantibodies or autoreactive T cells. The symptoms are rather diverse. The most characteristic include periodic fever attacks, skin rashes, arthralgia, myalgia, abdominal pain, arthritis, osteomyelitis, and other signs of systemic or organ specific inflammation (1–3). A number of autoinflammatory diseases are caused by a pathological hyperactivity of IL-1b pathway, either as a result of mutations in single genes affecting inflammasomes and other components of IL-1b activation machinery or from more complex causes in which the underlying genetic lesion is unknown (1, 3).

Bone damage or other types of bone involvement are common in IL-1b–driven autoinflammatory diseases (4). IL-1b promotes osteoclast activity by stimulating RANKL expression in osteoblasts and by direct binding to osteoclasts. This way it likely stimulates inflammatory bone resorption by these cells during the course of the disease (4, 5). Interestingly, different diseases of this group show different and distinct types of bone damage. Moreover, the bone damage is often observed only in a fraction of patients with a particular disease (4, 6, 7). These observations suggest that the character of genetic lesion, genetic modifiers, or other circumstances are critically affecting the outcome (4). However, the identity of these factors and the mechanisms of how they change the clinical picture are largely unknown.

One of the key activators of IL-1b pathway mutated in several autoinflammatory conditions is NLRP3 inflammasome. It is activated by aberrant ion fluxes; lysosomal damage by crystalline matter, such as silica or monosodium urate crystals; mitochondrial damage; presence of reactive oxygen species (ROS); and various microbial products and molecules associated with cellular damage (8–12). Several unifying mechanisms enabling recognition of such a variety of stress agents by a single type of inflammasome have been suggested, but none of them has yet gained universal

*Laboratory of Leukocyte Signalling, Institute of Molecular Genetics of the Czech Academy of Sciences, 14220 Prague, Czech Republic; †Laboratory of Adaptive Immunity, Institute of Molecular Genetics of the Czech Academy of Sciences, 14220 Prague, Czech Republic; ‡Laboratory of Transgenic Models of Diseases, Institute of Molecular Genetics of the Czech Academy of Sciences, 25242 Vestec, Czech Republic; xCzech Centre for Phenogenomics, Institute of Molecular Genetics of the Czech Academy of Sciences, 25242 Vestec, Czech Republic; {Faculty of Science, Charles University, 12800 Prague, Czech Republic; ‖Laboratory of Integra-tive Biology, Institute of Molecular Genetics of the Czech Academy of Sciences, 14220 Prague, Czech Republic; and #Max F. Perutz Laboratories, University of Vienna, 1030 Vienna, Austria

[1]J.K., A.D., and J.P. contributed equally to this work.

ORCIDs: 0000-0003-3017-2666 (J.K.); 0000-0003-1066-9413 (A.D.); 0000-0002-7310-3487 (F.S.); 0000-0002-4742-3196 (D.G.); 0000-0001-8445-2634 (S.B.); 0000-0003-2956-0944 (P.K.); 0000-0002-1560-4398 (T.B.).

Received for publication August 7, 2019. Accepted for publication January 13, 2020.

This work was supported by the Czech Science Foundation (Project 17-07155S). It also benefited from institutional funding by the Czech Academy of Sciences (RVO 68378050). In addition, it was supported by core facilities of the Institute of Molecular Genetics funded by Projects LM2015040 from the Czech Centre for Phenogenomics and LQ1604 NPU II from the Ministry of Education, Youth and Sports of the Czech Republic; Projects CZ.1.05/1.1.00/02.0109 from the Biotechnology and Biomedicine Centre of the Academy of Sciences and Charles University in Vestec and CZ.1.05/2.1.00/19.0395 Higher quality and capacity for transgenic models from the Ministry of Education, Youth and Sports of the Czech Republic and the European Regional Development Fund; Project CZ.02.1.01/0.0/0.0/16_013/0001789 Upgrade of the Czech Centre for Phenogenomics: developing towards translation research by the Ministry of Education, Youth and Sports of the Czech Republic and the European Structural and Investment Funds; the Light Microscopy Core Facility was supported by the Ministry of Education, Youth and Sports of the Czech Republic (LM2015062, CZ.02.1.01/0.0/0.0/16_013/0001775, and LO1419), and Operational Programme Prague - Competitiveness (CZ.2.16/3.1.00/21547). J.K. and D.G. received additional support from the Charles University Grant Agency (Project 923116).

Address correspondence and reprint requests to Dr. Tomas Brdicka, Institute of Molecular Genetics of the Czech Academy of Sciences, Videnska 1083, 14220 Prague, Czech Republic. E-mail address: tomas.brdicka@img.cas.cz

The online version of this article contains supplemental material.

Abbreviations used in this article: BM, bone marrow; CMO, chronic multifocal osteomyelitis; CRMO, chronic recurrent multifocal osteomyelitis; mCT, microcomputed tomography; PKC, protein kinase C; ROS, reactive oxygen species; WT, wild-type.

acceptance (8, 9, 11–13). Production of ROS represents one such a mechanism that could connect cellular stress to NLRP3 inflammasome activation (for review, see 10, 14). In most of the cell types, there appear to be at least two main sources of ROS, NADPH oxidases, and mitochondria (15). In phagocytes, NOX2 NADPH oxidase is activated downstream of receptors for mi-crobial products and other proinflammatory stimuli. It generates superoxide anion, which can be further converted to a number of additional ROS toxic to microorganisms. Various NADPH oxidases are also part of a broad array of signaling pathways in multiple cell types (16, 17). Mitochondrial ROS are produced mainly as a result of respiratory chain activity, and their genera-tion can be enhanced by stress or mitochondrial damage (18–20). Although initial reports suggested that NADPH oxidase–derived ROS are critical for NLRP3 inflammasome triggering, more recent studies rather support the view that mitochondria are the essential source of ROS required for its activation (21, 22). However, whether NADPH oxidase ROS can contribute to NLRP3 inflam-masome activation when deregulated as a result of neutrophil priming or during diseases that result in exaggerated NADPH oxidase-dependent ROS production has not been studied.

Several studies have shown increased production of ROS in monocytes from autoinflammatory disease patients (10, 23–28). In some of these works it has been proposed that these ROS are of mitochondrial origin (10, 23), but there are only limited options of how to study this aspect in patients. The effects of increased ROS production, whether of mitochondrial or NADPH oxidase origin, on the development and/or severity of autoinflammatory diseases is currently unknown.

There are relatively few mouse models of autoinflammatory bone diseases. One of the best characterized is Pstpip2^{cmo} mouse strain, which spontaneously develops severe bone and soft tissue inflammation mainly in hind paws and tail. In several aspects, the disease resembles a human condition known as chronic recurrent multifocal osteomyelitis (CRMO) and was thus termed chronic multifocal osteomyelitis (CMO). From there, the strain derives its name Pstpip2^{cmo} (29). The disease is caused by a point mutation in the gene coding for the adaptor protein PSTPIP2 (30). As a result, no PSTPIP2 is detectable in these mice at the protein level (31). The mechanism by which PSTPIP2 deficiency leads to CMO disease is only partially understood. It binds several inhibitory molecules, including PEST-family protein tyrosine phosphatases, phosphoinositide phosphatase SHIP1, and inhibitory kinase Csk, which likely mediate its negative regulatory effect on the inflammatory response (32, 33). In addition, it has been reported that osteomyelitis in Pstpip2^{cmo} mice is completely dependent on excessive IL-1b production by neutrophilic granulocytes (34–36). Genetic studies suggest a combined involvement of the NLRP3 inflammasome and a poorly characterized mechanism dependent on caspase-8. A relatively limited role of neutrophil proteases has also been demonstrated (36, 37). The involvement of NLRP3 inflammasome suggests that cellular stress and ROS might be involved in CMO disease pathology, especially, when we consider the fact that neutrophils are very potent producers of NADPH oxidase–derived ROS. Moreover, ROS are also activators of osteoclasts (38), a cell type likely responsible for inflammatory bone damage in CMO mice (39). In this study, we show that in Pstpip2^{cmo} neutrophils, superoxide generation by NADPH oxidase is profoundly dysregulated and these cells produce substantially increased amounts of superoxide in response to variety of stimuli. Strikingly, the dysregulated superoxide production by these neutrophils does not have a strong effect on IL-1b production and soft tissue inflammation, but rather on the bone inflam-mation and subsequent bone damage, suggesting that the role of NADPH-oxidase–derived ROS is not in triggering the CMO but rather in directing the damage accompanying this disease to the bones.

Materials and Methods

Abs

Abs to the following murine Ags were used: RAC1/2/3 (catalog no. 2465; Cell Signaling Technology, Danvers, MA); p47phox (D-10) and ERK2 (C-14) (Santa Cruz Biotechnology, Dallas, TX); B220-biotin, TER119-biotin, c-Kit-biotin, CD3ε-biotin, Ly6G-biotin, CD115-biotin, CD11b-allophycocyanin, CD11b-FITC, CD11b-PE, B220-FITC, Ly6C-PE-Cy7, Ly6C-FITC, Ly6G-FITC, Ly6G-allophycocyanin, c-Kit-PE, Sca-1-allophycocyanin, and CD16/32-PE/Cy7 (BioLegend, San Diego, CA); CD34-FITC, DX5-biotin, F4/80-biotin, and Thy1.2-FITC (eBioscience, ThermoFisher Scientific, Waltham, MA); Fc Block (2.4G2) (BD Biosciences, San Jose, CA); and HRP-conjugated goat anti-mouse IgG (Sigma -Aldrich) and HRP-goat anti-rabbit (Bio-Rad, Hercules, CA). The mouse mAb that recognizes murine PSTPIP2 has been described earlier (33). Heat-aggregated IgG was prepared as follows: IgG was purified from mouse serum (Sigma-Aldrich) on protein A–Sepharose (GE Healthcare, Uppsala, Sweden), transferred to PBS, and concentrated to 30 mg/ml on an Amicon Ultracel–30K unit (Millipore, Merck, Darmstadt, Germany). The aggregation was induced by heating to 63˚C for 30 min.

Other reagents

In this study we also used luminol, HRP, LPSs from Escherichia coli O127:B8, fMLP, PMA, (all from Sigma-Aldrich), L-012 (Wako Chem-icals), TNF-a, G-CSF (PeproTech, Rocky Hill, NJ), U0126 (Cell Signaling Technology), and Go¨6976 (Calbiochem, Merck). Silica (silicon dioxide crystals) was obtained from Sigma-Aldrich. To enable fluorescent labeling for microscopy, 5 mg/ml silica particles were first coated with nonfat dry milk (2% in PBS, 1 h at room temperature) and then labeled with 5 mM Cell Proliferation Dye eFluor 670 (eBioscience), 30 min at 37˚C.

Mice

Pstpip2^{cmo} mouse strain (C.Cg-Pstpip2^{cmo}/J) carrying the c.293T→C mutation in the Pstpip2 gene (on BALB/C genetic background) resulting in an L98P change in the PSTPIP2 protein (29, 30), B6.129S-Cybb^{tm1Din}/J lacking NADPH oxidase subunit gp91phox (40); MyD88 deficient mouse strain (B6.129P2(SJL)-MyD88$^{tm1.1Defr}$/J, derived from MyD88^{fl} mice (41); B6.SJL-Ptprca Pepcb/BoyJ (CD45.1^{+}) congenic strain (42), B6.Cg-Tg(S100A8-cre,-EGFP)1Ilw/J with granulocyte-specific CRE expression (MRP8-Cre) (43); and Gt(ROSA)26Sor$^{tm1(DTA)Lky}$/J strain (44), in which diphtheria toxin expression can be induced by CRE recombinase, were obtained from The Jackson Laboratory (Bar Harbor, ME). Pstpip2^{cmo} mouse strain was backcrossed on C57BL/6J background for at least 10 generations and then used in the majority of experiments, with the ex-ception of experiments in Figs. 1E, 4A, 4D–F and Supplemental Fig. 1. For these experiments, the original Pstpip2^{cmo} strain on BALB/c genetic background has been selected due to the higher number of neutrophils that could be obtained by the negative selection method and due to the better quality of immortalized granulocyte progenitors derived from this strain. Both genetic backgrounds showed similar disease symptoms and similar dysregulation in superoxide production. The BALB/c and C57BL/6J inbred strains were obtained from the animal facility of Institute of Mo-lecular Genetics, Academy of Sciences of the Czech Republic (Prague, Czech Republic). Pstpip2^{cmo}-DTA-MRP8-Cre mouse strain was generated by breeding of the Pstpip2^{cmo} mice on C57BL/6J background with Gt(ROSA)26Sor$^{tm1(DTA)Lky}$/J strain mouse strain. Breeding this strain to B6. Cg-Tg(S100A8-cre,-EGFP)1Ilw/J mice carrying Cre transgene under the control of granulocyte-specific MRP8 promoter resulted in the generation of Pstpip2^{cmo}-DTA-MRP8-Cre strain lacking almost all granulocytes (Supplemental Fig. 3B, 3C). Mice were housed and bred in an accredited animal facility at the Institute of Molecular Genetics of the Czech Acad-emy of Sciences (registration number CZ11760038). They were main-tained under specific pathogen-free conditions. Animals were fed by standard breeding fortified diet (Altromin) cereal-based (soy, wheat, corn) fixed formula, which is free of alfalfa and fish/animal meal and deficient in nitrosamines, containing 22.6% crude protein, 5% crude fat, 4.5% crude fiber, 7.1% crude ash, autoclavable, and increased vitamin content. The drinking water was purified via reverse osmosis system and chlorinated by chlorine dioxide (ClO_2) as an alternative disinfectant to prevent secondary contamination. The final concentration of active chlorine was maintained between 0.6 and 1.0 ppm (in acid pH 4–5). Experimental cohorts, sex and age matched, were made from both genders, and standard randomization

was applied. Unless indicated otherwise, age of animals ranged from 6 to 14 wk. Experiments in this work that were conducted on animals were approved by the Expert Committee on the Welfare of Experimental Animals of the Institute of Molecular Genetics and by the Academy of Sciences of the Czech Republic (registration numbers 69/2014, 62/2015, 50/2016, 66/2016, 45/2018) and were in agreement with local legal requirements and ethical guidelines.

Primary cells and cell lines

All primary cells and cell lines were cultured at 37˚C with 5% CO_2 in IMDM supplemented with 10% FCS and antibiotics. For bone marrow (BM) cell isolation, mice were sacrificed by cervical dislocation, BM was flushed with PBS supplemented with 2% FCS, and erythrocytes were lysed in an ACK buffer (150 mM NH_4Cl, 0.1 mM EDTA [disodium salt], 1 mM $KHCO_3$). Murine neutrophils were isolated from BM cells using anti-biotin MicroBeads and LS magnetic columns (Miltenyi Biotec, Bergisch Gladbach, Germany). For negative selection, cells were labeled with bio-tinylated Abs to B220, F4/80, DX5, c-Kit, CD3ε, CD115, and Ter119 prior to magnetic bead purification. For positive selection, only anti-Ly6G biotin was used. The purity of isolated cells was determined by flow cytometry. Primary murine monocytes were sorted from BM cells as Ly6G negative, Ly6C highly positive, and side scatter–low cells using BD Influx sorter (BD Biosciences). The following cell lines were used in this study: HEK293FT cells (Invitrogen), Platinum Eco cells (Plat-E cells; Cell Biolabs, San Diego, CA), and immortalized granulocyte progenitors. For preparation of immortalized granulocyte progenitors we used a modified version of the protocol for generation of immortalized macrophage progenitors (45). The progenitors were first enriched by the depletion of Mac-1^+, $B220^+$, and $Thy1.2^+$ from mouse BM cells and cultured in the presence of IL-3, IL-6, and SCF (supplied as culture supernatants from HEK293FT cells transfected with constructs coding for respective cytokines) for 2 d. Next, progenitors were transduced with ER-HoxB8 construct. The transduced cells were enriched for the GMP progenitor population by FACS (Lin^-, $Sca\text{-}1^-$, $c\text{-}Kit^+$, $FcgR^+$, $CD34^+$) and propagated in a medium containing 1 mM b-estradiol and 1% SCF-containing supernatant. Granulocyte differentiation was induced by b-estradiol withdrawal or by the b-estradiol withdrawal and replacement of SCF for G-CSF (50 ng/ml).

Flow cytometry

Single-cell suspensions of BM cells were incubated with Fc block and fluorophore-conjugated Abs and analyzed on a BD LSR II flow cytometer. For calcium response measurement, single-cell suspensions of BM from 6- to 8-wk-old mice were loaded with 2 mM calcium indicator Fura Red (Invitrogen). Samples were analyzed using a BD LSR II flow cytometer for 30 s at rest and then another 210 s after activation (with fMLP, Silica, or E. coli with OD = 0.8). The relative calcium concentration was mea-sured as a ratio of the Fura Red fluorescence intensity elicited by excitation wavelengths of 405 nm (emission measured at 635–720 nm) and 488 nm (emission measured at 655–695 nm). Data were acquired on a BD flow cytometer LSR II. Granulocytes were gated according to forward and side scatter properties. For F-actin detection, BM cells were fixed with 4% formaldehyde and labeled with fluorophore-conjugated Abs to CD11b, Ly6C, and Ly6G. Next, the cells were permeabilized with l-a-lysophosphatidylcholine (80 mg/ml; Sigma-Aldrich) and simultaneously stained with Alexa Fluor 488–conjugated phalloidin (Invitrogen). The cell fluorescence was measured on a BD LSR II flow cytometer. Gran-ulocytes were gated as $CD11b^+$, $Ly6C^{int}$, and $Ly6G^+$. The data were analyzed with FlowJo software (Tree Star, Ashland, OR).

Superoxide detection

Superoxide production in vitro was assessed by luminol-based chemiluminescence assay as published previously (46, 47). BM cells or purified murine neutrophils in IMDM supplemented with 0.2% FCS were plated in a density of 10^6 cells per well into a black 96-well plate (SPL Life Sci-ences, Naechon-Myeon, Korea). Cells were rested for 30 min at 37˚C and 5% CO_2. Then, luminol at final concentration 100 mM and stimuli (100 ng/ml LPS, fMLP 1 mg/ml, TNF-a 10 ng/ml, E. coli OD_{600} ~0.8– 53 diluted, silica 50 mg/cm^2, heat-aggregated murine IgG 300 mg/ml, PMA 100 ng/ml) were added. Luminescence was measured immediately on an EnVision plate reader (Perkin Elmer, Waltham, MA); each well was scanned every minute for 70 min. For fMLP-induced superoxide production, scanning every 10 s for 5 min was also used as indicated in figure legends. To measure superoxide production by cells in suspension, the cells were kept at 10^7 per 0.9 ml IMDM with 0.2% FCS and 100 mM luminol in an Eppendorf tube at 37˚C. After stimulation with 100 ml silica (1 mg/ml), every 5 min a 100-ml aliquot of cell suspension was gently transferred into an empty well of a black 96-well plate and the luminescence was immediately measured on an EnVision plate reader. When fMLP (1 mg/ml) was used as a stimulant, only a single aliquot of 10^6 cells was measured in 10-s intervals in a single well immediately after cell transfer to the plate and activation. For exogenous peroxidase treatment, cells were incubated with HRP (10 mg/ml) for 30 min prior to stimulation with silica.

To assess ROS production in vivo, mice were i.p. injected with luminescence reporter L-012 in final concentration 75 mg/kg (1.8 mg/25 g mouse) dissolved in PBS as previously described (48). Luminescence signal was acquired by Xtreme whole body imager (Bruker, Billerica, MA), with the following settings: binning 8 3 8, exposure time: 5 min. The quantification of photon counts was performed in Molecular Imag-ing Software (Bruker).

DNA constructs

Generation of MSCV-PSTPIP2-EGFP construct was as follows. The coding sequence of mouse PSTPIP2 was amplified from cDNA of mouse common myeloid progenitors and subcloned into pXJ41-EGFP cloning vector (Chum et al. 2016). IRES and Thy1.1 coding sequence was removed from MSCV-IRES-Thy1.1 retroviral vector (Clontech, Mountain View, CA) by digestion with EcoRI and ClaI followed by blunt ligation. PSTPIP2-EGFP coding sequence was then subcloned into modified MSCV vector using BglII and XhoI restriction sites to generate MSCV-PSTPIP2-EGFP.

Generation of MSCV-mPSTPIP2-TetOn inducible constructs. Wild-type (WT) and mutated sequences (W232A or 3YF) of mouse PSTPIP2 de-scribed earlier (33) were fused to C-terminal EGFP by PCR using P2A sequence as a linker. Fusion constructs were cloned into pLVX-Tet3G doxycycline inducible vector (Clontech) using AgeI and BamHI restriction sites. Resulting vectors were used as templates to amplify the Tet-On 3G, TRE3G, and PSTPIP2 sequences by PCR, and the resulting product was cloned into MSCV-IRES-EGFP vector using ClaI and BglII restriction sites.

Retroviral transduction

For confocal microscopy, c-kit+ stem and progenitor cells were obtained from BM of $Pstpip2^{cmo}$ (C57BL/6J) mice using magnetic purification (c-kit–biotin Ab, Anti-biotin microbeads). Cells were expanded in IL-3, IL-6, and SCF-supplemented media for 20 h, then infected with PSTPIP2-EGFP retroviral construct. For the production of replication incompetent retrovirus, ecotropic packaging cells (Plat-E) were plated in a 10-cm dish and transfected with 24 mg of plasmid DNA using Lipofectamine 2000 Reagent (Life Technologies) according to the manufacturer's instructions. Virus-containing supernatant was collected, concentrated with Amicon Ultra centrifugal filters with molecular mass cut-off 100 kDa (Merck Millipore), and immediately used to infect the cytokine expanded c-kit+ BM cells. These cells were centrifuged with 150 ml of concentrated virus supernatant and 2.4 ml of Lipofectamine 2000 Reagent (Sigma-Aldrich) at 1250 3 g for 90 min at 30˚C and then incubated for another 4 h at 37˚C in 5% CO_2 in a humidified incubator before the exchange of the media. Immortalized granulocyte progenitors were propagated in IMDM with 1 mM b-estradiol and 1% SCF-containing supernatant and then infected with PSTPIP2 mutant constructs using the same procedure described above.

Real-time quantitative PCR

RNA was purified with Zymo Research Quick-RNA Miniprep Plus Kit from neutrophils isolated by positive selection (see above). The reverse transcription was performed with RevertAid First Strand cDNA Synthesis Kit (ThermoFisher Scientific). Real-time quantitative PCR was carried out using LightCycler 480 SYBR Green I Master mix (Roche) and the following primers: 59-TGTAATGAAAGACGGCACACC-39 + 59-TCTTCTTTG-GGTATTGCTTGG-39 for IL-1b and 59-GATCTGGCACCACACCTTCT-39 + 59-GGGGTGTTGAAGGTCTCAAA-39 for b-actin on Roche LightCycler 480 Instrument II. The primer functionality was verified on LPS-stimulated BM-derived dendritic cells.

Microscopy

One day postinfection, EGFP-positive cells were sorted on an Influx sorter and injected into sublethally irradiated (6 Gy in a single dose) $CD45.1^+$ recipient mice. After 2 wk, mice were sacrificed, and BM cells isolated and resuspended in IMDM with 0.1% FCS. The cells were activated by 50 mg/cm^2 fluorescent silica (see above) in a 96-well plate for 10 min. The cells were transferred to 4% paraformaldehyde in PBS and fixed at room temperature for 20 min. Cell nuclei were stained with 10 mg/ml Hoechst 33258 (Sigma-Aldrich) for 15 min. Cells were than washed two

times with PBS, resuspended in 150 ml of ddH2O, and centrifuged on glass slide at 300 3 g for 5 min using Centurion Scientific K3 cytospin cen-trifuge (Centurion Scientific, Stoughton, U.K.). Cell samples were then mounted in 10 ml of DABCO mounting reagent (Sigma-Aldrich) and covered with glass coverslip (Zeiss, Oberkochen, Germany). The microscope setup was as follows: sequential two-color imaging was performed using a Leica TCS SP8 laser scanning confocal microscope (Leica, Wetzlar, Germany) with a 63 3 1.4 numerical aperture oil-immersion objective. Acquired images were manually thresholded to remove signal noise detected outside of the cell using ImageJ software.

Cell activation, lysis, and immunoprecipitation

For Western blotting, the cells were washed and resuspended in IMDM with 0.1% FCS at a concentration of 1–4 3 10^7 cells/ml. Subsequently, the cells were stimulated as indicated at 37˚C. The activation of cells was stopped by the addition of an equal volume of a 23 concentrated SDS-PAGE sample buffer (128 mM Tris [pH 6.8], 10% glycerol, 4% SDS, 2% DTT), followed by the sonication and heating of the samples (99˚C for 2 min). The samples were analyzed by SDS-PAGE followed by Western blotting. For detection of p47phox phosphorylation, phosphoproteins were isolated from BM cells using PhosphoProtein purification Kit (Qiagen, Hilden, Germany) according to manufacturer's instructions, followed by detection of p47phox by immunoblotting.

RAC activity assay

A total of 2 3 10^7 neutrophils (silica activated or not) were lysed in 1 ml lysis buffer (25 mM HEPES [pH 7.2], 150 mM NaCl, 10 mM $MgCl_2$, 1 mM EDTA, 1% NP-40, 10% glycerol, 100 3 diluted Protease Inhibitor Cocktail Set III [Calbiochem, Merck]) containing 5 mg PAK-RBD-GST (RAC-binding domain from PAK1 fused to GST, isolated from E. coli strain BL21 transformed with corresponding expression plasmid). After preclearing the lysate by centrifugation, the complexes of active RAC and PAK-RBD-GST were isolated on Glutathione Sepharose (GE Healthcare). RAC was then detected by immunoblotting.

Anesthesia

Mice for in vivo imaging were anesthetized by i.m. injection of Zoletil (20 mg/ml)–Xylazine (1 mg/ml) solution with Zoletil dose 100 mg/kg and Xylazine dose 1 mg/kg.

X-ray microcomputerized tomography

Hind paws were scanned in in vivo x-ray microcomputed tomography (mCT) Skyscan 1176 (Bruker). Scanning parameters were voltage, 50 kV; current, 250 mA; filter, 0.5 mm aluminum; voxel size, 8.67 mm; exposure time, 2 s; rotation step, 0.3˚ for 180˚ total; object to source distance, 119.271 mm; and camera to source distance, 171.987 mm; with time of scanning, 30 min. Reconstruction of virtual slices was performed in NRecon software 1.6.10 (Bruker) with setup for smoothing = 3, ring artifact correction = 4, and beam hardening correction = 36%. Intensities of interest for reconstruction were in the range of 0.0045 to 0.0900. For reorientation of virtual slices to the same orientation, the DataViewer 1.5.2 software (Bruker) was used.

For mCT data analysis, CT Analyzer 1.16.4.1 (Bruker) was used. The volume of interest was chosen there containing the distal part of hind paw starting from the half of metatarsus. Based on differences of x-ray absorption, three parts were analyzed separately: the whole volume of interest, the newly formed bone connected mostly with arthritis, and the area inhabited by the original bone of phalanges and metatarsi. The total volume was recorded for all three parts. For original and new bone, other parameters from two-dimensional and three-dimensional analysis were recoded to describe changes in the structure, namely, surface of the bone, surface/volume ratio, number of objects, closed porosity, mean fractal dimension, mean number of objects per slice, mean closed porosity per slice, and mean fractal dimension per slice. Scans with technical artifacts caused by spontaneous movements of animals were excluded from the analysis. Raw data are available upon request.

Cytokine detection

Murine paws were homogenized in 1 ml RIPA lysis buffer (20 mM TRIS [pH 7.5], 150 mM NaCl, 1% Nonidet P-40, 1% sodium deoxycholate, 0.1% SDS) containing 5 mM iodoacetamide (Sigma-Aldrich) and 100 3 diluted Protease Inhibitor Cocktail Set III (Calbiochem, Merck) using Avans AHM1 Homogenizer (30 s, speed 25). Any insoluble material was re-moved by centrifugation (20,000 3 g, 5 min, 2˚C), and concentration of the proteins in the samples were normalized to the same level using Bradford solution (AppliChem). Concentrations of IL-1b in the samples were determined by Ready-SET-Go! ELISA kits from eBioscience according to the instructions of the manufacturer.

Histology

The paws were fixed in 10% formol solution for 24 h and decalcified in Osteosoft (Merck) solution for 1 wk, followed by paraffin embedding and histological cutting. The slides were stained in automatic system Ventana Symphony (Roche), and slides were scanned in Axio Scan.Z1 (Zeiss). The image postprocessing and analysis was done in Zen software (Zeiss).

Statistical analysis

The p values were calculated in GraphPad Prism software (GraphPad Software, La Jolla, CA) using unpaired t test (two-tailed) for data in Figs. 2B–G, 2I, 3C, 5E; one-way ANOVA with Tukey–Kramer or Bonferroni multiple comparison posttest for data in Figs. 1E, 4A, 6E, 7B, and 7D; Mann–Whitney U test for Fig. 5C; and Gehan–Breslow–Wilcoxon test for disease-free curve in Fig. 6C. Symbol meanings are as follows: n.s. p . 0.05, *p # 0.05, **p # 0.01, ***p # 0.001, ****p # 0.0001. Unless stated otherwise, "n" in figure legends represent number of experi-ment repeats, points in column scatter plots represent biological replicates (in most cases animals), error bars in these plots show median with inter-quartile range, and points and error bars in superoxide production time course curves (arbitrary luminescence intensity curves) represent mean 6 SEM values obtained from two to eight technical replicates.

Results

Pstpip2^{cmo} neutrophils produce substantially more superoxide in response to inflammasome activator silica than WT neutrophils

Disease development in Pstpip2^{cmo} mice is, in part, dependent on NLRP3 inflammasome (37). Because ROS are involved in the NLRP3 inflammasome regulation, we tested if their production was dysregulated in Pstpip2^{cmo} BM cells. We isolated these cells from WT C57BL/6 and Pstpip2^{cmo} mice (backcrossed to the same genetic background) and stimulated these cells with silica parti-cles, a well-established activator of NLRP3 inflammasome (49) employed in previous studies of Pstpip2^{cmo} mice (33–35). Strik-ingly, this stimulation led to a substantially higher superoxide production by Pstpip2^{cmo} cells, when compared with their WT counterparts (Fig. 1A). This assay was performed in a 96-well plate, where the response could be affected by adhesion of the cells to plastic. Therefore, we carried out a similar measurement on the cells maintained strictly in suspension. This resulted in signals of lower intensity. However, the dysregulation of superoxide pro-duction by Pstpip2^{cmo} cells could still be observed (Fig. 1B).

Because superoxide generation is a characteristic feature of neutrophils, which form a large fraction of BM leukocytes (Fig. 1C), we have isolated these cells for further testing. Silica stimulation of adherent neutrophils, isolated by negative selection, led to even higher production of superoxide when compared with the full BM. Moreover, the difference between WT and Pstpip2^{cmo} cells was still preserved (Fig. 1D). In our experiments, negatively selected neutrophils were typically more than 90% pure. However, a large fraction of the contaminating cells were monocytes. Be-cause these cells are also known to respond by ROS production to a variety of stimuli, we have analyzed superoxide generation by purified monocytes. To determine the impact of these cells on our results, we have adjusted the quantity of monocytes to 10% of the neutrophil numbers, which is similar to the amount of monocytes contaminating our neutrophil samples prepared by negative se-lection. We compared the response of these monocytes with the superoxide production by neutrophils isolated by positive selec-tion on Ly6G. This purification resulted in virtually pure (more than 99%) neutrophils. The response of purified monocytes was almost two orders of magnitude lower than that of purified neu-trophils, and there was no significant difference between WT and

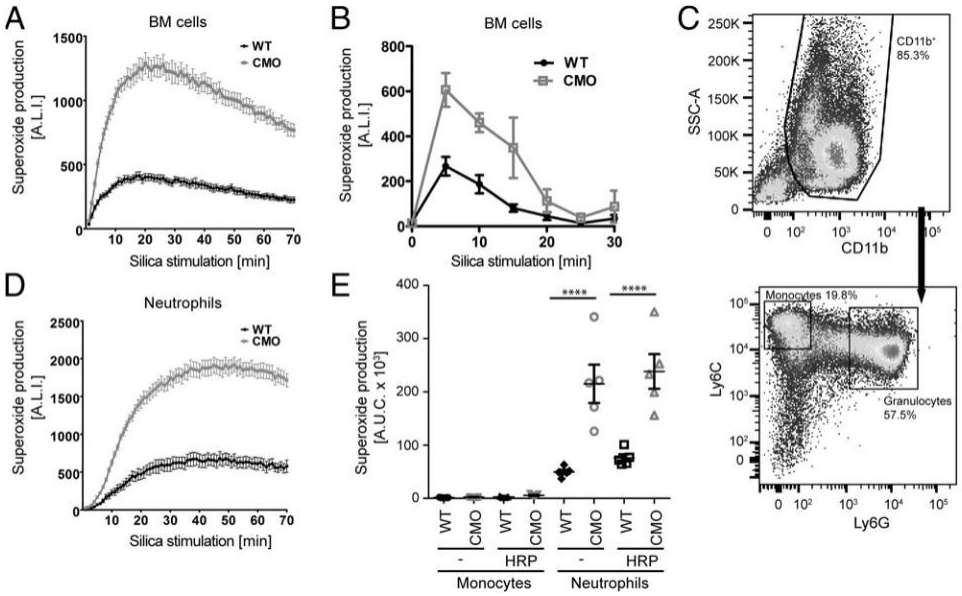

FIGURE 1. Pstpip2^{cmo} neutrophils produce higher amounts of superoxide. (A) Superoxide production by silica-stimulated Pstpip2^{cmo} (CMO) and WT BM cells measured in 1-min intervals by luminol-based chemiluminescence assay (for quantification of multiple experiments, see Fig. 2B). (B) Similar measurement as in (A) performed on BM cells held in suspension (5-min intervals; for quantification of multiple experiments, see Fig. 2C). (C) Representative flow cytometry dot plot showing percentages of monocytes and neutrophils in Pstpip2^{cmo} BM (n . 5). (D) Similar experiment as in (A) performed on neutrophils purified by negative selection (for quantification of multiple experiments, see Fig. 2B). (E) The superoxide production by silica-stimulated neutrophils purified by positive selection (10^6 per well) is compared with superoxide production by FACS-sorted (Ly6C$^+$, Ly6G^2) monocytes (10^5 per well) stimulated in the same manner in the presence or absence of HRP (n = 3). ****p # 0.0001. A.L.I., arbitrary luminescence intensity; A.U.C., area under the curve.

Pstpip2^{cmo} cells (Fig. 1E). Addition of exogenous peroxidase (HRP) to compensate for lower myeloperoxidase expression in monocytes (50) did not substantially alter the results (Fig. 1E). These data demonstrated that in the neutrophil samples prepared by negative selection, the monocyte contribution to the measured superoxide production is negligible. They also lead to the conclu-sion that even in nonseparated BM, the vast majority of superoxide originated from neutrophils and that neutrophils are responsible for enhanced superoxide production by Pstpip2^{cmo} BM cells.

Higher superoxide production by Pstpip2^{cmo} neutrophils is observed across a range of conditions

To find out how universal the superoxide overproduction in Pstpip2^{cmo} neutrophils is, we treated either BM cells or purified neutrophils with silica, PMA, live E. coli bacteria, heat-aggregated mouse IgG (as a model of immunocomplexes), TNF-a, LPS, or fMLP. All these experiments demonstrated dysregulated super-oxide production in Pstpip2^{cmo} BM cells (Fig. 2A–D, 2F) and purified neutrophils (Fig. 2B, 2E). The same dysregulation was also observed in the BM cells with Pstpip2^{cmo} mutation on BALB/c genetic background (Supplemental Fig. 1A). These results show that PSTPIP2 deficiency renders neutrophils more sensitive and prone to produce more ROS than WT cells. Interestingly, unsti-mulated BM cells from Pstpip2^{cmo} mice produced low but de-tectable levels of superoxide even in the absence of any stimulus.

This constitutive production has not been observed in WT BM (Fig. 2A, 2G). It also was not observed in both WT and Pstpip2^{cmo} cells maintained in suspension (data not shown). In addition, nonadherent cells also did not show any superoxide production in response to treatment with LPS, TNF-a, and fMLP when mea-sured in 5-min intervals (data not shown). However, in the case of fMLP, rapid transient response was detectable within the first 5 min of the measurement (Fig. 2H). Maximum superoxide pro-duction was not significantly altered in Pstpip2^{cmo} BM cells. However, it was more sustained, and total superoxide production was thus higher than in WT cells (Fig. 2I).

Pstpip2^{cmo} neutrophils do not produce excessive superoxide as a consequence of ongoing inflammation and do not show the signs of spontaneous priming

Higher superoxide production under resting conditions and after activation with a wide range of stimuli demonstrates general dysregulation of pathways leading to superoxide production in Pstpip2^{cmo} neutrophils. This dysregulation could be cell intrinsic because of PSTPIP2 deficiency or a side effect of ongoing bone inflammation, which could prime BM neutrophils located in the proximity of the inflamed tissue. It has previously been reported that autoinflammation in Pstpip2^{cmo} mice is completely dependent on IL-1b and its receptor (34, 35). Signaling through this receptor is critically dependent on MyD88 adaptor protein (51). To deter-mine whether the observed overproduction of ROS in Pstpip2^{cmo} neutrophils is not just the effect of ongoing inflammation, we crossed Pstpip2^{cmo} mice with MyD88-deficient strain to block IL-1b signaling. As expected, Pstpip2^{cmo} mice were in the absence of MyD88 completely protected from the disease development as determined by visual inspection (Fig. 3A) and x-ray mCT of hind paws (Fig. 3B). MyD88-deficient Pstpip2^{cmo} BM cells displayed the same dysregulation in superoxide production triggered by a variety of stimuli as Pstpip2^{cmo} cells. Treatments with LPS or E. coli were the only exceptions where the response was substantially lower in both Pstpip2^{cmo}/MyD88$^{2/2}$ and MyD88$^{2/2}$ cells, probably due to the higher dependence of signaling triggered by these activators on the TLR/MyD88 pathway. Nevertheless, even in MyD88-deficient cells, the cmo mutation gave rise to a stronger response to these two stimuli when compared with MyD88-deficient cells without the cmo mutation (Fig. 3C, Supplemental Fig. 1B). These results demonstrate the cell-intrinsic dysregulation of NADPH oxidase machinery that is not caused by chronic exposure to the in-flammatory environment.

Another potential explanation for the observed dysregulation of superoxide generation is that Pstpip2^{cmo} neutrophils are in a constitutively primed state. Increased superoxide production is

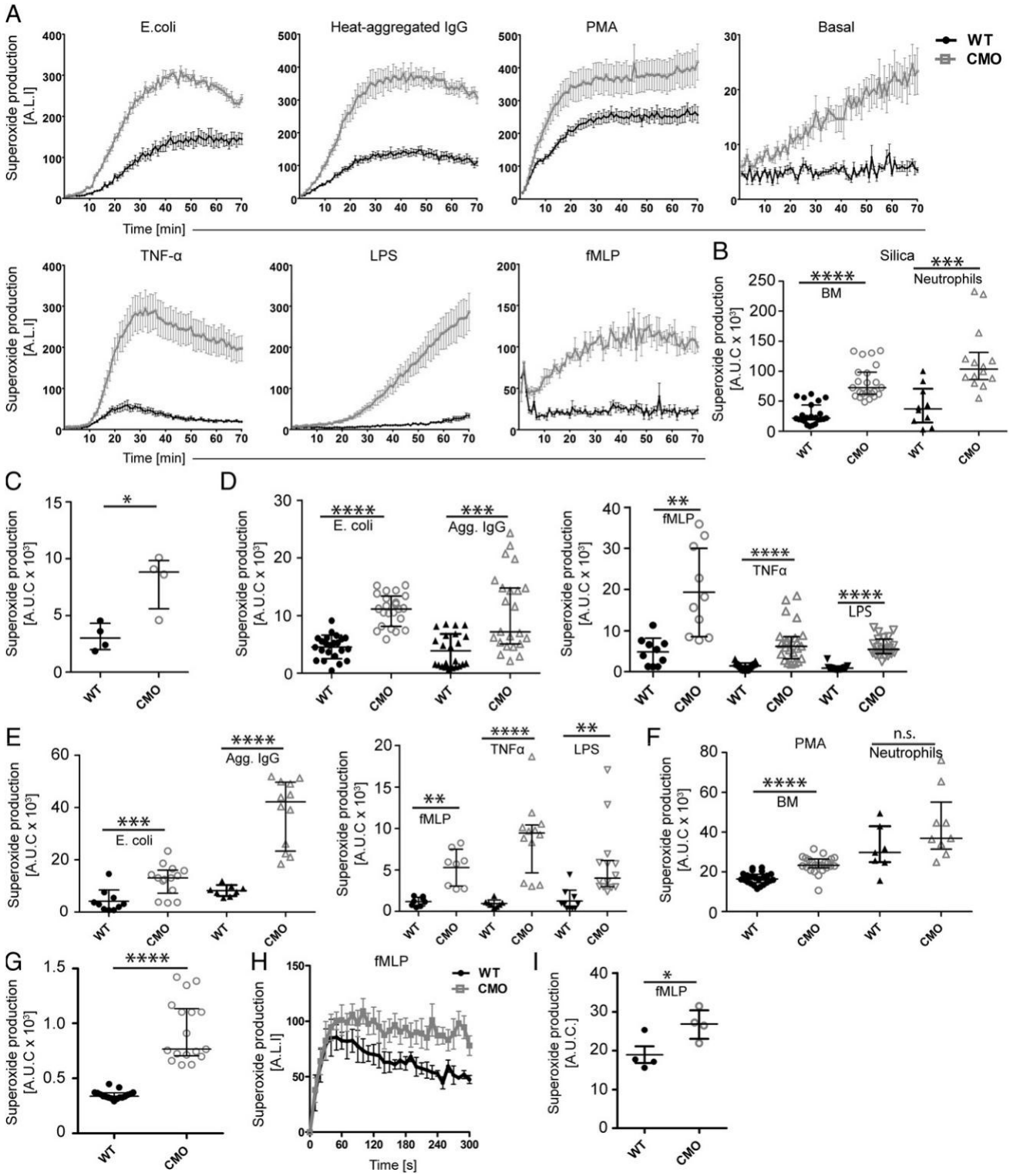

FIGURE 2. Increased superoxide production by Pstpip2^{cmo} neutrophils is triggered by a variety of stimuli. (A) Superoxide production by adherent Pstpip2^{cmo} (CMO) and WT BM cells treated with indicated agents (for quantification of multiple experiments, see D–G). (B) Quantification of superoxide production by adherent BM cells and neutrophils after silica treatment (n = 4 for BM and n = 5 for neutrophils). (C) Quantification of superoxide production by BM cells activated by silica in suspension (n = 2). (D) Quantification of superoxide production by adherent BM cells treated with live E. coli bacteria (E.coli), mouse aggregated IgG (IC), fMLP, TNF-a, and LPS (n = 4). (E) Similar analysis as in (D), performed on neutrophils purified by negative selection (n = 5 for E. coli and n = 3 for aggregated [Agg.] IgG). (F) Quantification of superoxide production by adherent BM cells and neutrophils after treatment with PMA (n = 4). (G) Quantification of basal superoxide production by nonstimulated adherent BM cells. (H) Superoxide production by nonadherent Pstpip2^{cmo} (CMO) and WT BM cells treated with fMLP. Measurement was performed in 10-s intervals, and data were normalized to basal ROS production. (I) Quantification of data in H (n = 2). "n" represents the number of independent experiments that were combined to generate the scatter plots in (B)–(I), and points in scatter plots represent biological replicates (i.e., cells from individual mice). *p # 0.05, **p # 0.01, ***p # 0.001, ****p # 0.0001. A.L.I., arbitrary luminescence intensity; A.U.C., area under the curve; n.s., p . 0.05.

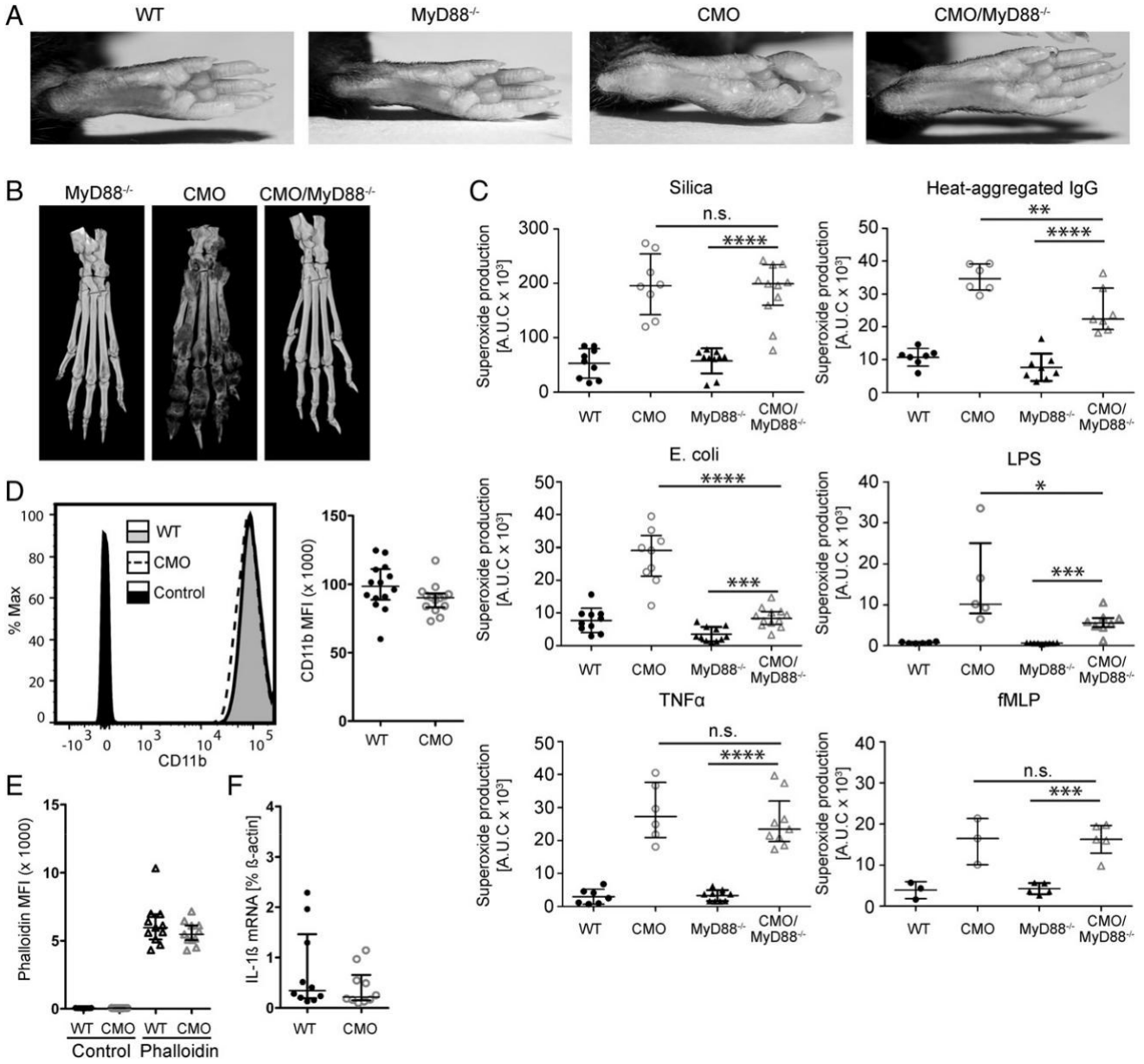

FIGURE 3. Overproduction of superoxide is not triggered by ongoing inflammation. (A) Representative hind paw photographs of 23- to 26-wk-old WT, MyD88$^{2/2}$, Pstpip2^{cmo} (CMO), and Pstpip2^{cmo}/MyD88$^{2/2}$ (CMO/MyD88$^{2/2}$) mice. (B) Representative x-ray mCT scans of hind paws from MyD88$^{2/2}$, Pstpip2^{cmo}, and Pstpip2^{cmo}/MyD88$^{2/2}$ mice, 14 wk old (n = 5 for Pstpip2^{cmo}/MyD88$^{2/2}$ and n = 3 for MyD88$^{2/2}$). (C) Quantification of superoxide production by BM cells isolated from WT, MyD88$^{2/2}$, Pstpip2^{cmo}, and Pstpip2^{cmo}/MyD88$^{2/2}$ mice and treated with indicated stimuli. For silica, n = 5; aggregated [Agg.] IgG, LPS, TNF-a, n = 4; E. coli, n = 6; fMLP, n = 3. (D) CD11b surface expression in resting neutrophils gated as Ly6G^{+} Ly6C^{+} (see Fig. 1B) measured by flow cytometry. Representative FACS plot and quantification of mean fluorescence intensities (MFI) measured in multiple experiments are shown (n = 3). (E) F-actin content in resting neutrophils gated as Ly6G^{+}Ly6C^{+} measured by flow cytometry with the use of fluorescent phalloidin on fixed and permeabilized cells. In controls, phalloidin staining was omitted (n = 3). (F) Real-time quantitative PCR quantification of IL-1b mRNA in resting neutrophils (n = 3). *p # 0.05, **p # 0.01, ***p # 0.001, ****p # 0.0001. n.s., p . 0.05.

one of the hallmarks of neutrophil priming. However, number of other changes also characterize primed neutrophils, including increased CD11b surface expression, actin cytoskeleton reorganization, and increase in IL-1b promoter activity (52–58). We have analyzed all these parameters, but we could not detect any alterations in these features (Fig. 3D–F).

Superoxide hyperproduction in Pstpip2^{cmo} neutrophils is suppressed by PSTPIP2 binding partners and is accompanied by hyperphosphorylation of p47phox

To elucidate the mechanism of how PSTPIP2 suppresses superoxide production, we employed conditionally immortalized Pstpip2^{cmo} granulocyte progenitors (45) we had established previously (33) and reconstituted these cells with doxycycline-inducible retroviral constructs coding for WT PSTPIP2 and its mutated versions unable to bind PEST-family phosphatases (W232A) and SHIP1 (3YF) (32, 33). After maturation of these progenitors into neutrophils and induction of PSTPIP2 expression with doxycycline, we treated these cells with silica and measured su-peroxide production. We observed around 50% reduction of su-peroxide generation in cells expressing WT PSTPIP2. In contrast, both mutated versions of PSTPIP2 were unable to substantially inhibit silica-induced superoxide production (Fig. 4A), despite similar expression levels of these constructs (Fig. 4B).

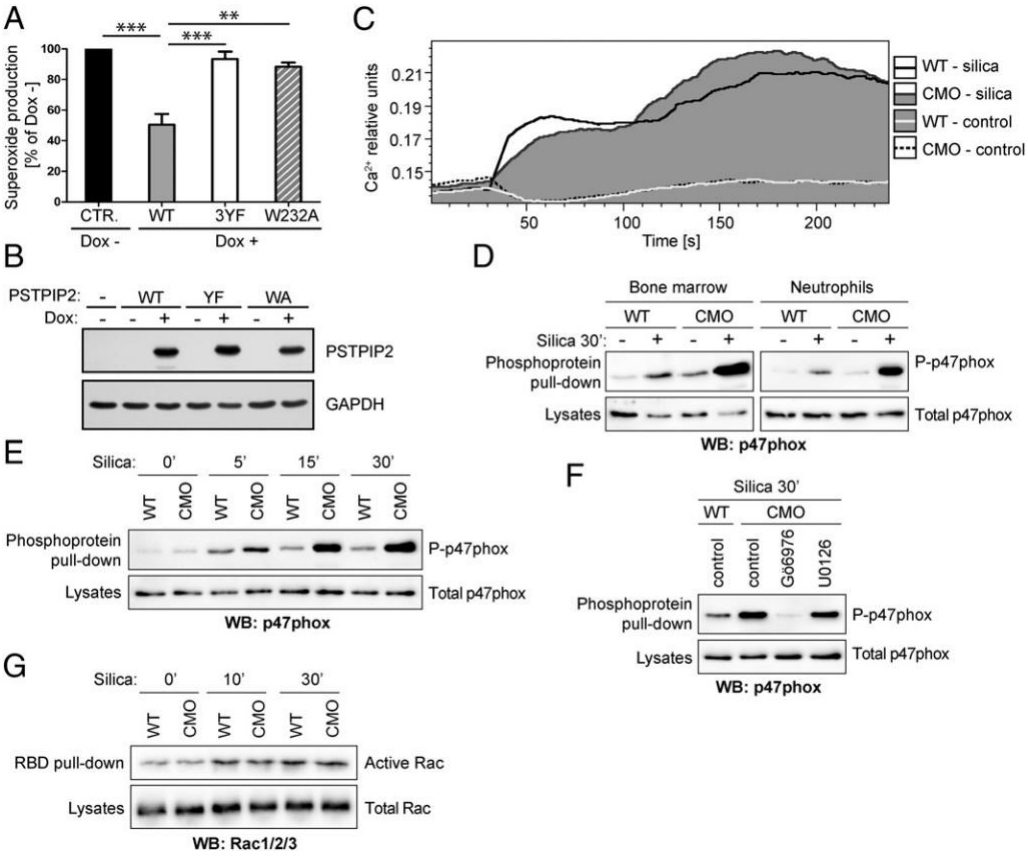

FIGURE 4. PSTPIP2-mediated suppression of superoxide production in neutrophils is dependent on PSTPIP2 binding partners and involves negative regulation of p47phox phosphorylation. (A) Suppression of superoxide production by WT and mutant PSTPIP2 in mature granulocytes differentiated from conditionally immortalized granulocyte progenitors. Expression of PSTPIP2 was triggered by overnight incubation with doxycycline. On the vertical axis, percentage of superoxide response by doxycycline-treated cells when compared with doxycycline nontreated cells is shown. Error bars represent SEM of three biological replicates. (B) Equal expression levels of PSTPIP2 variants from (A) after induction with doxycycline. (C) Calcium response of WT and Pstpip2^{cmo} neutrophils (gated from full BM) after silica treatment (n = 3). (D) Phosphorylation of p47phox in WT and Pstpip2^{cmo} BM cells and neutrophils after 30 min incubation with silica. To detect p47phox phosphorylation, total phosphoproteins were isolated from cell lysates followed by p47phox detection by immunoblotting (n = 3). (E) P47phox phosphorylation in BM cells at various time points. The phosphorylation was detected as in (D) (n = 3). (F) Phosphorylation of p47phox in Pstpip2^{cmo} neutrophils treated for 30 min with silica together with PKC inhibitor Go¨6976 or MEK inhibitor U0126. Phosphorylation of p47phox was detected as in (D) (n = 4 for Go¨6976 and n = 2 for U0126). (G) RAC activation in WT and Pstpip2^{cmo} neutrophils. Active RAC was isolated using PAK1-RBD-GST (RBD pull-down) and detected by immunoblotting with Ab to all three RAC proteins (RAC1/2/3) (n = 2). **p # 0.01, ***p # 0.001.

To analyze subcellular localization of PSTPIP2 during silica stimulation, we isolated BM progenitors from Pstpip2^{cmo} mice and transduced these cells with retroviral construct coding for PSTPIP2 fused to EGFP. Next, we transplanted these cells into lethally irradiated mice, and after 2 wk, we collected neutrophils expressing PSTPIP2-EGFP for microscopy analysis. In neutrophils, PSTPIP2 showed diffuse distribution throughout the cytoplasm, with occasional formation of speckles in a small fraction of cells (Supplemental Fig. 2, left panel, see an arrowhead). After addition of fluorescently labeled silica particles, neutrophils interacted with these particles and phagocytosed some of them (Supplemental Fig. 2, right panel, see an arrowhead). However, we did not observe any changes in PSTPIP2 subcellular localization during this process (Supplemental Fig. 2). This result suggests that large-scale redistribution of PSTPIP2 inside the cells is not part of the mechanism of how PSTPIP2 controls neutrophil activity during the treatment with silica.

To identify the dysregulated process leading to superoxide overproduction at the biochemical level, we measured the calcium response in WT and Pstpip2^{cmo} BM cells. Cells were loaded with Fura Red dye and stimulated with silica particles. We observed the same calcium response in both WT and Pstpip2^{cmo} cells (Fig. 4C), indicating that proximal signaling steps leading to calcium response are not responsible for increased ROS production in Pstpip2^{cmo} cells.

One of the major events further downstream is phosphorylation of NADPH oxidase cytosolic subunits by members of protein kinase C (PKC) family, including phosphorylation of p47phox, which then serves as an assembly hub for building the active NADPH oxidase complex (16, 59). To detect p47phox phosphorylation, we isolated phosphoproteins from untreated and silica-treated BM cells or purified neutrophils and detected p47phox in the isolated material by immunoblotting. In both Pstpip2^{cmo} BM cells and neutrophils, we found substantially stronger phosphorylation of p47phox when compared with WT cells (Fig. 4D). This difference was observed as early as 5 min after stimulation and was maintained for at least 30 min (Fig. 4E).

Although PKCs are critical for p47phox activation, costimulatory effects of other kinases have also been demonstrated (59, 60). Of these, ERK MAP kinase was shown to be dysregulated in silica-treated CMO neutrophils (33). To assess the roles of PKCs and ERK pathway in p47phox dysregulation, we have treated Pstpip2^{cmo} neutrophils either with PKC inhibitor Go¨6976 or MEK1/MEK2 inhibitor U0126 prior to activation with silica.

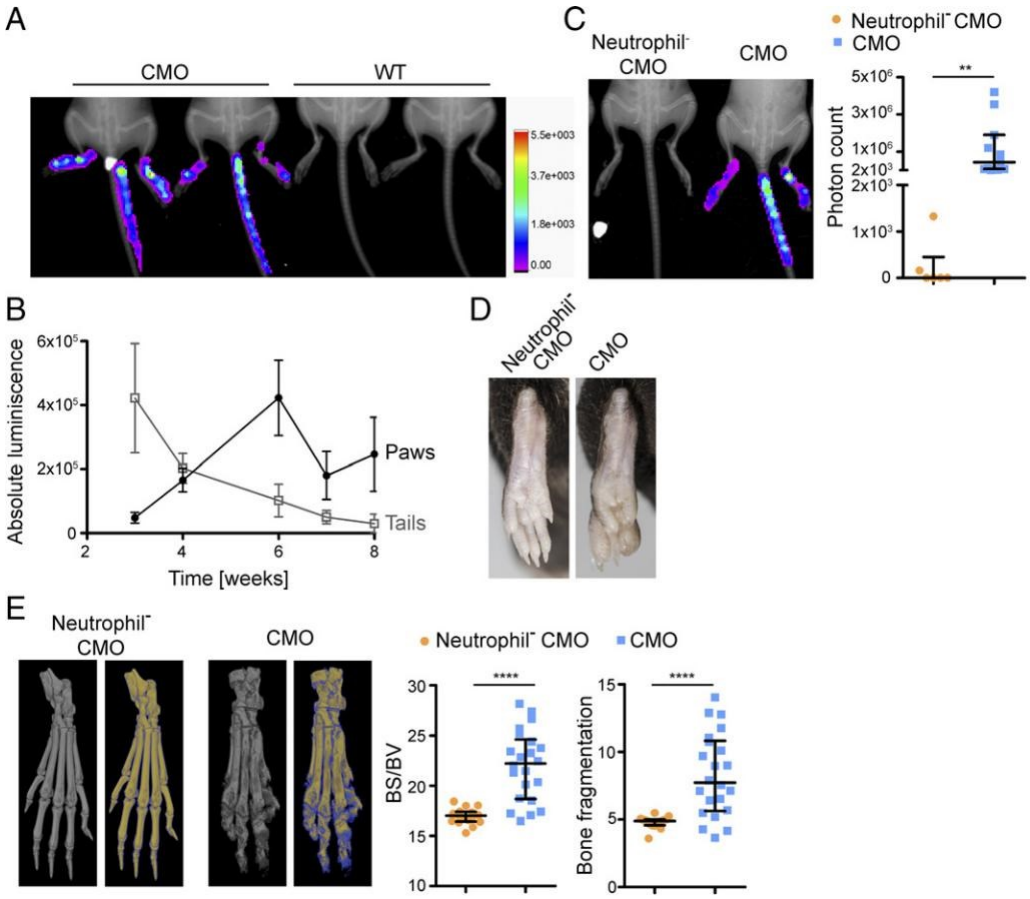

FIGURE 5. Neutrophil-dependent superoxide production in vivo precedes the onset of the disease. (A) Representative in vivo measurement of superoxide in 4-wk-old anesthetized WT and Pstpip2^{cmo} (CMO) mice injected i.p. with L-012 chemiluminescent probe. Superoxide-induced luminescence is shown as a heat-map in artificial colors on the background of an x-ray image. (B) Time course quantification of absolute L-012 luminescence driven by in vivo ROS production in Pstpip2^{cmo} mice. The luminescence was quantified separately for paws and tails (n = 6 per time point, mean 6 SEM). (C) Representative in vivo measurement of ROS production in anesthetized 4-wk-old Pstpip2^{cmo}-DTA mice where neutrophils were depleted or not via MRP8-CRE-dependent expression of diphtheria toxin (Neutrophil^2). The left panel shows quantification of in vivo ROS production in multiple mice of both genotypes (3–4 wk old). (D) Representative photographs of hind paws of 26-wk-old mice of the same genotypes as in (C). (E) Representative x-ray mCT scans of bones from 20-wk-old mice of the same genotypes as in (C). Gray images represent visualization of total bone tissue. Pseudocolor images distinguish between old (in yellow) and newly formed (in blue) bone mass. Quantification of bone surface/bone volume ratio (BS/BV) and bone fragmentation in paw bones of multiple mice is shown on the right. **p # 0.01, ****p # 0.0001.

Only the treatment with PKC inhibitor led to specific block of p47phox phosphorylation (Fig. 4F).

Small G-protein RAC is another critical component of active NADPH oxidase. We have tested the activation status of RAC after silica treatment of BM cells, but no difference between WT and Pstpip2^{cmo} cells has been observed (Fig. 4G).

Collectively, these data suggest that PSTPIP2 via its binding partners suppresses pathways leading to PKC-mediated p47phox phosphorylation and that this is the mechanism by which PSTPIP2 attenuates NADPH oxidase activity and superoxide production.

Unprovoked ROS production by neutrophils in vivo precedes the onset of the disease

To analyze the ROS production in vivo during the disease development, we used luminol derivative L-012 to visualize ROS generation in living anesthetized mice. Very interestingly, we observed a strong luminescent signal already in freshly weaned 3-wk-old mice that were otherwise asymptomatic (Supplemental Fig. 3A). The signal was mostly localized along the tail and with weaker intensity in the hind paws. Visualization at later time points revealed that at 4 wk of age, the ROS production was equally intensive in the tail and paws (Fig. 5A, 5B) and gradually moved to the hind paws during the weeks 6–8. At this age, ROS production became predominant in hind paws with more restricted focal localization (Fig. 5B, Supplemental Fig. 3A).

To test if neutrophils are the source of dysregulated ROS observed in vivo, we have generated Pstpip2^{cmo} mouse strain where the majority of neutrophils were deleted via MRP8-CRE-dependent expression of Diphtheria toxin (Pstpip2^{cmo}-DTA-MRP8-CRE, Supplemental Fig. 3B, 3C). In vivo ROS imaging revealed that ROS production in the tails and hind paws of these mice was almost completely abolished (Fig. 5C). In addition, these mice also did not show any symptoms of autoinflammatory disease, whether determined by visual inspection (Fig. 5D) or by x-ray mCT analysis (Fig. 5E). These data strongly support the idea that increased ROS production preceding the onset of the disease originates in neutrophils and, at the same time, confirm that neutrophils are critical for the development of disease symptoms (36).

NADPH oxidase deficiency has specific effects on bone destruction

Strong unprovoked production of ROS in very young mice preceding visible symptoms weeks before their demonstration suggested that ROS may act upstream of IL-1b in osteomyelitis development. To determine the contribution of high in vivo ROS

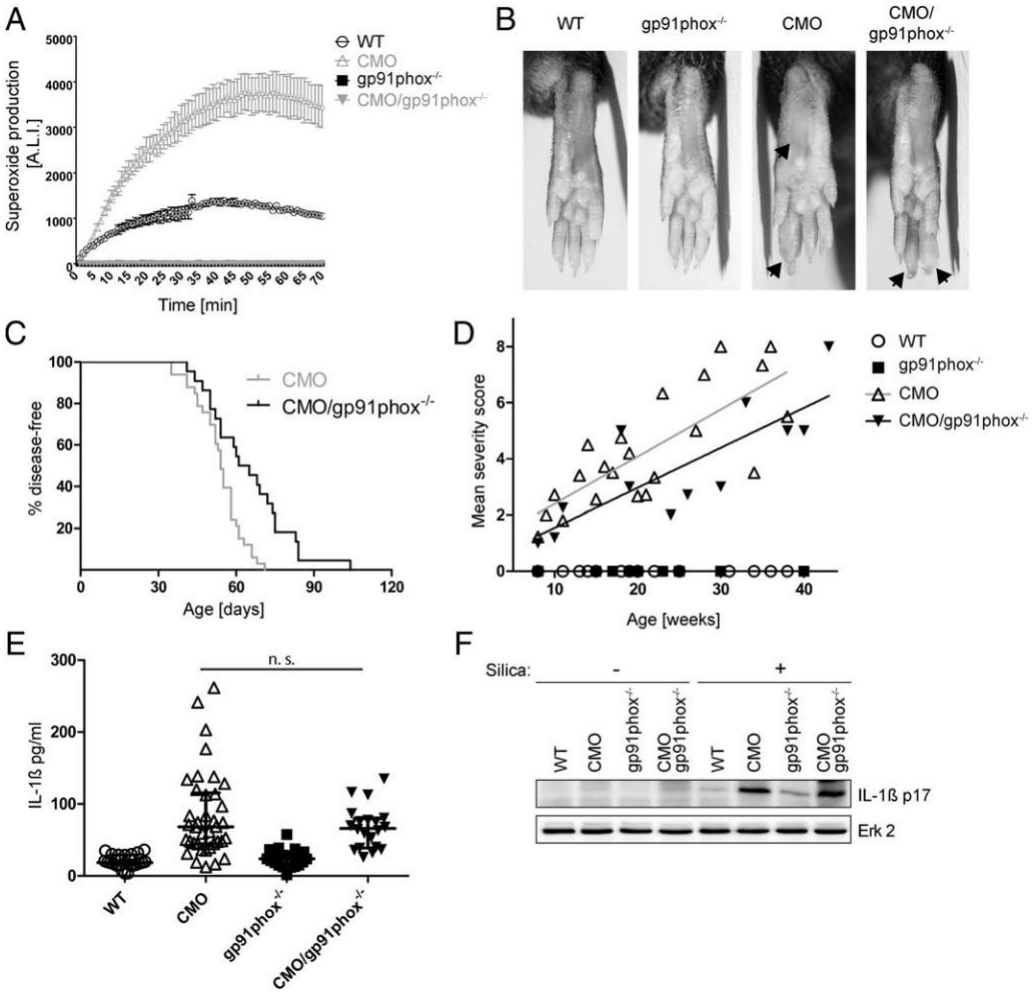

FIGURE 6. Limited effect of gp91phox deficiency on visible symptom development and IL-1b production. (A) In vitro superoxide generation induced by silica treatment in BM cells from 13- to 16-wk-old WT, Pstpip2^{cmo}, gp91phox$^{2/2}$, and Pstpip2^{cmo}/gp91phox$^{2/2}$ mice. Representative of two independent experiments. (B) Representative photographs of hind paws of 18- to 19-wk-old WT, Pstpip2^{cmo}, gp91phox$^{2/2}$, and Pstpip2^{cmo}/gp91phox$^{2/2}$ mice. (C) Disease-free curve comparing the time of disease appearance in Pstpip2^{cmo} and Pstpip2^{cmo}/gp91phox$^{2/2}$ mice. Development of visible symptoms was evaluated two to three times per week. (D) Disease severity was scored (scale from 0 to 8) by visual inspection of photographs of the hind paws collected over the course of this study. Each point represents mean value for the mice of the same age and genotype. Lines were generated using linear regression. (E) ELISA analysis of IL-1b from hind paw lysates. Samples were adjusted to the same protein concentration before analysis. Bars represent median with interquartile range. (F) Presence of processed IL-1b in the lysates from BM cells treated for 60 min (or not) with silica was detected by immuno-blotting (n = 4). n.s., p . 0.05.

generation to disease development, we crossed Pstpip2^{cmo} mice to gp91phox-deficient mouse strain. In the absence of gp91phox, we were unable to detect any superoxide production upon silica, E. coli, or aggregated IgG stimulation even in Pstpip2^{cmo} cells (Fig. 6A, data not shown). These data confirm that NADPH oxi-dase was responsible for the dysregulated ROS production in Pstpip2^{cmo} neutrophils. Surprisingly, Pstpip2^{cmo} mice lacking gp91phox developed similar disease symptoms as Pstpip2^{cmo} mice (Fig. 6B) and with similar, only slightly delayed, kinetics (Fig. 6C). Blind scoring of the disease severity by visual inspection of hind paw photographs collected throughout various experiments revealed that the symptoms of the disease are only partially alleviated in gp91phox-deficient animals, by approximately one to two points on 8-point scale (Fig. 6D). Moreover, ELISA analysis detected comparable amount of IL-1b in hind paw extracts from Pstpip2^{cmo} and Pstpip2^{cmo}/gp91phox$^{2/2}$ animals (Fig. 6E), and similar amount of processed IL-1b p17 was found in the lysates of silica-stimulated BM cells by immunoblot (Fig. 6F).

These data demonstrated that the phagocyte NADPH oxidase is dispensable for autoinflammatory disease initiation, but it affects the severity of the disease. We also noticed that the character of the hind paw edema was somewhat different in Pstpip2^{cmo}/gp91phox$^{2/2}$ mice. Typically, the swelling was most serious at the distal part of phalanges and only rarely affected metatarsal area in Pstpip2^{cmo}/gp91phox$^{2/2}$ animals, whereas in Pstpip2^{cmo} mice, metatarsi were frequently enlarged and the phalanges were often most seriously affected in their central parts (Fig. 6B).

To find out if these differences were caused by different character of bone inflammation, we performed x-ray mCT analysis of Pstpip2^{cmo} and Pstpip2^{cmo}/gp91phox$^{2/2}$ mice. Very surprisingly, bone destruction in Pstpip2^{cmo}/gp91phox$^{2/2}$ animals was almost entirely missing, whereas in Pstpip2^{cmo} mice substantial bone damage could be observed (Fig. 7A). To support this obser-vation with a quantitative analysis, we calculated bone surface to volume ratio and bone fragmentation from the x-ray mCT data. Pstpip2^{cmo}/gp91phox$^{2/2}$ mice showed similar values to WT, whereas values for Pstpip2^{cmo} mice were substantially higher (Fig. 7B). Timeline x-ray mCT scans of hind paws revealed progressive bone lesion formation in Pstpip2^{cmo} mice whereas

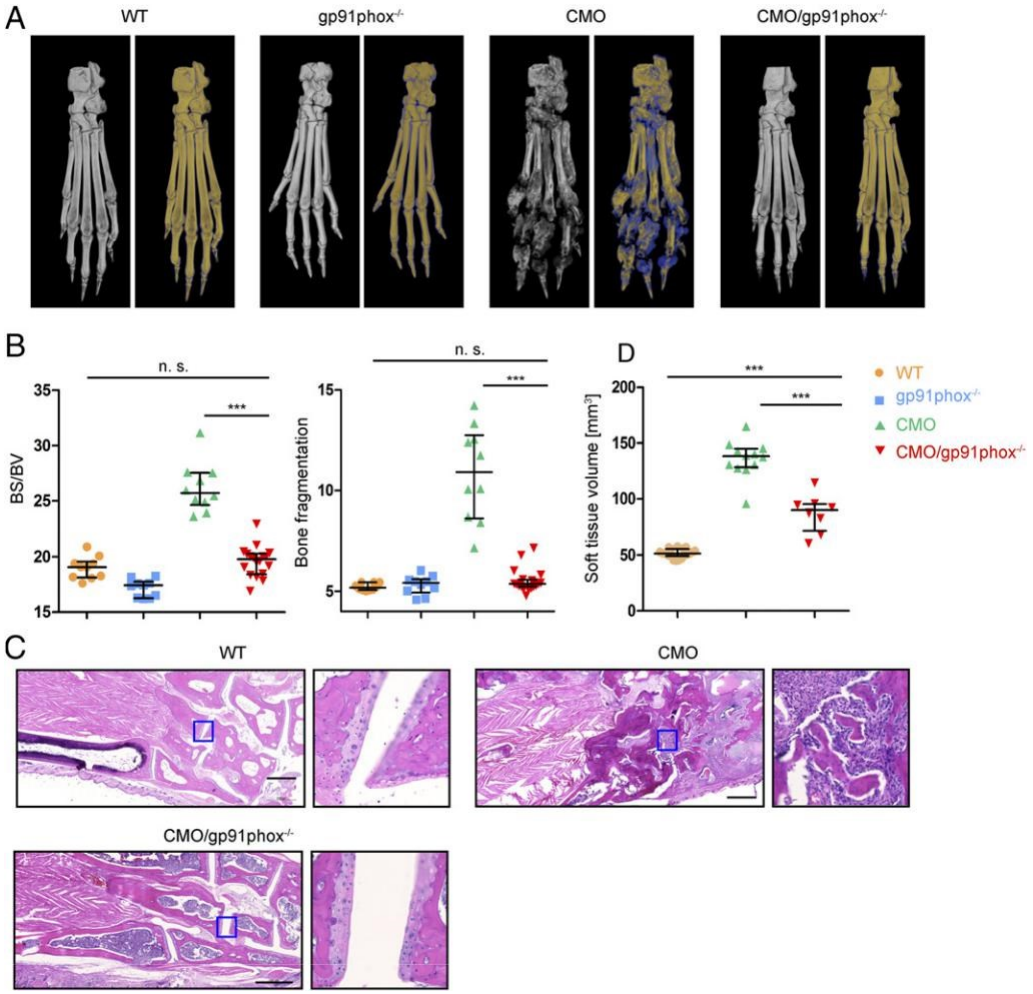

FIGURE 7. Almost complete absence of bone damage in gp91phox-deficient PSTPIP2^{cmo} mice. (A) Representative x-ray mCT scans of bones from 14-wk-old mice. Gray images represent visualization of total bone tissue. Pseudocolor images distinguish between old (in yellow) and newly formed (in blue) bone mass. (B) Quantification of bone surface/bone volume ratio (BS/BV) and bone fragmentation in paw bones of 14-wk-old mice. Bars represent median with interquartile range. (C) Sections of paraffin embedded tissue from tarsal area of hind paw stained with H&E. Scale bars, 500 mm. The regions in the blue squares are magnified and shown at the right of each image. (D) Volume of soft tissue in hind paws calculated as a total paw volume from which the bone volume has been subtracted. Values were calculated from x-ray mCT data. ***p # 0.001. n.s., p . 0.05.

Pstpip2^{cmo} gp91phox$^{2/2}$ littermates remained largely protected (Supplemental Fig. 4).

The lack of bone damage can also be demonstrated on tissue sections from tarsal area of hind paws (Fig. 7C). The CMO mice show very high level of osteolysis of tarsal bones, with almost missing joint cartilages due to arthritic changes accompanied with robust granulomatous infiltration. The WT mice have normally developed and structurally well-defined tarsal bones with undamaged joint cartilages with no infiltration of immune cells and no adverse changes in the BM. The Pstpip2^{cmo}/gp91phox$^{2/2}$ mice show a rescue effect in ossified parts of tarsal bones with no or minimal signs of bone damage by immune cells, and the soft tissue infiltration in the metatarsal area is minimal compared with CMO mice. The cartilages are also well shaped and are covering the joint areas comparably with WT animals. The difference from WT animals is in hypercellular structure of BM resulting in decreased volume of ossified tissue.

To address protection potential of gp91phox deficiency in old Pstpip2^{cmo} mice, we performed x-ray mCT scans on 7-mo-old mice. Old Pstpip2^{cmo} mice suffered from strong bone destruc-tion and remodeling but Pstpip2^{cmo}/gp91phox$^{2/2}$ mice were still protected from adverse effects of osteomyelitis (Supplemental Fig. 4). To gain a quantitative insight into the level of soft tissue inflammation, we have performed computational reconstruction of soft tissues from x-ray mCT scans described above in Fig. 7B and calculated soft tissue volume. This measurement revealed that soft tissues in Pstpip2^{cmo}/gp91phox$^{2/2}$ hind paws were significantly enlarged, albeit not to the same extent as in Pstpip2^{cmo} mice (Fig. 7D). Collectively, these data demonstrate that despite sig-nificant swelling that can be detected in the hind paw soft tissues of Pstpip2^{cmo}/gp91phox$^{2/2}$ mice, bones remain largely protected in the absence of NADPH oxidase activity.

Discussion

Monogenic autoinflammatory diseases develop as a result of dysregulation of the innate immune system. Although the speci-ficity of this branch of the immune system is relatively limited, these diseases still show tissue and organ selectivity. The mechanisms of this selectivity are often poorly understood (3). Pstpip2^{cmo} mice represent an important model of tissue-selective IL-1b–driven autoinflammatory disease that affects mainly bones and surrounding tissue in hind paws and tails (29–31). Our current studies demonstrate that IL-1b pathway is not the only pathway dysregulated in these animals. Superoxide production by neutrophil NADPH oxidase is also substantially enhanced, independently of IL-1b activity. Moreover, our data suggest that dysregulated ROS

production is a critical part of the selectivity mechanisms directing inflammatory damage to the bones.

Increased superoxide generation by neutrophil NADPH oxidase is one of the major consequences of neutrophil priming. It is a state of enhanced responsiveness attained after an exposure to priming agents such as LPS or TNF-a. These agents typically do not elicit superoxide production by themselves but rather increase its gen-eration triggered by other substances (53, 54). To find out if Pstpip2^{cmo} neutrophils are spontaneously constitutively primed, we have tested several additional parameters known to be associated with neutrophil priming, including increased expression of integrin subunit CD11b, changes in cytoskeleton organization, and IL-1b promoter activity (52–58). However, none of these traits were altered in Pstpip2^{cmo} neutrophils.

Neutrophil adhesion is also often considered a priming stimulus, because it results in similar phenotypic changes and is able to elicit enhanced superoxide production, even in response to solely priming agents such as TNF-a (54, 61). Accordingly, whereas we observed TNF-a– and LPS-induced superoxide production by adherent neutrophils, cells in suspension did not show any re-sponse, regardless of the genotype. The reaction to silica and fMLP was also substantially attenuated in nonadherent cells. However, the deregulation of responses in Pstpip2^{cmo} neutrophils could still be detected under these conditions. These data support the conclusion that dysregulation of NADPH oxidase activity in Pstpip2^{cmo} neutrophils is independent of adhesion. They also show that Pstpip2^{cmo} neutrophils are not fully primed and can still undergo priming.

Collectively, our data do not support the idea of spontaneous priming of Pstpip2^{cmo} neutrophils. They rather suggest dys-regulation of pathways controlling NADPH oxidase activity. However, it should be noted that different priming agents elicit varying sets of phenotypic changes in neutrophils (53), and some specific form of constitutive priming cannot be com-pletely disregarded.

We found that increased ROS production in Pstpip2^{cmo} mice was associated with p47phox hyperphosphorylation, leading to the conclusion that one or more pathways governing p47phox phos-phorylation are negatively regulated by PSTPIP2. MAP kinase ERK was shown to have a supporting role in p47phox activation by phosphorylating Ser 345 and 348 (62, 63). We have shown previously that ERK is also hyperactive in silica-treated CMO neutrophils (33). However, in this study we found that ERK pathway inhibition did not have any substantial effect on p47phox phosphorylation, whereas this phosphorylation could be almost completely abolished by inhibition of PKC (Fig. 4E). These data suggest that PSTPIP2 deficiency mainly affects the phosphorylation of p47phox that is PKC mediated. However, the precise mechanism is still unclear.

To our knowledge, genetically determined hyperactivation of NADPH oxidase has not yet been described or studied in the context of IL-1b activation or in autoinflammatory disease. Our observations show that elevated NADPH oxidase activity does not affect IL-1b pathway but rather the inflammatory bone damage in CMO. These data are in agreement with several other reports that disprove the role of NADPH oxidase–generated ROS in IL-1b processing by inflammasome. They are mainly based on analyses of monocytes and macrophages from NADPH oxidase–deficient patients and mice, where IL-1b production is not altered or it is even enhanced (64–67). In a single study on human neutrophils, NADPH oxidase deficiency also did not lead to reduction of NLRP3 inflammasome activity (68). In contrast, inhibition of mitochondrial ROS production in monocytes/macrophages results in an impairment of IL-1b production in these cells (19, 69), showing that the majority of ROS supporting inflammasome activation in these cell types is generated by mitochondria.

The roles of IL-1b and ROS in CMO pathophysiology appear to be different form each other. Whereas dysregulated IL-1b production is a critical trigger of the disease development, enhanced ROS production modifies the outcome. However, ROS are not able to initiate the disease on their own in the absence of IL-1b sig-naling. It is documented by our experiments with MyD88-deficient Pstpip2^{cmo} mice, which displayed the same ROS dysregulation as Pstpip2^{cmo} mice and yet they did not develop any symptoms of autoinflammation. These data also demonstrate that enhanced ROS production is not downstream of IL-1b because MyD88 is critical for signaling by IL-1R (70).

ROS are known to play a key role in differentiation and activity of osteoclasts. These cells are responsible for physiological bone resorption during bone remodeling processes. They are also involved in pathological bone damage in a number of disease states (71). Pstpip2^{cmo} mice exhibited increased osteoclastogenesis and osteoclast hyperactivity, suggesting that osteoclasts are responsible for inflammatory bone damage in these mice (39). Our data show that the bone damage can be almost completely abolished when phagocyte NADPH oxidase is inactivated by deletion of its gp91phox subunit. One possibility is that deficiency in osteoclast gp91phox results in defects in their differentiation and activity and reduced bone damage. However, in gp91phox$^{2/2}$ mice, no bone abnormalities have been observed. In addition, gp91phox-deficient osteoclasts differentiate normally and have normal bone resorp-tion activity (72–74). These results show that gp91phox expressed in osteoclasts is dispensable for differentiation and activity of these cells. In fact, other NADPH oxidases were shown to be more important for their function (72, 75). In contrast, exogenous ROS generated in culture media after addition of xanthine oxidase were shown to upregulate osteoclast numbers and activity in bone cultures in vitro (76). Our data together with published results thus favor the explanation that exogenous ROS originating from hy-peractive neutrophils, ample production of which we observed in Pstpip2^{cmo} mice in vivo, lead either directly or indirectly to in-creased differentiation and/or activity of osteoclasts and resulting bone damage.

PSTPIP2 mutations in humans have not yet been described. However, PSTPIP2 gene has been sequenced only in a limited number of CRMO patients and patients with closely related SAPHO syndrome (77–79). CRMO and SAPHO form a rather heterogeneous disease spectrum, which may in fact represent a number of distinct disorders in which various defects at the molecular level may lead to similar outcome, and so PSTPIP2 mutations in some of these patients may still be discovered in the future. The data on ROS production in these diseases are also largely missing. We are aware of only a single study in which the superoxide production by neutrophils was analyzed in two SAPHO patients from a single family without any mutations in PSTPIP2 gene. These data showed reduced superoxide generation after activation with multiple activators, including PMA, fMLP, and TNF-a, when compared with healthy controls (77). However, from the information provided, it was unclear whether the patients were undergoing anti-inflammatory treatment that could suppress the response at the time of analysis. Further studies are needed to fully understand the role of PSTPIP2 and ROS in CRMO, SAPHO, and other inflammatory bone diseases in humans.

Inflammatory bone damage is a serious problem accompany-ing a number of human disorders. Full understanding of possible mechanisms that can govern its development is critical for de-signing successful therapeutic interventions. Our data reveal how dysregulated ROS production results in bone damage in the specific

case of CMO. However, these findings may represent a more general mechanism with broader validity for other syndromes where inflammatory bone damage is involved, and analysis of ROS production in other instances of inflammatory bone damage may prove beneficial.

Acknowledgments

We thank the staff of Institute of Molecular Genetics core facilities for excellent support and help.

Disclosures

The authors have no financial conflicts of interest.

References

1. Manthiram, K., Q. Zhou, I. Aksentijevich, and D. L. Kastner. 2017. The monogenic autoinflammatory diseases define new pathways in human innate immunity and inflammation. [Published erratum appears in 2017 Nat. Immunol. 18: 1271.] Nat. Immunol. 18: 832–842.
2. Masters, S. L., A. Simon, I. Aksentijevich, and D. L. Kastner. 2009. Horror autoinflammaticus: the molecular pathophysiology of autoinflammatory disease (*). Annu. Rev. Immunol. 27: 621–668.
3. de Jesus, A. A., S. W. Canna, Y. Liu, and R. Goldbach-Mansky. 2015. Molecular mechanisms in genetically defined autoinflammatory diseases: disorders of amplified danger signaling. Annu. Rev. Immunol. 33: 823–874.
4. Bader-Meunier, B., E. Van Nieuwenhove, S. Breton, and C. Wouters. 2018. Bone involvement in monogenic autoinflammatory syndromes. Rheumatology (Oxford) 57: 606–618.
5. Takayanagi, H. 2007. Osteoimmunology: shared mechanisms and crosstalk between the immune and bone systems. Nat. Rev. Immunol. 7: 292–304.
6. Houx, L., E. Hachulla, I. Kone-Paut, P. Quartier, I. Touitou, X. Guennoc, G. Grateau, M. Hamidou, B. Neven, J. M. Berthelot, et al. 2015. Musculoskeletal symptoms in patients with cryopyrin-associated periodic syndromes: a large database study. Arthritis Rheumatol. 67: 3027–3036.
7. Tunca, M., S. Akar, F. Onen, H. Ozdogan, O. Kasapcopur, F. Yalcinkaya, E. Tutar, S. Ozen, R. Topaloglu, E. Yilmaz, et al; Turkish FMF Study Group. 2005. Familial Mediterranean fever (FMF) in Turkey: results of a nationwide multicenter study. Medicine (Baltimore) 84: 1–11.
8. Gong, T., Y. Yang, T. Jin, W. Jiang, and R. Zhou. 2018. Orchestration of NLRP3 inflammasome activation by ion fluxes. Trends Immunol. 39: 393–406
9. Lawlor, K. E., and J. E. Vince. 2014. Ambiguities in NLRP3 inflammasome regulation: is there a role for mitochondria? Biochim. Biophys. Acta 1840: 1433–1440.
10. Carta, S., S. Tassi, L. Delfino, A. Omenetti, S. Raffa, M. R. Torrisi, A. Martini, M. Gattorno, and A. Rubartelli. 2012. Deficient production of IL-1 receptor antagonist and IL-6 coupled to oxidative stress in cryopyrin-associated periodic syndrome monocytes. Ann. Rheum. Dis. 71: 1577–1581.
11. Hughes, M. M., and L. A. J. O'Neill. 2018. Metabolic regulation of NLRP3. Immunol. Rev. 281: 88–98.
12. Broz, P., and V. M. Dixit. 2016. Inflammasomes: mechanism of assembly, regulation and signalling. Nat. Rev. Immunol. 16: 407–420.
13. Zhen, Y., and H. Zhang. 2019. NLRP3 inflammasome and inflammatory bowel disease. Front. Immunol. 10: 276.
14. Abais, J. M., M. Xia, Y. Zhang, K. M. Boini, and P. L. Li. 2015. Redox regulation of NLRP3 inflammasomes: ROS as trigger or effector? Antioxid. Redox Signal. 22: 1111–1129.
15. Holmstro¨m, K. M., and T. Finkel. 2014. Cellular mechanisms and physiological consequences of redox-dependent signalling. Nat. Rev. Mol. Cell Biol. 15: 411–421.
16. Brandes, R. P., N. Weissmann, and K. Schro¨der. 2014. Nox family NADPH oxidases: molecular mechanisms of activation. Free Radic. Biol. Med. 76: 208–226.
17. Sumimoto, H. 2008. Structure, regulation and evolution of Nox-family NADPH oxidases that produce reactive oxygen species. FEBS J. 275: 3249–3277.
18. West, A. P., G. S. Shadel, and S. Ghosh. 2011. Mitochondria in innate immune responses. Nat. Rev. Immunol. 11: 389–402.
19. Zhou, R., A. S. Yazdi, P. Menu, and J. Tschopp. 2011. A role for mitochondria in NLRP3 inflammasome activation. [Published erratum appears in 2011 Nature 475: 122.] Nature 469: 221–225.
20. Brookes, P. S., Y. Yoon, J. L. Robotham, M. W. Anders, and S.-S. Sheu. 2004. Calcium, ATP, and ROS: a mitochondrial love-hate triangle. Am. J. Physiol. Cell Physiol. 287: C817–C833.
21. Swanson, K. V., M. Deng, and J. P. Ting. 2019. The NLRP3 inflammasome: molecular activation and regulation to therapeutics. Nat. Rev. Immunol. 19: 477–489.
22. Chen, Y., Z. Zhou, and W. Min. 2018. Mitochondria, oxidative stress and innate immunity. Front. Physiol. 9: 1487.
23. Bulua, A. C., A. Simon, R. Maddipati, M. Pelletier, H. Park, K. Y. Kim, M. N. Sack, D. L. Kastner, and R. M. Siegel. 2011. Mitochondrial reactive oxygen species promote production of proinflammatory cytokines and are elevated in TNFR1-associated periodic syndrome (TRAPS). J. Exp. Med. 208: 519–533.
24. van der Burgh, R., L. Nijhuis, K. Pervolaraki, E. B. Compeer, L. H. Jongeneel, M. van Gijn, P. J. Coffer, M. P. Murphy, P. G. Mastroberardino, J. Frenkel, and M. Boes. 2014. Defects in mitochondrial clearance predispose human monocytes to interleukin-1b hypersecretion. J. Biol. Chem. 289: 5000–5012.
25. Borghini, S., S. Tassi, S. Chiesa, F. Caroli, S. Carta, R. Caorsi, M. Fiore, L. Delfino, D. Lasiglie`, C. Ferraris, et al. 2011. Clinical presentation and pathogenesis of cold-induced autoinflammatory disease in a family with recurrence of an NLRP12 mutation. Arthritis Rheum. 63: 830–839.
26. Tassi, S., S. Carta, L. Delfino, R. Caorsi, A. Martini, M. Gattorno, and A. Rubartelli. 2010. Altered redox state of monocytes from cryopyrin-associated periodic syndromes causes accelerated IL-1beta secretion. Proc. Natl. Acad. Sci. USA 107: 9789–9794.
27. Omenetti, A., S. Carta, L. Delfino, A. Martini, M. Gattorno, and A. Rubartelli. 2014. Increased NLRP3-dependent interleukin 1b secretion in patients with familial Mediterranean fever: correlation with MEFV genotype. Ann. Rheum. Dis. 73: 462–469.
28. Carta, S., F. Penco, R. Lavieri, A. Martini, C. A. Dinarello, M. Gattorno, and A. Rubartelli. 2015. Cell stress increases ATP release in NLRP3 inflammasome-mediated autoinflammatory diseases, resulting in cytokine imbalance. Proc. Natl. Acad. Sci. USA 112: 2835–2840.
29. Byrd, L., M. Grossmann, M. Potter, and G. L. Shen-Ong. 1991. Chronic mul-tifocal osteomyelitis, a new recessive mutation on chromosome 18 of the mouse. Genomics 11: 794–798.
30. Ferguson, P. J., X. Bing, M. A. Vasef, L. A. Ochoa, A. Mahgoub, T. J. Waldschmidt, L. T. Tygrett, A. J. Schlueter, and H. El-Shanti. 2006. A missense mutation in pstpip2 is associated with the murine autoinflammatory disorder chronic multifocal osteomyelitis. Bone 38: 41–47.
31. Chitu, V., P. J. Ferguson, R. de Bruijn, A. J. Schlueter, L. A. Ochoa, T. J. Waldschmidt, Y. G. Yeung, and E. R. Stanley. 2009. Primed innate immunity leads to autoinflammatory disease in PSTPIP2-deficient cmo mice. Blood 114: 2497–2505.
32. Wu, Y., D. Dowbenko, and L. A. Lasky. 1998. PSTPIP 2, a second tyrosine phosphorylated, cytoskeletal-associated protein that binds a PEST-type protein-tyrosine phosphatase. J. Biol. Chem. 273: 30487–30496.
33. Drobek, A., J. Kralova, T. Skopcova, M. Kucova, P. Nova´k, P. Angelisova´, P. Otahal, M. Alberich-Jorda, and T. Brdicka. 2015. PSTPIP2, a protein associated with autoinflammatory disease, interacts with inhibitory enzymes SHIP1 and Csk. J. Immunol. 195: 3416–3426.
34. Cassel, S. L., J. R. Janczy, X. Bing, S. P. Wilson, A. K. Olivier, J. E. Otero, Y. Iwakura, D. M. Shayakhmetov, A. G. Bassuk, Y. Abu-Amer, et al. 2014. Inflammasome-independent IL-1b mediates autoinflammatory disease in Pstpip2-deficient mice. Proc. Natl. Acad. Sci. USA 111: 1072–1077.
35. Lukens, J. R., J. M. Gross, C. Calabrese, Y. Iwakura, M. Lamkanfi, P. Vogel, and T. D. Kanneganti. 2014. Critical role for inflammasome-independent IL-1b production in osteomyelitis. Proc. Natl. Acad. Sci. USA 111: 1066–1071.
36. Lukens, J. R., P. Gurung, P. Vogel, G. R. Johnson, R. A. Carter, D. J. McGoldrick, S. R. Bandi, C. R. Calabrese, L. Vande Walle, M. Lamkanfi, and T.-D. Kanneganti. 2014. Dietary modulation of the microbiome affects autoinflammatory disease. Nature 516: 246–249.
37. Gurung, P., A. Burton, and T. D. Kanneganti. 2016. NLRP3 inflammasome plays a redundant role with caspase 8 to promote IL-1b-mediated osteomyelitis. Proc. Natl. Acad. Sci. USA 113: 4452–4457.
38. Callaway, D. A., and J. X. Jiang. 2015. Reactive oxygen species and oxidative stress in osteoclastogenesis, skeletal aging and bone diseases. J. Bone Miner. Metab. 33: 359–370.
39. Chitu, V., V. Nacu, J. F. Charles, W. M. Henne, H. T. McMahon, S. Nandi, H. Ketchum, R. Harris, M. C. Nakamura, and E. R. Stanley. 2012. PSTPIP2 deficiency in mice causes osteopenia and increased differentiation of multipotent myeloid precursors into osteoclasts. Blood 120: 3126–3135.
40. Pollock, J. D., D. A. Williams, M. A. Gifford, L. L. Li, X. Du, J. Fisherman, S. H. Orkin, C. M. Doerschuk, and M. C. Dinauer. 1995. Mouse model of X-linked chronic granulomatous disease, an inherited defect in phagocyte superoxide production. Nat. Genet. 9: 202–209.
41. Hou, B., B. Reizis, and A. L. DeFranco. 2008. Toll-like receptors activate innate and adaptive immunity by using dendritic cell-intrinsic and -extrinsic mechanisms. Immunity 29: 272–282.
42. Shen, F. W., Y. Saga, G. Litman, G. Freeman, J. S. Tung, H. Cantor, and E. A. Boyse. 1985. Cloning of Ly-5 cDNA. Proc. Natl. Acad. Sci. USA 82: 7360–7363.
43. Passegue´, E., E. F. Wagner, and I. L. Weissman. 2004. JunB deficiency leads to a myeloproliferative disorder arising from hematopoietic stem cells. Cell 119: 431–443.
44. Voehringer, D., H. E. Liang, and R. M. Locksley. 2008. Homeostasis and effector function of lymphopenia-induced "memory-like" T cells in constitutively T cell-depleted mice. J. Immunol. 180: 4742–4753.
45. Wang, G. G., K. R. Calvo, M. P. Pasillas, D. B. Sykes, H. Ha¨cker, and M. P. Kamps. 2006. Quantitative production of macrophages or neutrophils ex vivo using conditional Hoxb8. Nat. Methods 3: 287–293.
46. Goodridge, H. S., C. N. Reyes, C. A. Becker, T. R. Katsumoto, J. Ma, A. J. Wolf, N. Bose, A. S. Chan, A. S. Magee, M. E. Danielson, et al. 2011. Activation of the innate immune receptor Dectin-1 upon formation of a 'phagocytic synapse'. Nature 472: 471–475.
47. Bedouhe`ne, S., F. Moulti-Mati, M. Hurtado-Nedelec, P. M. Dang, and J. El-Benna. 2017. Luminol-amplified chemiluminescence detects mainly superoxide anion produced by human neutrophils. Am. J. Blood Res. 7: 41–48.
48. Kielland, A., T. Blom, K. S. Nandakumar, R. Holmdahl, R. Blomhoff, and H. Carlsen. 2009. In vivo imaging of reactive oxygen and nitrogen species in

inflammation using the luminescent probe L-012. Free Radic. Biol. Med. 47: 760–766.
49. Cassel, S. L., S. C. Eisenbarth, S. S. Iyer, J. J. Sadler, O. R. Colegio, L. A. Tephly, A. B. Carter, P. B. Rothman, R. A. Flavell, and F. S. Sutterwala. 2008. The Nalp3 inflammasome is essential for the development of silicosis. Proc. Natl. Acad. Sci. USA 105: 9035–9040.
50. Aratani, Y. 2018. Myeloperoxidase: its role for host defense, inflammation, and neutrophil function. Arch. Biochem. Biophys. 640: 47–52.
51. Adachi, O., T. Kawai, K. Takeda, M. Matsumoto, H. Tsutsui, M. Sakagami, K. Nakanishi, and S. Akira. 1998. Targeted disruption of the MyD88 gene results in loss of IL-1- and IL-18-mediated function. Immunity 9: 143–150.
52. Condliffe, A. M., E. R. Chilvers, C. Haslett, and I. Dransfield. 1996. Priming differentially regulates neutrophil adhesion molecule expression/function. Immunology 89: 105–111.
53. Miralda, I., S. M. Uriarte, and K. R. McLeish. 2017. Multiple phenotypic changes define neutrophil priming. Front. Cell. Infect. Microbiol. 7: 217.
54. Vogt, K. L., C. Summers, E. R. Chilvers, and A. M. Condliffe. 2018. Priming and de-priming of neutrophil responses in vitro and in vivo. Eur. J. Clin. Invest. 48(Suppl. 2): e12967.
55. Crawford, N., and P. Eggleton. 1991. Dynamic changes in neutrophil cytoskeleton during priming and subsequent surface stimulated functions. Biochem. Soc. Trans. 19: 1048–1055.
56. Yao, Y., H. Matsushima, J. A. Ohtola, S. Geng, R. Lu, and A. Takashima. 2015. Neutrophil priming occurs in a sequential manner and can be visualized in living animals by monitoring IL-1b promoter activation. J. Immunol. 194: 1211–1224.
57. Jennings, R. T., M. Strengert, P. Hayes, J. El-Benna, C. Brakebusch, M. Kubica, and U. G. Knaus. 2014. RhoA determines disease progression by controlling neutrophil motility and restricting hyperresponsiveness. Blood 123: 3635–3645.
58. Liu, Z., T. Yago, N. Zhang, S. R. Panicker, Y. Wang, L. Yao, P. Mehta-D'souza, L. Xia, C. Zhu, and R. P. McEver. 2017. L-selectin mechanochemistry restricts neutrophil priming in vivo. Nat. Commun. 8: 15196.
59. Belambri, S. A., L. Rolas, H. Raad, M. Hurtado-Nedelec, P. M.-C. Dang, and J. El-Benna. 2018. NADPH oxidase activation in neutrophils: role of the phosphorylation of its subunits. Eur. J. Clin. Invest. 48(Suppl. 2): e12951.
60. El-Benna, J., P. M. Dang, M. A. Gougerot-Pocidalo, J. C. Marie, and F. Braut-Boucher. 2009. p47phox, the phagocyte NADPH oxidase/NOX2 organizer: structure, phosphorylation and implication in diseases. Exp. Mol. Med. 41: 217–225.
61. Dapino, P., F. Dallegri, L. Ottonello, and C. Sacchetti. 1993. Induction of neutrophil respiratory burst by tumour necrosis factor-alpha; priming effect of solid-phase fibronectin and intervention of CD11b-CD18 integrins. Clin. Exp. Immunol. 94: 533–538.
62. Dang, P. M., A. Stensballe, T. Boussetta, H. Raad, C. Dewas, Y. Kroviarski, G. Hayem, O. N. Jensen, M. A. Gougerot-Pocidalo, and J. El-Benna. 2006. A specific p47phox -serine phosphorylated by convergent MAPKs mediates neutrophil NADPH oxidase priming at inflammatory sites. J. Clin. Invest. 116: 2033–2043.
63. El Benna, J., J. Han, J. W. Park, E. Schmid, R. J. Ulevitch, and B. M. Babior. 1996. Activation of p38 in stimulated human neutrophils: phosphorylation of the oxidase component p47phox by p38 and ERK but not by JNK. Arch. Biochem. Biophys. 334: 395–400.
64. van de Veerdonk, F. L., S. P. Smeekens, L. A. Joosten, B. J. Kullberg, C. A. Dinarello, J. W. van der Meer, and M. G. Netea. 2010. Reactive oxygen species-independent activation of the IL-1beta inflammasome in cells from patients with chronic granulomatous disease. Proc. Natl. Acad. Sci. USA 107: 3030–3033.
65. van Bruggen, R., M. Y. Ko¨ker, M. Jansen, M. van Houdt, D. Roos, T. W. Kuijpers, and T. K. van den Berg. 2010. Human NLRP3 inflammasome activation is Nox1-4 independent. Blood 115: 5398–5400.
66. Meissner, F., R. A. Seger, D. Moshous, A. Fischer, J. Reichenbach, and A. Zychlinsky. 2010. Inflammasome activation in NADPH oxidase defective mononuclear phagocytes from patients with chronic granulomatous disease. Blood 116: 1570–1573.
67. Meissner, F., K. Molawi, and A. Zychlinsky. 2008. Superoxide dismutase 1 regulates caspase-1 and endotoxic shock. Nat. Immunol. 9: 866–872.
68. Gabelloni, M. L., F. Sabbione, C. Jancic, J. Fuxman Bass, I. Keitelman, L. Iula, M. Oleastro, J. R. Geffner, and A. S. Trevani. 2013. NADPH oxidase derived reactive oxygen species are involved in human neutrophil IL-1b secretion but not in inflammasome activation. Eur. J. Immunol. 43: 3324–3335.
69. Nakahira, K., J. A. Haspel, V. A. Rathinam, S. J. Lee, T. Dolinay, H. C. Lam, J. A. Englert, M. Rabinovitch, M. Cernadas, H. P. Kim, et al. 2011. Autophagy proteins regulate innate immune responses by inhibiting the release of mitochondrial DNA mediated by the NALP3 inflammasome. Nat. Immunol. 12: 222–230.
70. Deguine, J., and G. M. Barton. 2014. MyD88: a central player in innate immune signaling. F1000Prime Rep. 6: 97.
71. Okamoto, K., T. Nakashima, M. Shinohara, T. Negishi-Koga, N. Komatsu, A. Terashima, S. Sawa, T. Nitta, and H. Takayanagi. 2017. Osteoimmunology: the conceptual framework unifying the immune and skeletal systems. Physiol. Rev. 97: 1295–1349.
72. Lee, N. K., Y. G. Choi, J. Y. Baik, S. Y. Han, D. W. Jeong, Y. S. Bae, N. Kim, and S. Y. Lee. 2005. A crucial role for reactive oxygen species in RANKL-induced osteoclast differentiation. Blood 106: 852–859.
73. Yang, S., P. Madyastha, S. Bingel, W. Ries, and L. Key. 2001. A new superoxide-generating oxidase in murine osteoclasts. J. Biol. Chem. 276: 5452–5458.
74. Sasaki, H., H. Yamamoto, K. Tominaga, K. Masuda, T. Kawai, S. Teshima-Kondo, K. Matsuno, C. Yabe-Nishimura, and K. Rokutan. 2009. Receptor activator of nuclear factor-kappaB ligand-induced mouse osteoclast differentiation is associated with switching between NADPH oxidase homologues. Free Radic. Biol. Med. 47: 189–199.
75. Goettsch, C., A. Babelova, O. Trummer, R. G. Erben, M. Rauner, S. Rammelt, N. Weissmann, V. Weinberger, S. Benkhoff, M. Kampschulte, et al. 2013. NADPH oxidase 4 limits bone mass by promoting osteoclastogenesis. J. Clin. Invest. 123: 4731–4738.
76. Garrett, I. R., B. F. Boyce, R. O. Oreffo, L. Bonewald, J. Poser, and G. R. Mundy. 1990. Oxygen-derived free radicals stimulate osteoclastic bone resorption in rodent bone in vitro and in vivo. J. Clin. Invest. 85: 632–639.
77. Ferguson, P. J., M. A. Lokuta, H. I. El-Shanti, L. Muhle, X. Bing, and A. Huttenlocher. 2008. Neutrophil dysfunction in a family with a SAPHO syndrome-like phenotype. Arthritis Rheum. 58: 3264–3269.
78. Hurtado-Nedelec, M., S. Chollet-Martin, D. Chapeton, J. P. Hugot, G. Hayem, and B. Ge´rard. 2010. Genetic susceptibility factors in a cohort of 38 patients with SAPHO syndrome: a study of PSTPIP2, NOD2, and LPIN2 genes. J. Rheumatol. 37: 401–409.
79. Jansson, A., E. D. Renner, J. Ramser, A. Mayer, M. Haban, A. Meindl, V. Grote, J. Diebold, V. Jansson, K. Schneider, and B. H. Belohradsky. 2007. Classification of non-bacterial osteitis: retrospective study of clinical, immunological and genetic aspects in 89 patients. Rheumatology (Oxford) 46: 154–160.

Supplementary figures

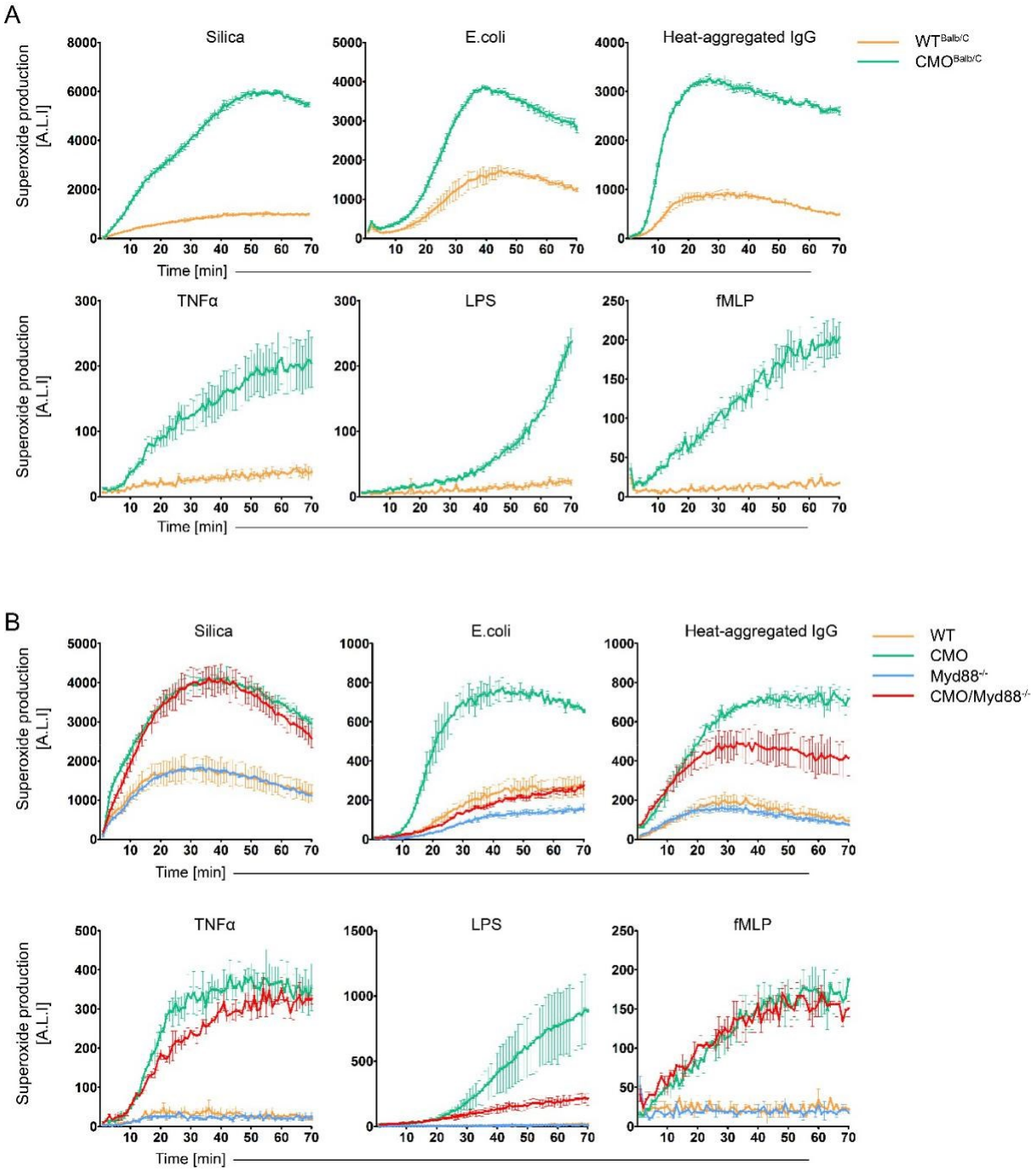

Supplemental Figure 1. Dysregulated superoxide production by bone marrow cells from *Pstpip2*^{cmo} mice of Balb/c (**A**) or MyD88$^{-/-}$ (**B**) genetic background. Superoxide production was detected by Luminol-based assay, exactly as described in Figure 2A.

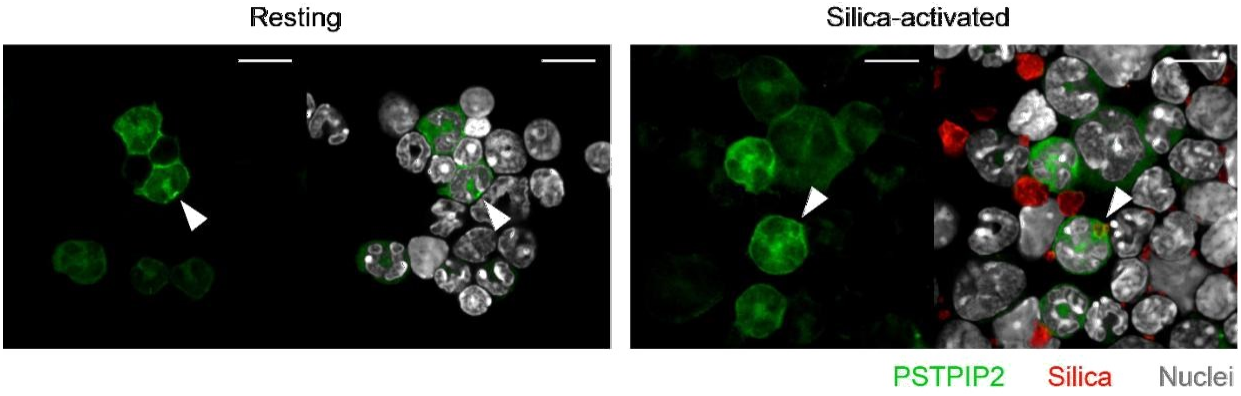

Supplemental Figure 2. Subcellular localization of PSTPIP2 in primary murine neutrophils. Neutrophils differentiated in vivo from bone marrow cells transduced with retroviral PSTPIP2-EGFP construct (green) were activated or not by silica (red) and imaged by confocal microscopy. Bar = 10 µm.

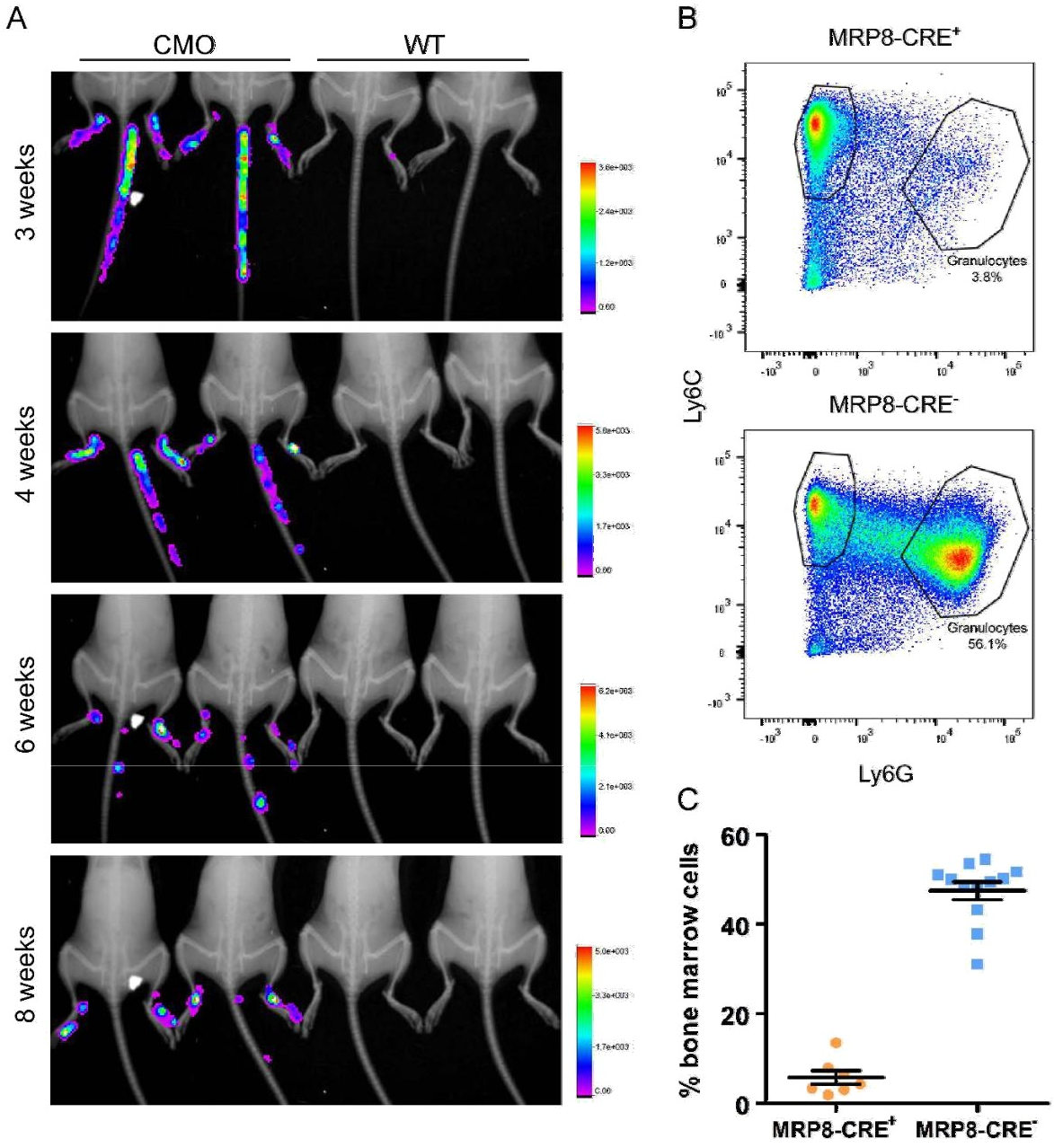

Supplemental Figure 3. Neutrophil-dependent ROS production in vivo. (**A**) In vivo ROS production in WT and *Pstpip2*^{cmo} (CMO) mice of various ages: representative images of the animals that were part of the analysis in Figure 5B. (**B**) Neutrophils were depleted in Pstpip2^{cmo} -DTA mice via MRP8-CRE-dependent expression of Diphtheria toxin (MRP8-CRE^{+}) or left untouched in the absence of MRP8-CRE (MRP8-CRE^{-}). Representative FACS plots of CD11b^{+} cells further gated for granulocytes (Ly6G^{High}, Ly6C^{Low}) and monocytes (Ly6G^{-}, Ly6C^{High}) are shown. (**C**) Efficiencies of granulocyte depletion in multiple animals. Shown are the percentages of granulocytes gated as in (B).

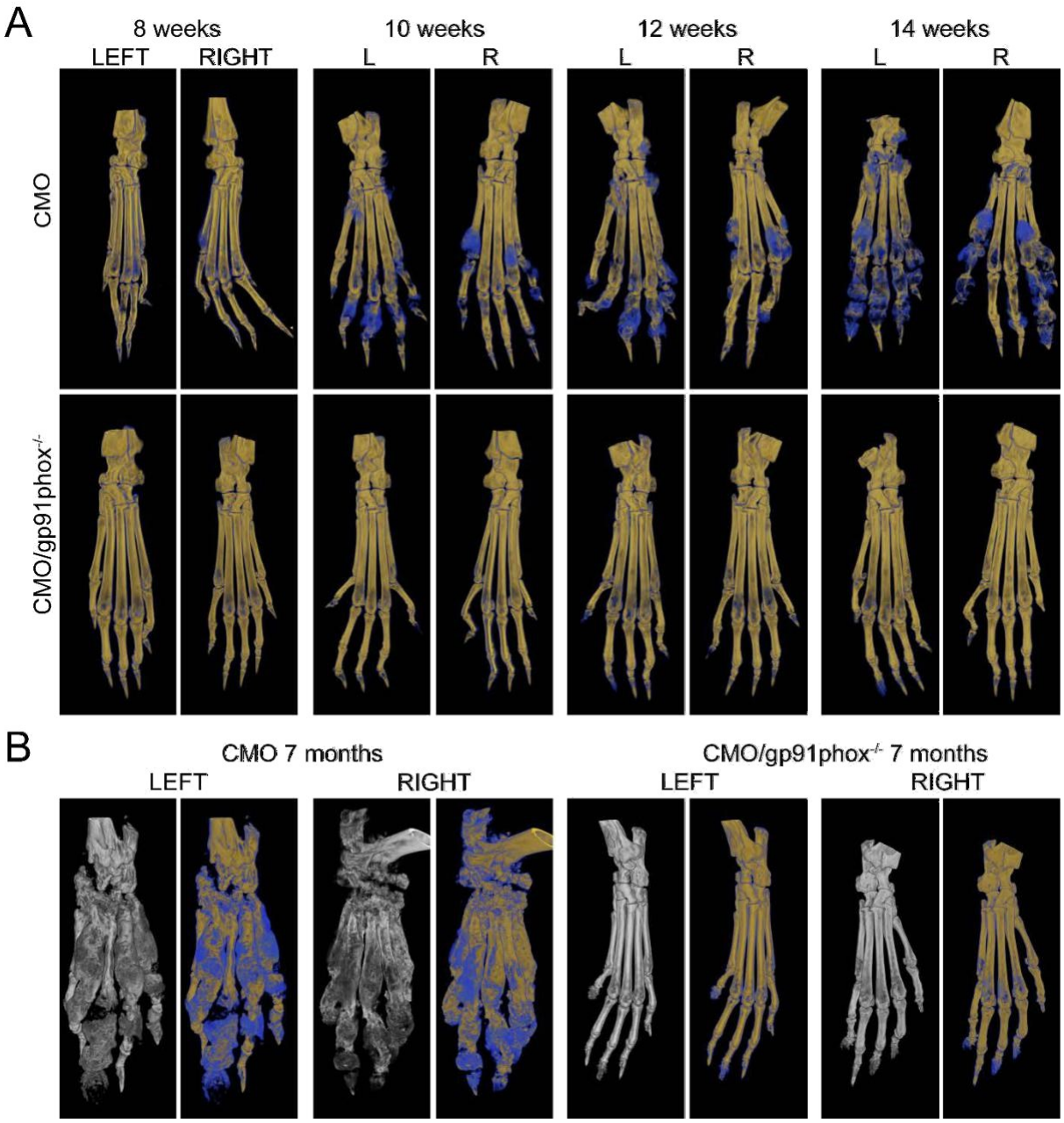

Supplemental Figure 4. Time course of bone damage development in *Pstpip2^{cmo}* and *Pstpip2^{cmo}/gp91phox$^{-/-}$* mice. (**A**) Mice at 8, 10, 12, and 14 weeks of age were anesthetized and their hind paw bones were imaged on X-ray μCT scanner. (**B**) The same analysis performed on 7 months old animals. Grey images represent visualization of total bone tissue. Pseudocolor images distinguish between old (in yellow) and newly formed (in blue) bone mass.

Received: 12 July 2019 | Revised: 23 October 2019 | Accepted: 19 November 2019

DOI: 10.1111/jcmm.14895

ORIGINAL ARTICLE

WILEY

Transmembrane adaptor protein WBP1L regulates CXCR4 signalling and murine haematopoiesis

Simon Borna[1,2] | Ales Drobek[1] | Jarmila Kralova[1] | Daniela Glatzova[1,2,3] | Iva Splichalova[4] | Matej Fabisik[1,2] | Jana Pokorna[1] | Tereza Skopcova[1] | Pavla Angelisova[1] | Veronika Kanderova[5] | Julia Starkova[5] | Petr Stanek[6] | Orest V. Matveichuk[7] | Nataliia Pavliuchenko[1,2] | Katarzyna Kwiatkowska[7] | Majd B. Protty[8] | Michael G. Tomlinson[9] | Meritxell Alberich-Jorda[10] | Vladimir Korinek[11] | Tomas Brdicka[1]

[1]Laboratory of Leukocyte Signaling, Institute of Molecular Genetics of the Czech Academy of Sciences, Prague, Czech Republic

[2]Faculty of Science, Charles University, Prague, Czech Republic

[3]Department of Biophysical Chemistry, J. Heyrovsky Institute of Physical Chemistry of the Czech Academy of Sciences, Prague, Czech Republic

[4]Laboratory of Immunobiology, Institute of Molecular Genetics of the Czech Academy of Sciences, Prague, Czech Republic

[5]CLIP - Childhood Leukaemia Investigation Prague and Department of Pediatric Hematology and Oncology, Second Faculty of Medicine, Charles University, Prague, Czech Republic

[6]Second Faculty of Medicine, Charles University, Prague, Czech Republic

[7]Laboratory of Molecular Membrane Biology, Nencki Institute of Experimental Biology, Warsaw, Poland

[8]Institute of Biomedical Research, University of Birmingham, Birmingham, UK

[9]School of Biosciences, University of Birmingham, Birmingham, UK

[10]Laboratory of Hematooncology, Institute of Molecular Genetics of the Czech Academy of Sciences, Prague, Czech Republic

[11]Laboratory of Cell and Developmental Biology, Institute of Molecular Genetics of the Czech Academy of Sciences, Prague, Czech Republic

Correspondence
Tomas Brdicka, Institute of Molecular Genetics of the Czech Academy of Sciences, Videnska 1083, 14220 Prague, Czech Republic.
Email: tomas.brdicka@img.cas.cz

Present address
Majd B. Protty, Sir Geraint Evans Cardiovascular Research Building, Cardiff University, Cardiff, UK

Funding information
European Regional Development Fund, Grant/Award Number: CZ.1.05/1.1.00/02.0109 and OPPK (CZ.2.16/3.1.00/21547); Grantová Agentura České Republiky, Grant/ Award Number: 16-07425S and P302-12-G101; H2020 Marie Skłodowska-Curie

Abstract

WW domain binding protein 1-like (WBP1L), also known as outcome predictor of acute leukaemia 1 (OPAL1), is a transmembrane adaptor protein, expression of which correlates with *ETV6-RUNX1* (t(12;21)(p13;q22)) translocation and favourable prog-nosis in childhood leukaemia. It has a broad expression pattern in haematopoietic and in non-haematopoietic cells. However, its physiological function has been un-known. Here, we show that WBP1L negatively regulates signalling through a critical chemokine receptor CXCR4 in multiple leucocyte subsets and cell lines. We also show that WBP1L interacts with NEDD4-family ubiquitin ligases and regulates CXCR4 ubiquitination and expression. Moreover, analysis of *Wbp1l*-deficient mice revealed alterations in B cell development and enhanced efficiency of bone marrow cell trans-plantation. Collectively, our data show that WBP1L is a novel regulator of CXCR4 signalling and haematopoiesis.

Actions, Grant/Award Number: 665735; Medical Research Council, Grant/Award Number: G0400247; Akademie Věd České Republiky, Grant/Award Number: RVO 68378050; Ministerstvo Školství, Mládeže a Tělovýchovy, Grant/Award Number: LM2015040, LM2015062, NPU I LO1419, NPU I LO1604 and OP RDI CZ.1.05/2.1.00/19.0395; Agentura pro zdravotnický výzkum České republiky (Czech Health Research Council), Grant/Award Number: NV15-28848A; Institute of Molecular Genetics

KEYWORDS

bone marrow homing, bone marrow transplantation, CXCR4, ETV6, haematopoiesis, haematopoietic stem cell, NEDD4 family, OPAL1, RUNX1, WBP1L

1 | INTRODUCTION

WW domain binding protein 1-like (WBP1L) also known as outcome predictor of acute leukaemia 1 (OPAL1) has attracted attention because of a report showing that its elevated expression at mRNA level correlates with favourable outcome in childhood acute lymphoblastic leukaemia (ALL).[1] These data suggested that it could potentially serve as a prognostic marker. Later, it was shown that its levels are particularly increased in B cell progenitor ALL (BCP-ALL) with chromosomal translocation t(12;21)(p13;q22), which results in expression of *ETV6-RUNX1* fusion transcription factor.[2,3] In BCP-ALL, this translocation is associated with good prognosis, which likely explains the correlation between WBP1L expression and favourable outcome.[2] However, it is not known whether WBP1L functionally contributes to it.

ETV6, a fusion partner in *ETV6-RUNX1*, is a transcriptional repressor and *WBP1L* is one of its target genes.[4-6] In general, ETV6 targets are of high interest because of critical importance of ETV6 in haematopoiesis and its involvement in leukaemia. Around 30 fusions of *ETV6* to different partner genes and a number of mutations in *ETV6* have been identified so far, many of them implicated in various haematological malignancies of myeloid and lymphoid origin.[7,8] In addition, its critical role in normal haematopoiesis has been revealed in studies of ETV6-deficient mice, which show profound defects in haematopoietic stem and progenitor cell function and inability of these cells to reconstitute haematopoiesis after bone marrow transplantation.[9,10]

Bioinformatic sequence analysis revealed that WBP1L is a transmembrane adaptor protein with a very short extracellular/luminal part followed by a single transmembrane domain and a larger cytoplasmic tail.[11] Although relatively short, the extracellular/lumi-nal part presumably forms a small compact domain held together by disulphide bridges formed among cysteines in the C*C*CC*CC motif.[11] The cytoplasmic part of WBP1L contains several potential interaction motifs corresponding to the consensus sequence of WW domain binding motifs L-P-X-Y or P-P-X-Y.[11]

Except for the limited bioinformatics analysis, WBP1L protein remained completely uncharacterized. Its physiological function has been unknown and whether it has any functional features that may link it to normal haematopoiesis or neoplasia has never been investigated. Here, we show that it binds several members of the NEDD4-family of ubiquitin ligases and that its deficiency results in enhanced surface expression and signalling of critical chemokine receptor CXCR4. WBP1L deficiency also results in alterations in B cell development and altered dynamics of stem and progenitor cells in the bone marrow. Taken together, we establish the role of WBP1L in CXCR4 signalling and in normal haematopoiesis. These findings also form the basis for further research on its potential role in leukaemia.

2 | MATERIALS AND METHODS

2.1 | Protein isolation, detection and quantification assays

Immunoprecipitations (IP) and immunoblotting were performed essentially as reported with adjustments described in online supplement. Western blot quantifications were carried out using Azure c300 imaging system (Azure Biosystems) and Aida Image Analysis software (Elysia-raytest). WBP1L expression in B cell lines was analysed by size exclusion chromatography-microsphere-based affinity proteomics analysis described in detail here,[3] and the data were quantified using Matlab (MathWorks). Tandem purification of WBP1L was based on the following publication[12] with modifications described in online supplement. WBP1L pal-mitoylation was analysed using metabolic labelling with palmitic acid analogue 17ODYA followed by reaction with biotin-azide and enrichment on streptavidin-coupled beads as described in detail in online supplement.

2.2 | Antibodies

Antibodies are listed in Tables S1 and S2. WBP1L antisera were generated by immunization of rabbits with KLH-conjugated peptide from WBP1L C-terminus while WBP1L monoclonal antibodies were prepared by standard hybridoma technology after immunization of mice with recombinant C-terminal part of murine WBP1L protein as described in online supplement.

2.3 | Cloning, qPCR, DNA transfection, virus preparation and cell infection

cDNA was generated using Quick-RNA kit (Zymo Research), revert aid reverse transcriptase (Thermo-Fisher) and oligo-dT primer. qPCR reactions were run on LightCycler 480 Instrument II using LightCycler 480 SYBR Green I Master mix (Roche). List of qPCR primers is in Table S3. For construct preparation see online supplement and Table S4. Phoenix cell transfection, virus generation and cell transduction were performed as described.[13] For lentivirus production, the procedure was to a minor extent modified as described in online supplement. Infected cells were sorted on Influx (BD) or selected on G418 (Thermo-Fisher).

2.4 | Mouse experiments, homing assays

Wbp1l$^{-/-}$ mice (*Wbp1l*$^{tm2a(EUCOMM)Hmgu}$) on C57Bl/6J genetic background were obtained from International Mouse Phenotyping Consortium. In these mice, gene trap flanked by FRT sites followed by coding region of exon 5 surrounded by LoxP sites were inserted into *Wbp1l* locus by homologous recombination (*Wbp1l*$^{-/-}$). Mice were bred in specific pathogen free conditions. To obtain inducible *Wbp1l*$^{fl/fl}$*CreERT* mice, we crossed animals of the *Wbp1l*$^{-/-}$ strain to *B6.Cg-Tg (ACTFLPe)9205 Dym/J* mice to remove the gene trap, and subsequently, to *B6.129-Gt(ROSA)26Sor*$^{tm1(cre/ERT2)Tyj}$*/J* animals. Both mouse strains were purchased from the Jackson Laboratory (Bar Harbor). To achieve *Wbp1l* deletion, mice were injected intraperitoneally with five daily doses of 2 mg of tamoxifen (Merck) in corn oil (Merck). For homing and transplantation assays, congenic *Ly5.1* (*C57BL/6NCr*) or *Ly5.1/Ly5.2* (*C57Bl/6J*) heterozygote recipients were sublethally (three Grey) or lethally (seven Grey) irradiated, followed by injection of transplanted cells into the tail vain. For experiments we used 8- to 12–week-old sex and age matched animals. Housing of mice and in vivo experiments were performed in compliance with local legal requirements and ethical guidelines. The Animal Care and Use Committee of the Institute of Molecular Genetics approved animal care and experimental procedures (Ref. No. 69/2014, 6/2016).

2.5 | Transwell migration

1 × 10^5 Cells in DMEM with 0.2% BSA were plated in the upper well of 5μm pore Transwell apparatus (Corning). After 4 hours, migrated cells in the bottom well were counted using a flow cytometer (LSRII; BD).

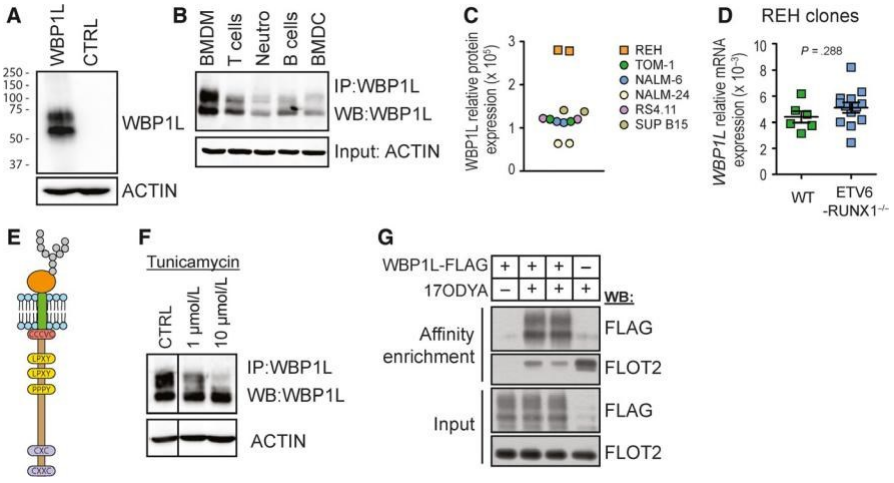

FIGURE 1 WBP1L is a palmitoylated glycoprotein, broadly expressed in haematopoietic cells. (A) Verification of new WBP1L rabbit antisera specificity on the lysates of HEK293 cells transfected or not with WBP1L construct. (B) Western blot analysis of WBP1L expression in murine leucocyte subsets. T cells (CD3$^+$), B cells (CD43$^-$, CD11b$^-$) and neutrophils (Ly6G$^+$) were isolated from the spleen or bone marrow. Bone marrow-derived macrophages (BMDM) and bone marrow-derived dendritic cells (BMDC) were differentiated in vitro from murine bone marrow. N = 3. (C) Expression of WBP1L in BCP-ALL cell lines was probed using size exclusion chromatography-microsphere-based affinity Proteomics method. Expression in *ETV6-RUNX1*$^+$ B cell line REH and *ETV6-RUNX1*$^-$ lines TOM-1, NALM-6, NALM-24, RS4.11 and SUB B15 was probed by two antibody clones to WBP1L (OPAL-01, OPAL-02) and quantified as an area under the curve on parts of chromatograms representing fractions corresponding to WBP1L (N = 1 per antibody clone). (D) Expression of *WBP1L* mRNA in different *ETV6-RUNX1*$^{-/-}$ REH clones from two independent sources of REH cells. Data are plotted as 2^{-ct} (N = 3). (E) Schematic representation of WBP1L structure and conserved sequence motifs (F) Analysis of WBP1L glycosylation in BMDM. BMDM treated or not with 1 or 10 μmol/L tunicamycin (overnight) were subjected to WBP1L immunoprecipitation followed by immunoblotting with WBP1L antisera. β-actin was stained in the corresponding cell lysates (N = 2). Irrelevant lines from the blot image were removed and replaced with a vertical dividing line. (G)Analysis of palmitoylation of WBP1L. HEK293 cells expressing WBP1L-FLAG-STREP were metabolically labelled with palmitate analogue 17ODYA and lysed. 17ODYA labelled proteins were tagged in a click chemistry reaction with biotin-azide, purified on streptavidin-coupled beads and analysed for the presence of WBP1L with anti-FLAG antibody (upper panel) or FLOTILLIN-2 as a representative of endogenous palmitoylated proteins (middle upper panel). WBP1L expression in cell lysates (middle lower panel) and comparable loading were verified by immunoblotting with antibodies to FLAG-tag (WBP1L) or FLOTILLIN-2, respectively (N = 3)

2.6 | Statistics

Results represent means ± SEM. If not specified otherwise, *P*-values were calculated using two-tailed Student's *t* test, one-way ANOVA or *Q* test. N represents number of animals or values per group or number of independent experiments.

3 | RESULTS

3.1 | WBP1L is a palmitoylated glycoprotein broadly expressed in haematopoietic cells

Analysis of WBP1L protein and mRNA expression in murine and human haematopoietic system with a newly generated polyclonal rabbit antibody (Figure 1A) and with Genevestigator tool, respectively, revealed that WBP1L is broadly expressed across multiple human and murine haematopoietic cell subsets (Figure 1B and S1). In addition and in agreement with previous reports of deregulated WBP1L expression in *ETV6-RUNX1*$^{+}$ BCP-ALL, we have found elevated levels of WBP1L protein in REH cell line, which is derived from *ETV6-RUNX1*$^{+}$ BCP-ALL. (Figure 1C and S2A). Interestingly, the genetic deletion of *ETV6-RUNX1* in REH cells (Figure S2B,C) did not alter WBP1L expression in these cells (Figure 1D).

Imaging of murine bone marrow-derived macrophages trans-duced with retroviral vector coding for murine WBP1L fused to EGFP revealed relatively broad distribution of WBP1L-EGFP within these cells. We have observed co-localization with plasma membrane, Golgi, endoplasmic reticulum, and to a limited extent with lysosomes and/or other acidic organelles (Figure S3). On the other hand, no co-localization with mitochondria could be detected (Figure S3).

The N-terminal part of WBP1L protein is highly conserved among major vertebrate classes (Figure S4). This region contains several conserved motifs, including potential N-glycosylation (NXS) and palmitoylation sites (Figure 1E and S4). Indeed, we could confirm that WBP1L is both glycosylated and palmitoylated (Figure 1F,G).

3.2 | WBP1L interacts with NEDD4-family E3 ubiquitin ligases

Cytoplasmic part of WBP1L contains three WW domain binding motifs ([L/P]PXY) (Figure 1E and S4). It has been speculated that they may interact with WW domains of NEDD4-family ubiquitin ligases.[11]

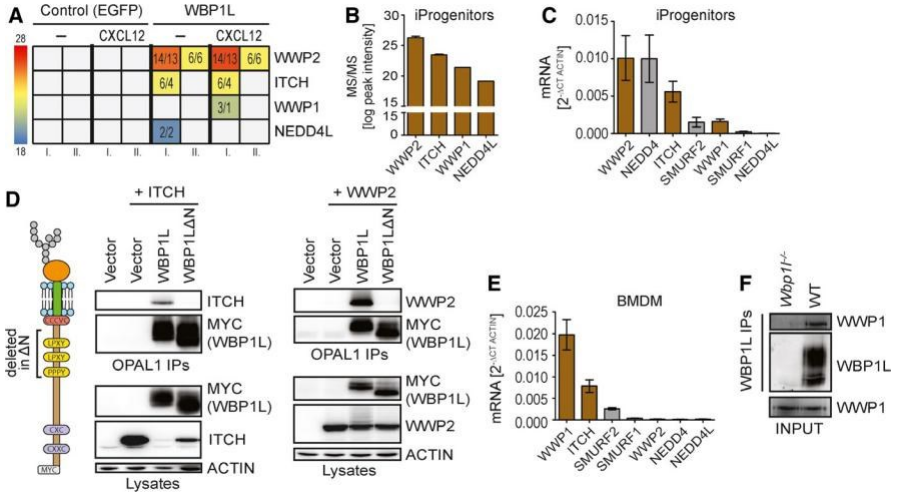

FIGURE 2 WBP1L binds multiple NEDD4-family E3 ubiquitin ligases. (A) Data from two independent mass spectrometry analyses (I. and II.) of WBP1L binding partners. *Wbp1l*$^{-/-}$ monocyte/macrophage progenitors were transduced with the constructs coding for WBP1L-FLAG-STREP or EGFP with the same tag. The cells were stimulated for 2 min with CXCL12 or left untreated. Tagged proteins with their binding partners were isolated by tandem purification and subjected to mass spectrometry analysis. The data are presented as colour-coded intensities obtained by label-free quantification of NEDD4-family E3 ubiquitin ligases. Values represent number of peptides used for intensity calculation/ number of unique peptides. Samples, where no peptides from a particular E3 ligase were detected, are coloured in grey (B) Label-free quantification of interacting E3 ligases from mass spectrometry experiment. Combined average intensities from both CXCR4 stimulated and non-stimulated samples are plotted (experiment I. form (A) only). (C) mRNA expression of NEDD4-family E3 ubiquitin ligases in immortalized monocyte/macrophage progenitors (iProgenitors). Plotted in brown are those ligases that interacted with WBP1L in mass spectrometry experiments (N = 3). (D) WBP1L interaction with NEDD4-family E3 ligases is dependent on WW binding motifs in WBP1L N-terminus. HEK293 cells were transfected with WBP1L-Myc or WBP1L N-Myc (with segment containing all WW binding motifs deleted) together with ITCH or WWP2. Following WBP1L immunoprecipitation, the isolated material and the original lysates were immunoblotted with antibody to ITCH or WWP2 and various controls as indicated (N = 3). (E) mRNA expression of NEDD4-family E3 ligases in BMDM. Plotted in brown are those ligases that interacted with WBP1L in mass spectrometry experiment (N = 3). (F) Endogenous interaction of WBP1L with WWP1 in BMDM. WBP1L immunoprecipitates from WT or *Wbp1l*$^{-/-}$ BMDM were immunoblotted with antibody to WWP1 and WBP1L. Input lysates were probed with antibody to WWP1 (N = 3). See also Figure S5

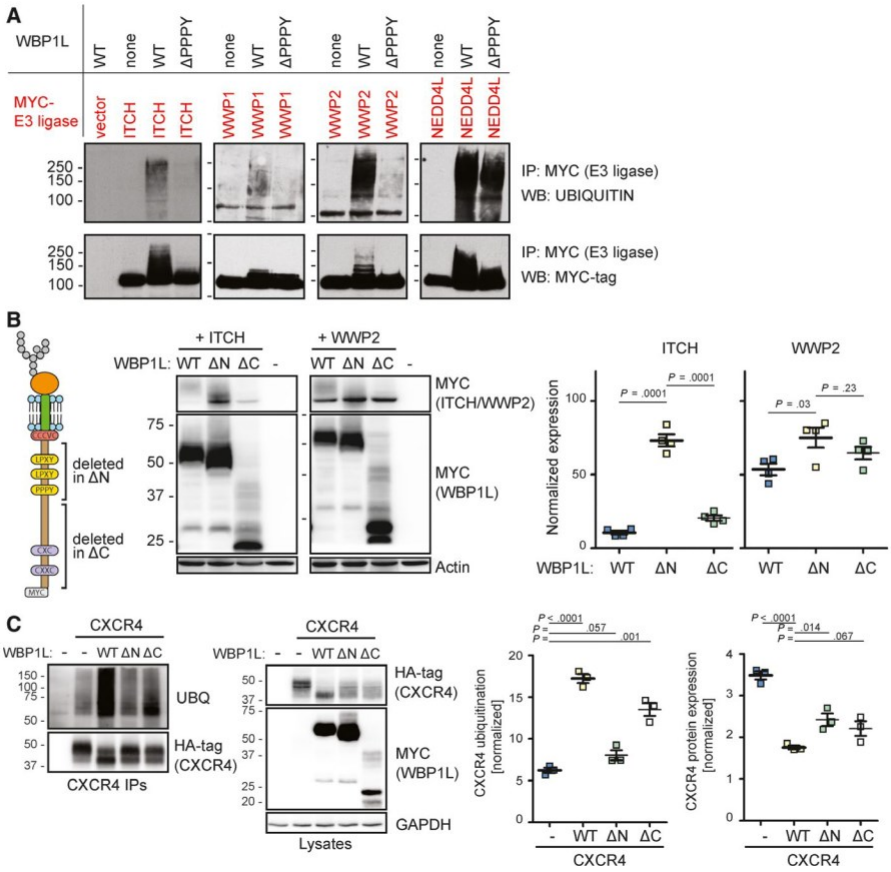

FIGURE 3 WBP1L regulates ubiquitination and expression of NEDD4-family E3 ubiquitin ligases and CXCR4. (A) HEK293 cells were cotransfected with individual Myc-tagged NEDD4-family E3 ubiquitin ligases and non-tagged WBP1L or its mutant lacking PPPY WW domain interacting motif. E3 ligases were immunoprecipitated via the Myc-tag from the lysates of these cells and subjected to immunoblotting with anti-MYC-tag or anti-UBIQUITIN antibody. (B) ITCH and WWP2 stability in HEK293 cells in the presence of WBP1L-MYC, WBP1L C-MYC (deletion of almost entire intracellular part of WBP1L except for WW binding motifs) or WBP1L N-MYC (deletion of WW binding motifs). Lysates from HEK293 cells transfected with ITCH-MYC or WWP2-MYC and WBP1L constructs were immunoblotted with antibody to MYC-tag to visualize ITCH, WWP2 and all forms of WBP1L and with antibody to ACTIN. Quantifications of the data are plotted as values normalized to ACTIN signal and then further normalized to experiment average to allow for comparison among the experiments (N = 3). (C) WBP1L-mediated increase in CXCR4 ubiquitination and down-regulation of CXCR4 protein levels in HEK293 cells. WBP1L-MYC, WBP1L C-MYC or WBP1L N-MYC were cotransfected with CXCR4-HA followed by CXCR4 imunoprecipitation and immunoblotting with antibodies to ubiquitin or HA-tag. Lysates were probed with antibodies to HA-tag (CXCR4), MYC-tag (WBP1L) or GAPDH (N = 3). For quantification, ubiquitination was normalized to HA-tag (CXCR4) signal (left panel) and CXCR4 expression to GAPDH (right panel). Both were further normalized to experiment average to allow for comparison among the individual experiments

However, this family has nine different members. To investigate whether WBP1L interacts with any of these ligases, we have expressed a FLAG-STREP-tagged WBP1L construct in immortalized monocyte/macrophage progenitors. We have selected this cell type because of a relatively high level of *Wbp1l* mRNA in myeloid progenitors (Figure S1). We isolated the FALG-STREP-tagged construct together with its associated binding partners from the lysates of these cells via a tandem purification on anti-FLAG and Streptactin beads. Mass spectrometry analysis of the isolated material revealed that WBP1L indeed interacts with several members of NEDD4-family. In this particular cell type, WWP2 was the most prominent. However, ITCH, WWP1 and NEDD4L could also be detected in one experiment (Figure 2A). Interestingly, the mass spectrometry signal intensities corresponded to the relative expression levels of these NEDD4-family members in immortalized monocyte/macrophage progenitors (Figure 2B,C). On the other hand, not all NEDD4-family members expressed in these cells could be co-isolated with WBP1L. These data suggest a certain level of WBP1L selectivity for individual NEDD4-family members.

To find out whether NEDD4-family ligases bind WBP1L via its [L/P]PXY WW domain binding motifs we have co-expressed the two highest scoring NEDD4-family ligases from the mass spectrometry experiment, WWP2 or ITCH, with wild-type WBP1L construct or with mutant WBP1L N lacking the membrane-proximal WW domain binding sequences (Figure 2D) in HEK293 cells. These cells allow for relatively high level of overexpression, which was ideal for reliable identification of NEDD4 family binding sites in WBP1L. Both E3 ligases could be readily co-immunoprecipitated with wild-type WBP1L but not with WBP1L N (Figure 2D). These data were further confirmed in a similar experiment in J774 macrophage-like cell line, which expresses relatively high level of

ITCH (not shown). The endogenous ITCH could be co-isolated with wild-type WBP1L but not with WBP1L N from these cells (Figure S5). To confirm the interaction of WBP1L with a NEDD4-family member at the endogenous protein level, we have selected bone marrow-derived macrophages (BMDM) which express the high-est levels of WBP1L among the cell types we have tested so far (Figure 1B). WWP1, which is the most abundant NEDD4-family member in this cell type (Figure 2E), could be co-isolated with WBP1L in this experiment (Figure 2F).

3.3 | WBP1L regulates ubiquitination and expression level of NEDD4-family E3 ubiquitin ligases and of CXCR4

Interaction with WW domain binding motifs is known to result in the activation and autoubiquitination of NEDD4-family ubiqui-tin ligases.[14,15] To test whether WBP1L can activate NEDD4 fam-ily members, we have cotransfected WBP1L-interacting (Figure 2A) NEDD4-family ligases with wild-type WBP1L, or its mutant lacking one of the conserved WW domain binding motifs, into HEK293 cells. This analysis demonstrated that cotransfection with wild-type but not mutant WBP1L resulted in a substantial increase in ubiquitina-tion of all these ligases, which is a sign of their activation (Figure 3A). Published work suggests that in the case of ITCH this ubiquitination results in down-regulation of its protein levels, while WWP2 appears relatively resistant to this negative feedback regulation. Thus, to fur-ther explore the mechanism of how WBP1L regulates these ubiquitin ligases, we co-expressed wild-type WBP1L, WBP1L N or WBP1L C (lacking C-terminal region of unknown function) with ITCH or WWP2 in HEK293 cells. Co-expression of ITCH with wild-type WBP1L and WBP1L C resulted in significantly reduced ITCH protein level when compared to co-expression with WBP1L N. As expected, this effect was much more limited in case of WWP2 (Figure 3B).

One of the best-studied targets of NEDD4-family ubiquitin li-gases in the haematopoietic system is the chemokine receptor CXCR4. It is involved in the maintenance of haematopoietic stem and progenitor cells and in promoting niche interactions in the bone marrow. It is also thought to support the survival and treatment re-sistance of leukaemic cells.[16,17] Based on these features, we have se-lected CXCR4 for a similar set of experiments to test whether WBP1L regulates its protein expression levels and ubiquitination. Indeed, co-expression of WBP1L with CXCR4 in HEK293 cells resulted in increased ubiquitination of CXCR4 (presumably by an endogenous NEDD4-family ligase). This effect was almost completely abolished by mutation of the WW domain binding motifs (WBP1L N) while deletion of the C-terminal sequence (WBP1L C) had a more limited effect (Figure 3C). CXCR4 ubiquitination was further accompanied by reduction in CXCR4 protein levels (Figure 3C). We also observed that WBP1L co-expression resulted in a striking increase in CXCR4 electrophoretic mobility (Figure 3C). The reason for this mobility shift is at present unknown.

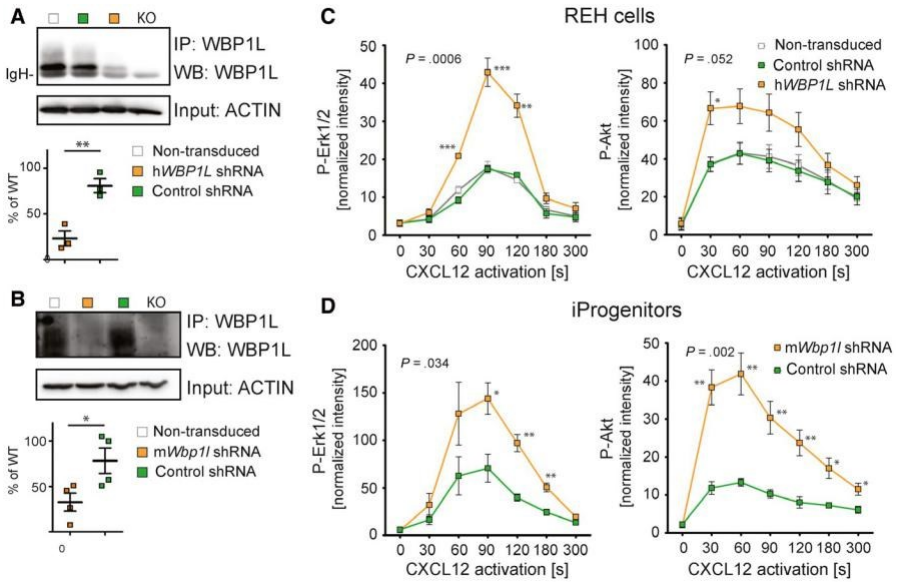

FIGURE 4 ShRNA-mediated down-regulation of WBP1L results in enhanced CXCR4 signalling in human and murine cell lines. (A, B) WBP1L immunoprecipitates from REH cells (A) or immortalized monocyte/macrophage progenitors (B) transduced with *Wbp1l* shRNA were stained with WBP1L antisera to demonstrate WBP1L down-regulation. Equal input of lysates to immunoprecipitation was verified by ACTIN immunoblotting. Quantification of multiple experiments (after normalization to ACTIN signal) was plotted as a percentage of WBP1L expression in non-transduced cells. (C, D) ERK1/2 and AKT phosphorylation downstream of CXCR4 in REH cells (C) and immortalized monocyte/macrophage progenitors (iProgenitors) (D), where WBP1L was down-regulated by shRNA. Cells were stimulated with 100 nmol/L CXCL12, lysed and subjected to Western blot analysis of ERK1/2 and AKT phosphorylation. Data represent mean of fluorescence intensity normalized to GAPDH. The *P*-value was calculated to compare maximum responses of cells transduced with non-silencing control and silencing shRNA. Asterisks denote significant differences in individual time-points. (N = 4)

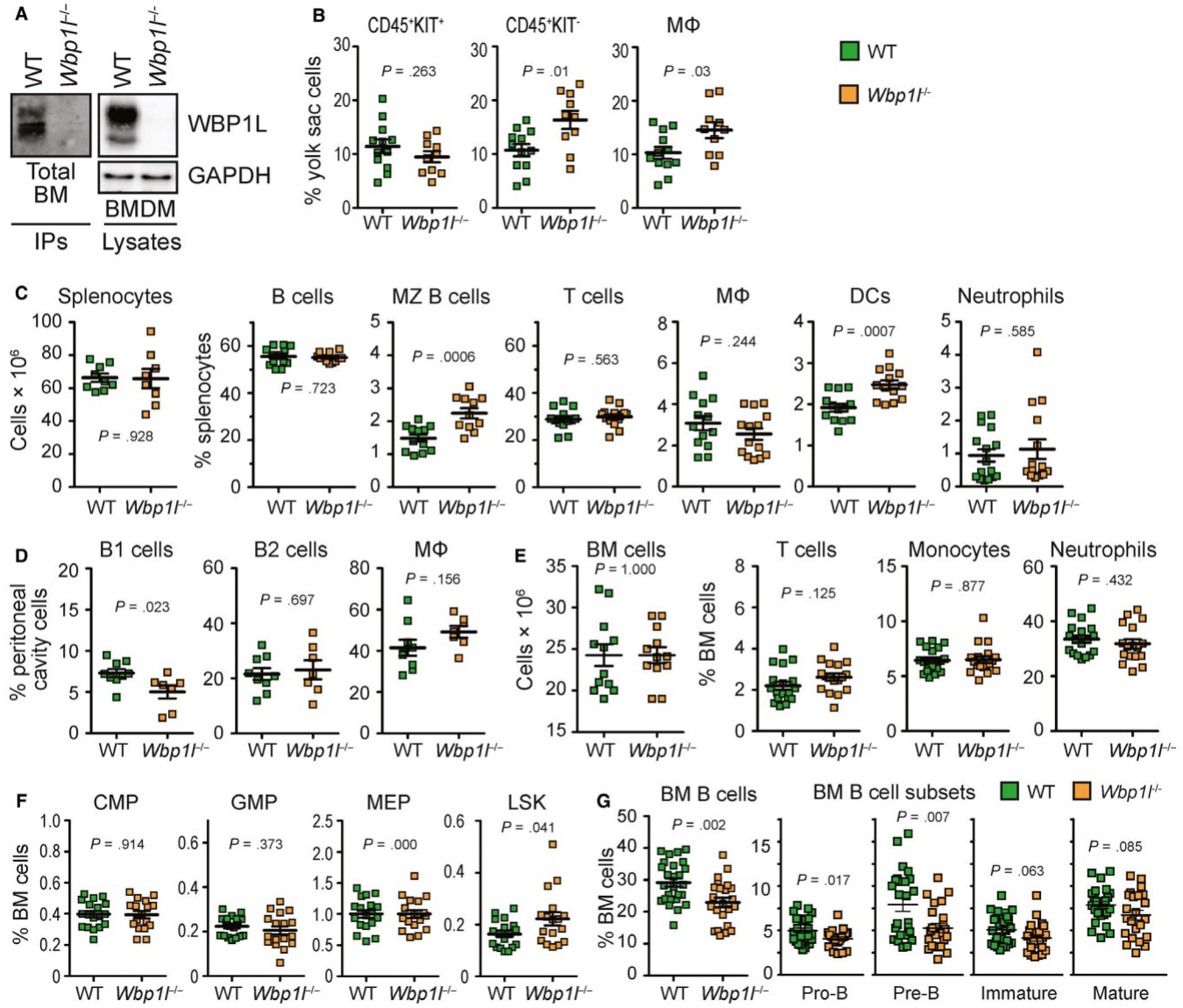

FIGURE 5 Altered leucocyte homeostasis in WBP1L-deficient mice. (A) Western blot analysis of WBP1L immunoprecipitates or whole cell lysates prepared from WT and *Wbp1l*$^{-/-}$ cells. mOPAL-01/03 antibodies were used for immunoprecipitation and WBP1L rabbit antisera for Western blotting. N = 3 (bone marrow), N = 5 (BMDM). (B) Flow cytometry analyses of E10.5 WT and *Wbp1l*$^{-/-}$ yolk sac cell subsets. Primitive macrophages were defined as Ter119^{-} CD11b^{+} F4/80^{+}. (C) Absolute numbers of splenocytes obtained from WT and *Wbp1l*$^{-/-}$ mice and flow cytometry analyses of WT and *Wbp1l*$^{-/-}$ splenocytes defined using the following markers: B cells (B220^{+}), MZ B cells (B220^{+}, AA4.1^{-}, CD23$^{-/low}$, CD1d^{+}), T cells (CD3^{+}), macrophages (F4/80^{+}, CD11b ^{int}), DC (CD11c^{+}, LY6C$^{-/low}$) and neutrophils (LY6G^{+}, CD11b^{+}, LY6C^{-}). (D) Flow cytometry analyses of WT and *Wbp1l*$^{-/-}$ leucocytes in the peritoneum, defined using the following markers: B1 cells (SSC^{low}, FSC^{low}, B220^{+}, CD23$^{-/low}$), B2 cells (SSC^{low}, FSC^{low}, B220^{+}, CD23^{+}) and macrophages (large peritoneal macrophages, CD11b^{high},F4/80^{high}). (E) Flow cytometry analyses of WT and *Wbp1l*$^{-/-}$ bone marrow cell subsets, defined using the following markers: T cells (CD3^{+}), monocytes (LY6C^{+}, CD11b^{+}, LY6G^{-}, CD19^{-}, TER119^{-}, CD3^{-}, NK1.1^{-}), neutrophils (KIT^{-}, B220^{-}, TER119^{-}, CD3^{-}, LY6G^{high}) (F) Flow cytometry analyses of stem and progenitor cells in the bone marrow. Cell subsets were defined using following markers: common myeloid progenitors—CMP (lin^{-}, c-kit^{+}, CD34^{+}, CD16/32$^{neg-low}$, SCA1^{-}), granulocyte-monocyte progenitors—GMP (lin^{-}, KIT^{+}, CD34^{+}, CD16/32^{High}, SCA1^{-}), megakaryocyte-erythroid progenitors—MEP (lin^{-}, KIT^{+}, CD34^{-}, CD16/32^{-}, SCA1^{-}) and LSK (lin^{-}, KIT^{+}, SCA1^{+}). (G) Flow cytometry analysis of bone marrow B cell subsets. B cells (B220^{+}), pro-B cells (CD43^{+}, B220^{+}, IgM^{-}), pre-B cells (CD43^{-}, B220^{low}, IgM^{-}), immature B cells (CD43^{-}, B220^{low}, IgM^{+}) and mature B cells (CD43^{-}, B220^{high}, IgM^{+})

3.4 | WBP1L inhibits CXCR4 signalling in murine and human cell lines

To analyse the effects of the endogenous WBP1L on CXCR4, we have selected two cell lines where the expression of WBP1L and/or CXCR4 is highly relevant. These included human leukaemic cell line REH as a representative of *ETV6-RUNX1*$^{+}$ leukaemia, where we have down-regulated WBP1L by a single shRNA specific for human *WBP1L* and immortalized murine monocyte/macrophage progenitors as a representative of bone marrow progenitors, where

we used a different shRNA targeting murine *Wbp1l* (Figure 4A,B). After stimulation with CXCR4 ligand CXCL12, these cells showed enhanced activity of downstream signalling pathways, resulting in increased phosphorylation of ERK1/2 and AKT (Figure 4C,D and S6). CXCR7, another known receptor for CXCL12, did not contribute to the signalling output under these conditions (Figure S7). These data demonstrated that WBP1L is involved in the negative regulation of CXCR4 signalling.

3.5 | Altered haematopoiesis in *Wbp1l*-deficient mice

To further analyse the physiological function of WBP1L, we have acquired *Wbp1l*-deficient mouse strain *Wbp1l*$^{tm2a(EUCOMM)Hmgu}$ (hereafter referred to as *Wbp1l*$^{-/-}$) from the International Mouse Phenotyping Consortium. These mice appeared grossly normal and healthy, were born in normal Mendelian ratios and did not express WBP1L protein (Figure 5A).

To characterize the haematopoietic system in *Wbp1l*$^{-/-}$ mice, we have analysed major cell subset frequencies in adult mice and in embryos. The embryonic haematopoietic cell numbers were grossly normal with small increases in the yolk sac CD45^{+} KIT^{-} cells and CD11b^{+} F4/80^{+} yolk sac macrophages (Figure 5B). In the peripheral tissues of the adult mice, there was a significant increase in marginal zone B cell fraction in the spleen (Figure 5C) and a reduction in B1 cell percentages in the peritoneal cavity (Figure 5D). We also observed increased frequencies of splenic dendritic cells in *Wbp1l*$^{-/-}$ mice (Figure 5C). Otherwise, the frequencies of other leucocyte subsets found in peripheral tissues were normal (Figure 5C,D). Bone marrows from *Wbp1l*$^{-/-}$ animals showed the same cell counts as wild-type bone marrows (Figure 5E). Most of bone marrow cell subsets were also found in normal numbers, including T cells, monocytes, neutrophils (Figure 5E) and the majority of progenitor populations (Figure 5F). However, there were two notable exceptions. First, the overall B cell percentages in the bone marrow were significantly reduced (Figure 5G). The reduction was most pronounced in early developmental stages (pro- and pre-B cells). At the later stages, including immature and mature B cells a similar trend was observed, but it was outside the threshold for statistical significance (*P*-values .06 and .08, respectively) (Figure 5G). The cell cycle of B cell progenitors was not substantially changed with the exception of a very

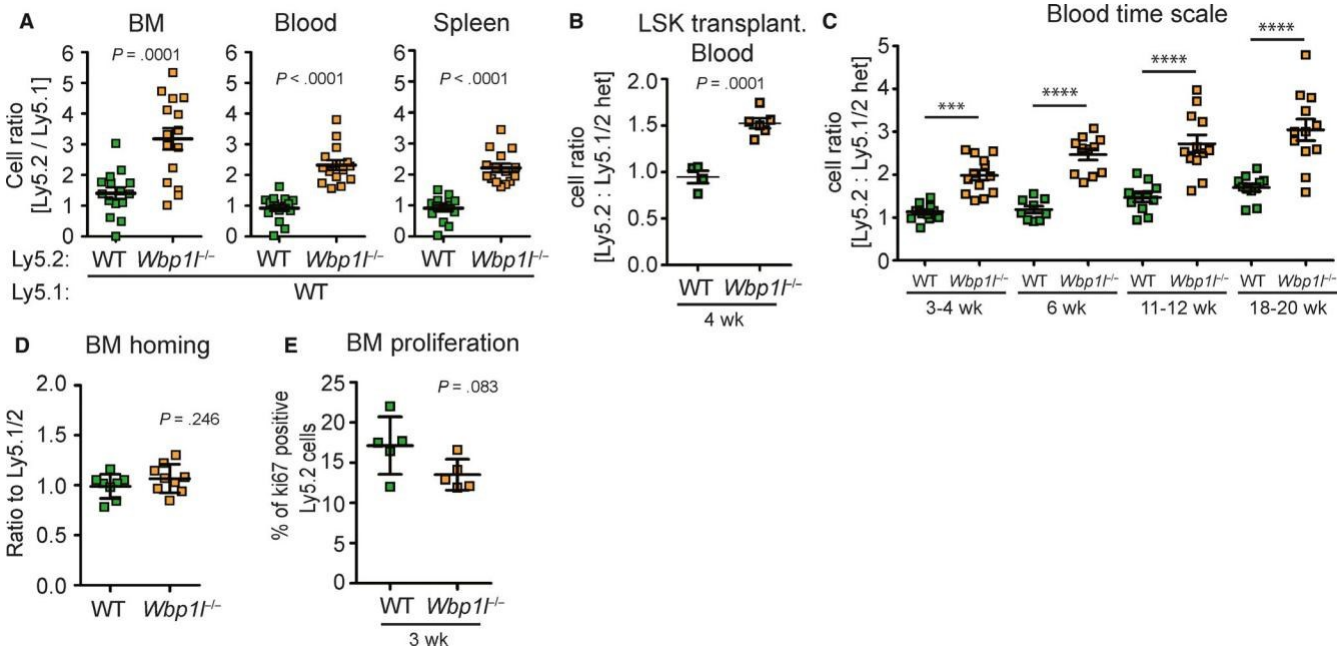

FIGURE 6 Enhanced engraftment of *Wbp1l*$^{-/-}$ bone marrow. (A) Ly5.2^{+} bone marrow (WT or *Wbp1l*$^{-/-}$) was mixed with Ly5.1^{+} bone marrow (always WT) in a ratio 1:1 and 2 × 10^{6} cells were transplanted into Ly5.1 lethally irradiated mice. Mice were analysed 2 months post-transplantation. Flow cytometry analyses show the ratio between Ly5.2 and Ly5.1 cells in the bone marrow, blood and spleen. (B) LSK cells sorted from Ly5.2^{+} bone marrow (WT or *Wbp1l*$^{-/-}$) were mixed with LSK from Ly5.1/Ly5.2^{+} heterozygous bone marrow (always WT) in a ratio 1:1 and 20 000 cells together with support of 0.5 × 10^{6} Ly5.1 bone marrow cells were injected into tail vain of Ly5.1 lethally irradiated mice. Data represent the ratio between Ly5.2^{+} and Ly5.1/Ly5.2^{+} cells detected in the recipient blood 4 wk post injection. One of two independent experiments is shown (N ≥ 8). (C) Ly5.2^{+} bone marrow (WT or *Wbp1l*$^{-/-}$) was mixed with Ly5.1/Ly5.2^{+} heterozygous bone marrow (always WT) in a ratio 1:1 and 2 × 10^{6} cells were transplanted into Ly5.1 lethally irradiated mice. At indicated time-points, the ratio between Ly5.2 and Ly5.1/Ly5.2 cells in blood was measured by flow cytometry. (D) Homing of WT and *Wbp1l*$^{-/-}$ bone marrow cells in a competitive set-up. WT or *Wbp1l*$^{-/-}$ bone marrow (Ly5.2^{+}) was each combined with WT bone marrow from Ly5.1/Ly5.2^{+} heterozygotes in a ratio 1:1 and 2 × 10^{6} cells were injected into the tail vain of sublethally irradiated recipient (Ly5.1^{+}). Data represent the ratio between Ly5.2^{+} and Ly5.1/Ly5.2^{+} cells detected in the recipient bone marrow 16 h post injection (N ≥ 8). (E) Competitive bone marrow transplantation was performed as in (C) and 3 wk after the transplantation expression of Ki67 proliferation marker was measured in transplanted cells

small but significant increase in G1 phase pre-B cells in *Wbp1l*$^{-/-}$ mice (Figure S8). Second, Lin^{-}SCA1^{+}KIT^{+} (LSK) cells encompassing early progenitors and stem cells (HSPC) showed slightly but significantly increased percentages in these animals (Figure 5F).

To test their functionality in vivo, we performed a competitive bone marrow transplantation assay, whereby we mixed wild-type or *Wbp1l*$^{-/-}$ Ly5.2 cells with wild-type Ly5.1 bone marrow cells in a 1:1 ratio and transplanted these mixtures into lethally irradiated recipient mice (Ly5.1). Nine weeks later, we have analysed their engraftment. Strikingly, *Wbp1l*$^{-/-}$ bone marrow engrafted significantly better and the ratio between *Wbp1l*$^{-/-}$ and wild-type cells increased from 1:1 to ca 3:1 (Figure 6A), whereas wild-type Ly5.2 and Ly5.1 BM engrafted with equal efficiency. The difference could be observed across all bone marrow leucocyte subsets analysed except for LSK cells, where a similar trend in favour of *Wbp1l*$^{-/-}$ cells was also present but was not statistically significant (Figure S9). The difference was also maintained in the periphery, where the ratio between *Wbp1l*$^{-/-}$ and wild-type cells was roughly 2:1 (Figure 6A). Similar difference in engraftment efficiency was also observed when we transplanted sorted LSK cells in the 1:1 ratio (Figure 6B). Next, we investigated how this ratio changes with time. A significant difference between the engraftment efficiency could be observed as early as 3 weeks after the transplantation and was maintained till at least 18 weeks after the transplantation (Figure 6C). The increased efficiency in the bone marrow engraftment was not the result of increased homing to the bone marrow or increased proliferation, which did not dis-play any alteration (Figure 6D,E). Collectively, these data are show-ing negative role of WBP1L in HSPC function. Persistence of the engraftment advantage for more than 16 weeks suggests that the haematopoietic system is affected already at the level of haemato-poietic stem cells.

3.6 | Compensatory mechanisms restore CXCR4 signalling when WBP1L is lost in the germline, but the effects of WBP1L deficiency on CXCR4 signalling can be observed upon its acute deletion

Part of the data described above are consistent with CXCR4 hyperactivity. However, the same homing capacity of the wild-type and *Wbp1l*$^{-/-}$ bone marrow cells (Figure 6D) is incompatible with enhanced CXCR4 function. These results prompted us to test whether bone marrow cells from *Wbp1l*$^{-/-}$ mice display similar CXCR4 dysregulation as shRNA-treated cell lines. Surprisingly, we did not observe any alterations in CXCL12-triggered ERK phosphorylation in bone marrow cells from *Wbp1l*$^{-/-}$ mice (Figure 7A). This result was in disagreement with our analysis of the effects of shRNA-mediated WBP1L down-regula-tion in cell lines (Figure 4). To exclude the possibility that enhanced CXCR4 signalling observed there was the result of non-specific off-tar-get effects of *Wbp1l* shRNAs, we expressed shRNA targeting *Wbp1l* in immortalized monocyte/macrophage progenitors from wild-type and *Wbp1l*$^{-/-}$ mice. Because of the absence of WBP1L, only non-specific activity of *Wbp1l* shRNA can be detected in *Wbp1l*$^{-/-}$ progenitors. As expected, *Wbp1l* shRNA significantly enhanced CXCL12-triggered ERK activation in wild-type cells. On the other hand, only negligible insignificant changes were detected in *Wbp1l*$^{-/-}$ cells (Figure 7B). These results demonstrated that the effects of *Wbp1l* shRNA are dependent on *Wbp1l* and, thus, specific. When we used the same cells in an in vivo homing experiment, we observed that WBP1L down-regulation significantly enhanced bone marrow homing of wild-type cells, when compared to *Wbp1l*$^{-/-}$ cells (Figure 7C). This outcome is consistent with the results of our in vitro analyses showing that WBP1L negatively regulates activity of CXCR4.

To definitely prove the validity of our shRNA data, we have generated a mouse strain *Wbp1l*$^{fl/fl}$*-CreERT* where the *Wbp1l* gene can be acutely inactivated upon injection of 4OH-tamoxifen. Acute *Wbp1l* deletion in this model resulted in enhanced ERK phosphorylation in response to CXCL12 stimulation in total bone marrow as well as in several major subsets, including T cells, monocytes and neutrophils, whereas in B cells, the difference was small and not statistically significant (Figure 7D and S10). No effects of WBP1L deficiency on total ERK expression were observed (Figure 7E). The enhanced CXCR4 signalling did not translate to any immediate effect on steady-state numbers of major bone marrow and splenic cell sub-sets (Figure S11A). However, it is likely that only much more substan-tial increase in CXCR4 signalling would be needed to alter leucocyte bone marrow retention within this timescale.

The data presented above suggested that the effects of WBP1L down-regulation can only be observed after its acute deletion. To further address this possibility, we have established primary culture of isolated KIT^{+} bone marrow cells from *Wbp1l*$^{fl/fl}$*-CreERT* mice, where *Wbp1l* could be deleted by 4OH-tamoxifen. Importantly, cells cultured outside the bone marrow are not exposed to continuous CXCL12 stimulation and desensitization and are, thus, having high expression of CXCR4 and stronger signalling capacity. In agreement with our pre-vious observations, after acute *Wbp1l* deletion by CRE recombinase (but not after germline deletion), these progenitors showed increased ERK phosphorylation in response to CXCL12 stimulation (Figure 7F and S11B). *Wbp1l* deletion also resulted in an increase in steady-state CXCR4 surface expression with no other effects on the rate of CXCL12-triggered receptor internalization in these cells (Figure 7G and S11C). The same increase in CXCR4 expression was also observed on KIT^{+} progenitors from peripheral blood of animals after acute *Wbp1l* deletion (Figure 7H). Similar, though not significant, trend was also observed when CXCR4 was measured on fixed and permeabilized cells (Figure S11D). Finally, cells with acute *Wbp1l* deletion showed in-creased migration towards CXCR4 ligand CXCL12 in a transwell assay in vitro (Figure 7I) and increased bone marrow homing efficiency in vivo (Figure 7J). These data confirm that WBP1L negatively regulates CXCR4 expression and signalling in primary cells.

4 | DISCUSSION

Expression of the *WBP1L* gene is heightened in *ETV6-RUNX1*$^{+}$ paediatric BCP-ALL and was shown to correlate with favourable

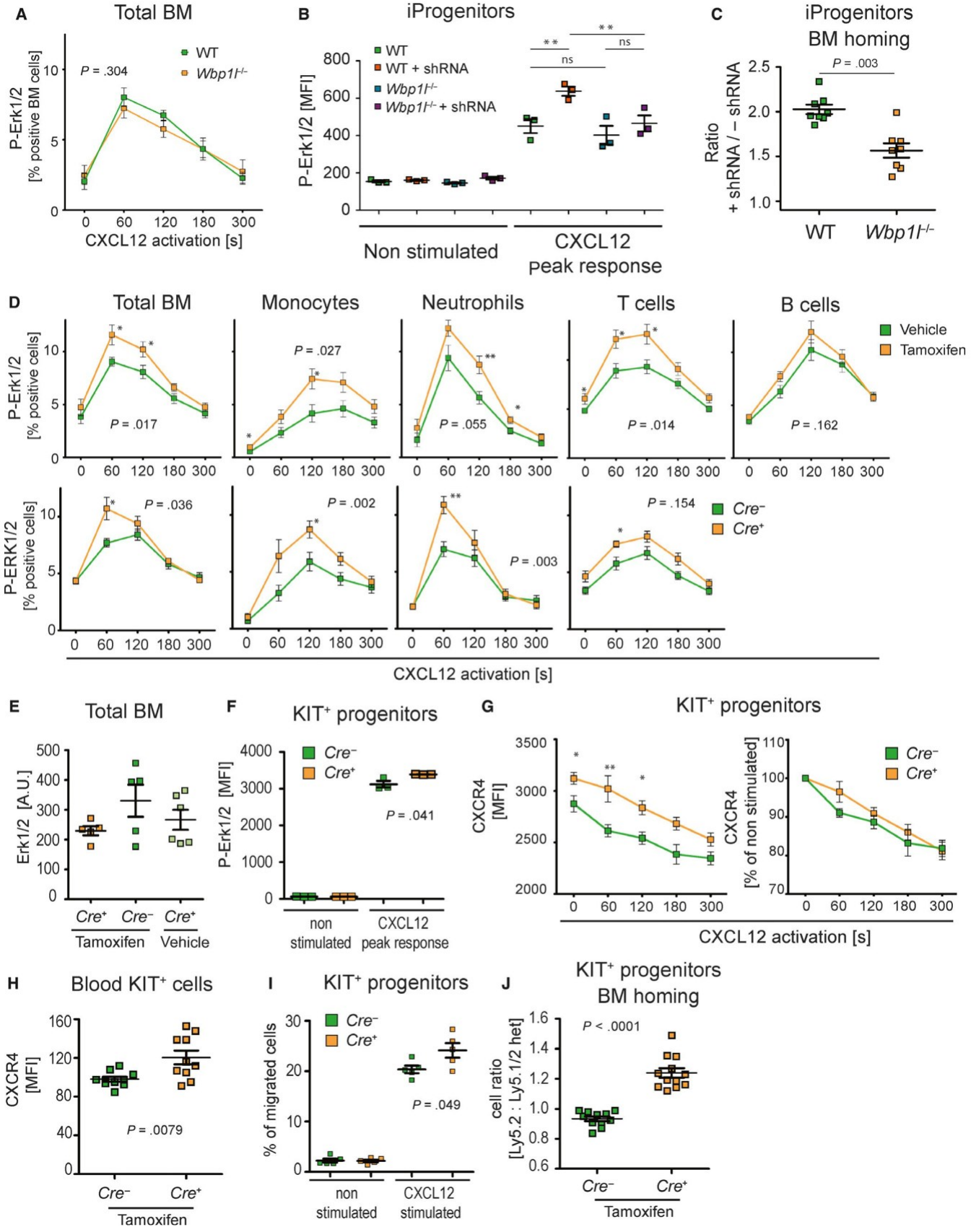

treatment response.[1-3] However, the function of its protein prod-uct WBP1L in healthy and leukaemic cells has not been investigated. Here, we attempted to uncover its physiological function. Our initial analysis shows that WBP1L binds several NEDD4-family E3 ubiquitin ligases and its deficiency results in augmented surface expression and signalling of CXCR4, one of their known target proteins.

FIGURE 7 Acute loss of WBP1L results in enhanced CXCR4 signalling but germline deficiency is compensated for. (A) ERK1/2 phosphorylation downstream of CXCR4 in WT and *Wbp1l*$^{-/-}$ (germline deletion) bone marrow cells. Cells were stimulated with 100 nmol/L CXCL12, fixed, stained for phosphorylated ERK1/2 and analysed by flow cytometry. Data represent percentage of responding cells (N = 6). *P*-value was calculated for maximum response of WT and *Wbp1l*$^{-/-}$ cells regardless of the time-point where it was reached. (B) Erk1/2 activation after CXCL12 stimulation (100 nmol/L) of immortalized monocyte/macrophage progenitors (iProgenitors) from WT and *Wbp1l*$^{-/-}$ mice and of the same cells transduced with *Wbp1l* shRNA. Erk phosphorylation was measured by flow cytometry of fixed and permeabilized cells stained with fluorescent P-Erk1/2 antibody. Peak response detected during 5 min measurement is shown. Data are represented as medians of fluorescence intensity (N = 3). *P*-values were calculated using 1way ANOVA with Bonferroni's multiple comparison test. (C) WT cells transduced or not with *Wbp1l* shRNA were mixed 1:1 and their bone marrow homing ability was analysed as in Figure 6D. As a control *Wbp1l*$^{-/-}$ cells transduced or not with *Wbp1l* shRNA and also mixed in a ratio 1:1 were used. Ratios of shRNA transduced and non-transduced cells are plotted for each genotype (n = 8). *P*-value was calculated for the differences between these two ratios. Significant outliers were discarded based on *q* test. As not all cells expressed shRNA containing vector after transduction, the true ratio was lower than 1:1 at the time of injection. The final data were normalized to this true ratio. (D) CXCR4 signalling in bone marrow cell subsets after acute deletion of *Wbp1l*. In the top row, *CreERT* expressing cells treated either with tamoxifen or vehicle (corn oil) are compared. In the bottom row, the comparison is made between tamoxifen-treated *Wbp1l*$^{fl/fl}$*-CreERT* and *Wbp1l*$^{fl/fl}$ (without *CreERT*) bone marrow cells. Cells were stimulated with 100 nmol/L CXCL12, fixed, stained for extracellular markers and intracellular P-ERK and analysed by flow cytometry. Data represent percentage of responding cells from whole bone marrow (N = 7), T cells (CD3$^+$, N = 7/8), monocytes (Ly6C$^+$ Ly6G$^-$, N = 11) and neutrophils (Ly6G$^+$ Ly6C$^-$,N = 7). Significant outliers were discarded based on *q* test. *P*-value was calculated for maximum response (regardless of the time-point at which this maximum was reached). In addition, significant differences in individual time-points are labelled with asterisks.
(E)Expression of total ERK1/2 in the bone marrow cells where *Wbp1l* was deleted as in (D). Protein level was measured using Western blot. ERK1 and ERK2 were probed separately and signal was summed and normalized to actin loading control (N ≥ 5) (F). CXCR4 signalling in in vitro 4-hydroxytamoxifen treated KIT$^+$ progenitors isolated from *Wbp1l*$^{fl/fl}$*-CreERT* and *Wbp1l*$^{fl/fl}$ (without *CreERT*) bone marrow. ERK phosphorylation was measured after stimulation with 100 nmol/L CXCL12 by flow cytometry on fixed and permeabilized cells. Peak response detected during 5 min measurement is shown. One of two independent experiments is shown, N = 6. (G) CXCL12-induced changes of CXCR4 surface expression on KIT$^+$ bone marrow progenitors. These cells were isolated from *Wbp1l*$^{fl/fl}$*-CreERT* and *Wbp1l*$^{fl/fl}$ bone marrow, treated with 4-hydroxytamoxifen to induce *Wbp1l* deletion and stimulated with CXCL12 for indicated time intervals. FACS data are plotted as median fluorescence intensities (left graph) or as percentage of expression level on non-stimulated cells (right graph) (n = 7). (H) CXCR4 expression on KIT$^+$ progenitors detected in the blood of tamoxifen-treated *Wbp1l*$^{fl/fl}$*-CreERT* and *Wbp1l*$^{fl/fl}$ mice. Significant outlier was discarded based on *q* test (N = 10). (I) Migration of 4-hydroxytamoxifen-treated KIT$^+$ progenitors from *Wbp1l*$^{fl/fl}$*-CreERT* and *Wbp1l*$^{fl/fl}$ mice towards 500 nmol/L CXCR4 in a transwell assay in vitro (N = 5). (J) Ly5.2$^+$ KIT$^+$ progenitors (from *Wbp1l*$^{fl/fl}$*-CreERT* or *Wbp1l*$^{fl/fl}$ mice, treated with 4-hydroxytamoxifen) were mixed 1:1 with Ly5.1/Ly5.2$^+$ heterozygous KIT$^+$ progenitors from WT mice and 10^7 cells were injected into Ly5.1 sublethally irradiated recipients. After 16 h, the ratio between Ly5.2 and Ly5.1/Ly5.2 cells in the bone marrow was measured by flow cytometry (N ≥ 11)

At the organismal level, WBP1L deficiency resulted in perturbations in B cell development and increased ability of bone marrow stem and progenitor cells to reconstitute haematopoietic system after the bone marrow transplantation. In addition, acute *Wbp1l* deletion resulted in increased progenitor homing to the bone marrow. How much of this phenotype can be attributed to CXCR4 hyperactivity is still an open question. There are at least two other mouse models that show increased CXCR4 activity. One of these strains carries a mutation in CXCR4 that prevents its desensitization and down-regulation (*CXCR4*^{WHIM}). The same mutation in humans causes immunodeficiency known as WHIM syndrome.[18-20] *CXCR4*^{WHIM} mice display a similar selective dysregulation in the bone marrow B cell compartment as *Wbp1l*$^{-/-}$ mice with the reduction in B cell percentages that is most profound at the B cell progenitor level.[20] They also show increase in marginal zone B cell percentages. On the other hand, some of their symptoms were not detected in *Wbp1l*$^{-/-}$ mice, including blood neutropenia and lymphopenia and reduced spleen size.[20] Increased CXCR4 expression and CXCR4-mediated signalling were also observed in mice deficient in the expression of BAR domain containing adaptor protein Missing In Metastasis (MIM). In these animals, leucocyte development and percentages appeared largely normal and no leukopenia has been observed. Rather they showed slightly increased white blood cell counts and splenomegaly.[21,22] Even though MIM deficiency has a number of CXCR4-independent effects, these data show that enhanced CXCR4 activity does not have to lead to leukopenia in the peripheral tissues, nor to major alterations in leucocyte subset numbers and frequencies in the bone marrow. It is possible that the lack of receptor desensitization rather than alterations in peak signal intensity may be the key factor driving peripheral leukopenia in *CXCR4*^{WHIM} mice.

Since in mice with germline *Wbp1l* deletion we have not observed up-regulation in CXCR4 activity, it is difficult to unequivocally answer the question if alterations in *Wbp1l*$^{-/-}$ B cell development are caused by CXCR4 dysregulation. This phenotype is strikingly similar to the one observed in *CXCR4*^{WHIM} animals. It is possible that not all haematopoietic cell subsets are able to compensate for the loss of WBP1L. Early B cell progenitors represent a relatively small population, and their WBP1L expression based on the data from ImmGen consortium[23] is similar to other B cell subsets (not shown). The options to analyse their CXCR4 signalling pathways are relatively limited. Those that can be analysed by flow cytometry, including ERK and STAT3 phosphorylation, as well as calcium response appear to be hypo/non-responsive in this particular cell type despite clearly measurable CXCR4 expression (not shown). As a result, B cell progenitors contribute very little to ERK phosphorylation of the entire B cell pool measured in our experiments where the more mature stages dominated the response. The other pathways we were not able to analyse in this relatively rare subpopulation and so it is still

possible that reduction in B cell progenitor numbers in *Wbp1l*$^{-/-}$ mice is caused by some aspect of CXCR4 signalling, which we could not measure.

WBP1L may also have other functions besides regulation of CXCR4. They may be responsible for a part of the phenotype of WBP1L-deficient cells and animals. WBP1L binds multiple NEDD4 family members and very likely other proteins, which can result in pleiotropic effects on leucocyte biology. It has been shown that in competitive transplantation assay HSPC with only one functional CXCR4 allele perform better than wild-type cells, which perform better than *CXCR4*^{WHIM} cells, clearly showing an inverse correlation between CXCR4 activity and transplantation efficiency.[24,25] This observation is rather counterintuitive and opposite to the results we obtained with *Wbp1l*$^{-/-}$ cells. An explanation suggested in these studies was that CXCR4 promotes haematopoietic stem cell quies-cence leading to competitive disadvantage when CXCR4 signalling is up-regulated. This leads to the conclusion that though CXCR4 role cannot be completely excluded by our experiments, effects of WBP1L on transplantation efficiency are likely CXCR4-independent. The molecular mechanism of how WBP1L regulates bone marrow engraftment will have to be addressed in future studies. On the other hand, functional effects of acute down-regulation of WBP1L are more clearly connected to CXCR4, leading to increased surface expression of CXCR4, increased CXCR4 signalling and improved homing efficiency, similar to mouse models with increased CXCR4 activity.

It is at present unclear what is the reason for the unequal effects of the acute and constitutive OPAL1 deletion on CXCR4 signalling. We can speculate that WBP1L may be rather general regulator of expression and/or activity of NEDD4 family ligases. However, there are many additional mechanisms regulating these enzymes. In the majority of cases, these might be able to compensate for the loss of WBP1L in the long-term. However, their ability to rapidly react to acute WBP1L loss would likely be more limited, as it may require changes in the gene expression pattern or other time-consuming adaptations.

Another important question is the role that WBP1L potentially plays in leukaemia. The *WBP1L* gene is a target gene of ETV6, which suppresses its expression.[4] In *ETV6-RUNX1*$^{+}$ BCP-ALL, one allele of *ETV6* is inactivated by fusion with *RUNX1*, while the other is often inactivated as well.[26] This could explain the increase of WBP1L ex-pression in *ETV6-RUNX1*$^{+}$ BCP-ALL. It is also in agreement with our data showing that in REH cells (which already have both *ETV6* alleles inactivated) *ETV6-RUNX1* genetic deletion did not have any further effect on WBP1L expression. *ETV6* inactivation likely represents part of the mechanism leading to the development of leukaemia and defining its features. In principle, WBP1L in this context can have two different functions. First, negative regulation of CXCR4 by WBP1L could dampen the interactions of leukaemic (stem) cells with protective bone marrow niches, making them more sensi-tive to treatment. Second, WBP1L may also have negative effect on leukaemic stem cells similar to its negative regulatory effects on HSPCs that were revealed in our competitive transplantation experiment. Our data do not specifically address the role of WBP1L in leukaemia. However, the effects of WBP1L deficiency on normal haematopoiesis that we observed here and the fact that WBP1L is an ETV6 target gene make WBP1L a relevant target of future re-search in this field.

ACKNOWLEDGEMENTS

This study was supported by Czech Science Foundation (GACR), projects 16-07425S and P302-12-G101, and by institutional funding from the Institute of Molecular Genetics, Academy of Sciences of the Czech Republic (RVO 68378050). We also acknowledge core facilities, including the Czech Centre for Phenogenomics (CCP, supported by project no. LM2015040 and OP RDI CZ.1.05/2.1.00/19.0395 'Higher quality and capacity for transgenic models') and Light Microscopy Core Facility, IMG ASCR, Prague, Czech Republic, supported by MEYS (LM2015062), OPPK (CZ.2.16/3.1.00/21547) and NPU I (LO1419). JS was sup-ported by Czech Health Research Council (AZV), project NV15-28848A. JS a V. Kanderova were also supported by Ministry of Education, Youth and Sports of the Czech Republic, project NPU I LO1604. OVM was supported by European Union's Horizon 2020 research and innovation program under the Marie Sklodowska-Curie grant No. 665735, MBP and MGT were supported by a MRC New Investigator Award (G0400247) to MGT We are grateful to Steve Watson from the University of Birmingham for helpful advice and comments. We also acknowledge Karel Harant and Pavel Talacko from Laboratory of Mass Spectrometry core facil-ity, Biocev, Charles University, Faculty of Science, where mass spectrometric analysis was performed. The mass spectromet-ric facility is supported by the project 'BIOCEV – Biotechnology and Biomedicine Centre of the Academy of Sciences and Charles University' (CZ.1.05/1.1.00/02.0109), from the European Regional Development Fund. The authors would like to thank Dusan Hrckulak from Laboratory of Cell and Developmental Biology IMG ASCR, Prague, for providing us with Cre recombinase construct and Peter Dráber from the Laboratory of Adaptive Immunity IMG ASCR for helping us to establish the method of tandem purifica-tion for mass spectrometry analysis. This work benefitted from the data assembled by ImmGen consortium.

CONFLICT OF INTEREST

The authors confirm that there are no conflicts of interest.

AUTHOR CONTRIBUTIONS

SB, A.D and JK with contribution from MF, PA, JP, TS, NP and TB conducted majority of experiments and data analysis. DG performed microscopy analysis. IS carried out analysis of *Wbp1l*$^{-/-}$ embryos. OVM and KK analysed palmitoylation of WBP1L. V. Kanderova pro-vided data on WBP1L expression in B cell lines. JS and PS gener-ated ETV6-RUNX1-deficient REH cell line. MBP and MGT generated rabbit antisera to WBP1L. MAJ contributed to design and analysis of homing and competitive transplantation assays. V. Korinek con-tributed to the generation of *Wbp1l*-CreERT mouse strain. TB with

contribution from SB and AD conceptualized the study, evaluated the data and wrote the paper.

DATA AVAILABILITY STATEMENT

The data that support the findings of this study are available from the corresponding author upon reasonable request.

ORCID

Orest V. Matveichuk https://orcid.org/0000-0002-4057-7598
Majd B. Protty https://orcid.org/0000-0001-8992-9120
Tomas Brdicka https://orcid.org/0000-0002-1560-4398

REFERENCES

1. Mosquera-Caro M, Helman P, Veroff R, et al. Identification, validation and cloning of a novel gene (OPAL1) and associated genes highly predictive of outcome in pediatric acute lymphoblastic leukemia using gene expression profiling [abstract]. *Blood*. 2003;102:4a.
2. Holleman A, den Boer ML, Cheok MH, et al. Expression of the outcome predictor in acute leukemia 1 (OPAL1) gene is not an indepen-dent prognostic factor in patients treated according to COALL or St Jude protocols. *Blood*. 2006;108:1984-1990.
3. Kanderova V, Kuzilkova D, Stuchly J, et al. High-resolution antibody array analysis of childhood acute leukemia cells. *Mol Cell Proteomics*. 2016;15:1246-1261.
4. Neveu B, Spinella J-F, Richer C, et al. CLIC5: a novel ETV6 target gene in childhood acute lymphoblastic leukemia. *Haematologica*. 2016;101:1534-1543.
5. Lopez RG, Carron C, Oury C, Gardellin P, Bernard O, Ghysdael J. TEL is a sequence-specific transcriptional repressor. *J Biol Chem*. 1999;274:30132-30138.
6. Chakrabarti SR, Nucifora G. The leukemia-associated gene TEL en-codes a transcription repressor which associates with SMRT and mSin3A. *Biochem Biophys Res Commun*. 1999;264:871-877.
7. De Braekeleer E, Douet-Guilbert N, Morel F, Le Bris MJ, Basinko A, De Braekeleer M. ETV6 fusion genes in hematological malignancies: a review. *Leuk Res*. 2012;36:945-961.
8. Rasighaemi P, Ward AC. ETV6 and ETV7: Siblings in hematopoiesis and its disruption in disease. *Crit Rev Oncol Hematol*. 2017;116:106-115.
9. Wang LC, Swat W, Fujiwara Y, et al. The TEL/ETV6 gene is required specifically for hematopoiesis in the bone marrow. *Genes Dev*. 1998;12:2392-2402.
10. Hock H, Meade E, Medeiros S, et al. Tel/Etv6 is an essential and selective regulator of adult hematopoietic stem cell survival. *Genes Dev*. 2004;18:2336-2341.
11. Pei J, Grishin NV. Unexpected diversity in Shisa-like proteins suggests the importance of their roles as transmembrane adaptors. *Cell Signal*. 2012;24:758-769.
12. Draber P, Kupka S, Reichert M, et al. LUBAC-recruited CYLD and A20 regulate gene activation and cell death by exerting oppos-ing effects on linear ubiquitin in signaling complexes. *Cell Rep*. 2015;13:2258-2272.
13. Kralova J, Glatzova D, Borna S, Brdicka T. Expression of fluorescent fusion proteins in murine bone marrow-derived dendritic cells and macrophages. *J Vis Exp*. 2018;140:e58081. https://doi.org/10.3791/58081
14. Lorenz S. Structural mechanisms of HECT-type ubiquitin ligases. *Biol Chem*. 2018;399:127-145.
15. Mund T, Pelham HRB. Control of the activity of WW-HECT domain E3 ubiquitin ligases by NDFIP proteins. *EMBO Rep*. 2009;10:501-507.
16. Ayala F, Dewar R, Kieran M, Kalluri R. Contribution of bone microenvironment to leukemogenesis and leukemia progression. *Leukemia*. 2009;23:2233-2241.
17. de Lourdes PA, Amarante MK, Guembarovski RL, de Oliveira CEC, Watanabe MAE. CXCL12/CXCR4 axis in the pathogenesis of acute lymphoblastic leukemia (ALL): a possible therapeutic target. *Cell Mol Life Sci*. 2015;72:1715-1723.
18. Hernandez PA, Gorlin RJ, Lukens JN, et al. Mutations in the chemo-kine receptor gene CXCR4 are associated with WHIM syndrome, a combined immunodeficiency disease. *Nat Genet*. 2003;34:70-74.
19. Kawai T, Malech HL. WHIM syndrome: congenital immune deficiency disease. *Curr Opin Hematol*. 2009;16:20-26.
20. Balabanian K, Brotin E, Biajoux V, et al. Proper desensitization of CXCR4 is required for lymphocyte development and peripheral compartmentalization in mice. *Blood*. 2012;119:5722-5730.
21. Zhan T, Cao C, Li L, Gu N, Civin CI, Zhan X. MIM regulates the traf-ficking of bone marrow cells via modulating surface expression of CXCR4. *Leukemia*. 2016;30:1327-1334.
22. Yu D, Zhan XH, Zhao XF, et al. Mice deficient in MIM expression are predisposed to lymphomagenesis. *Oncogene*. 2012;31:3561-3568.
23. Heng TS, Painter MW. The Immunological Genome Project: networks of gene expression in immune cells. *Nat Immunol*. 2008;9:1091-1094.
24. McDermott DH, Gao JL, Liu Q, et al. Chromothriptic cure of WHIM syndrome. *Cell*. 2015;160:686-699.
25. Gao JL, Yim E, Siwicki M, et al. Cxcr4-haploinsufficient bone marrow transplantation corrects leukopenia in an unconditioned WHIM syndrome model. *J Clin Invest*. 2018;128:3312-3318.
26. Sundaresh A, Williams O. Mechanism of ETV6-RUNX1 Leukemia. In: Groner Y, Ito Y, Liu P, Neil JC, Speck NA, van Wijnen A, eds. *RUNX Proteins in Development and Cancer*. Singapore: Springer Singapore; 2017:201-216.

SUPPORTING INFORMATION

Additional supporting information may be found online in the Supporting Information section.

How to cite this article: Borna S, Drobek A, Kralova J, et al. Transmembrane adaptor protein WBP1L regulates CXCR4 signalling and murine haematopoiesis. *J Cell Mol Med*. 2020;24:1980–1992. https://doi.org/10.1111/jcmm.14895

Supplemental methods

Cell culture

REH cells were cultured in RPMI (Thermo Fisher Scientific, Waltham, MA), 293T and J774 cells and Phoenix cells were cultured in DMEM (Thermo Fisher), other BCP-ALL cell lines were cultivated as described previously [1]. Media were supplemented with 10% fetal bovine serum (Thermo Fisher) and antibiotics. Immortalized monocyte-macrophage progenitors were cultivated and generated using conditional HOXB8 construct as described previously [2,3]. KIT^+ cells were cultured in IMDM media supplemented with 0.1% IL-6, 0.2% IL-3, 1% SCF, supplied as supernatants from HEK293 cells transfected with constructs coding for respective cytokines. CRE-mediated *Wbp1l* deletion was induced with 1μM 4-hydroxytamoxifen. BMDM were prepared and cultivated as described [4].

Antibody generation

Preparation of the rabbit anti-WBP1L polyclonal antibody was outsourced to Eurogentec (Seraing, Belgium). The QAREHGHPHLPRPPAC peptide, which is close to the WBP1L C-terminus and is identical in the human and mouse sequences, was conjugated to keyhole limpet hemocyanin (KLH) for use as the antigen. The same peptide was used to affinity purify the antibody. OPAL-01 and OPAL-02 antibodies to human WBP1L were described previously [1]. mOPAL-01 and mOPAL-03 mouse monoclonal antibodies to murine WBP1L were generated by standard hybridoma technology using splenocytes of mice (F1 hybrids of BALB/c × B10) immunized with recombinant intracellular part of murine WBP1L protein and Sp2/0 myeloma cells as a fusion partner.

Flow cytometry

For surface staining, cells were incubated with antibodies and Fc-block (Clone 2.4G2) in PBS with 2% FBS for 30 min. For intracellular staining, cells were fixed with 4% formaldehyde (Thermo Fisher), then stained for surface markers, permeabilized with 90% methanol (Lachner, Neratovice, Czechia), blocked with 5% BSA (Merck, Darmstadt, Germany) 0.3% Triton X-100 (Merck) in PBS and stained for intracellular antigens in 1% BSA 0,3% Triton X-100 in PBS. For cell cycle analyses or Ki67 staining, cells were not permeabilized by methanol and after antibody staining were stained with 2 μg/ml Hoechst 33342 (Merck). Data were collected on LSRII flow cytometer (BD Biosciences, San Jose, CA) and analyzed with FlowJo software (FlowJo LLC, Ashland, OR).

Other reagents and their sources

β-estradiol (Merck), 4-Hydroxytamoxifen (Merck), recombinant murine and human SDF1α (Immunotools, Friesoythe, Germany), Lipofectamine 2000 (Thermo Fisher), Protein A/G (Santa Cruz Biotechnology, Dallas, TX), tunicamycin, Lysotracker Red DND-99, ER-Tracker Red, MitoTracker Red (Thermo Fisher), TC14012 (RanD corporation), AMD3100 (Merck).

Analysis of WBP1L palmitoylation

Palmitoylation of WBP1L was analyzed using click reaction-based approach, essentially as described earlier [5]. Briefly, HEK293 cells (5.5 x 10^5 in 60-mm dish) were transfected with 6 µg of WBP1L- FLAG-STREP-bearing pBABE using FuGENE (Promega, Madison, WI) according to manufacturer's instruction. After 24 h, cells were labeled with 50 µM 17-octadecynoic acid (17ODYA) or exposed to 0.05% DMSO carrier (1.5 h, 37 °C). Cells were lysed in a buffer containing 4% SDS and lysates subjected to click reaction with biotin-azide (500 µM biotin-PEG3-azide; Merck). Proteins were precipitated with chloroform:methanol [6] and resupended in the presence of 0.5% SDS and 1% Brij97. Biotin-tagged proteins were enriched on streptavidin-coupled beads (Thermo Fisher), eluted in hot H_2O followed by series of buffers and analyzed by immunoblotting using mouse anti-FLAG IgG (Merck) and rabbit anti-FLOTILLIN-2 IgG (Cell Signaling Technology, Danvers, MA).

Microscopy

BMDM were plated overnight on eight well µ-plate (IBIDi). The next day the cells were directly imaged or stained with organelle specific dye (MitoTracker Red 1:500, LysoTracker Red DND-99 1:1000, ER-tracker Red 1:1000, all Thermo Fisher) and directly imaged, or stained with CD11b-APC (Table S1) and subsequently fixed with 4% formaldehyde (Merck) and stained with Hoechst 33342 (Merck). Sequential 2-color imaging was performed using Leica TCS SP8 laser scanning confocal microscope with a 63×1.4 NA oil-immersion objective. Acquired images were manually thresholded to remove signal noise detected outside of the cell using ImageJ software.

Isolation of cell subsets from organs

Mouse blood was collected by cheek bleeding to EDTA tubes (KABE Labortechnik, Numbrecht-Elsenroth, Germany). B cells and T cells were isolated from splenocyte suspensions and neutrophils and KIT^+ cells from bone marrow cell suspensions using magnetic microbeads (Miltenyi Biotec, Bergisch Gladbach, Germany, see *Supplementary Table S5*) on an AutoMACS magnetic cell sorter (Miltenyi Biotec). Cells from murine embryo proper and yolk sac were isolated by digestion of respective tissue in dispase (1mg/ml, Thermo Fisher) in HBSS for 10 min followed by erythrocyte lysis with ACK buffer.

Knock-out cell line preparation

ETV6-RUNX1$^{-/-}$ REH cell lines were established using CRISPR/Cas9 technology. pLV-U6g-EPCG plasmid (Merck) was used with guide RNA (GTGCCTCGAGCGCTCAGGATGG) against exon 2 of *ETV6* gene. Since the second allele of *ETV6* is deleted in REH cell line, this targeting sequence is specific for fusion gene only. Knockout of *ETV6-RUNX1* gene was confirmed by Sanger sequencing, on mRNA and protein level (Figure S2 and data not shown). As a control, REH cell line transduced with non- targeting CRISPR/Cas9 vector was used.

Tandem purification of WBP1L for mass spectrometry analysis of WBP1L-binding proteins

Cells were lysed in lysis buffer (30mM TRIS, pH 7.4, 120 mM NaCl, 2 mM KCl, 10% Glycerol, 1% β-D-dodecylmaltoside, 10 mM Chloroacetamide, Phosphatase inhibitor tablets (PhosSTOP, Roche, Basel, Switzerland), Protease Inhibitor Cocktail (Roche)) and tagged proteins were immunoprecipated from postnuclear supernatants on anti-flag M2 affinity gel (Merck), eluted with 3x FLAG peptide (Merck), followed by second round of affinity purification on Strep-Tactin sepharose (IBA Lifesciences, Goettingen, Germany) and elution with 2% sodium deoxycholate (Merck) in 50mM TRIS (pH 8.5). Cysteines in eluted proteins were reduced with 5mM final concentration of TCEP (Tris(2-carboxyethyl)phosphine hydrochloride) and blocked with 10mM final concentration of MMTS (methyl methanethiosulfonate). Samples were cleaved with 1µg of trypsin. After digestion, samples were acidified with TFA (Trifluoroacetic acid) to 1% final concentration. Sodium deoxycholate was removed by extraction to ethylacetate [7]. Peptides were desalted on Michrom C18 column.

nLC-MS 2 Analysis

Nano Reversed phase column (EASY-Spray column, 50 cm x 75 µm ID, PepMap C18, 2 µm particles, 100 Å pore size) was used for LC/MS analysis. Mobile phase buffer A was composed of water and 0.1% formic acid. Mobile phase B was composed of acetonitrile and 0.1% formic acid. Samples were loaded onto the trap column (Acclaim PepMap300, C18, 5 µm, 300 Å Wide Pore, 300 µm x 5 mm, 5 Cartridges) for 4 min at 15 µl/min. Loading buffer was composed of water, 2% acetonitrile and 0.1% trifluoroacetic acid. Peptides were eluted with Mobile phase B gradient from 4% to 35% B in 60 min. Eluting peptide cations were converted to gas-phase ions by electrospray ionization and analyzed on a Thermo Orbitrap Fusion (Q-OT- qIT, Thermo Fisher). Survey scans of peptide precursors from 400 to 1600 m/z were performed at 120K resolution (at 200 m/z) with a 5×10^5 ion count target. Tandem MS was performed by isolation at 1.5 Th with the quadrupole, HCD (Higher-energy collisional dissociation) fragmentation with normalized collision energy of 30, and rapid scan MS analysis in the ion trap. The MS 2 ion count target was set to 10^4 and the max injection time was 35 ms. Only those precursors with charge state 2–6 were sampled for MS 2. The dynamic exclusion duration was set to 45 s with a 10 ppm tolerance around the selected precursor and its isotopes. Monoisotopic precursor selection was turned on. The instrument was run in top speed mode with 2 s cycles [8].

Data analysis of mass spectrometry

All data were analyzed and quantified with the MaxQuant software (version 1.5.3.8) [9]. The false discovery rate (FDR) was set to 1% for both proteins and peptides and we specified a minimum length of seven amino acids. The Andromeda search engine was used for the MS/MS spectra search against the *Mus musculus* database (downloaded from Uniprot on March 2018, containing 25 527 entries). Enzyme specificity was set as C-terminal to Arg and Lys, also allowing cleavage at proline bonds and a maximum of two missed cleavages. Dithiomethylation of cysteine was selected as fixed modification and N-terminal protein acetylation and methionine oxidation as variable modifications. The “match between runs” feature of MaxQuant was used to transfer identifications to other LC- MS/MS runs based on their masses and retention time (maximum deviation 0.7 min) and this was also used in quantification experiments. Quantifications were performed with the label-free algorithms described recently [9]. Data analysis was performed using Perseus 1.5.2.4 software.

Protein immunoprecipitation

Cells were lysed in lysis buffer described in the tandem purification method above. In co-Immunoprecipitation experiments 1% β-D-dodecylmaltoside was replaced with 1% NP-40 substitute (AppliChem GmbH) and in WBP1L immunoprecipitation from multiple B cell lines (Figure S2) RIPA buffer (50 mM TRIS pH7.4, 150 mM NaCl, 1% NP-40 substitute, 1% Deoxycholate (Merck), 0.1% SDS (Merck)) with the same protease and phosphatase inhibitors was used. Lysates were incubated with WBP1L monoclonal antibodies followed by isolation of antibody-bound complexes on protein A/G agarose beads (Santa Cruz Biotechnology) and elution with SDS-PAGE sample buffer.

Construct preparation and lentiviral production

If not otherwise specified, inserts were amplified from cDNA using Q5 polymerase (New England BioLabs, Boston, MA). Myc-tagged *WBP1L WT*, *N* (with deletion of the following sequence QQRQHEINLIAYREAHNYSALPFYFRFLPNSLLPPYEEVVNRPPTPPPPYSAFQL deleted) *C* (lacking entire C-terminus starting from PPPPQGGPPGGSPPGAD...) were generated by PCR and cloned into pcDNA3 vector. For WBP1L palmitoylation analysis and tandem purification, *WBP1L* or *EGFP* were cloned into tagging vector (pBABE containing C-terminal 3xFlag-2x Srep-tag-UGA –IRES-G418). For microscopy, *WBP1L* was cloned into MSCV vector in front of *MYC-tag-EGFP-UAA*. *Golgi-mApple* was amplified from mApple-Golgi-7 (mApple-Golgi-7 was a gift from Michael Davidson, Addgene plasmid # 54907) and subcloned into MSCV. E3 ligase cloning is summarized in Table S3. *WBP1L* shRNA (silencing/nonsilencing murine TRCN0000297606/085, human TRCN0000282025/275362) was obtained from Merck. Full length *Cre* (a gift from Dušan Hrčkulák) was cloned into pHIV-EGFP vector (pHIV-EGFP was a gift from Bryan Welm & Zena Werb, Addgene plasmid # 21373 [10]).

For lentiviral transductions HEK293T cells were transfected with Lentiviral Packaging vector (Thermo Fisher) and a vector of interest in ratio 1:2.5 using polyethyleneimine (PEI) (Polysciences, Warrington, PA). Virus was concentrated on centrifugal filter (Amicon 100K, Millipore). Cell infection was performed similarly to retroviruses as described here [4]. After infection with shRNA constructs, the infected cells were sorted based on the reporter (EGFP) expression and used in experiments no later than 3 weeks after the infection.

Table S1. List of flow cytometry antibodies

Antigen	Clone	Species tested	Conjugate	Company
P-ERK	197G	Mus musculus	Alexa 647	Cell Signalling Technology
Ly5.1	A20	Mus musculus	APC, FITC	BioLegend
Ly5.2	104	Mus musculus	PE-Cy7, PB,	BioLegend
CD3	17A2, 1452/C11	Mus musculus	PE, PB	BioLegend
Ly6C	HK1.4	Mus musculus	FITC, PE-Cy7	BioLegend
Ly6G	1A8	Mus musculus	PB, FITC, PB, APC	BioLegend
B220	RA3-6B2	Mus musculus	e450	Thermo-Fisher
IgM	EB121-15F9	Mus musculus	FITC	eBioscience
CD43	eBioR2/60	Mus musculus	PE	eBioscience
KIT	2B8	Mus musculus	PE, FITC	BioLegend
SCA-1	E13-161.7	Mus musculus	APC	BioLegend
CD16/32	93	Mus musculus	FITC	BioLegend
CD19	6D5	Mus musculus	FITC	BioLegend
CD11c	N418	Mus musculus	APC	BioLegend
F4/80	BM8	Mus musculus	PE, FITC, PE-Cy7	BioLegend
CD11b	M1/70	Mus musculus	PE, BV785, A700, APC	BioLegend, Sony
TER119	TER-119	Mus musculus	PB, Qdot605	BioLegend,
CD34	RAM34	Mus musculus	FITC	eBioscience
CD93	AA4.1	Mus musculus	PerCP-Cy5.5	BioLegend
CD23	B3B4	Mus musculus	e660, APC	Thermo-Fisher
CD1d	1B1	Mus musculus	FITC	BioLegend
CD5	57-7.3	Mus musculus	PE	Thermo-Fisher
CD45	30-F11	Mus musculus	PerCP-Cy5.5	Biolegend
Ki67	16A8	Mus musculus	APC	Biolegend
anti-mouse Lineage Cocktail	17A2/RB6-8C5/RA3-6B2/Ter-119/M1/70	Mus musculus	PB	BioLegend
KOMBITEST™ CD3 FITC / CD16+ CD56 + PE / CD45 PerCP / CD19 APC	UCHT1/3G8/LT56/MEM-28/LT19	Homo sapiens	FITC, PE, PerCP, APC	Exbio
CD14	MEM-18	Homo sapiens	FITC	Exbio
CXCR4	2B11	Mus musculus and Homo sapiens	APC	Thermo-Fisher

Table S2. List of antibodies for immunoprecipitation and Western blotting.

Antigen	Clone	Company	Comments
WBP1L	Rabbit polyclonal	Custom made, Eurogentec	Human/mouse WBP1L for Western Blotting
WBP1L	OPAL-01	Made in house	Human WBP1L
WBP1L	OPAL-02	Made in house	Human WBP1L
WBP1L	mOPAL-01	Made in house	Mouse WBP1L
WBP1L	mOPAL-03	Made in house	Mouse WBP1L
β-ACTIN	AC15	Merck	
P-ERK	197G2	Cell Signalling Technology	
ERK 1	MK12	BD Bioscience	
ERK 2	Rabbit polyclonal	Santa Cruz Biotechnology	
P-AKT	D9E	Cell Signalling Technology	
GAPDH	Rabbit polyclonal	Merck	
MYC-tag	9B11	Cell Signalling Technology	
UBIQUITIN	Rabbit polyclonal (A100)	Boston Biochem	
UBIQUITIN	P4D1	Cell Signalling Technology	CXCR4 ubiquitination
ITCH	Rabbit polyclonal	LifeSpan BioSciences	Itch staining in Fig. 5C
ITCH	D8Q6D	Cell Signalling Technology	Itch expression in progenitors
WWP1	Rabbit polyclonal	Abcam	
WWP2	Rabbit polyclonal	Abcam	
CXCR4	2B11	BD Bioscience	
HA-tag	C29F4	Cell Signalling Technology	
FLOTILLIN-2	Rabbit monoclonal	Cell Signalling Technology	Western Blotting
FLAG	M2	Merck	
Mouse Anti-Rabbit IgG Antibody conjugated to peroxidase	M205	Genscript	For I.P.
Goat Anti-Mouse, light chain specific, conjugated to peroxidase	Monoclonal, not specified	Jackson Immunoresearch	For I.P.
Mouse Anti-Rabbit, light chain specific, conjugated to peroxidase	Monoclonal, not specified	Jackson Immunoresearch	For I.P.
Goat anti-Mouse IgG (H+L), conjugated to peroxidase	Polyclonal	Bio-Rad	For lysates
Goat anti-Mouse IgG (H+L), conjugated to peroxidase	Polyclonal	Bio-Rad	For lysates

Table S3. List of qPCR primers

Primer	Sequence	Species tested	Company
WBP1L forward	CTCAGCGCTGCCATTTTATT	Homo sapiens	Merck
WBP1L reverse	GCTGGAAGGCACTGTATGGT	Homo sapiens	Merck
GAPDH forward	CCACATCGCTCAGACACCAT	Homo sapiens	Merck
GAPDH reverse	CCAGGCGCCCAATACG	Homo sapiens	Merck
WBP1L forward	CGTTGCCGTTTTACTTCAGG	Mus musculus	Merck
WBP1L reverse	GAGCTGGAAGGCACTGTACG	Mus musculus	Merck
WWP1 forward	GTTGCTGCCAGACCCAAA	Mus musculus	Merck
WWP1 reverse	TAGGACAGATGATGATTCTCCATTA	Mus musculus	Merck
WWP2 forward	GCCGGTTACCAGCTCAAA	Mus musculus	Merck
WWP2 reverse	TCAAAGATACAGGTCTGCAAGC	Mus musculus	Merck
SMURF2 forward	TTACATGAGCAGGACACACTTACA	Mus musculus	Merck
SMURF2 reverse	GCTGCGTTGTCCTTTGTTC	Mus musculus	Merck
SMURF1 forward	GGGTCAGTGGTGGACTGC	Mus musculus	Merck
SMURF1 reverse	CCAGGGCCTGAGTCTTCATA	Mus musculus	Merck
NEDD4L forward	TGAGCAAGCTCACCTTCCA	Mus musculus	Merck
NEDD4L reverse	CCCGTGACAGTTGACGAAC	Mus musculus	Merck
NEDD4 forward	GCCGGTTACCAGCTCAAA	Mus musculus	Merck
NEDD4 reverse	TCAAAGATACAGGTCTGCAAGC	Mus musculus	Merck
ITCH forward	TTGATGCGAAGGAATTAGAGG	Mus musculus	Merck
ITCH reverse	GGTGTAGTGGCGGTAGATGG	Mus musculus	Merck
β-ACTIN forward	GATCTGGCACCACACCTTCT	Mus musculus	Merck
β-ACTIN reverse	GGGGTGTTGAAGGTCTCAAA	Mus musculus	Merck

Table S4. List of Nedd4-family cDNA constructs.

E3 ligase	Species	Plasmid or insert origin	Recloned to pK-MYC-C1 and thus adding Myc-tag
NEDD4L	Homo sapiens	Addgene, Plasmid: 27000 Gift from Joan Massague [11]	+
ITCH	Mus musculus	Addgene, Plasmid 11427 Gift from Allan Weissman [12]	-
WWP1	Homo sapiens	Gift from Paul Bieniasz, ADARC, NY	+
WWP2	Homo sapiens	Gift from Paul Bieniasz, ADARC, NY	+

Table S5 List of magnetic cell sorting reagents.

Antigen	Clone	Species tested	Conjugate	Company
Ly6G	17A2	Mus musculus	Biotin	BioLegend
CD3	145/2C11	Mus musculus	Biotin	BioLegend
CD11b MicroBeads	M1/70	Mus musculus and Homo sapiens	Coated	MiltenyiBiotec
CD43 (Ly48) MicroBeads	not specified by the company	Mus musculus	Coated	MiltenyiBiotec
KIT	Ack2	Mus musculus	Biotin	In house

Supplemental figures

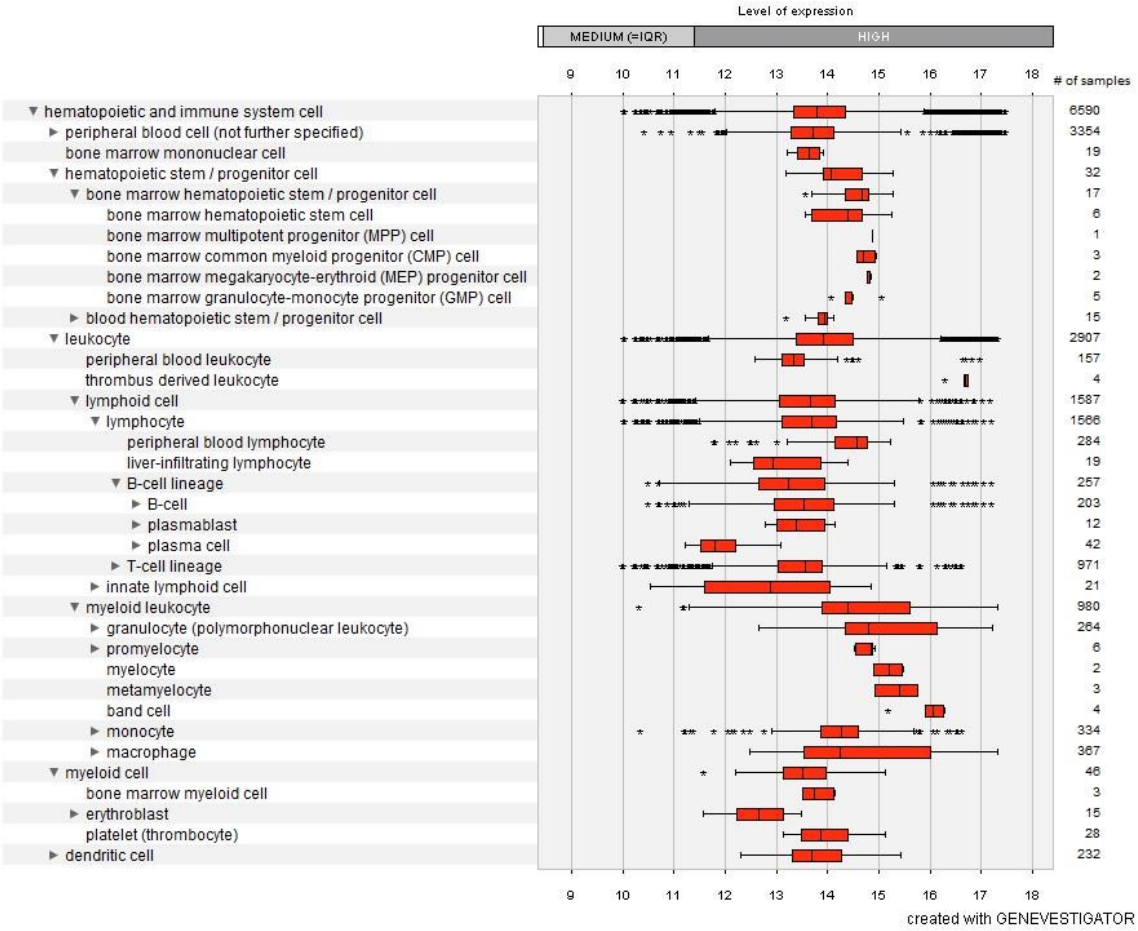

Figure S1. *WBP1L* expression in human leukocytes and leukocyte progenitor subsets. Expression profile of *WBP1L* mRNA generated by Genevestigator gene expression analysis tool, based on manually curated gene expression data from public repositories [13]. The box delimits the area between the upper and lower quartiles. Whiskers represent the lowest or highest data point still within 1.5 times this area in each direction. Stars represent data points outside this range.

A

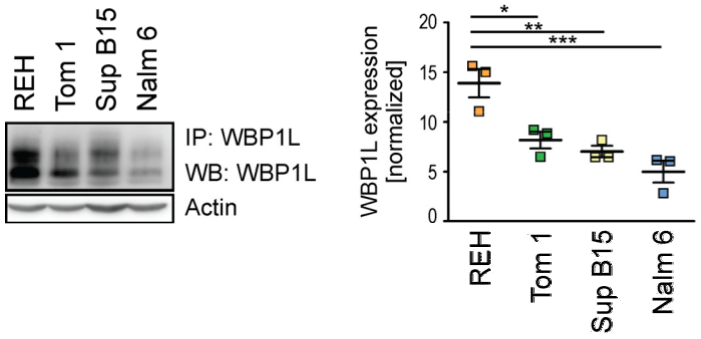

B

```
Original sequence  150 GCCTCGAGCGTCA--------GGATGGAGGAAGACTCG 180
Clone #17               ..............AA------..................
Clone #23               ..............CG------..................
Clone #190              ..............GG------..................
Clone #192              ..............GGGGC---..................
Clone #200              ..............AGATAGAC..................
```

C

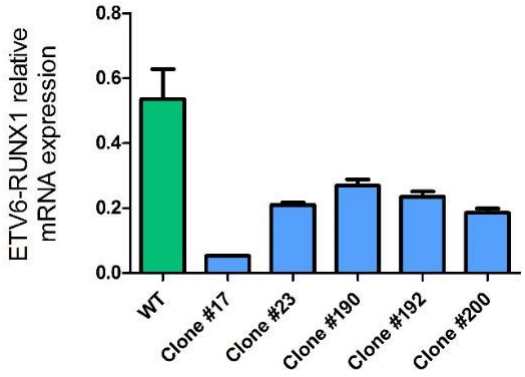

Figure S2. Expression of WBP1L in ETV6-RUNX1^{+} and ETV6-RUNX1^{-} cell lines and deletion of ETV6-RUNX1 in REH cells. (A) WBP1L immunoprecipitates from *ETV6-RUNX1*$^{+}$ B cell line REH and *ETV6-RUNX1*$^{-}$ lines TOM-1, NALM-6, and SUB B15 were immunoblotted with antibody to WBP1L and actin. For quantification, data were normalized in each experiment to actin and then to experiment average to allow comparison among experiments. Statistical significance was calculated using one way ANOVA with Dunnett's post test. (N=3). **(B)** Results of *ETV6* exon2 CRISPR/CAS9 target site sequencing in individual *ETV6-RUNX1*-deficient REH clones. **(C)** *ETV6-RUNX1* mRNA expression in the clones from (B) determined by qPCR. The data are plotted as 2^{-CT}.

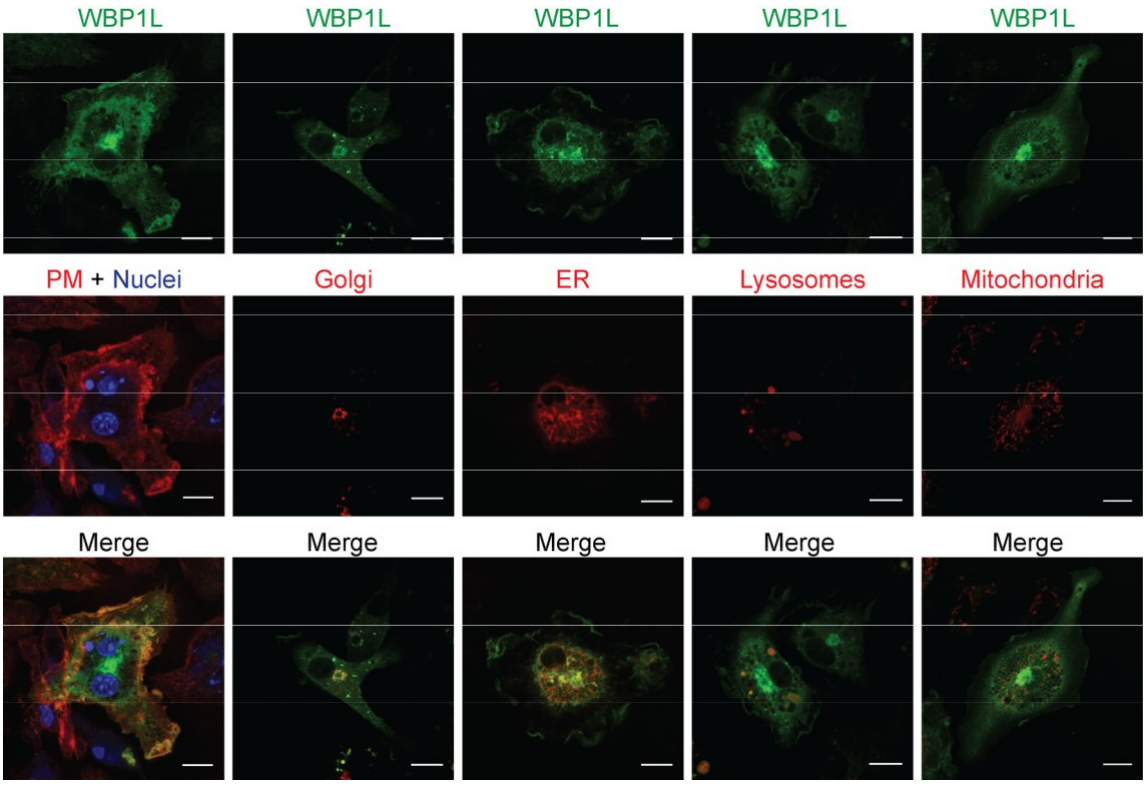

Figure S3. Subcellular localization of WBP1L. Confocal imaging of BMDM from *Wbp1l*$^{-/-}$ mice transduced with WBP1L-EGFP. The following markers were used: Plasma membrane (PM) – CD11b, Nuclei – Hoechst 33342, both on fixed cells; Golgi – Golgi-7-mApple retroviral construct, Endoplasmic reticulum (ER) – ER-Tracker-Red, Lysosomes and other acidic organelles – LysoTracker Red, Mitochondria – MitoTracker Red, all live cell imaging. Bar = 10 µm. N ≥ 3.

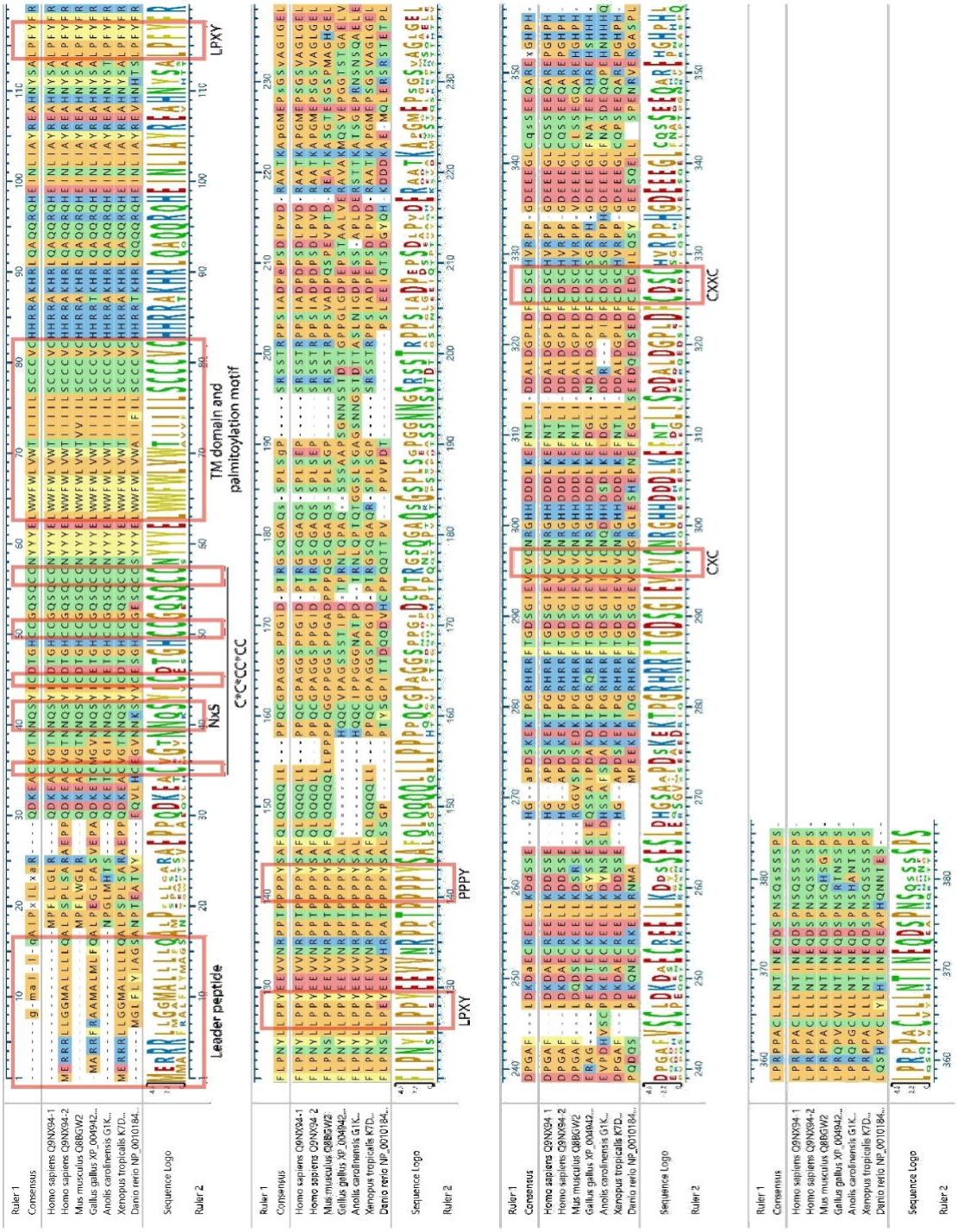

Figure S4. Alignment of WBP1L sequences from representatives of major vertebrate classes. Sequences were aligned with MUSCLE algorithm using MegAlign Pro software from DNASTAR Lasegene suite. Conserved features are highlighted with red boxes.

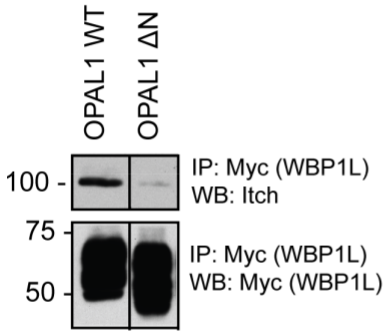

Figure S5. WBP1L interaction with ITCH in J774 macrophage-like cell line. MYC-tag imunoprecipatates from J774 cells stably expressing MYC-tagged WBP1L wild-type form or WBP1L N lacking WW domain interacting motifs. Western blots were stained with anti-ITCH antibody and anti MYC-tag antibody. Irrelevant lines from the blot image were removed and replaced with vertical dividing lines. N=2.

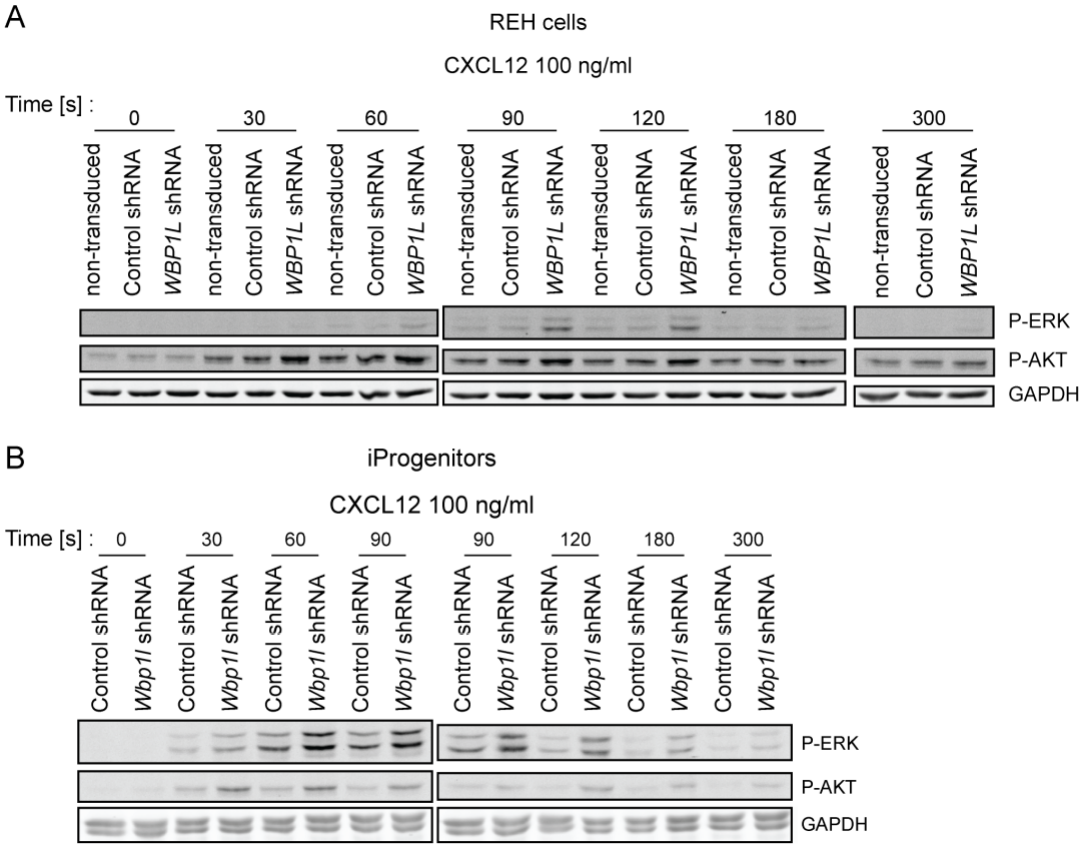

Figure S6. Representative Western blots showing data quantified in Figure 4C (A) and 4D (B).

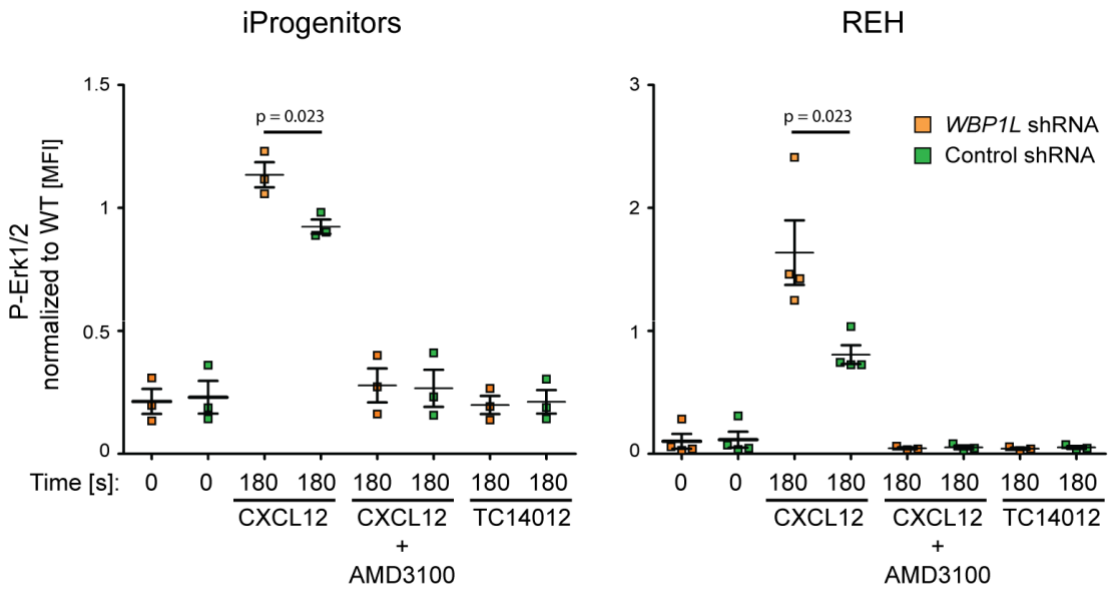

Figure S7. ERK1/2 phosphorylation downstream of CXCR4 or CXCR7 in immortalized monocyte/macrophage progenitors and REH cells transduced with *WBP1L* or control shRNA. Cells were treated with 100 nM CXCL12 alone or together with 1 µg/ml of CXCR4 antagonist AMD3100 or treated with 1 µM specific agonist of CXCR7 TC14012. ERK1/2 phosphorylation was analyzed by flow cytometry. Data are normalized to non-transduced cells (left panel N=3, right panel N=4).

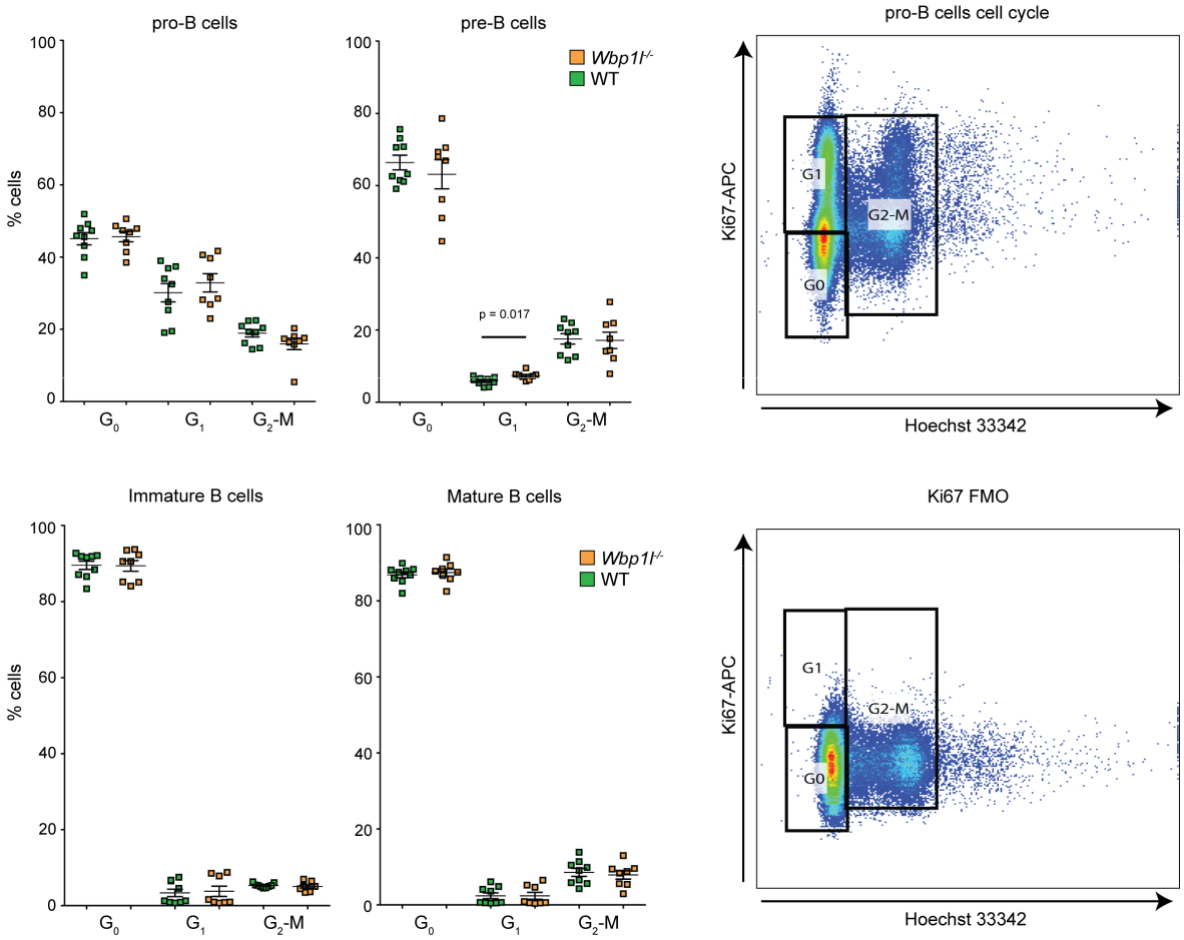

Figure S8. Analysis of cell cycle in bone marrow B cell progenitors from wild-type and *Wbp1l*-deficient mice. Bone marrow cells were fixed, stained for surface markers, permeabilized, and stained with Ki67 and Hoechst 33342. Individual B cell subsets were defined using following markers: Pro-B cells ($CD43^+$, $B220^+$, IgM^-), Pre-B cells ($CD43^-$, $B220^{low}$, IgM^-), Immature B cells ($CD43^-$, $B220^{low}$, IgM^+), Mature B cells ($CD43^-$, $B220^{high}$, IgM^+). The right panel of FACS plots shows gating strategy of cell cycle analyses. Representative FACS plots of stained cells with and without (Ki67 FMO) Ki67 staining are shown.

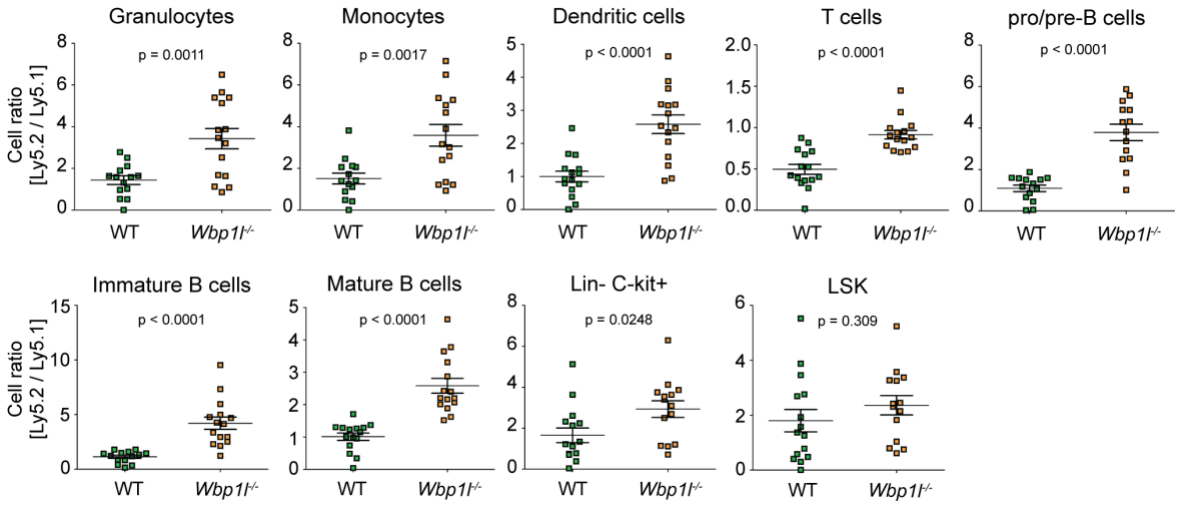

Figure S9. Enhanced engraftment of *Wbp1l*$^{-/-}$ bone marrow. Ly5.2^{+} bone marrow (WT or *Wbp1l*$^{-/-}$) was mixed with Ly5.1^{+} bone marrow (always WT) in a ratio 1:1 and 2 × 10^{6} cells were transplanted into Ly5.1 lethally irradiated mice. Mice were analyzed two months post transplantation. Flow cytometry analyses show the ratio between Ly5.2 and Ly5.1 cells determined for individual bone marrow cell subsets. Individual cell subsets were defined using following markers: Granulocytes (LY6C^{-}, CD11b^{+}, LY6G^{+}), Monocytes (LY6C^{+}, CD11b^{+}, LY6G^{-}), Dendritic cells (CD11c^{+}), T cells (CD3^{+}), Pro/Pre B cells (B220^{low}, IgM^{-}), Immature B cells (B220^{low}, IgM^{+}), Mature B cells (B220^{high}, IgM^{+}), Lin^{-}C-kit^{+} cells (lin^{-}, c-kit^{+}), LSK cells (lin^{-}, c-kit^{+}, SCA1^{+}).

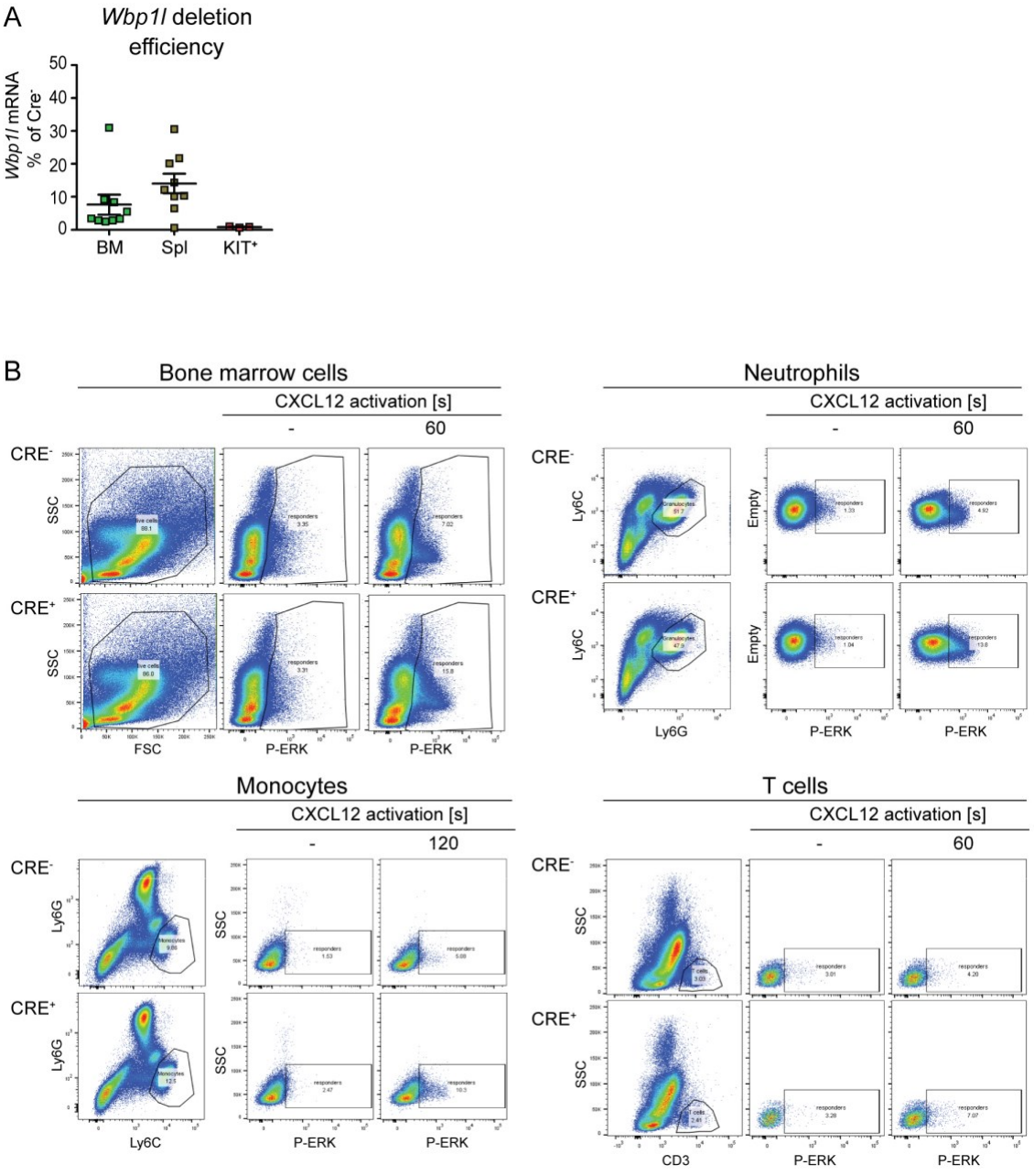

Figure S10. Effects of inducible *Wbp1l* deletion on ERK activation in bone marrow cell subsets. (A) *Wbp1l* mRNA expression after in vitro 4-hydroxytamoxifen induced deletion in samples from Figure 7F compared to 4- hydroxytamoxifen-induced deletion in vivo in the whole bone marrow and spleen from *Wbp1l-CreERT* mice (samples from Figure 7D). (B) Representative FACS plots for data shown in Figure 7D.

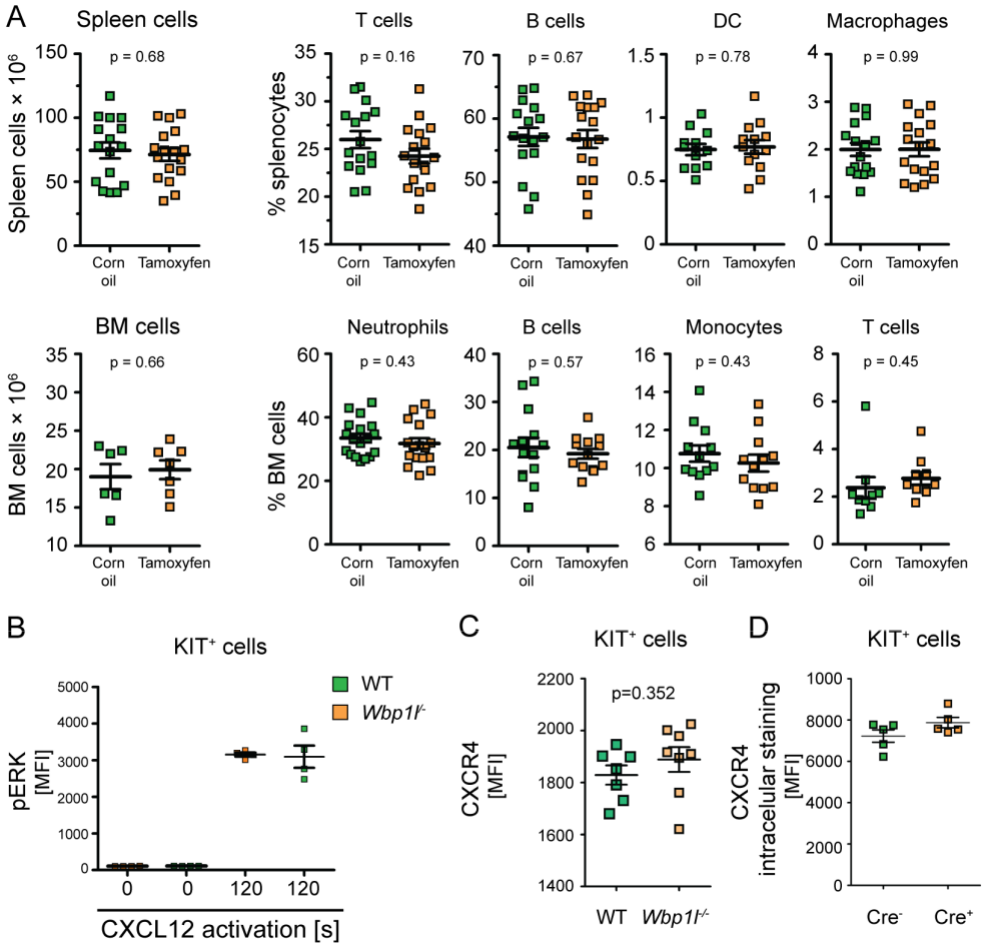

Figure S11. Additional analyses of *Wbp1l*$^{-/-}$ cells. (A) Total numbers of splenocytes and bone marrow cells and percentages of major leukocyte subsets 5-7 days after Tamoxifen-induced deletion of *Wbp1l*. The splenocyte subsets were defined using the following markers: T cells (CD3^{+}), B cells (B220^{+}), DC (CD11c^{+}, Ly6C$^{-/low}$), Macrophages (F4/80^{+}, CD11b^{int}). The bone marrow cell subsets were defined using the following markers: Neutrophils (Ly6C^{int}, CD11b^{+}, Ly6G^{+}), B cells (B220^{+}), Monocytes (Ly6C^{high}, CD11b^{+}, Ly6G^{-}), T cells (CD3^{+}). (B) Similar experiment as in Figure 7F. However, here the cells with constitutive *Wbp1l* inactivation were used (N=4). (C) CXCR4 surface expression was measured in cultured KIT^{+} bone marrow progenitors with constitutive *Wbp1l* inactivation by flow cytometry. One significant outlier was removed based on Q test. (D) Total CXCR4 expression was measured in cultured KIT^{+} bone marrow progenitors with constitutive *Wbp1l* inactivation by flow cytometry of fixed and permeabilized cells.

Supplemental References

1. **Kanderova V, Kuzilkova D, Stuchly J, Vaskova M, Brdicka T, Fiser K, Hrusak O, Lund-Johansen F, Kalina T.** High-resolution Antibody Array Analysis of Childhood Acute Leukemia Cells. *Mol Cell Proteomics*. 2016; 15: 1246-61.
2. **Wang GG, Calvo KR, Pasillas MP, Sykes DB, Hacker H, Kamps MP.** Quantitative production of macrophages or neutrophils ex vivo using conditional Hoxb8. *Nat Methods*. 2006; 3: 287- 93.
3. **Drobek A, Kralova J, Skopcova T, Kucova M, Novak P, Angelisova P, Otahal P, Alberich-Jorda M, Brdicka T.** PSTPIP2, a Protein Associated with Autoinflammatory Disease, Interacts with Inhibitory Enzymes SHIP1 and Csk. *J Immunol*. 2015; 195: 3416-26.
4. **Kralova J, Glatzova D, Borna S, Brdicka T.** Expression of Fluorescent Fusion Proteins in Murine Bone Marrow-Derived Dendritic Cells and Macrophages. *J Vis Exp*. 2018; 140: e58081.
5. **Sobocinska J, Roszczenko-Jasinska P, Zareba-Koziol M, Hromada-Judycka A, Matveichuk OV, Traczyk G, Lukasiuk K, Kwiatkowska K.** Lipopolysaccharide Upregulates Palmitoylated Enzymes of the Phosphatidylinositol Cycle: An Insight from Proteomic Studies. *Mol Cell Proteomics*. 2018; 17: 233-54.
6. **Wessel D, Flugge UI.** A method for the quantitative recovery of protein in dilute solution in the presence of detergents and lipids. *Anal Biochem*. 1984; 138: 141-3.
7. **Masuda T, Tomita M, Ishihama Y.** Phase transfer surfactant-aided trypsin digestion for membrane proteome analysis. *J Proteome Res*. 2008; 7: 731-40.
8. **Hebert AS, Richards AL, Bailey DJ, Ulbrich A, Coughlin EE, Westphall MS, Coon JJ.** The one hour yeast proteome. *Mol Cell Proteomics*. 2014; 13: 339-47.
9. **Cox J, Hein MY, Luber CA, Paron I, Nagaraj N, Mann M.** Accurate proteome-wide label-free quantification by delayed normalization and maximal peptide ratio extraction, termed MaxLFQ. *Mol Cell Proteomics*. 2014; 13: 2513-26.
10. **Welm BE, Dijkgraaf GJ, Bledau AS, Welm AL, Werb Z.** Lentiviral transduction of mammary stem cells for analysis of gene function during development and cancer. *Cell Stem Cell*. 2008; 2: 90-102.
11. **Gao S, Alarcon C, Sapkota G, Rahman S, Chen PY, Goerner N, Macias MJ, Erdjument-Bromage H, Tempst P, Massague J.** Ubiquitin ligase Nedd4L targets activated Smad2/3 to limit TGF-beta signaling. *Mol Cell*. 2009; 36: 457-68.
12. **Magnifico A, Ettenberg S, Yang C, Mariano J, Tiwari S, Fang S, Lipkowitz S, Weissman AM.** WW domain HECT E3s target Cbl RING finger E3s for proteasomal degradation. *J Biol Chem*. 2003; 278: 43169-77.
13. **Hruz T, Laule O, Szabo G, Wessendorp F, Bleuler S, Oertle L, Widmayer P, Gruissem W, Zimmermann P.** Genevestigator v3: a reference expression database for the meta-analysis of transcriptomes. *Adv Bioinformatics*. 2008; 2008: 420747.